UCLA
UCLA Electronic Theses and Dissertations

Title
Synthesis and Characterization of Salicylideneaniline Functionalized Molecular Rotors

Permalink
https://escholarship.org/uc/item/4ws2f51h

Author
Staehle, Ira Owen

Publication Date
2014

Peer reviewed|Thesis/dissertation

eScholarship.org Powered by the California Digital Library
University of California

UNIVERSITY OF CALIFORNIA

Los Angeles

Synthesis and Characterization of Salicylideneaniline Functionalized Molecular Rotors

A dissertation submitted in partial satisfaction of the requirements for the degree

Doctor of Philosophy in Chemistry

by

Ira Owen Staehle

2014

© Copyright by

Ira Owen Staehle

2014

ABSTRACT OF THE DISSERTATION

Synthesis and Characterization of Salicylideneaniline

Functionalized Molecular Rotors

By

Ira Owen Staehle

Doctor of Philosophy in Chemistry

University of California, Los Angeles 2014

Professor Miguel A. Garcia-Garibay, Chair

Artificial molecular machines have drawn much interest over the past twenty years. Several physical organic chemists have been actively involved in the study and development of different types of molecular machines. In nature many biological macromolecules have the ability to act as “molecular machines” and generate work. The most well known example of this is ATPsynthase, which functions by rotation of a central stock in order to convert ADP to ATP. These biological “molecular machines” are typically highly complex and consist of several subunits. However it is in this complexity that the function of these biological machines is manifested. In order to attain this level of complexity in artificial molecular machines, a gradual development of concepts and a deeper understanding of intermolecular interactions are required. Several molecular machine motifs have been identified and further functionality has been explored by

many physical organic chemists, incorporating useful material properties. One way to create artificial molecular machines is by controlling non-brownian motion. A common motif is a system that has two distinct energy states that can interconvert between one another in response to an external stimulus. These types of molecular machine motifs can be used for generating materials that are capable of energy harnessing. Research in the Garcia-Garibay group has focused on the use of light as an external stimulus to facilitate a conformational change between two distinct states in a molecular rotor.

Chapter 2 of this thesis will discuss the functionalization of molecular rotors with salicylideneanilines rotators. In work done in collaboration with Dr. Braulio Rodriguez-Molina, three different photoresponsive molecular rotors were synthesized, characterized, and crystallized. The photochromism of these solids was tested, with all systems converting from the low energy *cis*-enol to the transient *trans*-keto. The best performing of these three different molecular rotors was identified by the generation of the most *trans*-keto upon photoexcitation. A deuterated rotator analog was synthesized and the activation energy for rotation in the solid state was determined. Prior to this work, the preferred isomerization pathway for salicylidenenanilines was through a bicycle pedal mechanism, which does not account for rotation. The ssNMR data for the deuterated analog indicated that isomerization could also occur through rotation.

Chapters 3 and 4 will discuss the functionalization of molecular rotors with salicylideneanilines stators to act as potential molecular brakes. In chapter 3, an amino substituted stator was synthesized and characterized. Crystallization proved

challenging due to the preference of these compounds for the formation of spherulites, which are radial fibrous microcrystalline aggregate structures. Nonetheless, solid-state photochromism of the spherulites was determined for both systems by diffuse reflectance with the generation of a transient *trans*-keto form after photoexcitation. In chapter 4, an ester-substituted stator was synthesized and characterized. Single crystals could not be obtained and ssNMR was utilized to explore both the photochromism and thermochromism of the salicyladenanilines.

In chapter 5 of this thesis, I will discuss the synthesis and characterization of tetra-substituted salicylideneaniline adamantanes. Adamantanes are unique because they are the simplest diamonds and provide a rigid framework with minimal stress. Furthermore, tetra-substitution of adamantane generates a tetrahedral geometry around the adamantane core. Two adamantane systems were synthesized and single crystals were grown. However, only the connectivity was determined, due to poor quality crystals. These generated molecules could have up to 64 isomers, depending on the conformations of the four salicylideneanilines moieties. The photochromism of these solids was then tested with both systems generating the transient *trans*-keto species.

The dissertation of Ira Owen Staehle is approved.

Yu Huang

Patrick G. Harran

Miguel A. Garcia Garibay, Committee Chair

University of California, Los Angeles

2014

For my parents Dale & Sue
My grandparents (Carl & Myrtle) & (Harold & Claudia)

Table of Contents

List of Abbreviations

Ar	aryl
ca	circa
$CDCl_3$	deuterated chloroform
CP	cross polarization (NMR)
CP/MAS	NMR technique combining CP and MAS
d	deuterium
d_n	deuterium labeled compound with n deuterons
d	doublet (NMR)
dd	doublet of doublets (NMR)
ddd	doublet of doublets of doublets (NMR)
DMF	dimethylformamide
DSC	differential scanning calorimetry
E_a	activation energy
et al.	and others
FT-IR	fourier transform infrared (spectroscopy)
g	gram
GC	gas chromatography
hr.	hour
HRMS	high resolution mass spectrometry
Hz	hertz
IR	infrared (spectroscopy)
J	homo-nuclear coupling constant
K	Kelvin
k	exchange rate (Hz)
k_o	pre-exponential factor, or maximum exchange rate in Hz
k_{rot}	rate of rotation (Hz)
kcal	kilocalories
M	molar
MAS	magic-angle spinning (NMR)

m	multiplet (NMR)
MHz	megahertz
Min	minute
mL	milliliter
mm	millimeter
mmol	millimole
mol	mole
m.p.	melting point
ms	millisecond
m/z	mass to charge ratio
MS	mass spectrometry
NMR	nuclear magnetic resonance (spectroscopy)
NS	number of scans (NMR)
ns	nanosecond
Ph	phenyl
ppm	parts per million
q	quartet (NMR)
rt	room temperature
s	singlet (NMR)
t	triplet (NMR)
TGA	thermogravimetric analysis
THF	tetrahydrofuran
TLC	thin layer chromatography
UV-Vis	ultraviolet-visible (spectroscopy)
PXRD	powder x-ray diffraction
Å	angstrom
Λ	wavelength

Acknowledgements

I would first like to acknowledge my advisor, Professor Miguel Garcia-Garibay, for accepting me into his group and guiding me to be a better scientist. He always believed in me, even when I sometimes did not believe in myself. He provided opportunities for me to learn about several fields, including photochemistry and laboratory safety, and also taught me synthetic skills. I would like to thank my committee members, Professor Jeffrey Zink and Patrick Harran. I would also like to thank all past and present Garcia-Garibay group members. I would like to thank my classmates and friends: Andrew Roberts, Theresa Nguyen, Kady Bell, Alex Huters, Ilya Yakovlev, Joseph Fan, Patrick Commins, Salvador Perez-Estrada, and, especially, Antoine Stopin, Braulio Rodriguez-Molina, and Brianda Barrios for all the helpful discussions and collaborations, and, most importantly, for their friendship. I would like to thank my family. They have supported me during my journey and helped me pursue my dreams. Specifically, I want to thank my brother, Will, who helped me get through some of the challenges of graduate school. Finally I would like to thank my wife, Tania Maria Guardado-Alvarez. She has always supported me, no matter what, and helped motivate me to complete my research. Thank you, all, for your support and help finishing my doctoral studies.

VITA

2005-2008	Undergraduate Research Assistant Coe College, Cedar Rapids, IA Department of Chemistry Advisor: Dr. Scott Stoudt
2008	Bachelor of Arts in Chemistry Coe College
2008-2014	Teaching Assistant Department of Chemistry and Biochemistry University of California, Los Angeles

Publications and Presentations

Staehle, I; Rodriguez-Molina, B.; Garcia-Garibay, M. A. "Engineered Photochromism in Crystalline Salicylidene Anilines by Facilitating Rotation to Reach the Colored *trans*-Keto Form." *Cryst. Growth Des*., **2014**, *14,* 3667-3673.

Staehle, I; Chung, T. SJ.; Stopin, A.; Vadehra, G. S.; Hsieh, S. I.; Gibson, J. H.; Garcia-Garibay, M. A. "An Approach to Enhance the Safety Culture of an Academic Chemistry Research Laboratory by Addressing Behavioral Factors" in press.

Vadehra, G; Staehle, I; Chung, T; Commins, P.; Garcia-Garibay, M. A. "Cultivating a Culture of Safety in an Organic Chemistry Research Laboratory at UCLA." UC Center for Laboratory Safety Workshop, Irvine CA 2014.

Staehle, I; Garcia-Garibay, M. A. "Towards the Synthesis of a TEMPO Modified Rotor." US-Argentina Workshop on Nanomaterials (The International Center for Materials Research) in Bariloche, Argentina 2009.

Chapter 1

Photoresponsive Solid-State Artificial Molecular Machines

1.1 Introduction

Significant advances in the field of artificial molecular machines have occurred over the past two decades.[1,2] Chemists have synthesized molecular analogies to macroscopic machines such as: propellers,[3] gears,[4] turnstiles,[5] and ratchets[6], among others. Although these systems provided molecular analogs, there was no reason to believe that the molecular motion would emulate the macroscopic machine. Mislow and Iwamura, while studying ditriptycyl methanes and ethers, demonstrated that the triptycenes were geared and highly correlated, in approximation to the macroscopic bevel gears (Figure 1.)

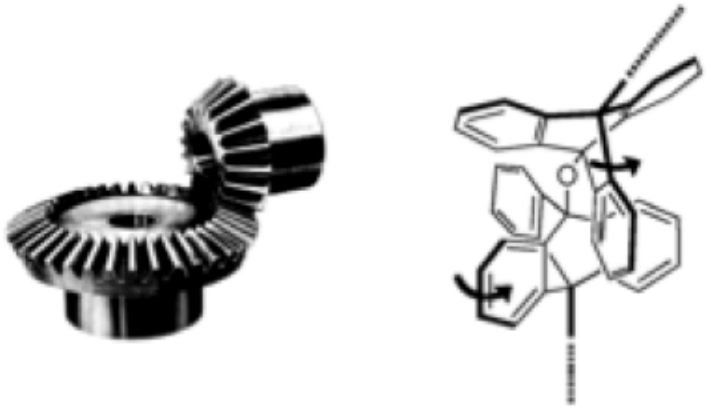

Figure 1. Structural and analogical similarities between a macroscopic bevel gear and a di-9-triptycylether in solution. Reprinted with permission from ref. 1f.

The resemblance between systems at the macroscopic level to the molecular level is not only structural but also functional.[7] While macroscopic objects continue to guide the efforts of chemists in the field of artificial molecular machines, the incorporation of properties that help control the behavior of the molecule by taking advantage of an external stimuli have been explored recently.[8] An example of this

approach comes from Feringa, who developed a sophisticated photochemically-driven molecular motor.[9] Feringa's system provided the first light-driven molecular motor, which can undergo repetitive 360° rotations in a unidirectional manner, as illustrated in Scheme 1.

Scheme 1. from reference 9.

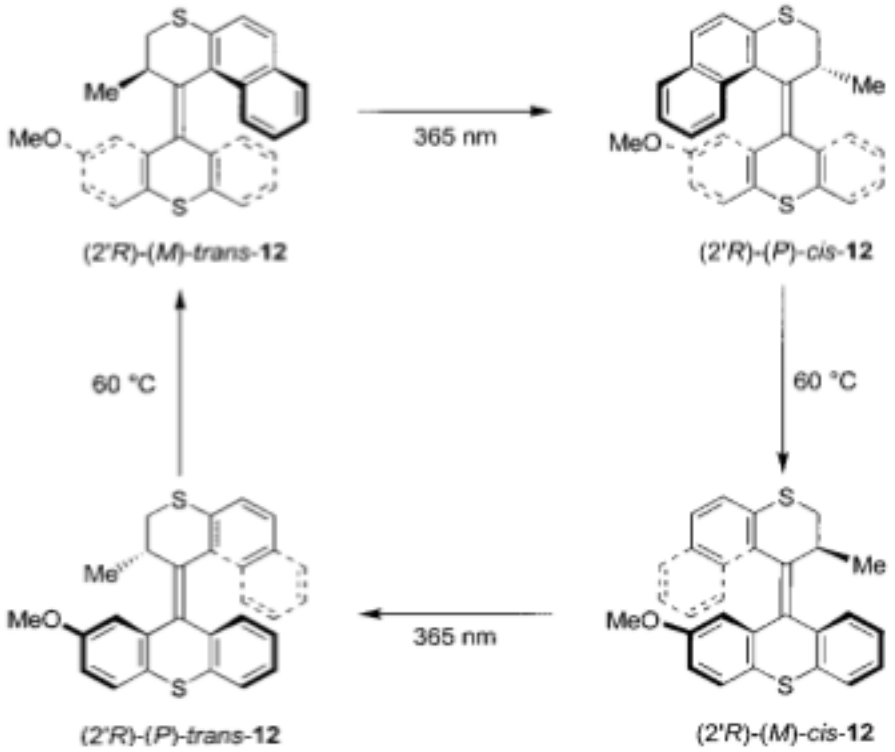

It is unlikely that "artificial molecular machines" will find applications similar to those of their macroscopic counterparts; these resemblances have stimulated an understanding of molecular interactions and association.[10] Thermal forces influence the driving force on the function of molecular machines on the molecular level in a viscous environment, while macroscopic machines are largely based on the relation between inertial forces and friction. Due to this reason, artificial molecular machines are more likely to be successful when they incorporate design

elements from biomolecular machines. These biomolecular machines range in function from solar energy capture and transduction (photosynthesis), ion pumping (ATP synthase), and internal transport (bacterial flagellum) to sensory functions (vision), among other things.[11] The complexity of these examples illustrates that artificial molecular machines should be more complex than isolated molecules in solution, if they are expected to be useful. In order to address a more defined environment, a crystalline solid state would be an ideal starting point. This environment would address the relationship between molecular structure and aggregation, allow for the determination of the relationship between aggregate structure and internal dynamics, and help develop concepts to control aggregate function.

1.2. Designing molecular machines

A machine is defined as an assemblage of parts that transmits force, motion, or energy from one component to another.[12] In contrast to the individual components, a machine has a large reduction of entropy, as a result of the change in the number of degrees of freedom.[13] A wristwatch, for example, is a macroscopic object made of 200 parts (N = 200) that work collectively as one. The individual components have 6N = 1200 independent degrees of freedom, but, when they are assembled in a specific manner, the assembly has only a few internal degrees of freedom, as illustrated in Figure 2.

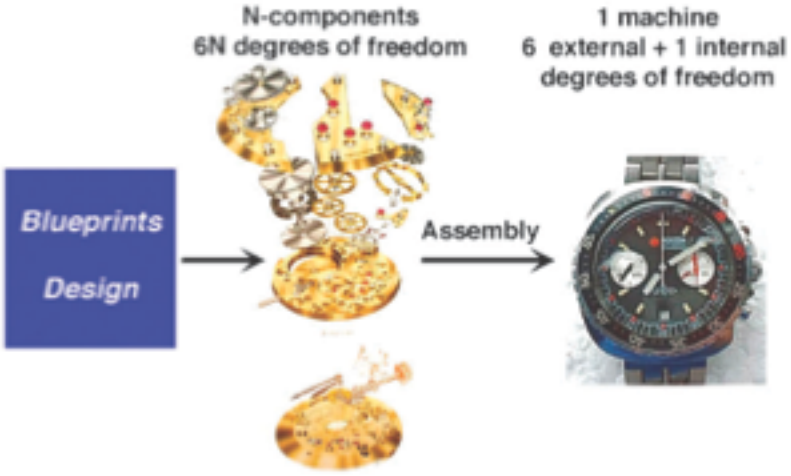

Figure 2. A machine is a dense, multicomponent assembly of precisely built units designed to assemble in a specific orientation that results in a limited number of internal degrees of freedom. Reprinted with permission from ref. 15. Copyright © 2006 American Chemical Society.

The function of the watch is derived from the combination of a large number of components within a structurally complex and dense assembly. The wristwatch function is governed by inertial forces and friction, which may be described using deterministic models.

Borrowing from macroscopic machines, an artificial molecular machine could be described and built by the blueprints, which describe the composition and structure of all the components (atoms and molecules) and the instruction for the assembly (chemical synthesis, self assembly and organization). Analogous to macroscopic systems, molecular machines should be dense, multicomponent assemblies that function under the influence of a suitable driving potential. These molecular systems, however, do not possess a resting state and cannot have functions based on inertial motion. Molecular machines have 3N-6 internal degrees of freedom for every conformation, with those degrees of freedom containing a large

number of quanta. These systems are subject to Brownian dynamics and their motion can only be described in a probabilistic manner.[14] Due to these forces, dissipating rapidly through the many degrees of freedom, the molecular machine's function will depend on the structural changes between states with different properties.

1.3. Molecular design of artificial molecular machines utilizing amphidynamic crystals

The development of artificial molecular machines will encompass several disciplines (chemistry, physics, materials science, etc.), but only synthetic chemists have the tools to establish the relationship between structure, internal dynamics, and function. In order to correlate the relationship between structure and dynamics of molecules in the condensed-phase, a qualitative phase diagram was proposed that related phase order and dynamics, shown in Figure 3.[15]

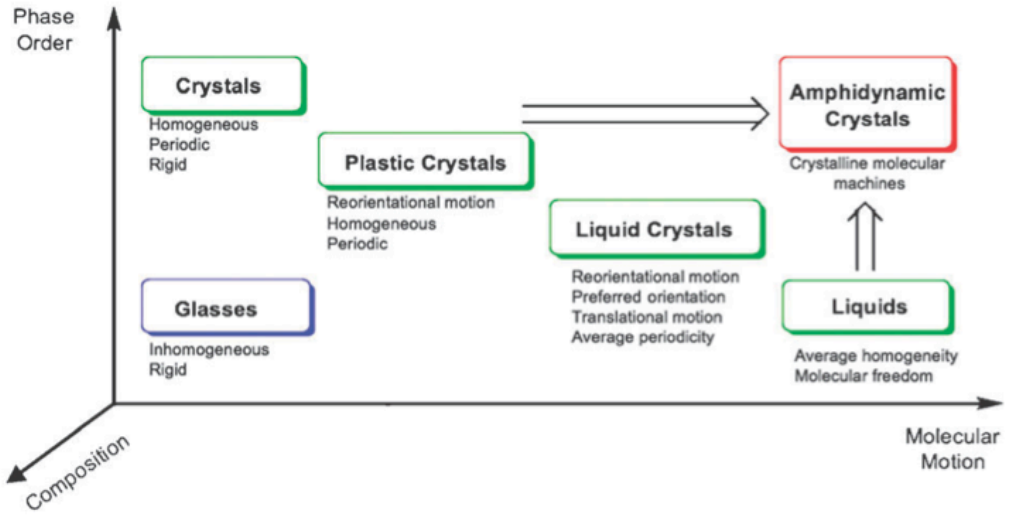

Figure 3. Phase order compared to molecular motion for condensed-phase matter from reference 1f.

Knowledge and intuition suggests an inverse relationship between phase order and molecular motion in the condensed-phase. Starting in the bottom right corner (Figure 3), molecules in the liquid phase have molecular freedom and can undergo rapid diffusion, collisions, and tumbling that make the bulk material dynamically isotropic. Located in the bottom left corner are glasses, which have arrested diffusion and rotation, rendering the system structurally inhomogeneous. Additionally glasses have no net molecular order and very little motion. The top left corner of the phase diagram is occupied by crystals, which have the greatest long-range order. Molecular crystals fill-in the largest amount of volume and form aggregates with very short-range forces. The corresponding close-packing results in a structure that is rigid, homogeneous, and periodic.

Two intermediate phases possessing molecular dynamics and phase order between those observed for liquids and crystals are the result of weak enthalpic forces. The plastic crystalline phase possesses one or more degrees of rotational freedom, as well as limited translational motion, and are typically spherical or cylindrical shaped moieties (C_{60}, ferrocene, adamantane, norbornadiene, etc.)[16] Plastic crystalline molecules are located at discrete sites within a homogeneous periodic lattice, yet the components can undergo high frequency re-orientation.[17] With this "dynamic disorder," these globular shaped molecules experience low barriers to rotation in the solid state. Plastic crystals possess an anchored center of mass, but having multiple rotational axes does not make them ideal for controlled molecular motion.

Liquid crystals (LC) are the other intermediate phase with order and motion between plastic crystals and liquids, located in the middle-right portion of Figure 3. Liquid crystals have long-range orientational order and can undergo fast translational self-diffusion, molecular rotation, and internal conformational dynamics. The structure of liquid crystals is characterized by rigid cores (rod-like or disc-shaped) and floppy side chains, and is not possible for molecules with arbitrary shapes. Phase order and dynamics are influenced by the characteristics of the corresponding molecular structures, but an inherent trade-off for these systems exists between phase order and molecular dynamics.

Utilizing proper structural design, we can integrate rigid molecular components that make an ordered lattice with components capable of experiencing high functional mobility to generate high order and fast motion. This phase, with components at the extremes of the dynamics spectrum, was termed "amphidynamic crystals," by our group, as illustrated in the top right corner of Figure 3.[18] These amphidynamic crystals would offer the ideal framework for artificial molecular machines, due to the highly anisotropic manner and well-defined frame of reference.

1.4. Molecular machines utilizing amphidynamic crystals

Taking inspiration from macroscopic machines, which are densely packed with components that undergo periodic motions (rotary and oscillatory), the following three design elements were utilized: an amount of pre-programmed free volume; the use of volume-conserving processes, like rotating cylinders that do not displace shape or volume; and correlated motions, where the moving objects intermesh in a gearing fashion, taking turns to occupy the same space. Based on

these design elements, rapid molecular motion within a close-packed environment should be possible in molecular crystals.

The most successful structures for forming amphidynamic crystals are based upon molecular rotors. These molecules are designed with rigid frames, which generate local free volume within a dense packed environment, linked through axles to support rotation. The molecular rotor is comprised of three components: 1) the stator, which provides the static frame of reference, 2) the rotator, which is the component undergoing motion, and 3) the axle, which links the rotator to the stator and should be a near barrierless linker. These molecular rotors are analogous to the structural designs of macroscopic gyroscopes and compasses, however it is unlikely that they will function like their macroscopic object. The molecular gyroscope framework should provide well-defined motion within a densely packed crystal, as illustrated in Figure 4.

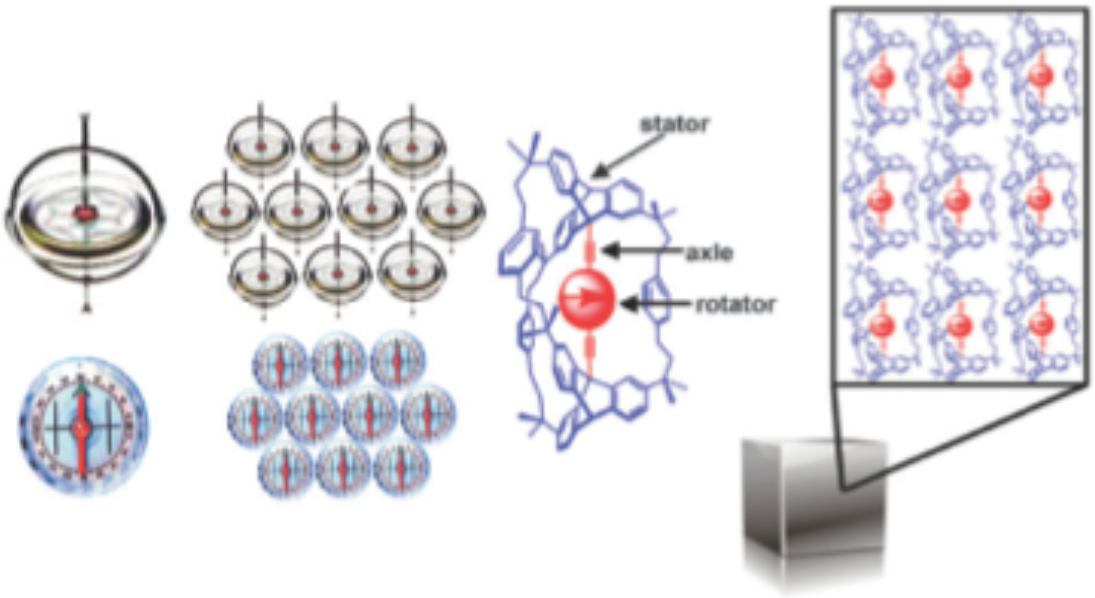

Figure 4. From left to right: macroscopic gyroscope and compass, an array of both, a detailed molecular gyroscope, an array of molecular gyroscopes in the crystalline phase from reference 15.

The molecular gyroscope in Figure 4 represents an idealized system with elements to form crystals that would support rotary motion. The rotary component is a phenylene ring linked by a rigid dialkynyl axle, shown in red, while the bridged triptycene stator is shown in blue. The rotation about C(sp)-C(sp) bonds is almost barrierless in the gas phase, and alkynyl axles facilitate the rotation of the central rotator.[19] The stator portion provides a static frame of reference and creates internal free-volume where rotation can occur. The bridging groups connecting the two stators help to further define a boundary of free volume around the rotator. These three features may be mainstays in molecular rotors for stimuli-responsive bulk materials, however, variations in size, aspect ratio, and symmetry of the

components should allow for systematic variation in the packing, solid-state dynamics and function.

1.5. External stimuli responsive molecular machines

Harnessing the potential of amphidynamic molecular rotors as collective molecular machines will require the functionalization of the rotors with stimuli-responsive moieties, so that their rotation may be externally controlled. It has been previously suggested that molecular rotors functionalized with dipolar groups would provide interesting ferroelectric and electro-optic materials.[20] Crystalline molecular rotors with dipolar rotators bear functional and structural analogies to macroscopic "compasses," which would have a dependence on the orientation of the central rotator, with respect to an external magnetic field. Molecular compasses have been prepared to investigate the interfacing rotary dynamics with an external electric field, as illustrated in Figure 5.

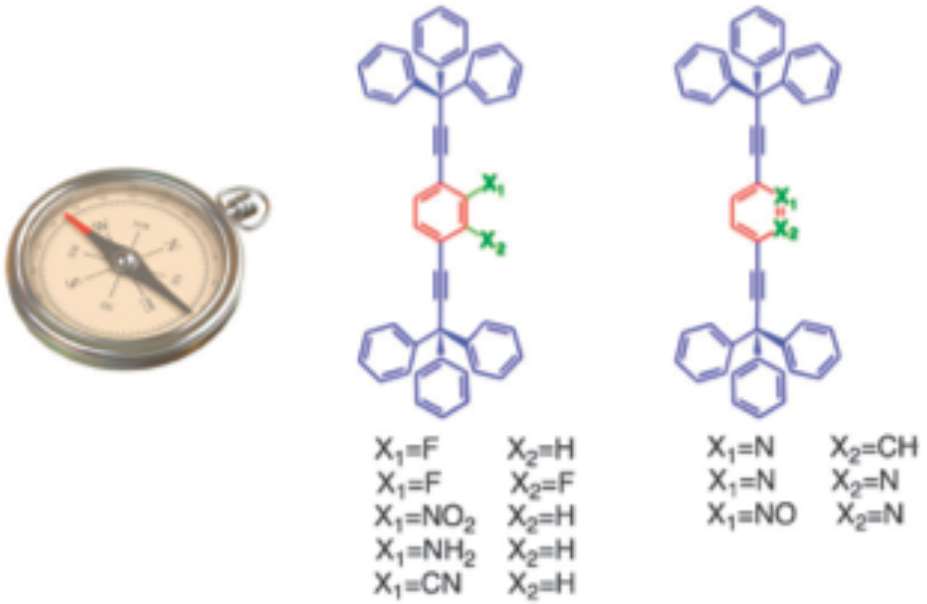

Figure 5. Molecular compasses that have a dipole-functionalized rotation unit that allows for directional responsive dynamics. Imaged from reference 20.

The substitution of polar groups (F, CN, NO_2, NH_2) onto the phenylene ring resulted in isomorphic structures to that of the parent molecular rotors. These systems show structural similarities in space groups and unit cell parameters to the unsubstituted molecular rotors. This indicates that amphidynamic molecular rotors may be integrated with dipolar functionality on the rotator, without drastically altering the solid-state, which dictates the rotational dynamics.

However an external magnetic field is not the only possibility for external stimuli of a molecular rotor**.** Light could be utilized as an external stimulus to facilitate changes at the molecular level, which could change the rotational rate of a molecular rotor. Photochromism is the reversible transformation of a single chemical species between two states that absorb in different regions of the ultraviolet and visible spectrum.[21] Photochromic molecules are of considerable

interest, due to their potential use in many new technologies, including non-linear optics,[22] information storage,[23] sensors,[24] and molecular machines.[25] These and other applications require photochromism to operate in solid matter, *i.e.* crystals, polymers, or thin films. For that reason, the solid-state photochromism of an increasing number of compounds like diarylethenes, [26] spiropyrans, [27] azobenzenes,[5, 28] and salicylideneanilines [29] have been explored with increasing interest. Photochromism generally entails changes in bonding patterns and extent of conjugation, resulting from electrocyclic reactions, proton transfer, and tautomerism, as well as *trans*-to-*cis* double bond isomerizations.[1] Photochromism also causes changes in size and shape that are generally not allowed within the rigid environment of a solid matrix. Feringa reported a homochiral molecular motor embedded in a unidirectionally-aligned liquid crystalline film.[30] The molecular motor was used to dope the film (1%) that results in a system that undergoes submicron changes in surface topology, as a function of a four-step cycle characterized by diastereospecific photoisomerizations and thermal atropisomerizations. The surface of this film was large enough to generate a collective torque to rotate a 28 mm glass rod, as shown in Figure 6.

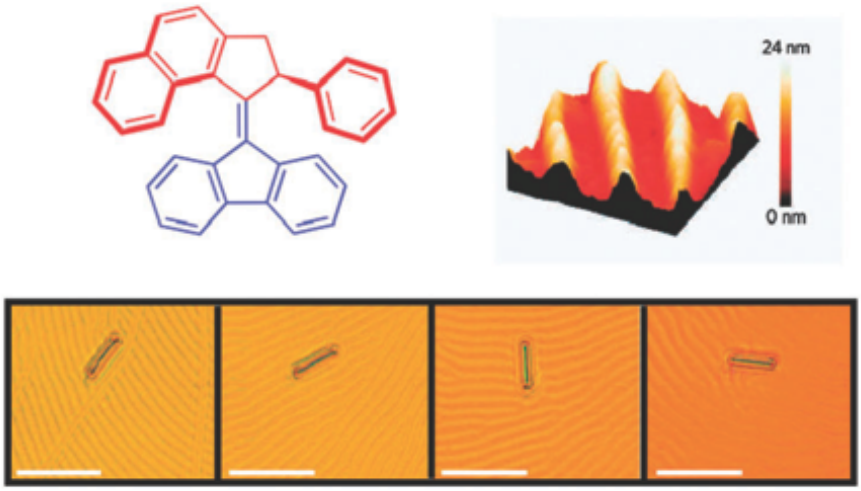

Figure 6. A liquid crystalline film doped with a light-driven unidirectional molecular motor resulting in a stimuli-responsive multicomponent system, which rotates a glass rod. Scale bars = 50 mm. Reprinted with permission from Macmillan Publishers Ltd: *Nature,* reference 30, copyright © 2006.

Recently in our group, molecular rotors have been functionalized with azobenzene linkers, which connect the two stators together.[25b] This idea was developed because of the tendency of bridges collapsing toward the rotator, inhibiting all rotation. Installation of a photoactivatable-bridging group could serve as a simple molecular brake, which could facilitate or inhibit rotation in the respective form (*trans* or *cis*), illustrated in Figure 7.[31]

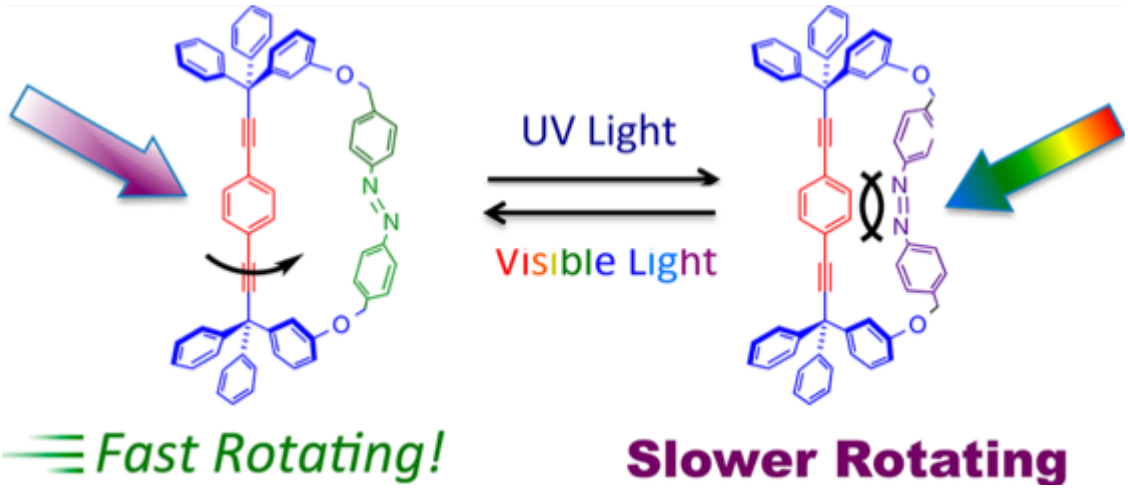

Figure 7. Azobenzene linked rotor exhibiting fast rotation in the *trans* form, after irradiation the azobenzene isomerizes to the respective *cis* form inhibiting the rotation from reference 31.

However, due to the large displacement required in the solid-state for the isomerization of azobenzene, this process does not occur in a bulk crystalline solid. As a result, nanocrystals of azobenzene-linked rotors were generated and showed to undergo both forward and reverse isomerizations with the proper wavelength of light.

Addition of a photoresponsive moiety to molecular rotors that does not displace much volume between states would be an ideal candidate for solid-state stimuli responsive molecular machines. One of the most promising photochromes for this application is the salicylideneaniline functionality. In the specific case of salicylideneanilines (SAs), they exist in thermal equilibrium between *cis*-enol and *cis*-keto tautomeric forms, with the aromatic hydroxyl-bearing tautomer being the most stable. Photochromism in these molecules occurs upon electronic excitation of the stable *cis*-enol, followed by an adiabatic oxygen-to-nitrogen proton transfer reaction, and an isomerization process that positions the N-H group opposite to the carbonyl oxygen to form the longer-lived, *trans*-keto species, which has a red

colored *ortho*-quino-dimethane chromophore [32] (Figure 8). While the proton-transfer step should not be hindered in a solid-state environment, isomerization from the *cis*-enol to the *trans*-keto structure is expected to be difficult, especially in close-packed crystals.[33] In fact, substantial X-ray structural evidence suggests that this event occurs by a volume conserving bicycle pedal motion[34], involving a reorientation of the central imine/enamine atoms.

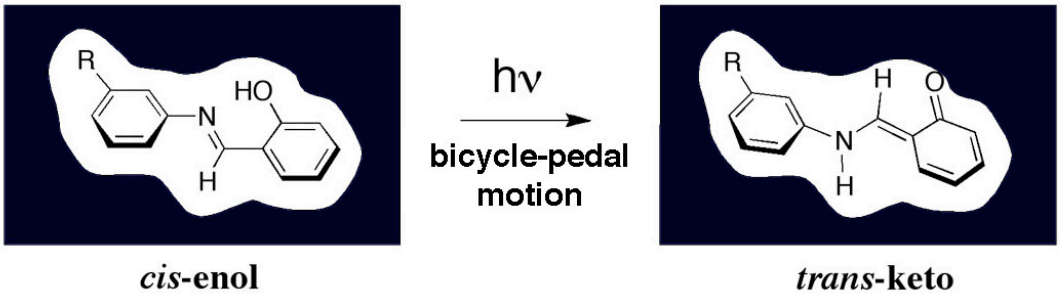

Figure 8. Volume conserving bicycle-pedal motion of the *cis*-enol form and the trans-keto form of a substituted salicylideneaniline moiety adapted from reference 35.

Exploration of salicylideneaniline functionalized molecular rotors would be a important step to the development of photoresponsive solid-state molecular machines.

1.6. References

[1] a) E. R. Kay, D. A. Leigh and F. Zerbetto, *Angew. Chem., Int. Ed.*, **2007**, *46,* 72; b) K. Skopek, M. C. Hershberger and J. A. Gladysz, Coord. *Chem. Rev.*, **2007**, *251*, 1723; c) W. R. Browne and B. L. Feringa, *Nat. Nanotechnol*., **2006**, *1*, 25; d) G. S. Kottas, L. I. Clarke, D. Horinek and J. Michl, *Chem. Rev.*, **2005**, *105*, 1281; e) V. Balzani, A. Credi, F. M. Raymo and J. F. Stoddart, *Angew. Chem., Int. Ed.*, **2000**, *39*, 3348. f) Vogelsberg C S.; Garcia-Garibay, M.A. *Chem. Soc. Rev*., **2012**, *41*, 1892.

[2] a) R. A. van Delden, M. K. J. Wiel, M. M. Pollard, J. Vicario, N. Koumura and B. L. Feringa, *Nature*, **2005**, *437*, 1337; b) D. Horinek and J. Michl, *Proc. Natl. Acad. Sci. U. S. A.*, **2005**, *102*, 14175; c) K. Skopek and J. A Gladysz, *J. Organomet. Chem*., **2008**, *693*, 857; d) A. R. Karim, A. Linden, K. K. Baldridge and J. S. Siegel, *Chem. Sci.*, **2010**, *1*, 102; e) A. Scarso, H. Onagi and J. Rebek Jr., *J. Am. Chem. Soc*., **2004**, *126*, 12728; f) D. A. Leigh, J. K. Y. Wong, F. Dehez and F. Zerbetto, *Nature*, **2003**, *424,* 174; g) A. R. Pease, J. O. Jeppesen, J. F. Stoddart, Y. Luo, C. O. Collier and J. R. Heath, *Acc. Chem. Res.*, **2001**, *34*, 433; h) H. Jian and J. M. Tour, *J. Org. Chem*., **2003**, *68,* 5091; i) T. Akutagawa, K. Shitagami, S. Nishihara, S. Takeda, T. Hasegawa, T. Nakamura, Y. Hosokoshi, K. Inoue, S. Ikeuchi, Y. Miyazaki and K. Saito*, J. Am. Chem. Soc.,* **2005**, *127*, 4397; j) H. Kitagawa, Y. Koboria, M. Yamanakaa, K. Yozab and K. Kobayashia, *Proc. Natl. Acad. Sci. U. S. A*., **2009**, *106*, 10444.

[3] a) K. Mislow, *Acc. Chem. Res*., **1976**, *9,* 26; b) K. Mislow, D. Gust, P. Finocchiaro and R. J. Boettcher, *Top. Curr. Chem.,* **1974**, *47*, 1; c) P. Finocchiaro, D. Gust, W. D. Hounshell, J. P. Hummel, P. Maravigna and K. Mislow, *J. Am. Chem. Soc.,* **1976**, *98,* 4945.

[4] a) W. D. Hounshell, C. A. Johnson, A. Guenzi, F. Cozzi and K. Mislow, *Proc. Natl. Acad. Sci. U. S. A.*, **1980**, *77*, 6961; b) I. Iwamura and K. Mislow, *Acc. Chem. Res.,* **1988**, *21*, 175; c) M. Oki, The Chemistry of Rotational Isomers, Springer-Verlag, Berlin, 1993.

[5] T. C. Bedard and J. Moore, *J. Am. Chem. Soc*., **1995**, *117*, 10662.

[6] a) T. R. Kelly, I. Tellitu and J. P. Sestelo*, J. Org. Chem.,* **1997**, *63*, 3655; b) T. R. Kelly, I. Tellitu and J. P. Sestelo, *Angew. Chem., Int. Ed. Engl*., **1997**, *36*, 1866.

[7] a) K. Mislow, *Chemtracts—Organic Chemistry*, **1989**, *2*, 151; b) J. Tomasi, *THEOCHEM*, **1988**, *179*, 273.

[8] a) E. Maligaspe, N. V. Tkachenko, N. K. Subbaiyan, R. Chitta, M. E. Zandler, H. Lemmetyinen and F. D'Souza, *J. Phys. Chem. A,* **2009**, *113,* 8478; b) P. D. W. Boyd and C. Reed, *Acc. Chem. Res.,* **2005**, *38*, 235; c) C. M. Drain, A. Varotto and I. Radivojevic, *Chem. Rev.*, **2009**, *109*, 1630; d) S. Takagi, M. Eguchi, D. A. Tryk and H. Inoue, *J. Photochem. Photobiol., C,* **2006**, *7*, 104; e) M. R. Waseilewski, *Chem. Rev*., **1992**, *92*, 435; f) D. Gust, T. A. Moore and A. L. Moore, *Acc. Chem. Res.*, **2001**, *34*, 40.

[9] B. L. Feringa, *Acc. Chem. Res*., **2001**, *34*, 504.

[10] a) J. P. Sauvage, *Acc. Chem. Res*., **1998**, *31*, 611; b) A. Harada, *Acc. Chem. Res.*, **2001**, *34*, 456; c) S. J. Rowan, S. J. Cantrill, G. R. L. Cousins, J. K. M. Sanders and J. F. Stoddart, *Angew.* Chem., Int. Ed., 2002, 41, 898.

[11] a) D. Gust, T. A. Moore and A. L. Moore, Acc. Chem. Res., 2001, 34, 40. b) P. D. Boyer, Annu. Rev. Biochem., 1997, 66, 717; c) D. Stock, A. G. W. Leslie and J. E. Walker, Science, 1999, 286, 1700; d) H. Noji, R. Yasuda, M. Yoshida and K. Kinosita, Nature, 1997, 386, 299; K. Kinbara and T. Aida, Chem. Rev., 2005, 105, 1377; e) T. Atsumi, L. McCarter and Y. Imae, Nature, **1992**, *395*, 182.

[12] Webster's Ninth New Collegiate Dictionary, Merriam-Webster, Inc., Springfield, MA, 1991.

[13] M. A. Garcia-Garibay, *Proc. Natl. Acad. Sci. U. S. A.*, **2005**, *102*, 10771.

[14] a) R. D. Astumian, *Science*, **1997**, *276*, 917; b) R. D. Astumian, *Philos. Trans. R. Soc. London, Ser. B*, **2000**, *355*, 511. c) Quantum Aspects of Life, ed. D. Abbott, P. C. W. Davies and A. K. Pati, Imperial College Press, London, 2008.

[15] M. A. Garcia-Garibay, *Proc. Natl. Acad. Sci. U. S. A.*, **2005**, *102*, 10771.

[16] a) J. H. Strange, *Acta Crystallogr., Sect. B: Struct. Crystallogr. Cryst. Chem*., **1972**, *28*, 1645; b) N. G. Parsonage and L. A. K. Stavely, Disorder in Crystals, Clarendon Press, Oxford, 1978.

[17] W. J. Dunning, *J. Phys. Chem. Solids*, **1961**, *18*, 21.

[18] T.-A.V.Khuong; J.E.Nun˜ez;,C.E.Godinez; M.A.Garcia-Garibay, *Acc. Chem. Res*., **2006**, *39*, 413.

[19] S. Saebo, J. Almolof, J. E. Boggs; J. G. Stark, *THEOCHEM*, **1989**, *200*, 361

[20] a) Z. Dominguez, T.-A. V. Khuong, C. N. Sanrame, H. Dang, J.E.Nun˜ezandM.A.Garcia-Garibay,*J.Am.Chem.Soc*.,**2003**, *125*, 8827; b) R. D. Horansky, L. I. Clarke, J. C. Price, T.-A. V. Khuong, P. D. Jarowski and M. A. Garcia-Garibay, *Phys. Rev. B.*, **2005**, *72*, 014302; c) B. Rodriguez-Molina, M.E.Ochoa,N.Farfa´n,R.Santillan; M.A.Garcia-Garibay*, J. Org. Chem*., **2009**, *74*, 8554

[21] a) Hadjoudis, E.; Mavridis, I. M. *Chem. Soc. Rev.* **2004**, *33*, 579. b) Irie, M. *ChemRev.* **2000**, *100*, 1683; c) Heinz Dürr, H.; Bouas-Laurent, H., Eds., Photochromism: Molecules and Systems, Elsevier, Amsterdam, 2003

[22] a) Castet, F.; Rodriguez, V.; Pozzo, J.-L.; Ducasse, L.; Plaquet, A.; Champagne, B. *Acc. Chem. Res.* **2013**, *46*, 2656. b) Safin, D. A.; Robeyns, K.; Garcia, Y. *Cryst. Eng. Comm.* **2012***, 14,* 5523. c)Delaire, J. A.; Nakatani, K. *Chem. Rev.* **2000**, *100*, 1817.

[23] a) Moorthy, J. N.; Mandal, S.; Mukhopadhyay, A.; Samanta, S. *J. Am. Chem. Soc.* **2013**, *135*, 6872. b) Bruder, F.-K.; Hagen, R.; Rolle, T.; Weiser, M.-S.; Facke, T. *Angew. Chem. Int. Ed.* **2011,** *50,* 4552. c) Feringa, B. L.; Jager, W. F.; Lange, B. De. *Tetrahedron* **1993**, *49*, 8267.

[24] a) Zhang, J.; Zou, Q.; Tian, H. *Adv. Mater.* **2013**, *25*, 378. b) Natali, M.; Giordani, S. *Chem. Soc. Rev.* **2012**, *41*, 4010. c) Byrne, R. J.; Stitzel, S. E.;Diamond, D. *J. Mater. Chem.* **2006**, *16*, 1332.

[25] a) Yamada, M.; Kondo, M.; Mamiya, J. I.; Yu, Y. L.; Kinoshita, M.; Barrett, C. J.; Ikeda, T. *Angew. Chem., Int. Ed*., **2008**, *47*, 4986. b) Commins, P.; Garcia-Garibay, M. A. *J. Org. Chem.* **2014**, 1611.

[26] a) Terao, F.; Morimoto, M.; Irie, M. *Angew. Chem. Int. Ed.* **2012**, *51*, 901. b) Uno, K.; Niikura, H.; Morimoto, M.; Ishibashi, Y.; Miyasaka, H.; Irie, M. *J. Am. Chem. Soc.* **2011**, *133*, 13558. c)

Fukaminato, T.; Doi, T.; Tamaoki, N.; Okuno, K.; Ishibashi, Y.; Miyasaka, H.; Irie, M. *J. Am. Chem. Soc.* **2011**, *133*, 4984.

[27] a) Klajn, R. *Chem. Soc. Rev.* **2014**, *43*, 148. b) Liu, F.; Morokuma, K. *J. Am. Chem. Soc.* **2013**, *135*, 10693. c) Harada, J.; Kawazoe, Y.; Ogawa, K. *Chem. Commun.* **2010**, *46*, 2593.

[28] a) Bushuyev, O. S.; Tomberg, A.; Fris, T.; Barrett, C. J. *J. Am. Chem. Soc.* **2013**, 135, 12556. b) Kolpak, A. M.; Grossman, J. C. *Nano Lett.* **2011**, *11*, 3156.

[29] a) Koshima, H.; Matsuo, R.; Matsudomi, M.; Uemura, Y.; Shiro, M. *Cryst. Growth Des.,* **2013**, *13*, 4330. b) Harada, J.; Nakajima, R.; Ogawa, K. *J. Am. Chem. Soc.* **2008**, *130*, 7085. c) Amimoto, K.; Kawato, T. *J. Photochem. Photobiol. C Photochem. Rev.* **2005**, *6*, 207.

[30] R. Eelema, M. M. Pollard, J. Vicario, N. Katsonis, B. S. Ramon, C. W. M. Bastiaansen, D. J. Broer and B. L. Feringa, *Nature*, **2006**, *440*, 163.

[31] Commins, P.; Garcia-Garibay, M. A. *J. Org. Chem.* **2014**, 1611.

[32] (a) Flynn, C. R.; Michl, J. *J. Am. Chem. Soc.* **1974**, *96*, 3280. (b) Migirdicyan, E.; Baudet, J. J. Am. Chem. Soc. **1975**, *97*, 7400.

[33] (a) Cohen, M. D.; Schmidt, G. M. J.; Flavian, S. *J. Chem. Soc.*, **1964**, 2041. (b) Bregman, J.; Leiserowitz, L.; Osaki, K. *J. Chem. Soc*. **1964**, 2086.

[34] a) Harada, J.; Uekusa, H.; Ohashi, Y. *J. Am. Chem. Soc*., **1999**, *121*, 5809. b) Harada, J.; Ogawa, K. *J. Am. Chem. Soc.,* **2001**, *123*, 10884.

[35] Staehle, I. O.; Rodriguez-Molina, B.; Khan, S. I.; Garcia-Garibay, M. A. *Cryst. Growth Des.* **2014**, *14*, 3667.

Chapter 2

Engineered Photochromism in Crystalline Salicylidene Anilines by Facilitating Rotation to Reach the Colored *trans*-Keto Form

Adopted from recently published Staehle, I. O., Rodriguez-Molina, B., Khan, S. I., Garcia-Garibay, M. A. "Engineered Photochromism in Crystalline Salicylidene Anilines by Facilitating Rotation to Reach the Colored *trans*-Keto Form" (*Crys. Growth. Des.,* **2014**. DOI: 10.1021/cg500762a)

2.1. Introduction

Photochromism is the reversible transformation of a single chemical species between two states that absorb in different regions of the ultraviolet and visible spectrum.[1] Photochromic molecules are of considerable interest, due to their potential use in many new technologies, including non-linear optics,[2] information storage,[3] sensors,[4] and molecular machines.[5] These and other applications require photochromism to operate in solid matter, *i.e.* crystals, polymers, or thin films. For this reason, the solid-state photochromism of an increasing number of compounds like diarylethenes,[6] spiropyrans,[7] azobenzenes,[5, 8] and salicylideneanilines[9] have been explored with increasing interest.

Photochromism generally entails changes in bonding patterns and extent of conjugation resulting from electrocyclic reactions, proton transfer, and tautomerism, as well as *trans*-to-*cis* double bond isomerizations.[1] Photochromism also causes changes in size and shape that are generally not allowed within the rigid environment of a solid matrix. In fact, the detailed nature of the crystalline environment plays a critical role in determining the presence or absence of photochromic behavior for a homologous series that consistently displays it in solution.[10] For example, out of three polymorphs of *N*-3,5-di-tert-butylsalicylidene-3-carboxyaniline, only the α and β forms exhibit photochromism, while the structure of the γ form remains unchanged upon exposure to light.[11] In the specific case of salicylideneanilines (SAs), they exist in thermal equilibrium between *cis*-enol and *cis*-keto tautomeric forms, as shown in Figure 1, with the aromatic hydroxyl-bearing tautomer being the most stable.

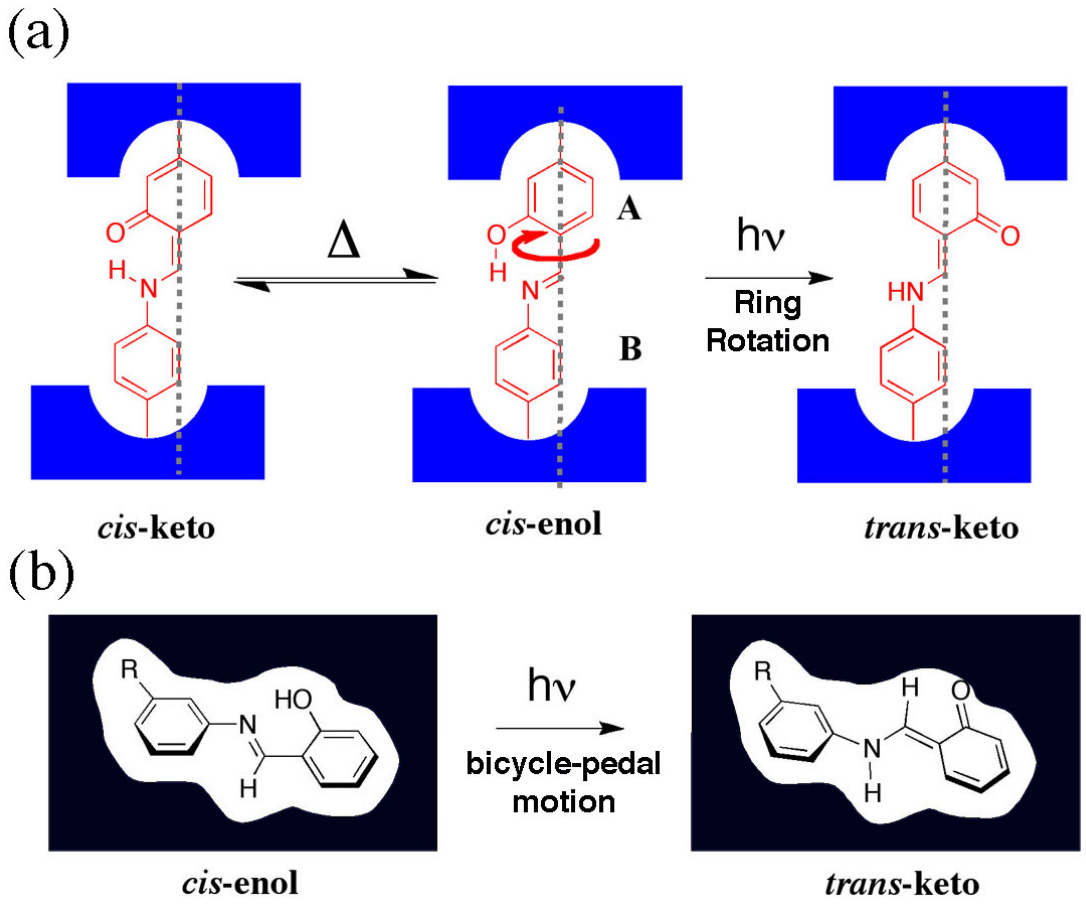

Figure 1. Photochromism of crystalline salicylideneanilines (SA) through (a) hypothetical ring rotation in a crystal-engineered molecular rotator built with a shielding stator that creates free volume for rotation, and (b) by a volume conserving, bicyle-pedal motion in the cavity of a close-packed crystal.

Photochromism in these molecules occurs upon electronic excitation of the stable *cis*-enol followed by an adiabatic oxygen-to-nitrogen proton transfer reaction and an isomerization process that positions the N-H group opposite to the carbonyl oxygen to form the longer-lived, *trans*-keto species,[1a] which has a red colored *ortho*-quino-dimethane chromophore[12] (Figure 1). While the proton-transfer step should not be hindered in a solid-state environment, isomerization from the *cis*-enol to the *trans*-keto structure is expected to be difficult, especially in close-packed crystals.[13] In fact, substantial X-ray structural evidence suggests that this event occurs by a

volume conserving bicycle pedal motion[1a,14,15,] involving a reorientation of the central imine/enamine atoms (Figure 1b). One strategy to facilitate this process takes advantage of bulky substituents that twist the aromatic rings out of plane and generate some free volume in the lattice.[15] Considering simple alternatives, and based on our experience in the field of crystalline molecular rotors,[16] we recognized that solid-state photochromism in SAs may be deliberately enabled by engineering crystals that allow the full rotation of the hydroxyl-containing ring (Figure 1a). In analogy with crystalline molecular rotor **1**[17] in Figure 2, which has a phenylene rotator shielded by two trityl groups acting as the stator, we decided to explore analogous structures with the two SA rings shielded by a bulky framework (Figures 1a and 2).

Using this basic design, we confirmed the solid state photochromism of salicylideneaniline-bearing structures **2**, **3,** and **4** (Figure 2). Evidence that rotation of the phenol ring is possible was obtained by measuring the rotational dynamics of an isomorphous crystal of a d_4-labeled Schiff base analogue of **3**, where the hydroxyl group was removed (see below).

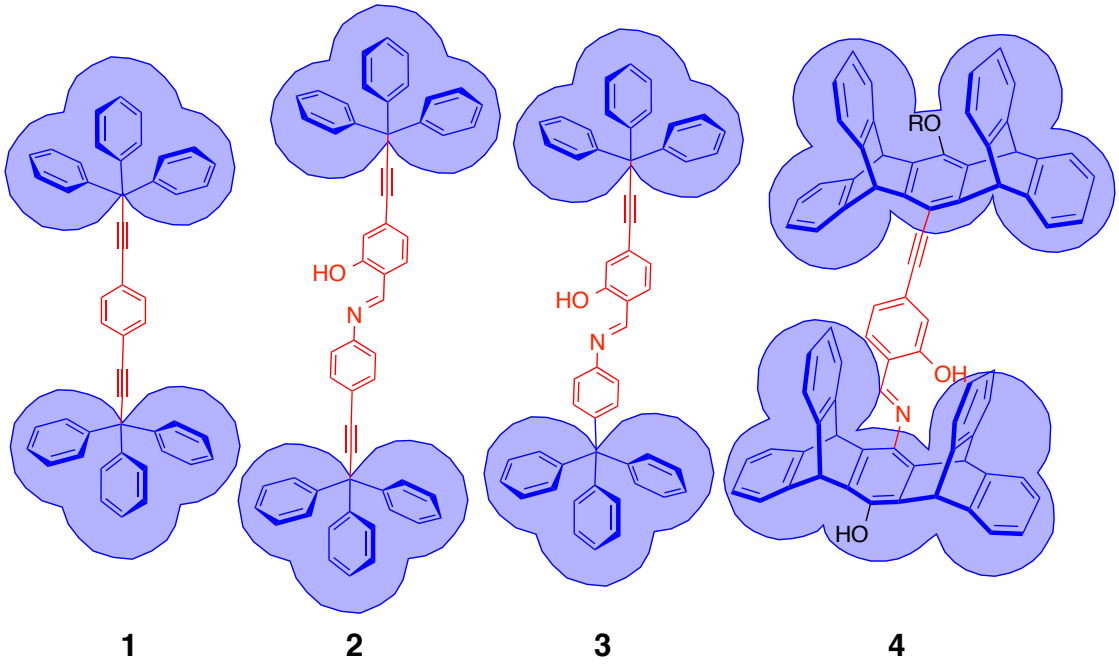

Figure 2. Phenylene molecular rotor **1** along with SA modifided rotors **2**, **3**, and **4** (R=hexyl) with structures intended to faciltate the rotation of the phenol ring so that it can form the colored trans-keto form.

2.2. Synthesis and Characterization

The SA molecular rotors **2** and **3** were obtained by the convergent strategy shown in Scheme 1. For the synthesis of **2**, samples of tritylacetylene were converted into the salicylaldehyde half molecular rotor **5,** using commercial 4-bromo-2-hydroxybenzaldehyde and standard Sonogashira conditions.[18] Compound **6** was obtained in a similar manner from the same alkyne and 4-bromoaniline, and the desired SA **2** was prepared in 73% yield by condensation of **5** and **6**. Compound **3** was obtained by condensation of commercial 4-amino-tetraphenylmethane with SA **5** in 89% yield. The ^{1}H NMR spectra of **2** and **3** have the characteristic signals of the aldimine hydrogens with chemical shifts of 8.60 and 8.62 ppm, respectively, and those of the phenol hydrogens at 13.21 and 13.37 ppm. Their corresponding ^{13}C

NMR spectra showed the signals of the aromatic hydroxyl-bearing carbon at 160.8 ppm for both compounds, and the imine carbons at 161.8 and 161.5 ppm. Four signals in the range of 84 and 97 ppm, in the case of **2**, correspond to the two distinct alkynes present in the molecule. Accordingly, only two signals at 84.8 and 98.4 are observed for **3**. Two signals at 56.17 and 56.20 ppm correspond to the two quaternary trityl carbon atoms in the case of **2**, while the corresponding values in the case of **3** are 56.2 and 64.8 ppm. These assignments were corroborated in the case of **2** by analysis of a 2D HMBC spectrum. The FTIR spectra of solids **2** and **3** had a very broad signal that spanned from ca 3400-2600 $cm^{-1,}$ attributed to the O-H stretch and a signal at ca. 1620 cm^{-1} assigned to the C=N functionality, in agreement with the *cis*-enol form.[19]

Scheme 1

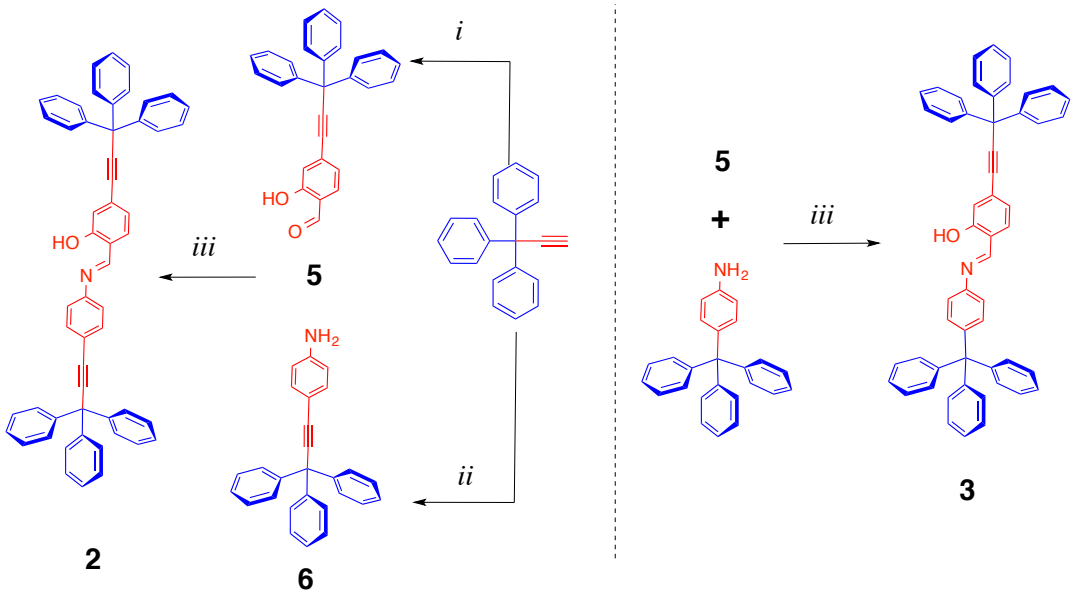

Reaction conditions: i. 4-bromo-2-hydroxybenzaldehyde, $Pd(PPh_3)_4$, CuI, diisopropylamine, benzene, reflux 8h. *ii.* 4-bromoaniline, $Pd(PPh_3)_4$, CuI, diisopropylamine, benzene, reflux 48h. *iii.* 4 Å molecular sieves, toluene, reflux 20h.

Scheme 2

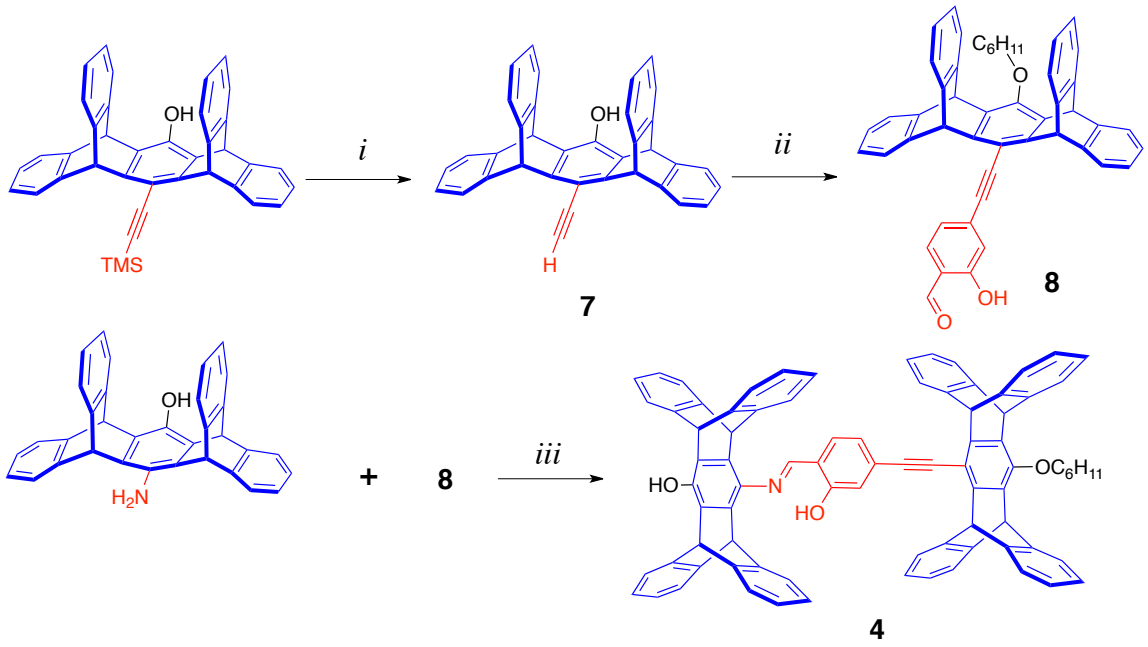

Reaction conditions: i. potassium carbonate, 1-bromo-hexane, dry acetone, reflux 12h. Followed by TBAF, THF at 50^{0}C for 0.5h. *ii.* 4-bromo-2-hydroxybenzaldehyde, $Pd(PPh_3)_4$, CuI, diisopropylamine, benzene, reflux 48h. *iii.* 4 Å molecular sieves, toluene, reflux 20h.

As shown in Scheme 2, the synthesis of the bis-pentiptycene derivative **4** was completed by condensation of the known 6-amino-13-hydroxy-pentiptycene[20] with salicylaldehyde pentiptycene **8** with a yield of 74%, as shown in Scheme 2. This synthesis started with the preparation of compound **8** by Sonogashira coupling of commercial 4-bromo-2-hydroxybenzaldehyde with the pentiptycene derivative **7**. Precursor **7** was formed in two steps, starting from the TMS-protected alkyne pentiptycene,[21] which was alkylated using 1-bromohexane to increase its solubility. The ^{1}H NMR spectrum of compound **4** showed that the protons on the bridgehead carbons of the different pentiptycene halves were resolved with chemical shifts at 5.62, 5.74, 5.75, and 5.94 ppm, with each signal integrating for two protons for a

total of eight bridgehead protons. All the ^{1}H and ^{13}C NMR signals from the central SA chromophore were consistent with those described above for compounds **2** and **3**. Similarly, in addition to the stretching bands assigned to the SA unit, the IR spectrum of **4** had two broad phenolic O-H bands in the 3500-3100 cm^{-1} region, corresponding to the OH of the pentiptycene portion and the *cis*-enol form.

Scheme 3

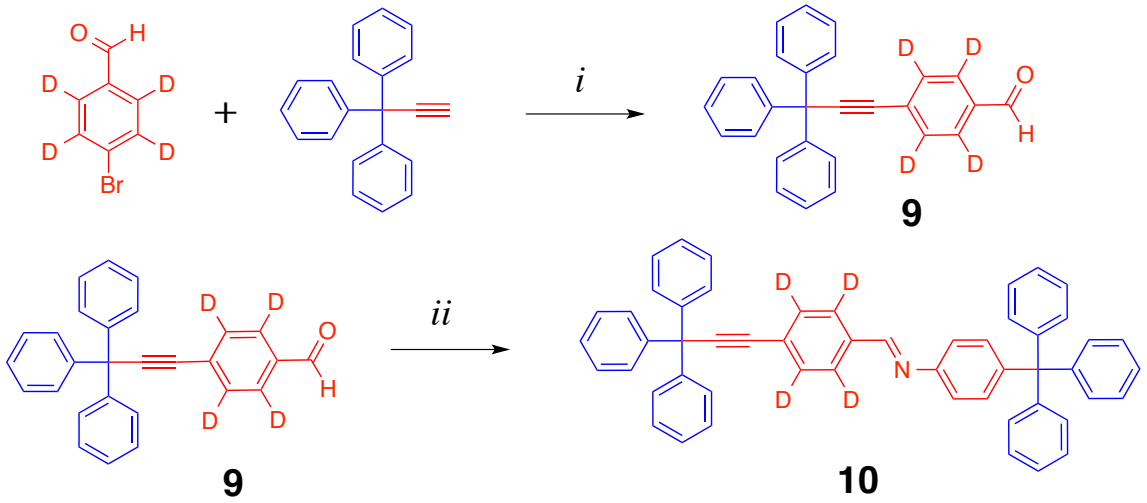

Reaction conditions: i. 4-bromo-2-hydroxybenzaldehyde, $Pd(PPh_3)_4$, CuI, diisopropylamine, benzene, reflux 8h. *ii.* 4 Å molecular sieves, toluene, reflux 20h.

Finally, in order to explore the rotational dynamics of the trityl group-shielded SA phenolic ring (ring A in Figure 1), we synthesized d_4-labeled compound **10** by condensing 4-amino-tetraphenylmethane with deuterated aldehyde **9** in 62% yield (Scheme 3). The spectroscopic properties of this model compound were in good agreement with expectations, including the degree of deuterium labeling, which was also confirmed by high-resolution mass spectrometry. Satisfyingly, as described below, the powder X-ray diffraction of imine **10** is essentially identical to

that of the analogous SA rotor **3**, which is indicative of a nearly identical packing structure.

2.3. Crystallization Studies and Single Crystal X-Ray Diffraction Analyses

Crystallization studies for compounds **2**-**4** were carried out at room temperature using different dry solvents and solvent mixtures. The selection of solvents was based on sample solubility and on the stability of the imine groups. Samples were soluble in chloroform, dichloromethane, toluene, and xylenes, but their solubility was low in acetonitrile and in hexanes. Traces of water in methanol and ethanol caused the slow hydrolysis of **2** and these solvents were avoided. In a typical experiment, *ca.* 15 mg of the selected compound was placed in a small glass vial, dissolved with the appropriate solvent or solvent mixture (ca. 1 mL), and capped. Samples were monitored regularly until the appearance of the first crystals, which were taken out of the solution and immediately covered with oil, to prevent the escape of solvent of crystallization. X-Ray data were collected at 100(2) K and selected crystallographic parameters for all three compounds are compiled in the SI.

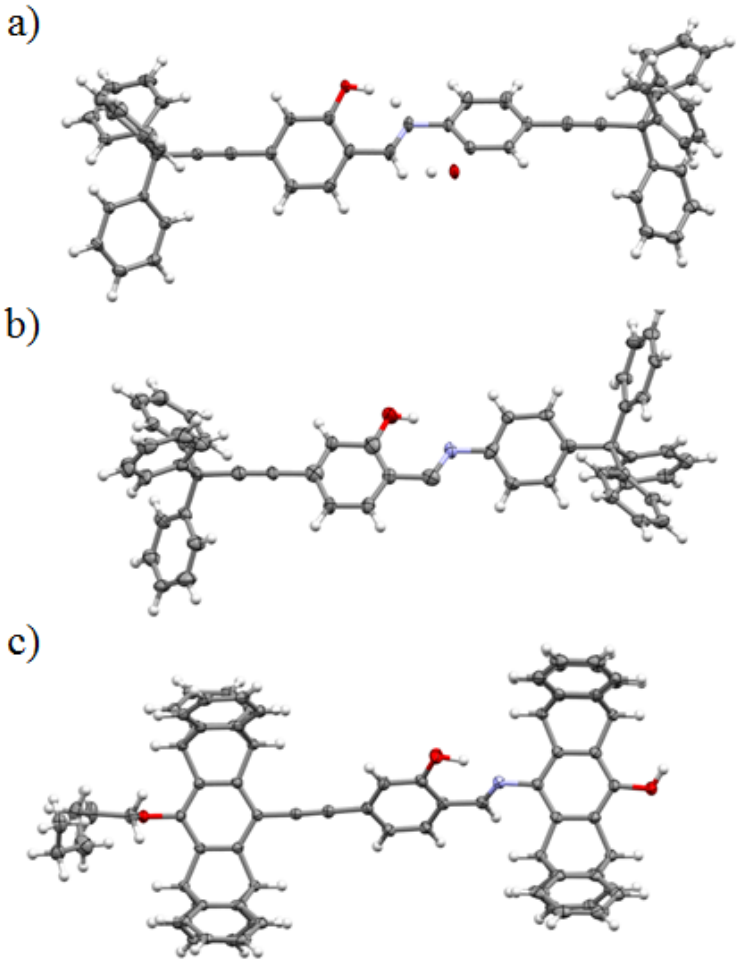

Figure 3. (a) Molecular structure of SA molecular rotor **2** showing a superposition of two disordered positions with occupancy of 56:44 and the central phenyl rings adopting a twisted conformation. (b) One of the two disordered positions with occupancy 87% of **3** that crystallizes with one cyclohexane molecule (not shown). (c) Molecular structure of the solvate of pentiptycene SA molecular rotor **4** obtained from acetonitrile (solvent molecules omitted). All the thermal ellipsoids are shown at 50% probability.

Small crystals of **2,** which were obtained by slow evaporation from dichloromethane, had their structure solved in the triclinic space group *P*-1, with one SA molecular rotor and one highly disordered solvent molecule per asymmetric unit. The crystals became opaque when exposed to open air, suggesting a rapid desolvation process. The molecular structure showed disorder in the

salicylideneaniline portion and was particularly evident in the C-OH and C=N groups, which were disordered over two positions related by a 180° rotation over an axis perpendicular to the molecular axis (Figure 3), with an occupancy 56:44. As a result of the disorder, a confirmation of the *cis*-enol previously determined by spectroscopic means was not possible. The C_{Ar}-OH and the C_{Ar}-H bond distances displayed an average 1.289(2) Å, instead of values of ca. 1.35 Å and 0.95 Å, which were expected for phenolic and C-H bonds, respectively.[14a] The Schiff base had a conformation where the two aromatic rings in the salicylidene aniline portion were not planar, with the angle between mean planes being slightly larger than 45°. This twisted conformation is characteristic of compounds with photochromic behavior,[22] which, in the case of compound **2,** was explored by diffuse reflectance in the solid state, as discussed in the following sections. The packing structure showed the lattice-forming trityl groups guiding the crystallization in a displaced parallel arrangement, by adopting a Ph···Ph interaction known as a four-fold phenyl embrace, or quadruple phenyl embrace (QPE),[23] with two phenyl rings showing edge-to-face propagating interactions with neighboring trityl groups. Some interdigitation occured between adjacent molecules, such that the trityl group of adjacent molecules was in close proximity with the salicylideneaniline component (Figure 4a).

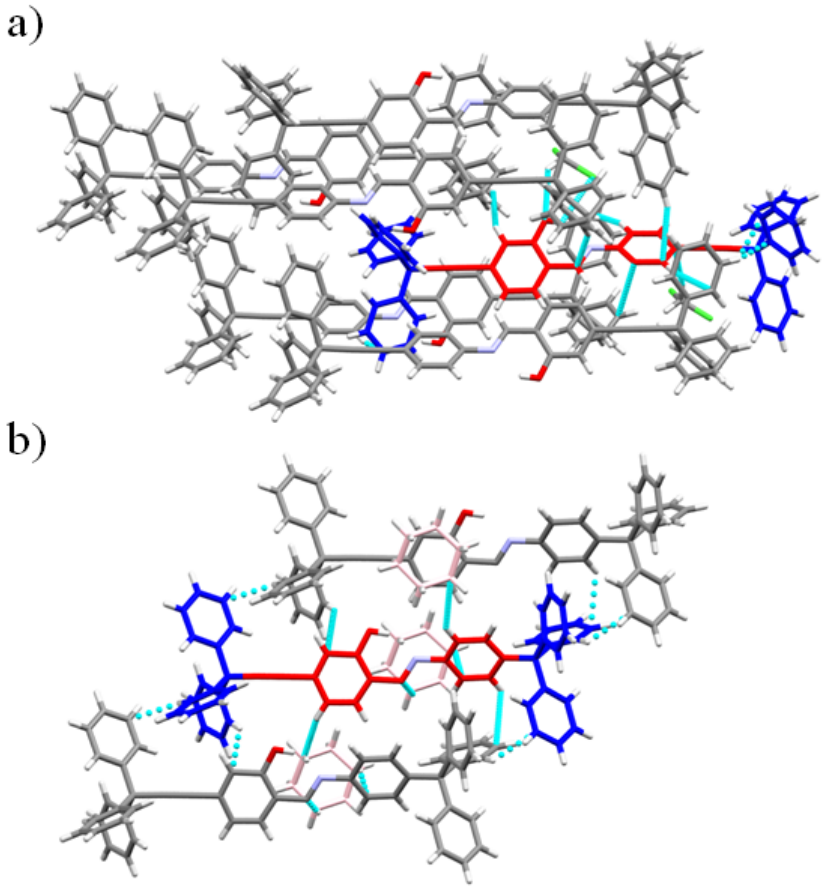

Figure 4. Comparison of the crystal packing of compounds **2** and **3,** showing the parallel array of molecules along close contacts (light blue line), with the salicylideneaniline portion (highlighted in red). (a) Compound **2,** showing four intermolecular contacts of the adjacent trityl groups over the aniline ring and two over the salicylidene ring. (b) In compound **3,** the aniline portion has three close contacts, two of them with the loosely bound solvent highlighted in pink, while the salicylidene ring has two (one with solvent).

Crystals of SA molecular rotor **3** were obtained from a mixture of cyclohexane/dichloromethane. Small single crystals had a tendency to degrade when exposed to ambient conditions. X-Ray diffraction data was solved in the monoclinic system, space group *C*2, with one molecule of cyclohexane per molecule of **3**. Structural analysis was complicated by the disorder of the salicylideneaniline part over two alternate positions related by 180° over an axis perpendicular to the

molecular axis, with an occupancy of 87:13. In our model, only the major component was refined anisotropically, and is shown in Figure 3b. In this structure, the central aromatic rings adopt a more planar conformation with an angle between mean aromatic planes close to 23°. Packing interactions between adjacent trityl groups favored a herringbone-like packing of aromatic molecules, where molecules of compound **3** crystallize in perpendicular layers with the molecular axis roughly parallel to the *b*,*c*-crystallographic plane. Compared to compound **2**, the salicylideneaniline moiety in **3** showed fewer intermolecular interactions, mainly with the cyclohexane molecules in the lattice (Figure 4b).

2.4. Solid State Photochromism

As mentioned above, the ^{1}H NMR, Compound **4** showed the lowest solubility of all and crystals obtained from dichloromethane or chloroform became opaque within seconds when exposed to air. Plates obtained by slow evaporation from a mixture of dichloromethane/acetonitrile were suitable for X-ray diffraction. Data were collected at 100(2) K and solved in the monoclinic space group $P2_1/c$. A considerable amount of highly disordered solvent was found within the cavity generated by the pentiptycene framework, which is well known to form host-guest complexes.[24] In our model, five molecules of acetonitrile were found per molecule of **4**. In contrast to the molecular structures of compounds **2** and **3**, that of compound **4** did not present disorder of the salicylideneaniline moiety, with C_{Ar}-OH and C=N bond distances of 1.354(3) and 1.287(3) respectively, indicating the presence of a *cis*-enol tautomer. The salicylidene rings adopt a twisted conformation with an angle between mean planes of 45.6°. In this array, the pentiptycene halves

acquire a coplanar conformation, allowing adjacent molecules to aggregate in a head-to-head fashion, forming parallel-displaced layers in a zig-zag pattern (please see *SI*). The rigid framework efficiently protects the inner part of the molecule by generating a relatively large cavity filled with acetonitrile. ^{13}C NMR and IR spectra are consistent with the stable *cis*-enol as the predominant form. In order to determine the relative contributions of the *cis*-enol and *trans*-keto forms of SA molecular rotors **2**-**4**, spectroscopic measurements were carried out using UV-Vis diffuse reflectance before and after exposure to UV light.

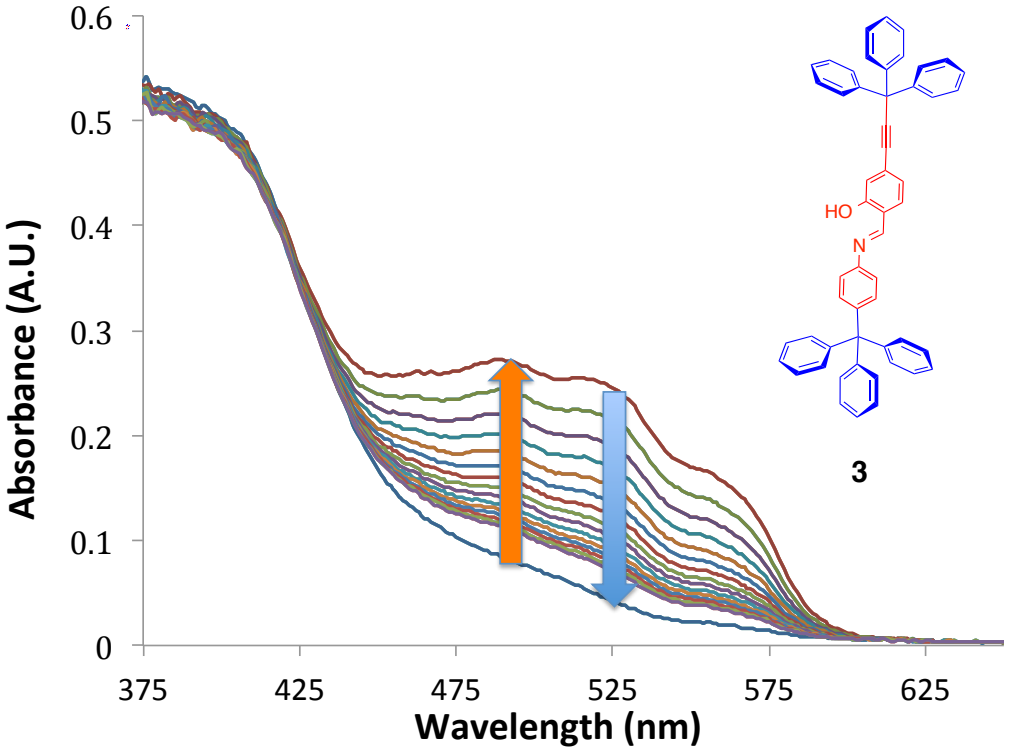

Figure 5. Optical absorption from the Kubelka-Monk function analysis of diffuse reflectance measurements of SA rotor **3** obtained immediately after irradiation with λ=365 nm (orange arrow) and after various decay periods (blue arrow).

Well-characterized polycrystalline powders were placed onto a barium sulfate plate, pressed, and their diffuse reflectance measured before irradiation with

365 nm UV light for 15 min at 300 K.[25] After that, as illustrated in Figure 5 for the case of compound **3**, diffuse reflectance measurements of the photogenerated *trans*-keto form were carried out over time scales that ranged from 6,000 (ca 1.6 h) to 50,000 s (ca. 13.9 h). While a photochromic response was observed for all three samples, their increase in the visible absorption band was different, in the order **3** > **2** >> **4** (Table 1). The spectrum of compound **2** was characterized by an absorption band that extended from ca. 270-450 nm with a λ_{max} at ca. 380 nm that could be assigned to the *cis*-enol. A weak shoulder in the range of 450-550 was assigned to the small equilibrium concentrations of the *cis*-keto form. Exposure to 365 nm UV light resulted in the growth of a broad band that extended up to 600 nm with a λ_{max} at ca. 475, with an absorbance increased by a factor of 1.69 (Table 1) from 0.065 to 0.110±0.003. This band was assigned to the *trans*-keto form, which decays in a manner that be described by a biexponential function with components having lifetimes of 174±14 s and 1392±71 s, respectively.

Table 1. Extent of reaction, lifetime of the *trans*-keto form, and parameters that may affect the photochromism of the three SA rotors.

	SA Rotor **2**	SA Rotor **3**	SA Rotor **4**
Increase factor in keto form absorption after h λ[1]	1.69	4.5	1.06
Lifetime T_1 (s)	174±14	405±2	1819±472
Lifetime T_2 (s)	*1392*±71	*1952*±13	16468±1920
Density, ρ [Mg m^{-3}]	1.271	1.208	1.216
Near neighbors / number of solvent[2]	6/2	5/2	2/5

[1]Equilibration attained after ca. 15 min irradiation at 365 nm, [2]Number of atoms from neighboring molecules within a threshold of 3 Å. The distances for these close contacts can be found in the SI.

The solid state spectra obtained from compound **3** (Figure 5) were similar to those of **2**. Before irradiation, the spectrum had a λ_{max} at 376 nm and a weak shoulder that extended to ca. 600 nm, which we tentatively assigned, respectively, to the *cis*-enol and the *cis*-keto forms. Exposure to UV light resulted in the growth of a new broad, vibrationally resolved absorption band between ca. 400-600 nm, with a 4.5-fold increase in absorbance from 0.060 to 0.270±0.002 at 525 nm (Figure 5). The lifetime for **3** was also fit to a biexponential function, with fast component of 405±2 s and a slow component of 1952±13 s. Solid samples of compound **4** showed a spectrum with a broad band between 275-450 nm and a λ_{max} at ca. 350 nm, and weaker broad band that extended from 450-600 nm. Notably, irradiation with UV light resulted in a very small growth of the latter with a change in absorbance by a factor of only 1.06, from 0.240 to 0.255±0.005. The lifetime for **4** was fit with a biexponential function, with a fast component having a lifetime of 1820±470 seconds and the slow component having a lifetime of 16470±1920 seconds. The long wavelength absorbance and small photochromic response, in the case of **4,** was likely the result of electron donation by the hydroxyl group.[26]

A potential correlation between crystal density, or number of close neighbors in the lattice and the magnitude of the photochromic response observed, was not evident. A clear distinction between compounds **2** and **3**, which had reasonably high responses, and compound **4**, which showed a very small variation, indicated the importance of electronic factors. It is worth noting that the lifetime of the *trans*-keto tautomers of compounds **2** and **3** were relatively short, as compared to those of

other structures, which was in agreement with a molecular design intended to facilitate the rotations of the hydroxyl-bearing aromatic group.[15c,27]

2.5. Solid-State ^{2}H NMR

In order to support the suggested role for molecular rotation on the solid state photochromism of salicylideneanlines (Figure 1), we analyzed the rotation of a model Schiff base prepared with aldehyde analog **9**, which lacked the *ortho*-hydroxyl group. Considering the relatively large photochromic response observed in the case of compound **3**, we prepared analog **10** with a deuterium-labeled aldimine ring (Scheme 3). We reasoned that removal of the hydroxyl group would likely result in a crystalline solid with a packing arrangement isomorphous to that of **3.** Gratifyingly, X-ray powder diffraction data corroborated this hypothesis (see SI), which allowed us to confirm that the shielding provided by the trityl framework would allow for the fast rotation of the aldimine. Without energetic contributions from the intramolecular hydrogen bond, we expected the rotational potential to be symmetric with equivalent sites related by 180° jumps. We selected a d_4-labeled aldimine derivative, because solid-state ^{2}H NMR is an ideal technique to probe the solid state dynamics of groups bearing C-D bonds.[28] Quadrupolar echo spectra acquired with static powdered samples as a function of temperature (ca. 100 mg) were expected to display changes in line shape that depended on the frequencies and trajectories of motion. In the case of 1,4-phenylene groups undergoing 180° rotations in crystalline environments, a very broad spectrum characteristic of static samples, known as a Pake pattern, could be obtained at sufficient low temperature.[29]

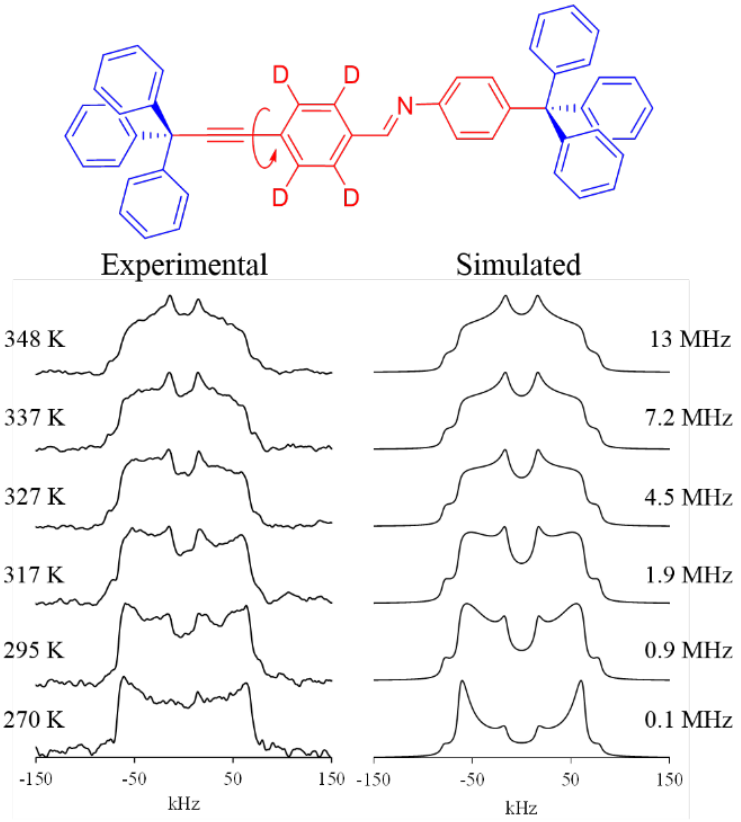

Figure 6. Experimental (left) and simulated (right) ^{2}H lineshapes of model compound **10**. The experimental data was obtained at the temperatures indicated and the simulated spectra were obtained with the program NMRweblab using the rotational exchange frequencies noted and the parameters listed in the text.

Changes in the spectral line shape occur in a predictable manner as a function of rotational exchange rates, as the temperature increases. In practice, the experimental spectrum is simulated using a suitable dynamic model that includes a set of parameters that are characteristic of the molecules of interest. Excellent simulation models developed by experts are currently available on the Internet.[30,31] In the case of deuterated phenylenes, we considered (1) a quadrupolar coupling constant QCC=180 kHz, (2) an asymmetry parameter η =0, (3) the number of sites along a symmetric potential, which, in this case, was n=2, (4) a value of $\alpha=60^o$ for the cone angle made by the rotating C-D bond vector and the rotational axis, and (5) the

frequency of exchange between sites.[28,29] Spectral changes displayed a relatively high sensitivity in the intermediate regime between ca. 10^4 and 10^8 Hz. Slow exchanging ($<10^4$ Hz) and static samples were characterized by symmetric spectrum with two intense peaks separated by ca. 130 kHz that were flanked by two outer shoulders that extended up to ca. 250 kHz.[28,29] By contrast, the spectrum observed for rotational exchange in the fast exchange limit ($>10^8$ s^{-1}) consisted of two peaks with a separation of only 32 Hz, tall shoulders that expanded a width of ca. 125 kHz, and a second set of small peaks separated by ca. 155 kHz. Intermediate rotation frequencies lead to spectra whose appearance was in between.

As illustrated in Figure 6, ^{2}H NMR spectra obtained in the temperature range between 270 K and 348 K displayed changes in line shape with the intensity of the outer peaks decreasing and that of the inner peaks increasing, as expected for rotational motion within the 10^4 to 10^7 Hz range. The general features of the spectra and the changes observed as a function of temperature above 295 K were reasonably matched with a simulation model that assumed a Log-Gaussian distribution of rotational frequencies, with a width σ =1.0 centered in the range of 1.2 to 10 MHz.[31,32] A Log-Gaussian distribution is indicative of a Gaussian distribution of activation energies,[32] which was consistent with the orientationally disordered nature of the sample. Notably, the spectrum obtained at 270 K was poorly matched by a simulation carried out with values extrapolated from the other five data points, and the frequency suggested should be considered as an upper limit. Although this disagreement may be due to the greater uncertainty of the data near the slow exchange regime, it may also arise from a temperature-dependent

potential energy surface related to the "softening" of the crystal within the corresponding temperature range.[33] Measurements at temperatures higher than 350 K did not cause significant changes in the spectra, indicating that rotation occurred with rates that were faster than the timescale of the ^{2}H NMR experiment (fast exchange regime).

Using the experimental temperatures and the mean exchange frequencies of the simulations, we were able to construct an Arrhenius plot to determine the approximate activation energy (Ea) and pre-exponential factor (A) (Figure 7). While a value of Ea = 11.2 kcal mol^{-1} was in line with our design and expectations for the phenylene rotation, a pre-exponential factor A= 1.5 $x10^{14}$ s^{-1} was greater than that expected for a phenylene rotator based on its moment of inertia.[17] Notably, computational analysis of a model (*E*)-*N*-benzylideneaniline carried out at the B3LYP and M06 levels of theory by rotation of the phenyl-aldimine sigma bond (Ph—C=N-), while the rest of the structure was allowed to minimize, suggested barriers to rotation of 8.43 and 8.76 kcal/mol, respectively. These values suggested that the experimental barrier in the case of **10** might be largely determined by molecular electronic factors, rather than by steric barriers in the crystal lattice. Thus, recognizing that aldimine **10** was isomorphous with SA **3**, it was reasonable to conclude that rotation of the oxygen-bearing ring should not be significantly inhibited by nearest neighbors.

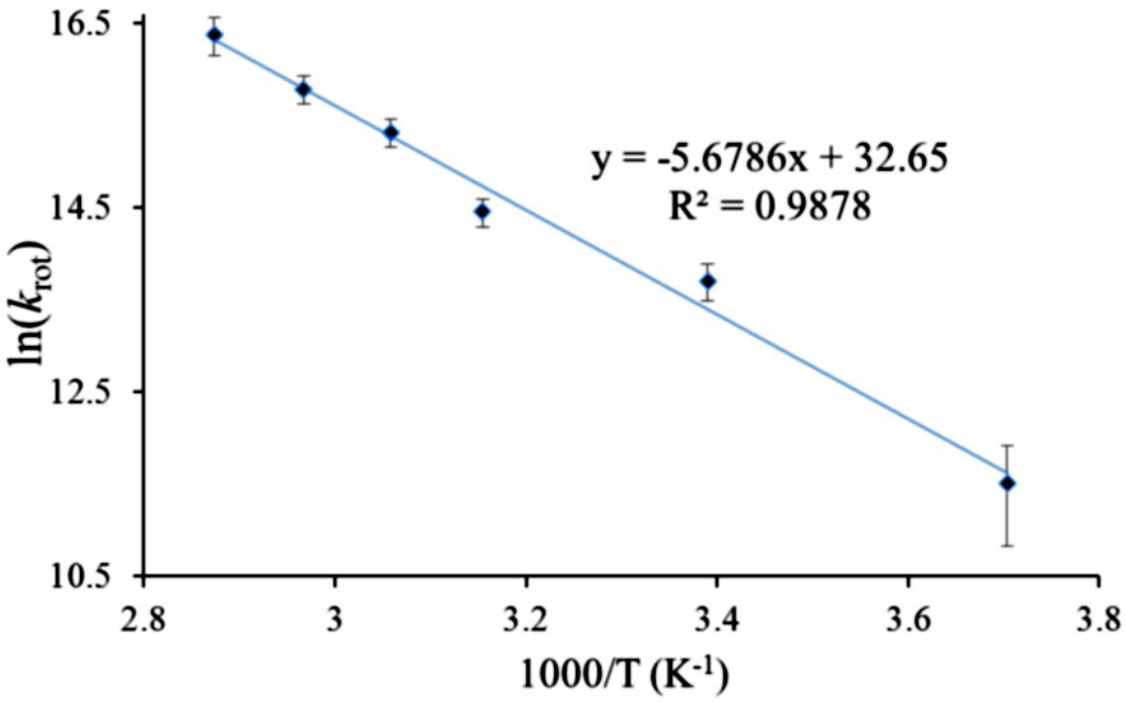

Figure 7. Arrhenius plot of **10** indicating a mean barrier to rotation of 11.2 kcal in the crystalline state.

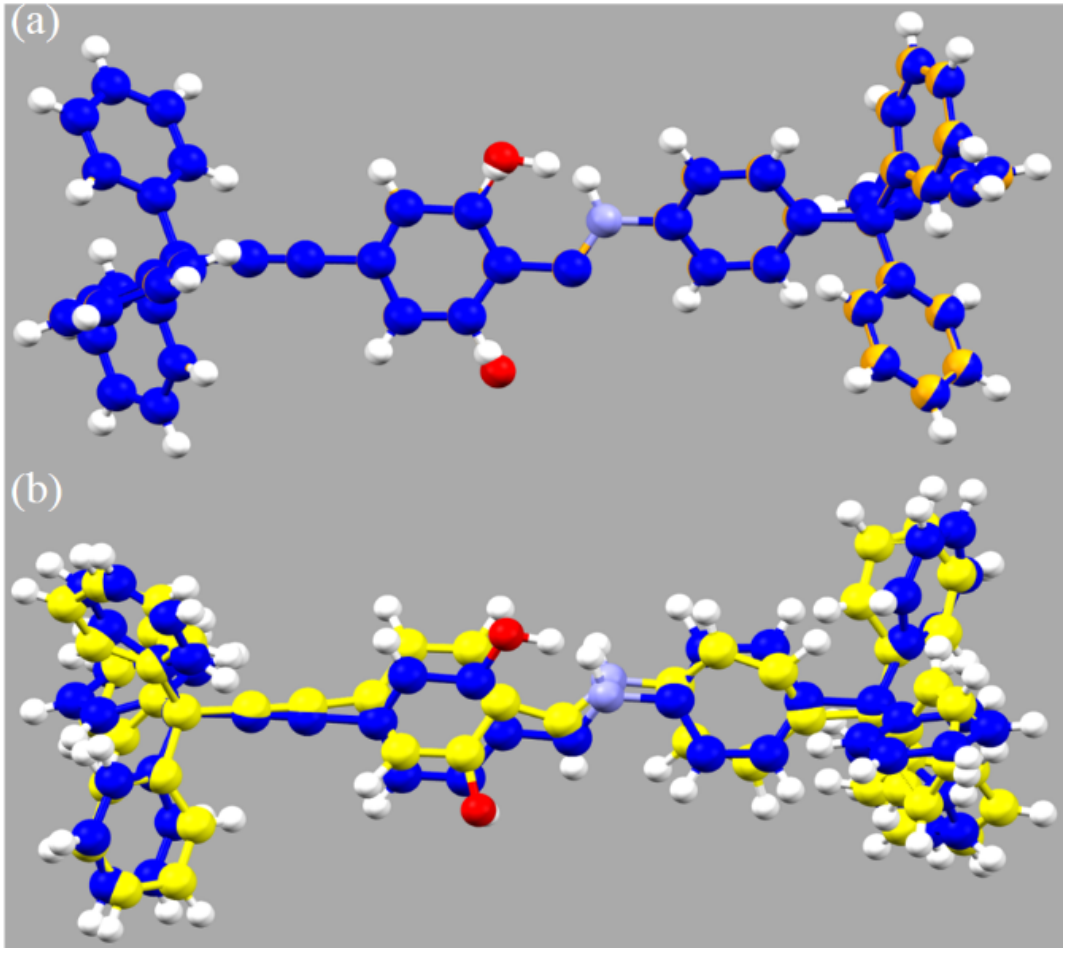

Figure 8. (a) Crystal structure of *cis*-enol **3** in blue superimposed on the *trans*-keto via 180° rotation in orange. (b) Crystal structure of cis-enol **3** in blue superimposed on the *trans*-keto via bicycle pedal functionalized to emulate **3** in yellow.

2.6. Reaction Cavity Analysis

Reactions in crystals require that the size and shape of the transition states, intermediates, and final products match those of the reaction cavity determined by the boundary formed by the nearest neighbors of the reactant.[34] The relative preference of two competing products can be determined by measuring the root mean square deviation (RMSD) of the best overlap between each of their structures and that of the reactant, which is a measure of how well they would fit in the

reaction cavity. Considering that the *trans*-keto forms in Figure 1, originating either from ring rotation or bicycle pedal motion, are actually different structures, we decided to analyze the RMSD of their best overlap with the structure of the *cis*-enol, as shown in Figure 8. The structure of the *trans*-keto form was modeled by simple rotation of the oxygen-bearing ring. In contrast, the structure corresponding to the bicycle pedal mechanism was modeled by taking the coordinates of the salicylideneaniline portion of the crystal data for the *trans*-keto form, which Harada *et al*. demonstrated could occur by this mechanism,[14a] and attaching the bulky trityl and tritylethynyl groups. It has been shown that bicycle pedal motion requires not only the reorientation of the central C=N double bond, but also a change in the direction of the two aromatic rings, which requires some motion of the trityl groups that are likely to act as anchors and prevent this motion. The RMSD[35] calculated for the ring rotation mechanism was only 3.3×10^{-5} and that for the bicycle pedal motion was 0.67. Both these values and inspection of Figure 8 indicated that the bicycle pedal mechanism required significantly greater structural changes and should be more demanding than the 2-fold ring flip, supporting the latter as the preferred mechanism.

2.7. Conclusions

In conclusion, we synthesized and fully characterized three molecular rotors with salicylideneaniline rotators encapsulated by bulky groups that generate a low density region for rotation of the oxygen-bearing aromatic group to rotate in the solid state. While all three SA molecular rotors generated the colored *trans*-keto tautomer upon irradiation with UV light, the extent of the photochromic reaction

was significantly larger for the simpler SA chromophores **2** and **3,** as compared to the *para*-hydroxy substituted chromophore in molecular rotor **4**, which highlighted the importance of electronic factors. In order to obtain evidence for a mechanism that involved the postulated ring rotation, we prepared and analyzed the rotational dynamics of molecular rotor **10**, an isotopically labeled deoxo-analog of **3** that crystallized in an isomorphous crystal stucture. Using ^{2}H NMR line shape analysis, we determined the ground state barrier for rotation of **10** to be 11.2 kcal/mol. Furthermore, a very small RMSD value for the best structural overlap between the starting *cis*-enol and the *trans*-keto form obtained by ring rotation suggested an allowed solid state reaction. The evidence presented, here, strongly supports the use of crystal-engineered ring rotation as an alternative to bicycle pedal motion to obtain photochromic salicylideneanilines.

2.8. APPENDIX

General Methods

IR spectra were obtained with a Perkin-Elmer spectrum 100 HATR FTIR instrument. ^{1}H and ^{13}C NMR spectra were acquired on a Brüker NMR spectrometer at 400 and 100 MHz or 300 and 75 MHz, respectively, with $CDCl_3$ as the solvent. NMR coupling constants were calculated using gNMR[36]. Mass spectra were acquired on an Applied Biosystems voyager-DE-STR MALDI-TOF. Solution UV-Vis measurements were taken on an Ocean Optics USB2000+ while solid-state diffuse reflectance measurements were taken on a UV-3101PC UV-Vis N/R Scanning Spectrophotometer. Samples for diffuse reflectance were placed on a barium sulfate plate and pressed. This was then irradiated using a Rayonet Photochemical Reactor with 6-12 inch 8W (BLE-8T365) 365nm bulbs. A Coherent 405 nm CUBE laser was used to excite the solid in a NMR tube at both room temperature and 77K, and the subsequent emission spectra were monitored using a Princeton Instruments Roper CCD detector, which was cooled to liquid nitrogen temperatures. The 4-Tritylaniline, 4-bromo-2-hydroxybenzaldehyde, 2.5 M *n*-butyllithium in hexanes, acetyl chloride, 0.5 M ethynylmagnesium bromide in THF, 4-bromoaniline, diisopropylamine, CuI, bis(triphenylphosphine) palladium (II) chloride, potassium carbonate, tetra-n-butylammonium fluoride, 1-bromohexane, dibromobenzene-d_4 were commercially available and were used without further purification. THF and benzene were distilled from sodium and kept under argon. Toluene was distilled from calcium hydride and kept under argon.

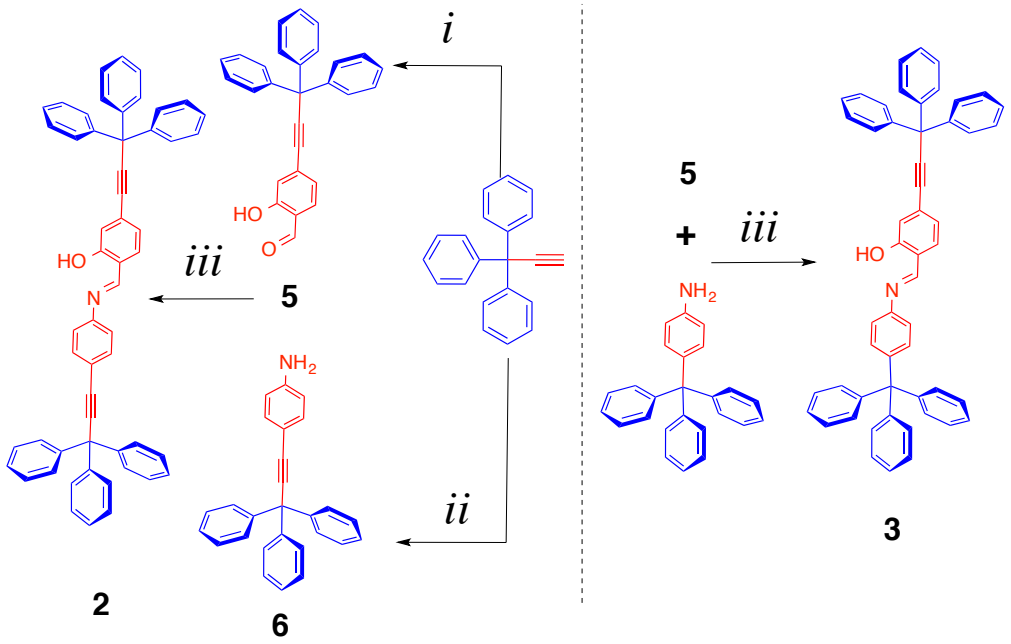

Reaction conditions: i. 4-bromo-2-hydroxybenzaldehyde, $Pd(PPh_3)_4$, CuI, diisopropylamine, benzene, reflux 8h. ii. 4-bromoaniline, $Pd(PPh_3)_4$, CuI, diisopropylamine, benzene, reflux 48h. iii. 4 Å molecular sieves, toluene, reflux 20h.

Synthesis of Salicylidine Aniline Rotor 2.

In a round bottom flask with a condenser adapted, under argon atmosphere, 150 mg of salicylaldehyde trityl alkyne **5** (0.13 mmol) powder were combined with 142 mg of aniline trityl alkyne **6** (0.14 mmol) powder. To the flask 4 A molecular sieves were added along with dry toluene (30 mL). The solution was then allowed to reflux 20 h. The reaction was worked up by filtering and then reduced under reduced pressure to yield a yellow solid. This was then purified by column chromatography using silica gel and hexanes/dichloromethane (4:1) to afford 198 mg (73 %) of **2** as a yellow solid m.p. 272 °C (decomposition). ^{1}H NMR ($CDCl_3$) δ: 13.21 (s, 1H), 8.60 (s, 1H), 7.56 (d, *J* = 8.5 Hz, 2H), 7.36–7.22 (m, 33H), 7.17 (d, *J* = 1.1 Hz, 1H), 7.07 (dd, *J* = 7.9, 1.2 Hz, 1H). ^{13}C NMR (CDCl3) δ: 161.8, 160.8, 147.7, 145.2, 145.0, 132.8, 132.1, 129.19, 129.18, 128.12, 128.1, 127.0, 126.9, 122.5, 122.4, 121.2,

120.2, 119.0, 98.6, 96.8, 84.8, 84.6, 56.2, 56.17. FTIR (powder, HATR, cm $^{-1}$): 3200-2400 (very broad), 3059, 2922, 2851, 2226, 1952, 1615, 1592, 1490, 1447, 1188. HRMS (ESI+, m/z) calculated for $C_{55}H_{40}NO$ = 730.3104, found 730.3132, error: 3.8 ppm.

Synthesis of the Salicylidine Aniline Rotor 3.

In a round bottom flask with a condenser adapted, under argon atmosphere, 95 mg of 4-Tritylaniline (0.28 mmol) powder were combined with 100 mg of salicylaldehyde trityl alkyne **5** (0.26 mmol) powder. To the flask 4 A molecular sieves were added along with dry toluene (30 mL). The solution was then allowed to reflux for 20 h. The reaction was worked up by filtering and then reduced under reduced pressure to yield a yellow solid. This was then purified by column chromatography using silica gel and hexanes/dichloromethane (4:1) to afford 161 mg (89 %) of **3** as a yellow solid m.p. 266 °C (decomposition). ^{1}H NMR (500 MHz, $CDCl_3$) δ 13.37 (s, 1H), 8.62 (s, 1H), 7.34−7.16 (m, 35H), 7.15 (d, J =1.5 Hz, 1H), 7.05 (dd, J =8.0 Hz, 1.5 Hz, 1H) : ^{13}C NMR (125 MHz, $CDCl_3$) δ: 161.5, 160.8, 146.6, 146.1, 145.8, 145.0, 132.2, 132.0, 131.1, 129.2, 128.1, 127.6, 127.0, 126.0, 122.3, 120.3, 120.2, 119.0, 98.4, 84.8, 64.8, 56.2. FTIR (powder, HATR, cm $^{-1}$): 3200-2400 (very broad), 3079, 3061, 3025, 2953, 2861, 1617, 1591, 1544, 1489, 1445, 1359, 1178. HRMS (LIFDI-TOF, m/z) calculated for $C_{53}H_{39}NO$ =705.3026, found 705.3022, error: -0.6 ppm.

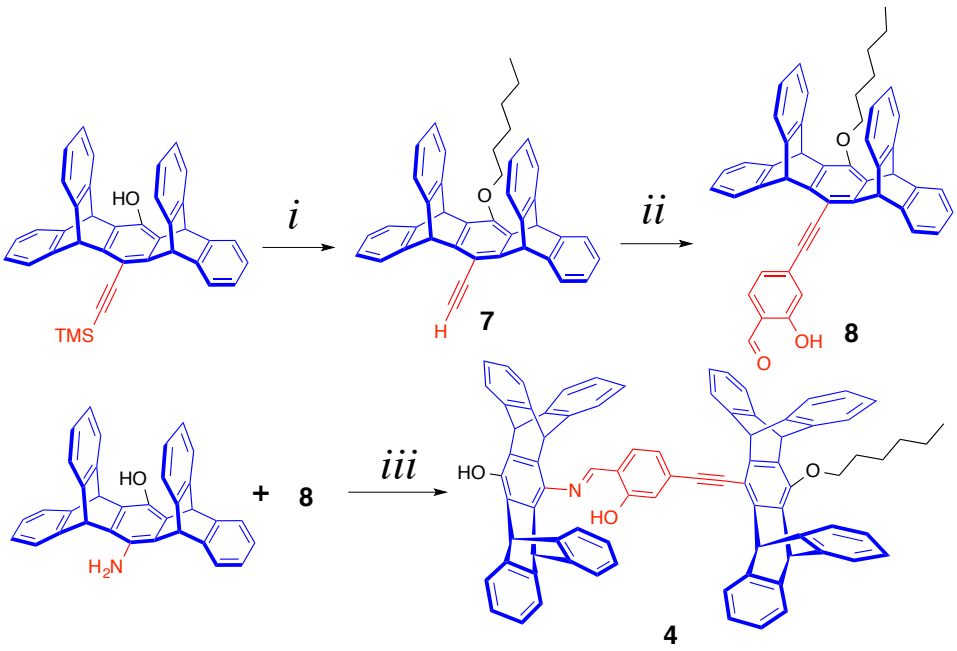

Reaction conditions: i. potassium carbonate, 1-bromohexane, dry acetone, reflux 12h. Followed by TBAF, THF at 50^{0}C for 0.5h. *ii.* 4-bromo-2-hydroxybenzaldehyde, $Pd(PPh_3)_4$, CuI, diisopropylamine, benzene, reflux 48h. *iii.* 4 Å molecular sieves, toluene, reflux 20h.

Synthesis of the Pentiptycene Salicylidine Aniline Rotor 4.

In a round bottom flask with a condenser adapted, under argon atmosphere, 94 mg of p-hydroxy pentiptycene amine (0.21 mmol) powder were combined with 125 mg of salicylaldehyde hexyl pentiptycene alkyne **8** (0.19 mmol) powder. To the flask 4 A molecular sieves were added along with dry toluene (30 mL). The solution was then allowed to reflux 20 h. The reaction was worked up by filtering and then reduced under reduced pressure to yield a yellow solid. This was then purified by column chromatography using silica gel and hexanes/dichloromethane (6:1) to afford 153 mg (74 %) of **4** as a yellow solid m.p. 360 °C (decomposition) .^{1}H NMR (500 MHz, $CDCl_3$) δ 13.70 (s, 1H), 8.56 (s, 1H), 7.66 (d, *J* = 8.0 Hz, 1H), 7.65 (d, *J* = 1.5 Hz, 1H), 7.51 (dd, *J* = 8.0, 1.5 Hz, 1H), 7.46 (ddd, *J* = 7.2, 1.2, 0.6 Hz, 4H), 7.40 (ddd, *J* =

7.2, 1.2, 0.6 Hz, 4H), 7.37 (ddd, *J* = 7.2, 1.2, 0.6 Hz, 4H), 7.35 (ddd, *J* = 7.2, 1.2, 0.6 Hz, 4H), 7.02 (ddd, *J* = 7.6, 7.2, 1.2 Hz, 4H), 7.00 (ddd, *J* = 7.6, 7.2, 1.2 Hz, 8H), 6.99 (ddd, *J* = 7.6, 7.2, 1.2 Hz, 4H), 5.94 (s, 2H), 5.75 (s, 2H), 5.74 (s, 2H), 5.62 (s, 2H), 4.01 (t, *J* = 7.0 Hz, 2H), 2.05 (app. p, *J* = 7.9 Hz, 2H), 1.71 (app. p, *J* = 7.9 Hz, 2H), 1.57–1.47 (m, 4H), 1.05 (t, *J* = 7 Hz, 3H): ^{13}C NMR (125 MHz, $CDCl_3$) δ: 167.3, 161.4, 150.2, 146.3, 145.12, 145.08, 145.03, 145.0, 143.5, 135.7, 135.6, 135.5, 132.5, 130.4, 128.8, 125.4, 125.39, 125.36, 125.34, 124.0, 123.7, 123.5, 122.8, 120.5, 119.1, 110.5, 94.5, 88.2, 76.2, 52.6, 49.5, 48.3, 47.5, 31.9, 30.6, 26.1, 22.8, 14.2. FTIR (powder, HATR, cm $^{-1}$): 3600-3100 (broad), 3100-2400 (very broad), 3294, 3067, 3019, 2929, 1940, 1724, 1708, 1600, 1457.55, 1299, 1253, 1198, 1109. HRMS (ESI+, m/*z*) calculated for $C_{83}H_{60}NO_3$ = 1118.4568, found 1118.4608, error: 3.6 ppm.

Synthesis of Salicylaldehyde Trityl Alkyne 5.

In a two-neck round bottom flask with an condenser adapted, 220 mg of 3,3,3-tris(phenyl)-1-propyne (0.82 mmol) powder were mixed with 150 mg of 4-bromo-2-hydroxybenzaldehyde (0.74 mmol) powder, 52 mg of $PdCl_2(PPh_3)_2$ (0.07 mmol) powder and 28 mg of CuI (0.15 mmol) powder under argon atmosphere. In a separate two-neck round bottom flask, 8 mL of THF and 2 mL of diisopropylamine were previously degassed with argon (45 min) and this mixture was transferred into the previous flask. The resulting mixture was refluxed 8 h. The reaction was quenched with a saturated solution of ammonium chloride, and the organic phase was extracted with dichloromethane. The combined organic layers were dried over Na_2SO_4 and the mixture was purified by column chromatography using silica gel and hexanes/EtOAc (93:7) to afford 240 mg (75.5 %) of compound **5** as a pale white

solid m.p. 153-154 °C. ^{1}H NMR (500 MHz, $CDCl_3$) δ 11.04 (s, 1H), 9.88 (s, 1H), 7.50 (d, *J* = 8.5 Hz, 1H), 7.36–7.25 (m, 15H), 7.14 (s, 1H), 7.14 (d, *J* =6.0 Hz, 1H) : ^{13}C NMR (125 MHz, $CDCl_3$) δ: 195.8, 161.3, 144.7, 133.4, 132.2, 129.14, 129.09, 128.13, 128.08, 127.1, 123.1, 120.5, 120.0, 100.6, 84.2, 56.2. FTIR (powder, HATR, cm $^{-1}$): 3650, 3575, 2225, 1903, 1651, 1621, 1490, 1444. HRMS (ESI+, m/*z*) calculated for $C_{28}H_{19}O_2$ = 389.1536, found 389.1538, error: 0.5 ppm.

Synthesis of Aniline Trityl Alkyne 6.

In a two-neck round bottom flask with a condenser adapted, 501 mg of 3,3,3-tris(phenyl)-1-propyne (1.86 mmol) powder were mixed with 384 mg of 4-bromoaniline (2.23 mmol) powder, 64 mg of $Pd(PPh_3)_4$ (0.05 mmol) powder and 10 mg of CuI (0.05 mmol) powder under argon atmosphere. In a separate two-neck round bottom flask, 35 mL of benzene and 12 mL of diisopropylamine were previously degassed with argon (45 min) and this mixture was transferred into the previous flask. The resulting brown solution turned black after 48 h reflux. The reaction was quenched with a saturated solution of ammonium chloride, and the organic phase was extracted with EtOAc (2 x 25 mL). The combined organic layers were dried over Na_2SO_4 and the mixture was purified by column chromatography using silica gel and hexanes/EtOAc (97:3) to afford 235 mg (35 %) of compound **6** as a pale yellow solid m.p. 168-169 °C. ^{1}H NMR (500 MHz, $CDCl_3$) δ 7.35–7.22 (m, 17H), 7.14 (s, 1H), 6.61 (d, *J* =8.5 Hz, 2H), 3.76 (s, 1H): ^{13}C NMR (125 MHz, $CDCl_3$) δ: 146.4, 145.7, 132.8, 129.2, 127.9, 126.7, 114.7, 113.1, 93.3, 85.5, 56.0. FTIR (powder, HATR, cm $^{-1}$): 3475, 3378, 2212, 1887, 1616, 1603, 1514, 1489, 1443. HRMS (ESI+, m/*z*) calculated for $C_{27}H_{21}NH$ = 360.1752, found 360.1747, error: 1.4 ppm.

Synthesis of Hexyl Pentiptycene Alkyne 7.

In a round bottom flask, TMS-protected pentiptycene (0.250 g, 0.460 mmol) powder was dissolved in dry acetone (10 mL) with potassium carbonate (0.076 g, 0.552 mmol) powder was stirred 10 min. Then, 1-bromohexane (0.19 mL, 1.38 mmol) was added via syringe. The mixture was stirred 12 h at 50 °C, and the potassium carbonate was then removed through filtration. The acetone in the filtered solution was evaporated and the resulting brown solid was redissolved with dry THF (10 mL). The brownish solution was warmed up at 50 °C before TBAF (0.69 mL, 0.691 mmol) was added. Upon addition, the mixture turned yellowish and the stirring continued 0.5 h. The mixture was cooled down to room temperature, worked up with ammonium chloride saturated solution and the organic layer was extracted with dichloromethane (2 x 20 mL). The combined organic layers were dried over sodium sulfate and the residue was purified by silica gel column chromatography using hexanes/ethyl acetate (97:3) as eluent, to afford 221 mg of **7** as a white powder (isolated yield: 86% over two steps) m.p. 278^{0}C (decomposition). ^{1}H NMR (500 MHz, $CDCl_3$) ^{1}H NMR (500 MHz, $CDCl_3$) δ 7.39 (ddd, *J* = 5.16, 3.30, 1.05 Hz, 4H), 7.34 (d, *J* = 5.22, 3.46, 1.05 Hz, 4H), 6.97 (ddd, *J* = 5.07, 5.10, 3.46, 4H), 6.95 (ddd, *J*= 5.06, 5.11, 3.32), 5.86 (s, 2H), 5.70 (s, 2H), 3.97 (t, *J* = 7.0 Hz, 2H), 3.61 (s, 1H), 2.05 (app. p, *J* = 7.9 Hz, 2H), 1.71 (app. p, *J* = 7.9 Hz, 2H), 1.57−1.47 (m, 4H), 1.05 (t, *J* = 7 Hz, 3H): ^{13}C NMR (125 MHz, $CDCl_3$) δ: 150.0, 146.6, 145.2, 145.0, 135.4, 125.3, 124.0, 123.5, 109.8, 82.6, 79.4, 76.1, 52.2, 48.2, 31.8, 30.5, 26.1, 22.8, 14.2. FTIR (powder, HATR, cm $^{-1}$): 3300, 3068, 3020, 2971, 2930, 2856, 2303, 1583, 1457, 1390, 1301,

1258. 1443. HRMS (ESI+, m/*z*) calculated for $C_{42}H_{34}O$ = 555.26879, found 555.26841, error: 0.6 ppm.

Synthesis of Salicylaldehyde Hexyl Pentiptycene Alkyne 8.

In a two-neck round bottom flask with an condenser adapted, 117 mg of **7** (0.21 mmol) powder were mixed with 46 mg of 4-bromo-2-hydroxybenzaldehyde (0.23 mmol), 0.007 mg of $PdCl_2(PPh_3)_2$ (0.01 mmol) powder and 0.002 mg of CuI (0.01 mmol) powder under argon atmosphere. In a separate two-neck round bottom flask, 15 mL of THF and 1 mL of diisopropylamine were previously degassed with argon (45 min) and this mixture was transferred into the previous flask. The resulting mixture was refluxed 20 h. The reaction was quenched with saturated solution of ammonium chloride, and the organic phase was extracted with dichloromethane. The combined organic layers were dried over Na_2SO_4 and the mixture was purified by column chromatography using silica gel and hexanes/EtOAc (9:1) 112 mg (79%) of compound **8** as a pale white solid m.p 300 °C (decomposition) ^{1}H NMR (500 MHz, $CDCl_3$) δ 11.23 (s, 1H), 10.00 (s, 1H), 7.69 (d, *J* = 7.5 Hz, 1H), 7.42–7.39 (m, 2H), 7.39 (ddd, 7.2, 1.2, 0.6 Hz, 4H), 7.33 (ddd, 7.2, 1.2, 0.6 Hz, 4H), 6.97 (ddd, 7.6, 7.2, 1.2 Hz, 8H), 5.83 (s, 2H), 5.70 (s, 2H), 3.98 (t, 6.5 Hz, 2H), 2.00 (app. p, 6.5 Hz, 2H), 1.67 (app. p, 8.0 Hz, 2H), 1.01 (t, 7.0 Hz, 3H).^{13}C NMR (125 MHz, $CDCl_3$) δ: 195.8, 161.6, 150.5, 146.4, 145.0, 144.9, 135.7, 133.7, 132.4, 125.4, 125.3, 124.0, 123.5, 123.1, 120.4, 120.2, 109.9, 93.8, 89.9, 76.2, 52.5, 48.3, 31.8, 30.5, 26.0, 22.8, 14.2. FTIR (powder, HATR, cm $^{-1}$): 2920, 2851, 2211, 1653, 1621, 1557, 1503, 1457, 1390, 1321, 1301, 1276, 1257, 1230. HRMS (ESI+, m/*z*) calculated for $C_{49}H_{39}O_3$ = 675.2894, found 675.2913, error: 2.9 ppm.

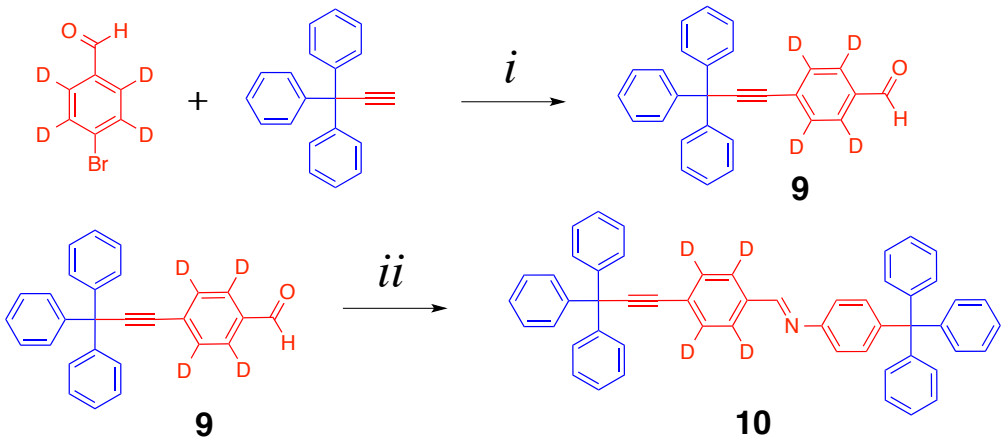

Reaction conditions: i. 4-bromo-2-hydroxybenzaldehyde, $Pd(PPh_3)_4$, CuI, diisopropylamine, benzene, reflux 8h. ii. 4 Å molecular sieves, toluene, reflux 20h.

Synthesis of d_4-Benzaldehyde Trityl Alkyne 9.

In a three-neck round bottom flask, 0.240 g of dibromobenzene-d_4 (1.0 mmol) were dissolved in 8 mL of dry THF and the solution was cooled down to -78°C using a dry ice/acetone bath. After stirring 10 min, 0.49 mL of *n*-BuLi (1.2 mmol, 2.42 M in hexanes) were added dropwise using a syringe. The mixture was stirred at -78°C for 2 h. Afterwards, 0.15 mL of dry DMF (2 mmol) were added dropwise and the mixture was stirred 12 h at room temperature. The reaction mixture was then treated with 10 mL of HCl (1 M) and diluted with brine. The desired compound was extracted using methylene chloride (2 x 25 mL) and the organic layers were combined and dried over Na_2SO_4. The resulting crude was carried on the next reaction without further purification. In a three-neck round bottom flask, 0.805 g of 3,3,3-triphenyl-1-propyne (3 mmol), and recently synthesized 4-bromobenzaldehyde-d_4 (189 mg, 1 mmol) were dissolved in 10 mL of dry THF and bubbled with N_2 for 45 min. In a second round bottom flask, $PdCl_2(PPh_3)_2$ (70 mg, 0.1 mmol), CuI (9 mg, 0.05 mmol) and 2 mL of diisopropylamine were mixed with

10 mL of dry THF and also bubbled with N_2 for 45 min. After degassing, the yellow mixture of the flask containing the catalyst and co-catalyst was transferred to the first flask by using a cannula. The resulting mixture was refluxed 8 h under inert atmosphere and quenched with saturated solution of NH_4Cl. The organic compounds were extracted with diethyl ether (2 x 30 mL) and the organic layers were combined and dried over Na_2SO_4. After rotary evaporation of the solvent, the brownish residue was purified by column chromatography using hexanes/ethyl acetate (9:1) as the eluent to afford 106 mg (28 % over two steps) of a white solid. After ^{1}H NMR, This was then purified by column chromatography using silica gel and hexanes/EtOAc (9:1). ^{1} m.p. 154-156 °C H NMR ($CDCl_3$) δ: 10.01 (s, 1H), 7.33-7.25 (m, 15H). ^{13}C NMR (CDCl3) δ: 191.5, 144.8, 135.2, 131.8 (t, 27.7 Hz), 129.7, 129.1, 128.2, 127.1, 100.1, 84.3, 56.3. FTIR (powder, HATR, cm $^{-1}$): 3060, 3020, 2956, 2925, 2826, 2736, 2221, 1690, 1571, 1490, 1448, 1322, 1287, 1236. HRMS (ESI+, m/*z*) calculated for $C_{28}H_{16}D_4O$ = 377.1838, found 377.1825, error: -3.39 ppm.

Synthesis of d_4-Imine Full Rotor 10. (Analog of 3)

In a round bottom flask with a condenser adapted, under argon atmosphere, 78 mg of 4-Tritylaniline (.234 mmol) were combined with 80 mg of **9** (.21 mmol). To the flask 4 A molecular sieves were added along with dry toluene (20 mL). The solution was then allowed to reflux 20 h. The reaction was worked up by filtering and then reduced under reduced pressure to yield a yellow solid 91 mg (62%) m.p. 268-270 °C. ^{1}H NMR ($CDCl_3$) δ: 8.47 (s, 1H), 7.33-7.31(m, 12H), 7.30-7.27 (m, 5H), 7.25-7.20 (m, 15H) 7.11 (d, *J* = 8.5 Hz, 2H). ^{13}C NMR (CDCl3) δ: 159.2, 149.4, 146.8, 145.1, 144.9, 144.4, 135.6, 132.0, 131.6, 131.4, 131.2, 129.2, 128.4, 128.1, 127.5, 127.1,

127.0, 126.3, 126.0, 120.0, 98.3, 84.8, 64.7, 56.2. FTIR (powder, HATR, cm^{-1}): 3030, 2952, 2857, 1622, 1596, 1570, 1490, 1445, 1326, 1033. Mass calculated for $[C_{53}H_{35}D_4N+H]^+$ 694.3406, found 694.3389, error: -2.45 ppm.

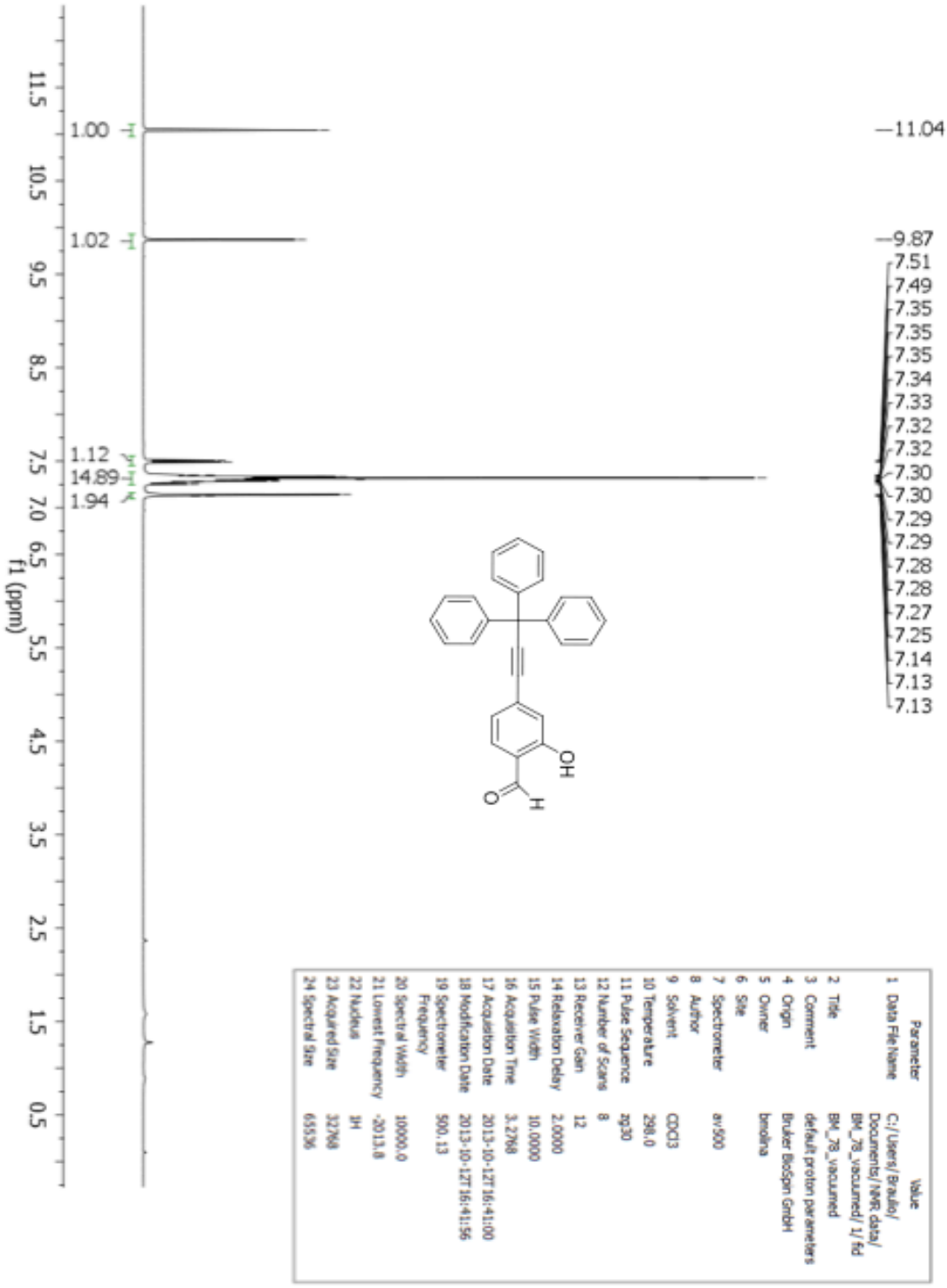

Figure S1. ^{1}H NMR of **Salicylaldehyde Trityl Alkyne 5**
500 MHz ^{1}H NMR spectrum of compound **5** in $CDCl_3$

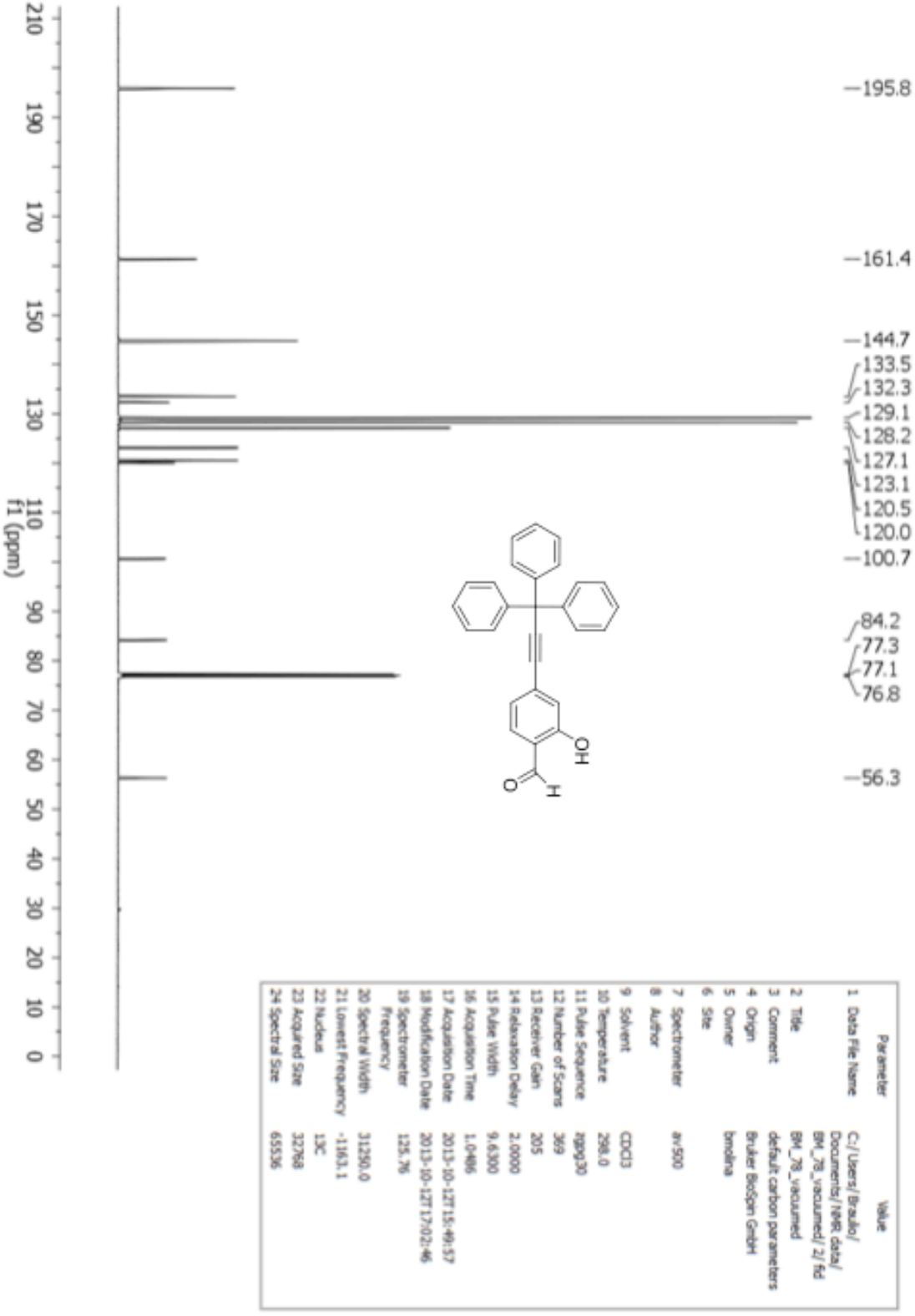

Figure S2. ^{13}C NMR of the **Salicylaldehyde Trityl Alkyne 5**
125 MHz ^{13}C NMR spectrum of compound **5** in $CDCl_3$

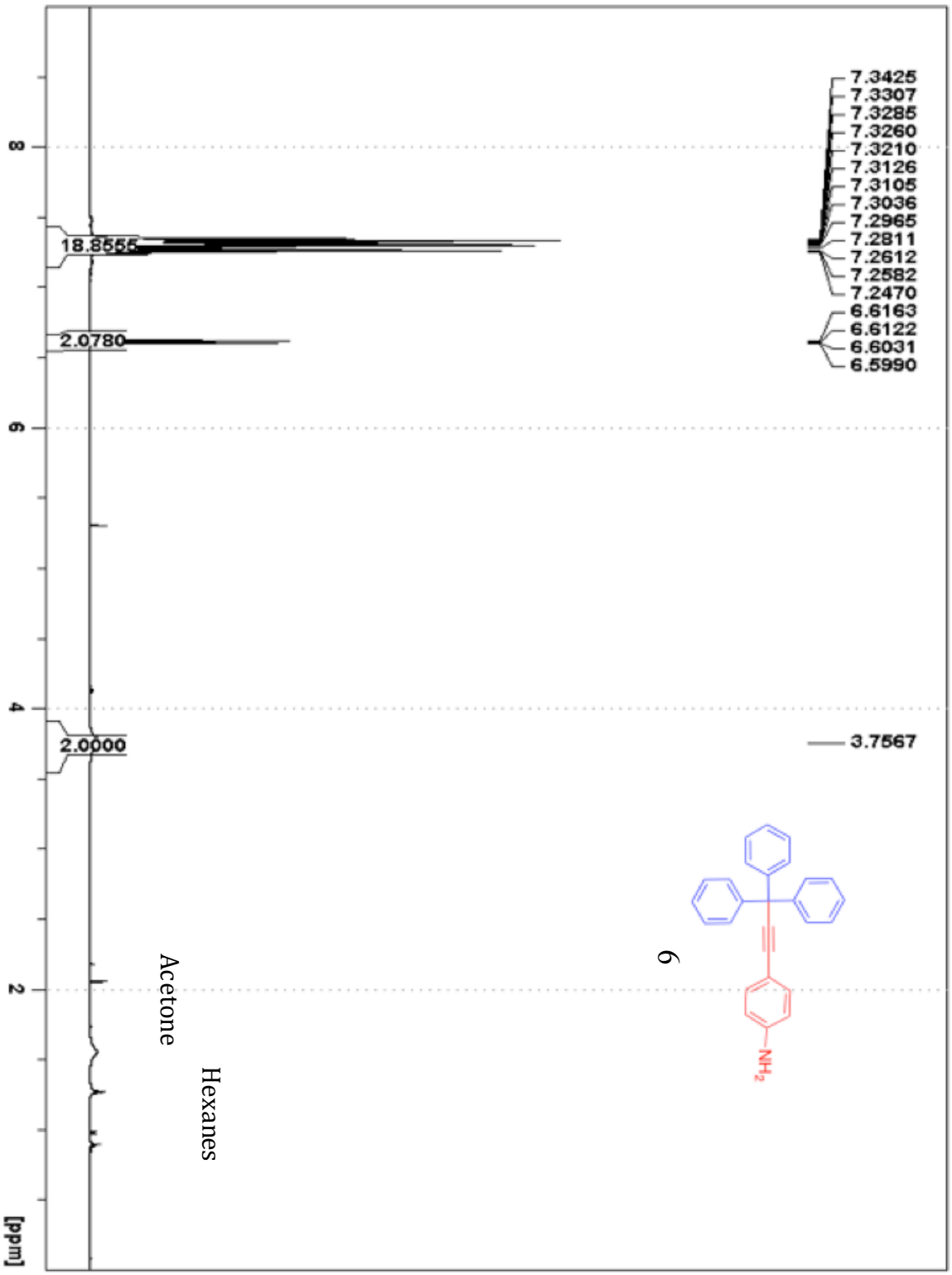

Figure S3. ^{1}H NMR of **Aniline Trityl Alkyne 6**
400 MHz ^{1}H NMR spectrum of compound **6** in $CDCl_3$

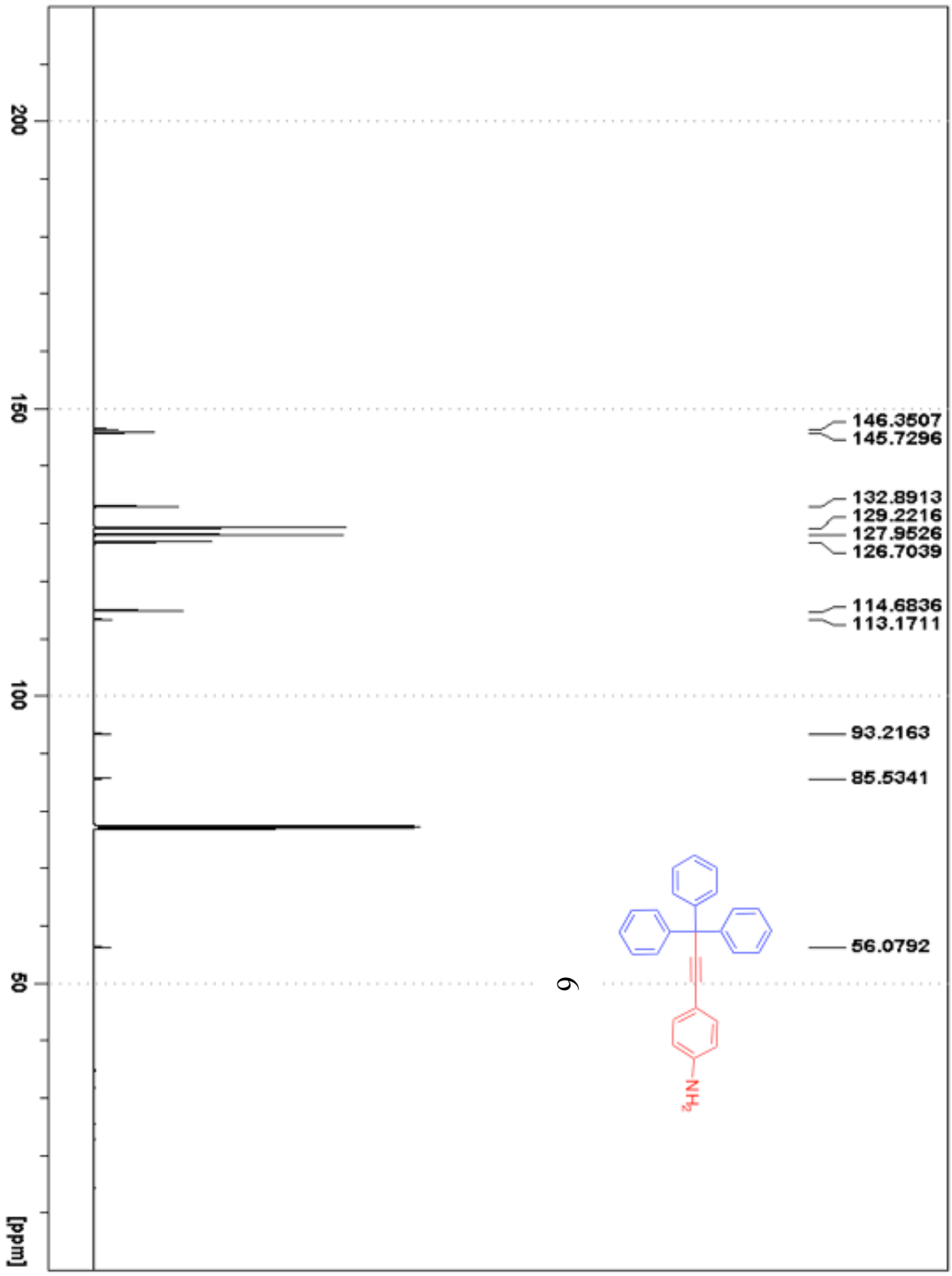

Figure S4. ^{13}C NMR of **Aniline Trityl Alkyne 6**
100 MHz ^{13}C NMR spectrum of compound **6** in $CDCl_3$

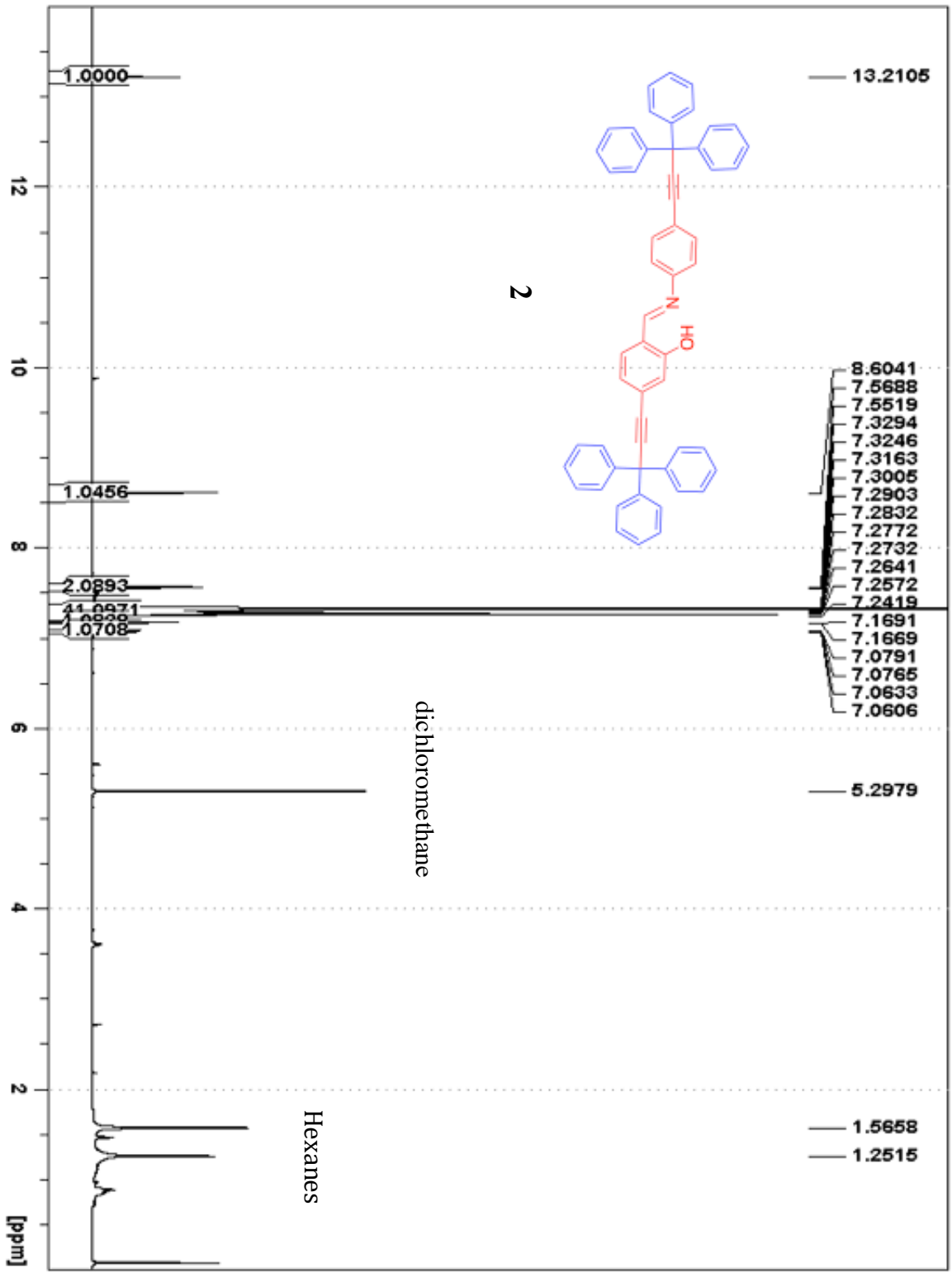

Figure S5. ^{1}H NMR of Salicylidine Aniline Rotor **2**
400 MHz ^{1}H NMR spectrum of compound **2** in $CDCl_3$

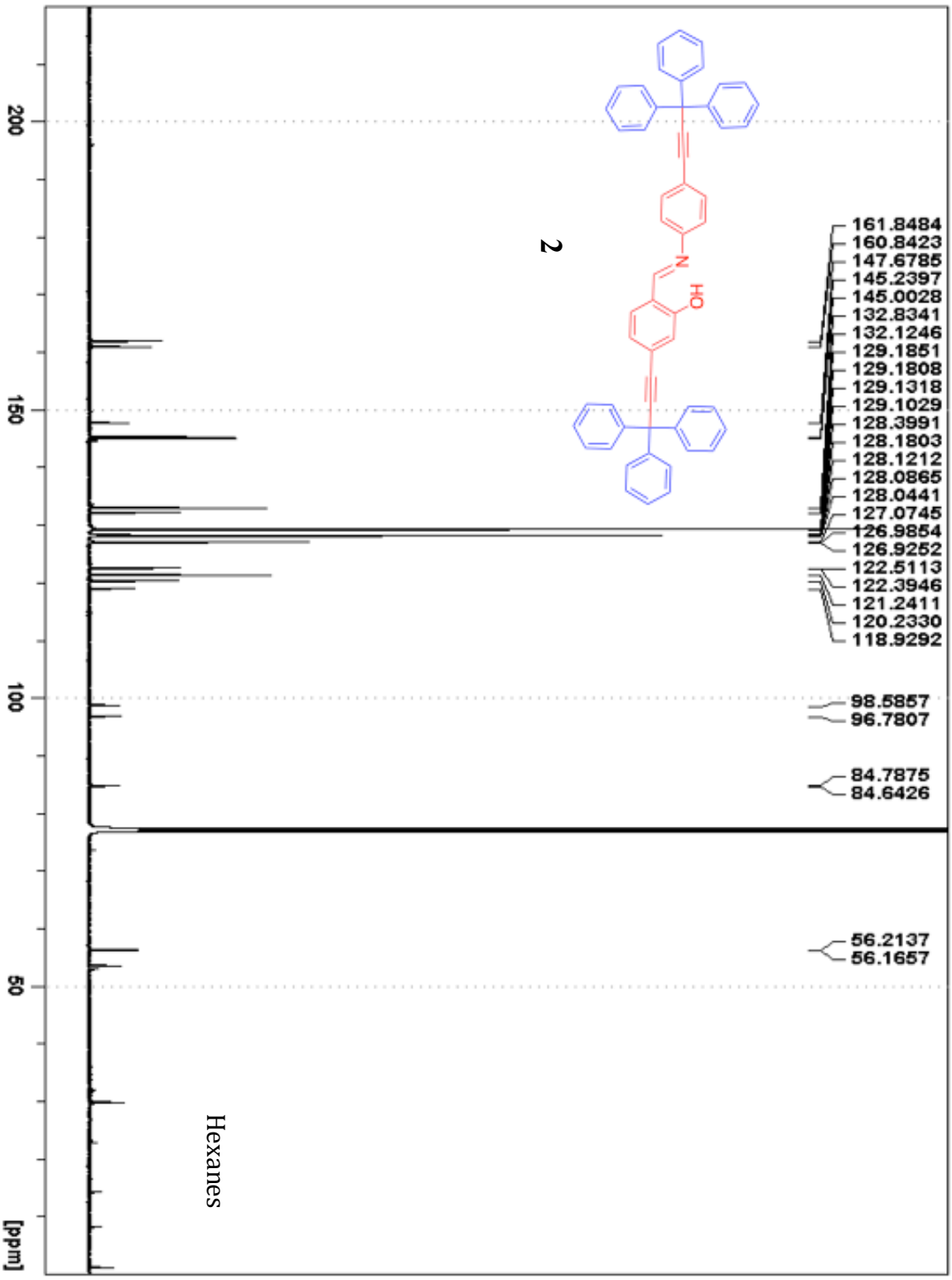

Figure S6. ^{13}C NMR of Salicylidine Aniline Rotor **2**
100 MHz ^{13}C NMR spectrum of compound **2** in $CDCl_3$

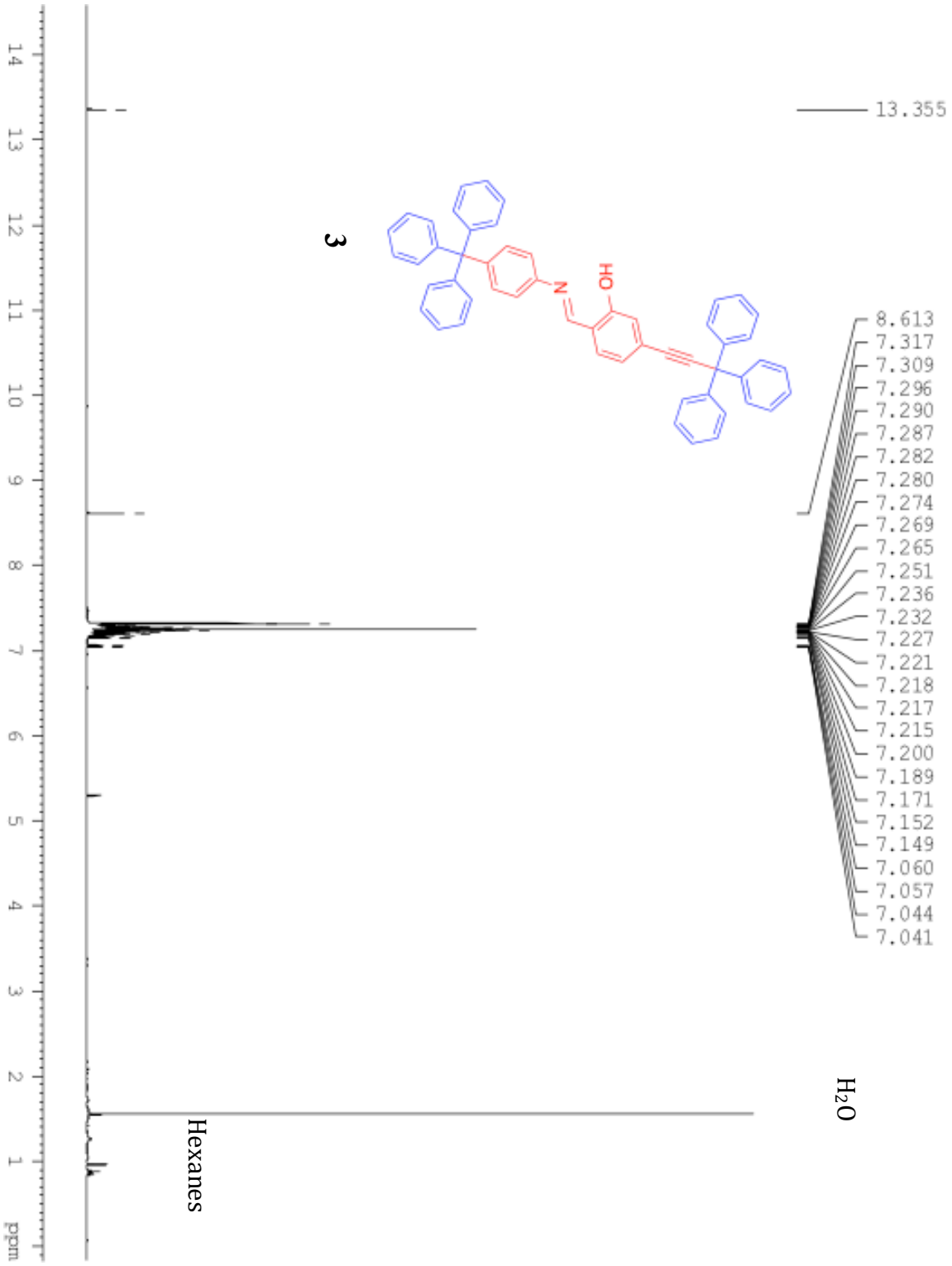

Figure S7. ^{1}H NMR of Salicylidine Aniline Rotor **3**
400 MHz ^{1}H NMR spectrum of compound **3** in $CDCl_3$

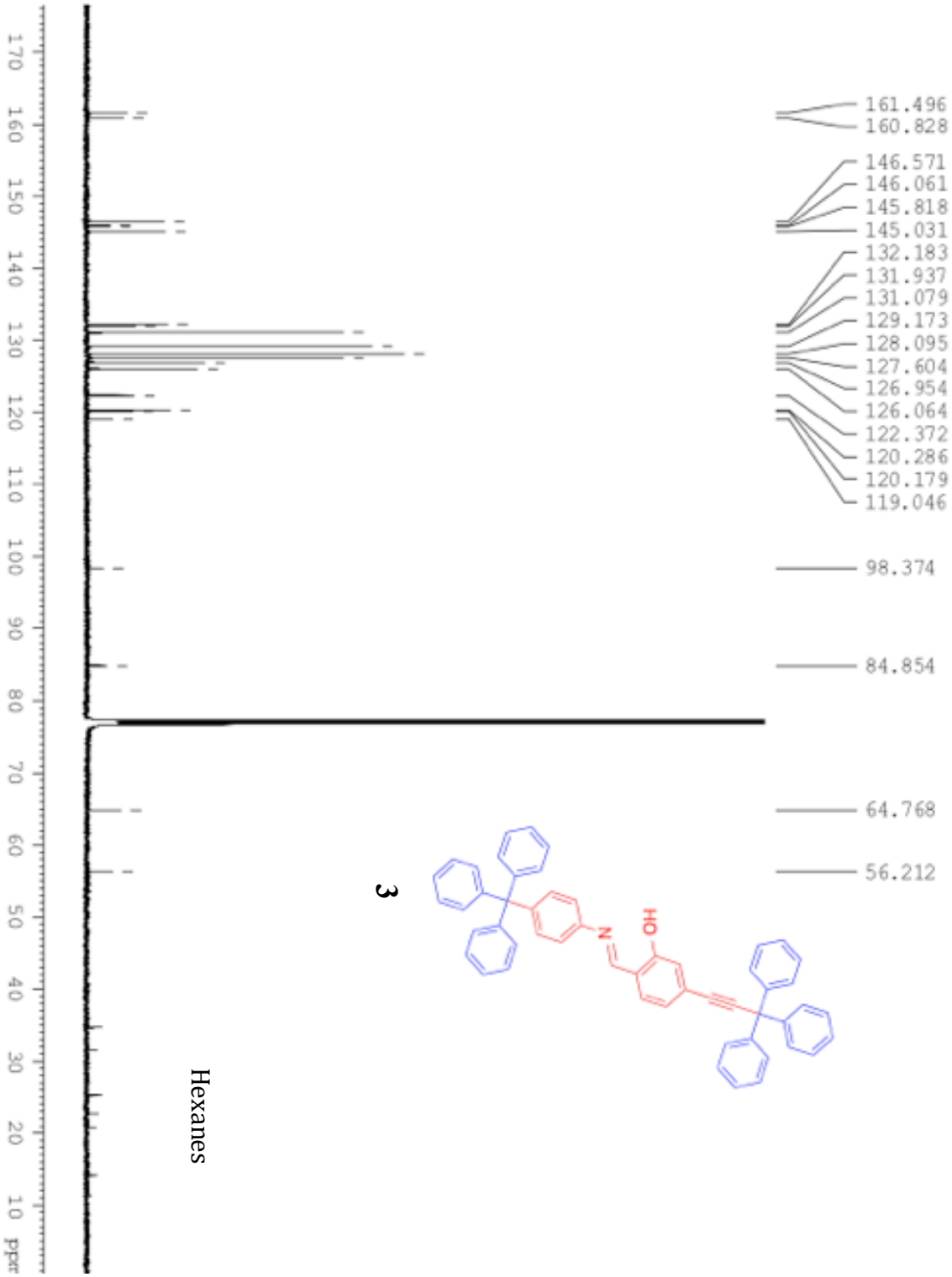

Figure S8. ^{13}C NMR of Salicylidine Aniline Rotor **3**
100 MHz ^{13}C NMR spectrum of compound **3** in $CDCl_3$

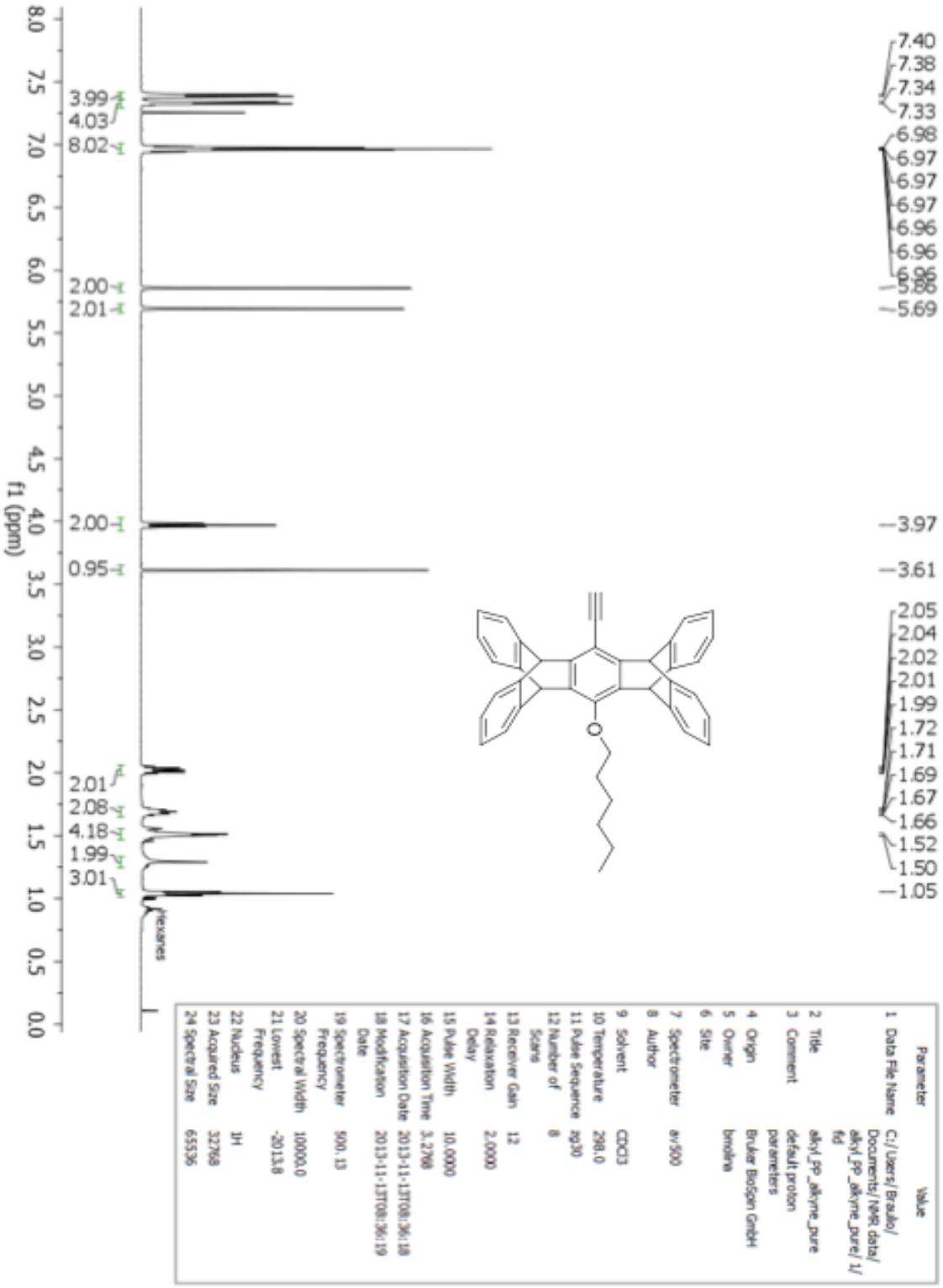

Figure S9. ^{1}H NMR of Hexyl Pentiptycene Alkyne **7**
500 MHz ^{1}H NMR spectrum of compound **7** in $CDCl_3$

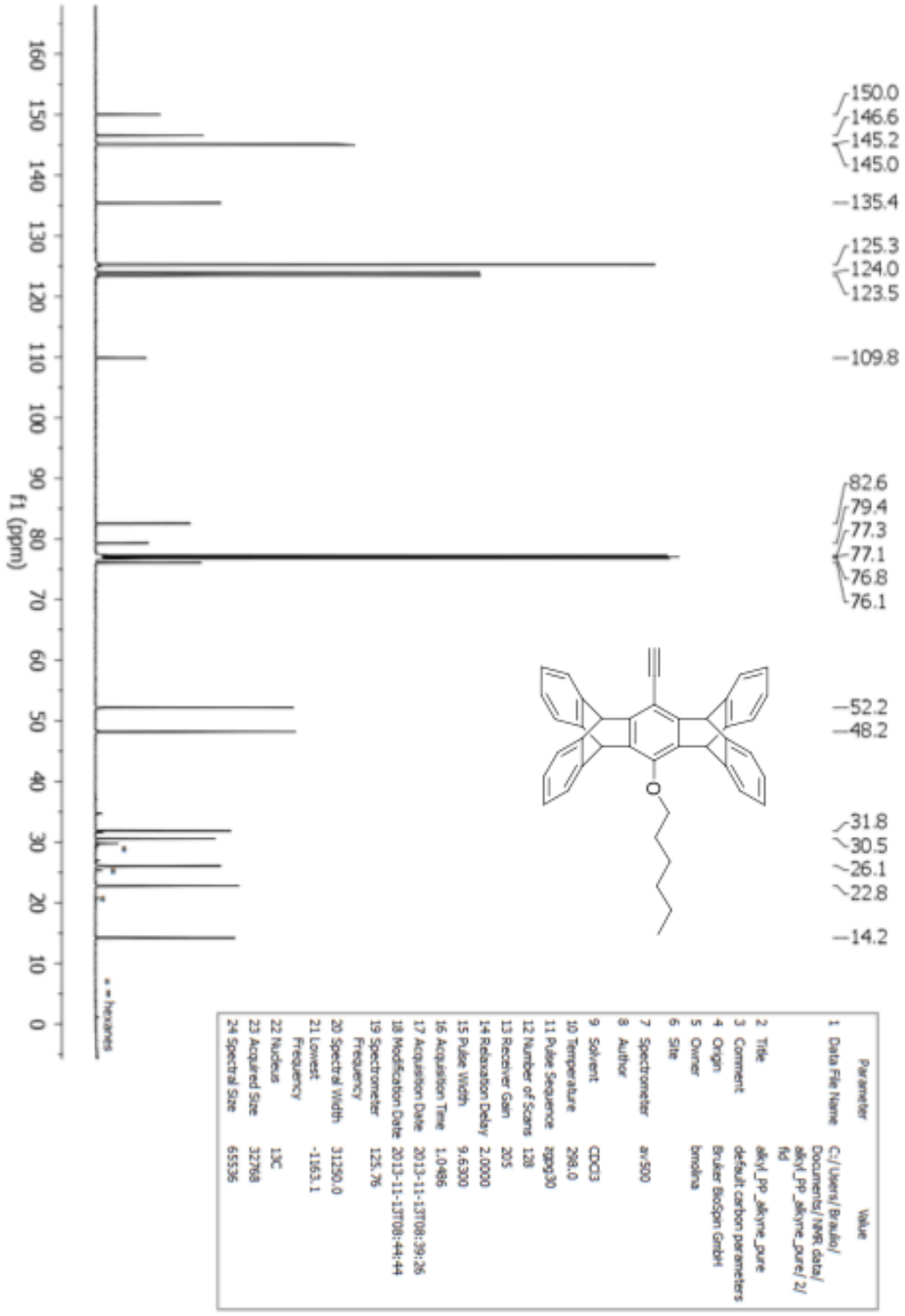

Figure S10. ^{13}C NMR of Hexyl Pentiptycene Alkyne **7**
125 MHz ^{13}C NMR spectrum of compound **7** in $CDCl_3$

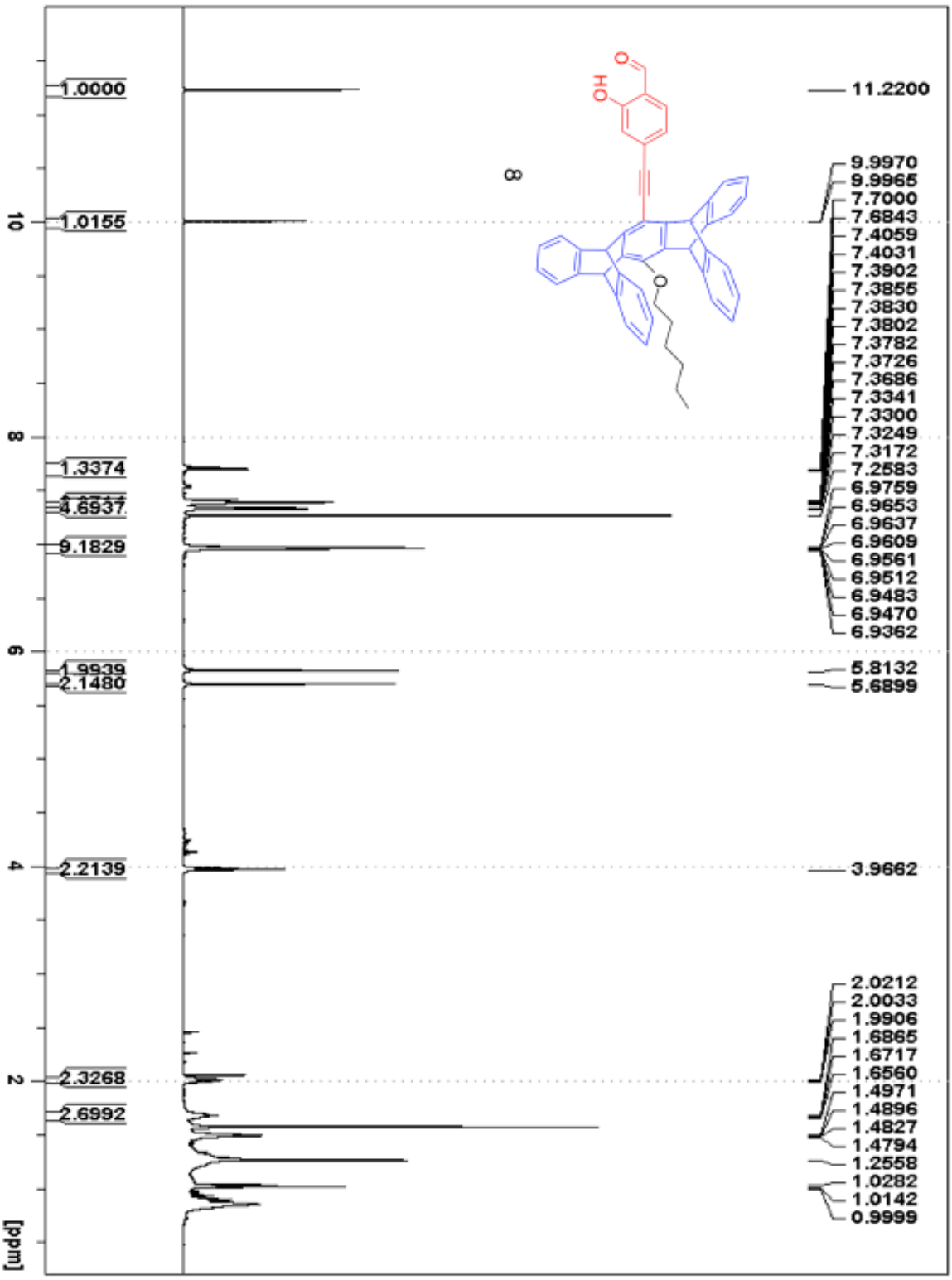

Figure S11. ^{1}H NMR of Salicylaldehyde Hexyl Pentiptycene Alkyne **8**
400 MHz ^{1}H NMR spectrum of compound **8** in $CDCl_3$

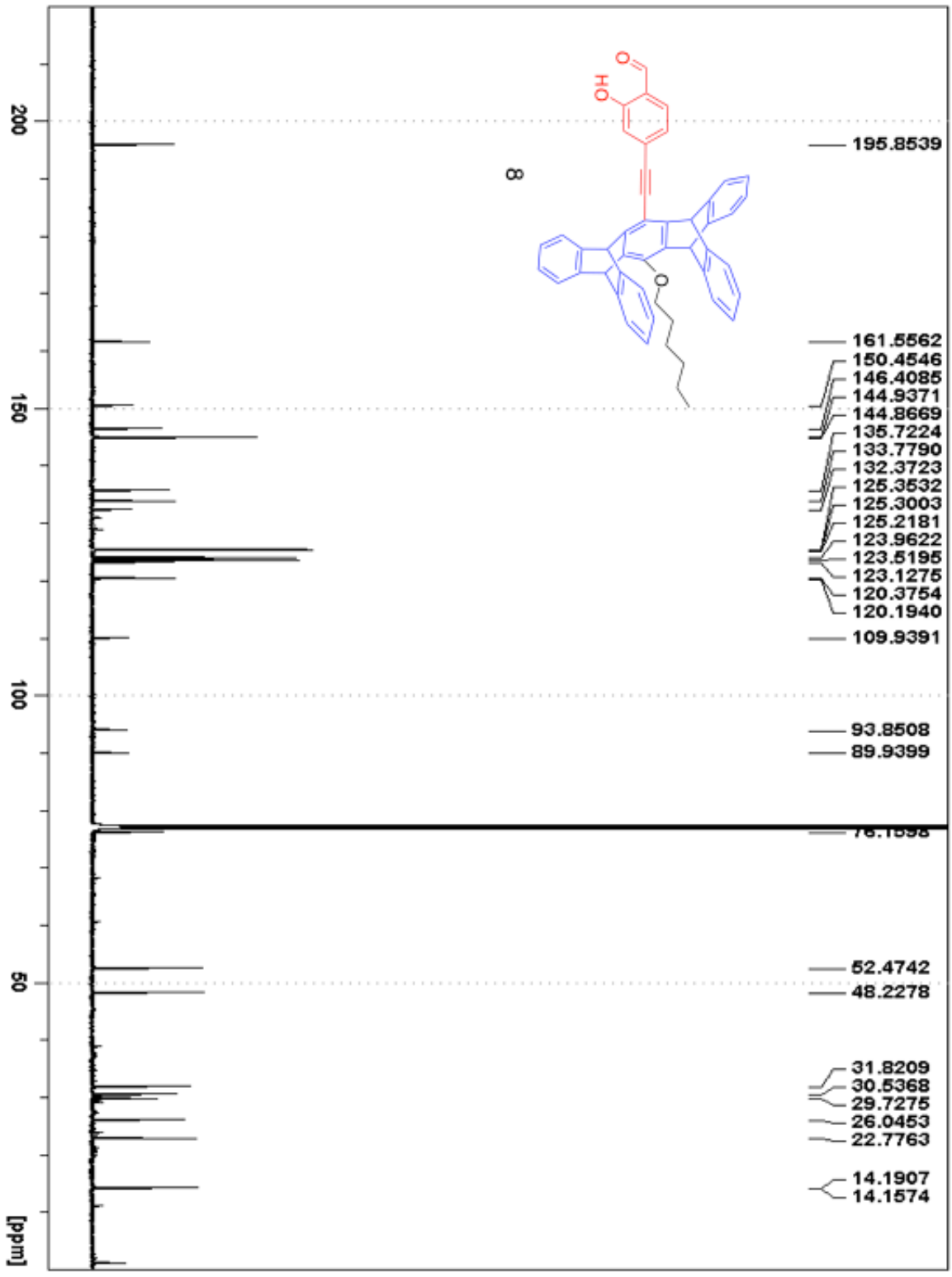

Figure S12. ^{13}C NMR of Salicylaldehyde Hexyl Pentiptycene Alkyne **8**
100 MHz ^{13}C NMR spectrum of compound **8** in $CDCl_3$

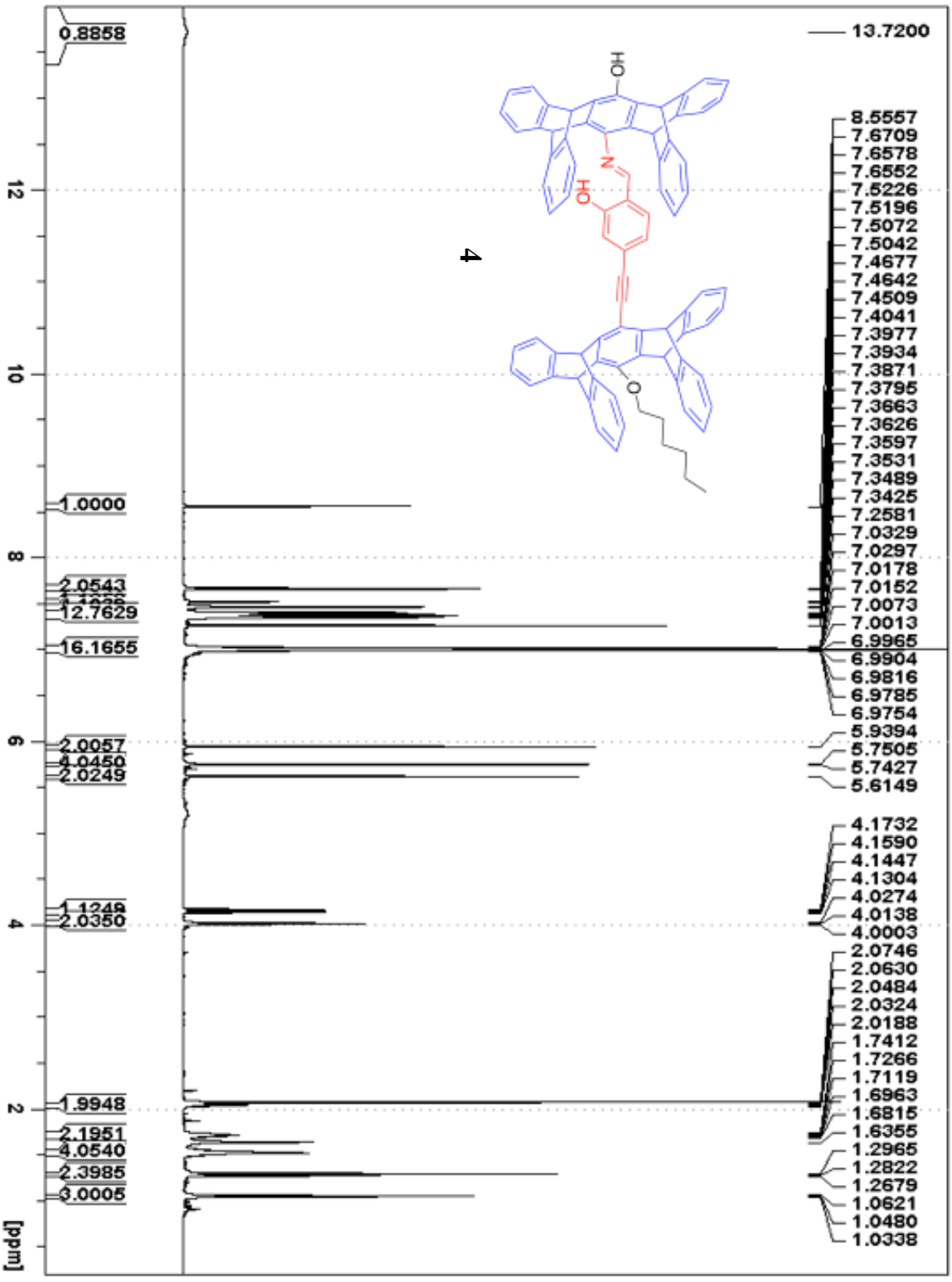

Figure S13. ^{1}H NMR of Pentiptycene Salicylidine Aniline Rotor **4**
500 MHz ^{1}H NMR spectrum of compound **4** in $CDCl_3$

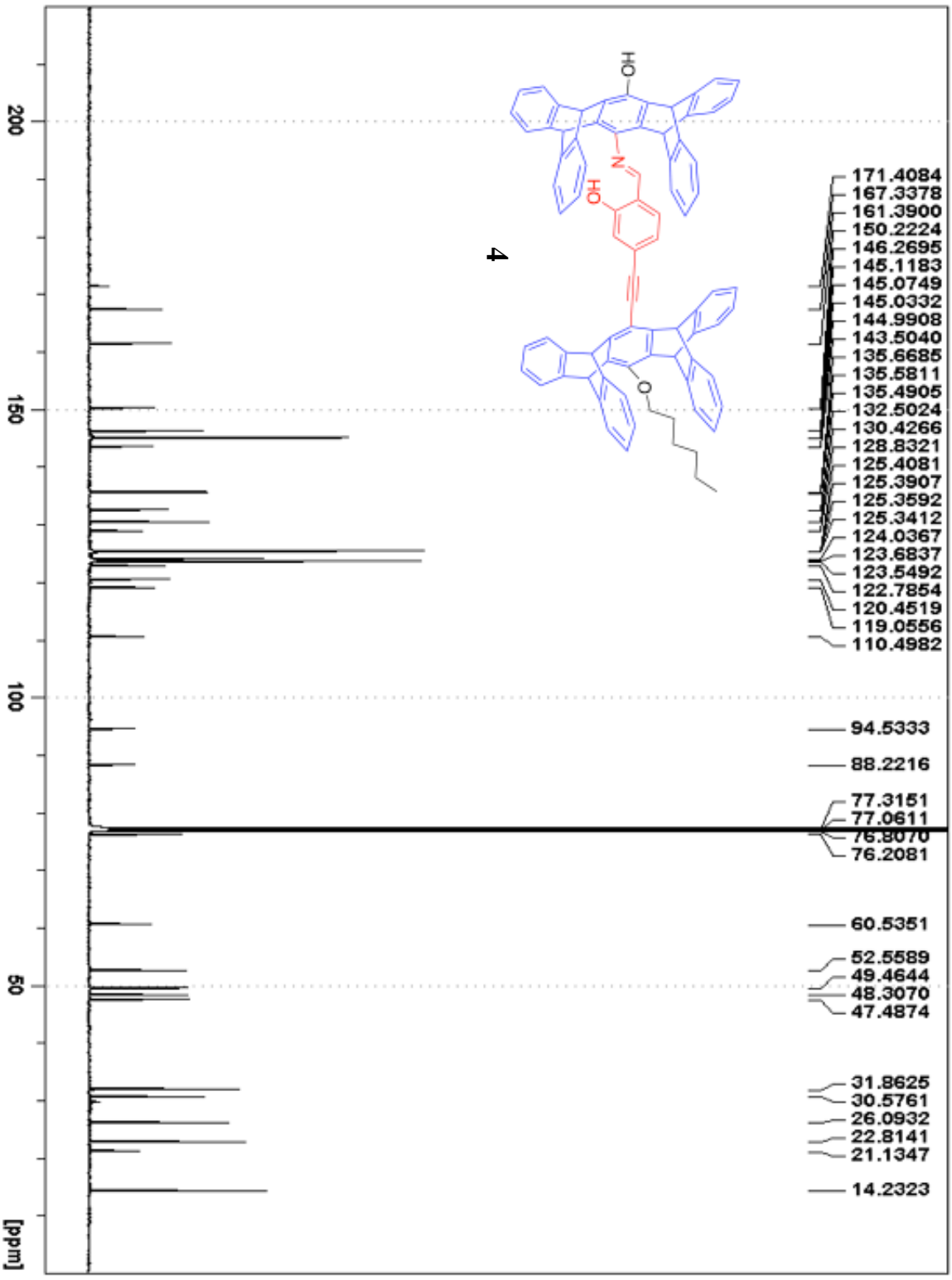

Figure S14. ^{13}C NMR of Pentiptycene Salicylidine Aniline Rotor **4**
125 MHz ^{13}C NMR spectrum of compound **4** in $CDCl_3$

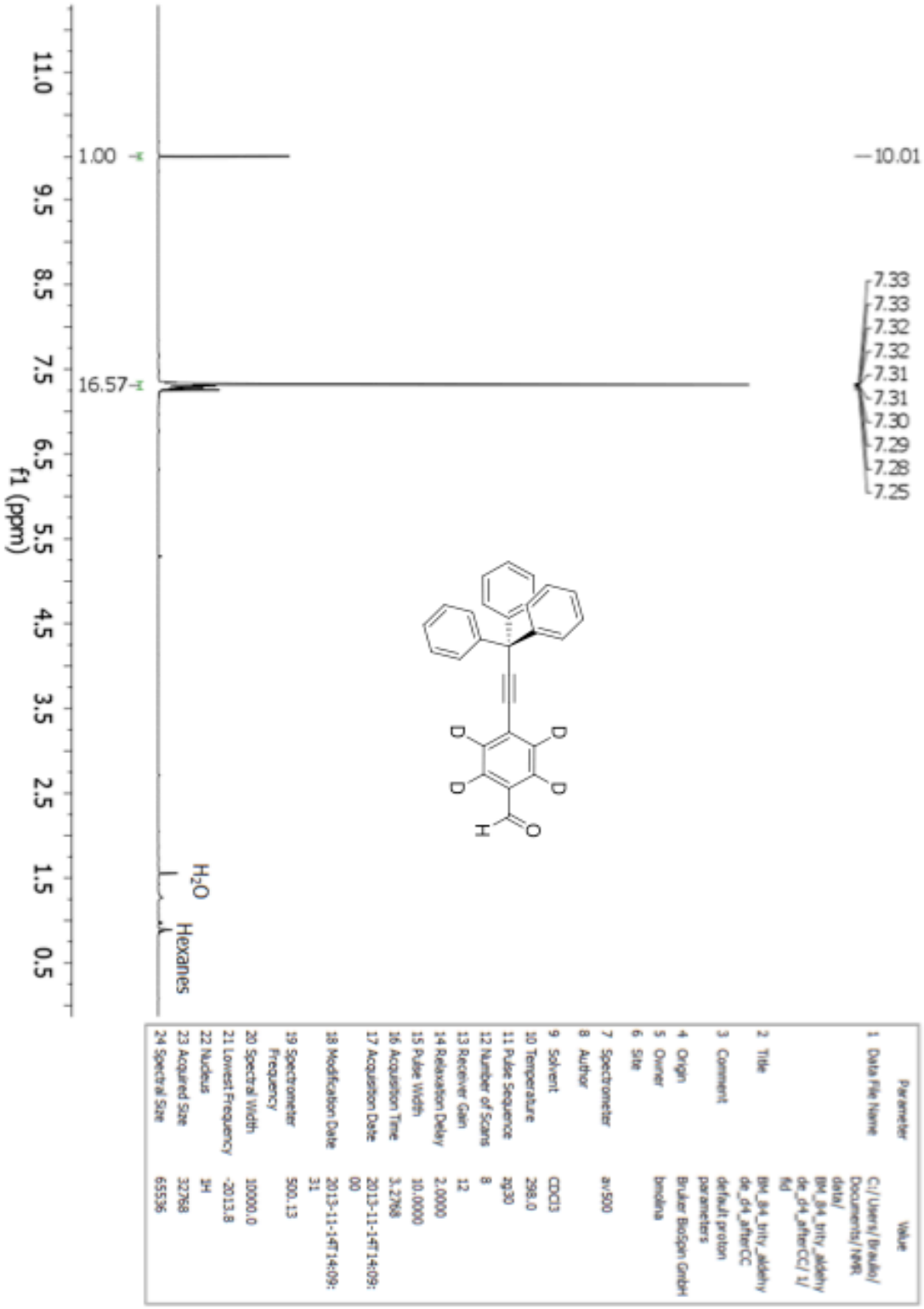

	Parameter	Value
1	Data File Name	C:/Users/Braulio/Documents/NMR data/BM_84_trity_aldehyde_d4_after CC/ 1/fid
2	Title	BM_84_trity_aldehyde_d4_after CC
3	Comment	default proton parameters
4	Origin	Bruker BioSpin GmbH
5	Owner	bnsdna
6	Site	
7	Spectrometer	av500
8	Author	
9	Solvent	CDCl3
10	Temperature	298.0
11	Pulse Sequence	zg30
12	Number of Scans	8
13	Receiver Gain	12
14	Relaxation Delay	2.0000
15	Pulse Width	10.0000
16	Acquisition Time	3.2768
17	Acquisition Date	2013-11-14T14:09:00
18	Modification Date	2013-11-14T14:09:31
19	Spectrometer Frequency	500.13
20	Spectral Width	10000.0
21	Lowest Frequency	-2013.8
22	Nucleus	1H
23	Acquired Size	32768
24	Spectral Size	65536

Figure S15. ^{1}H NMR of **d_4-Benzaldehyde Trityl Alkyne 9**
500 MHz ^{1}H NMR spectrum of compound **9** in $CDCl_3$

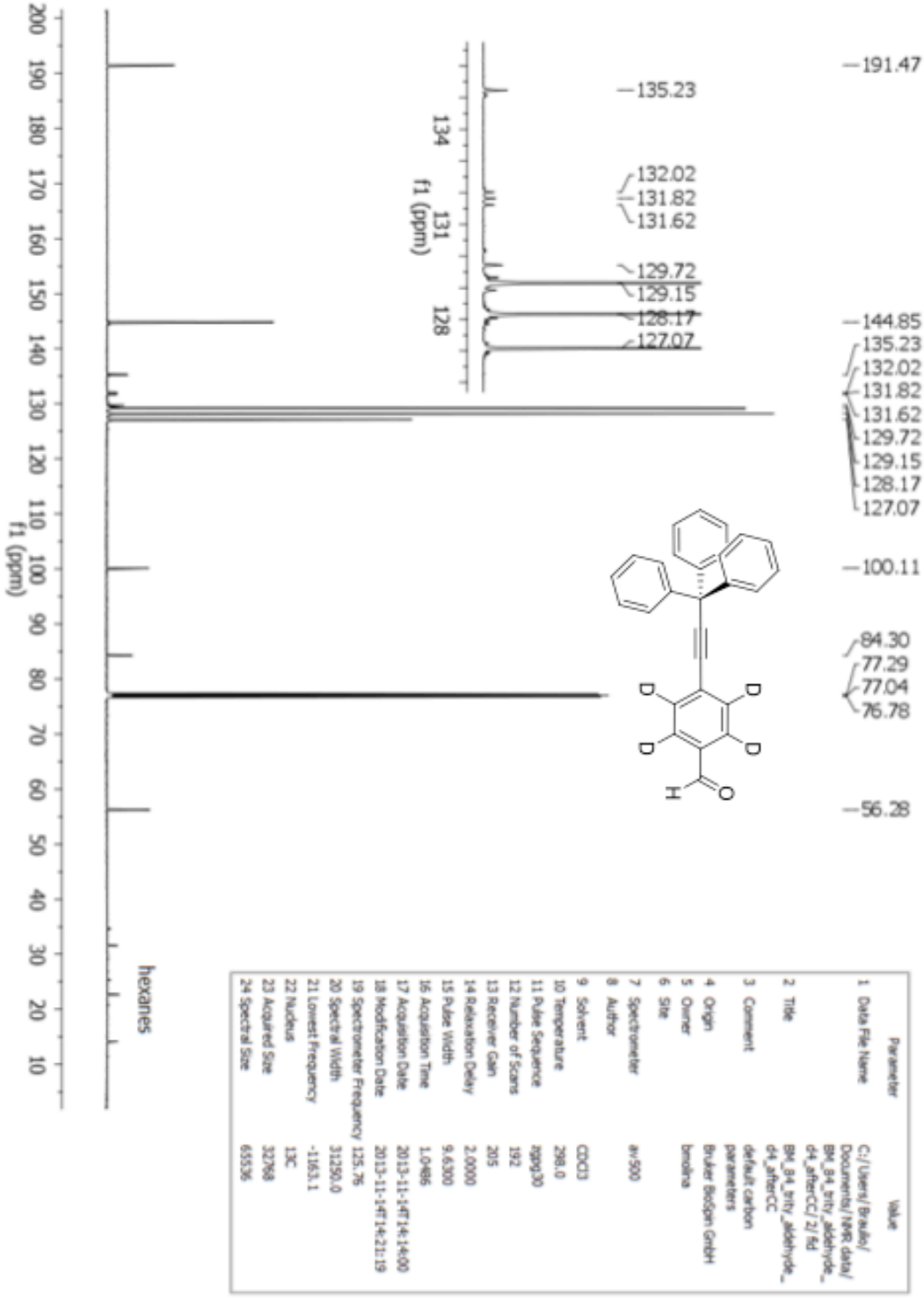

Figure S16. ^{13}C NMR of **d_4-Benzaldehyde Trityl Alkyne 9**
125 MHz ^{13}C NMR spectrum of compound **9** in $CDCl_3$

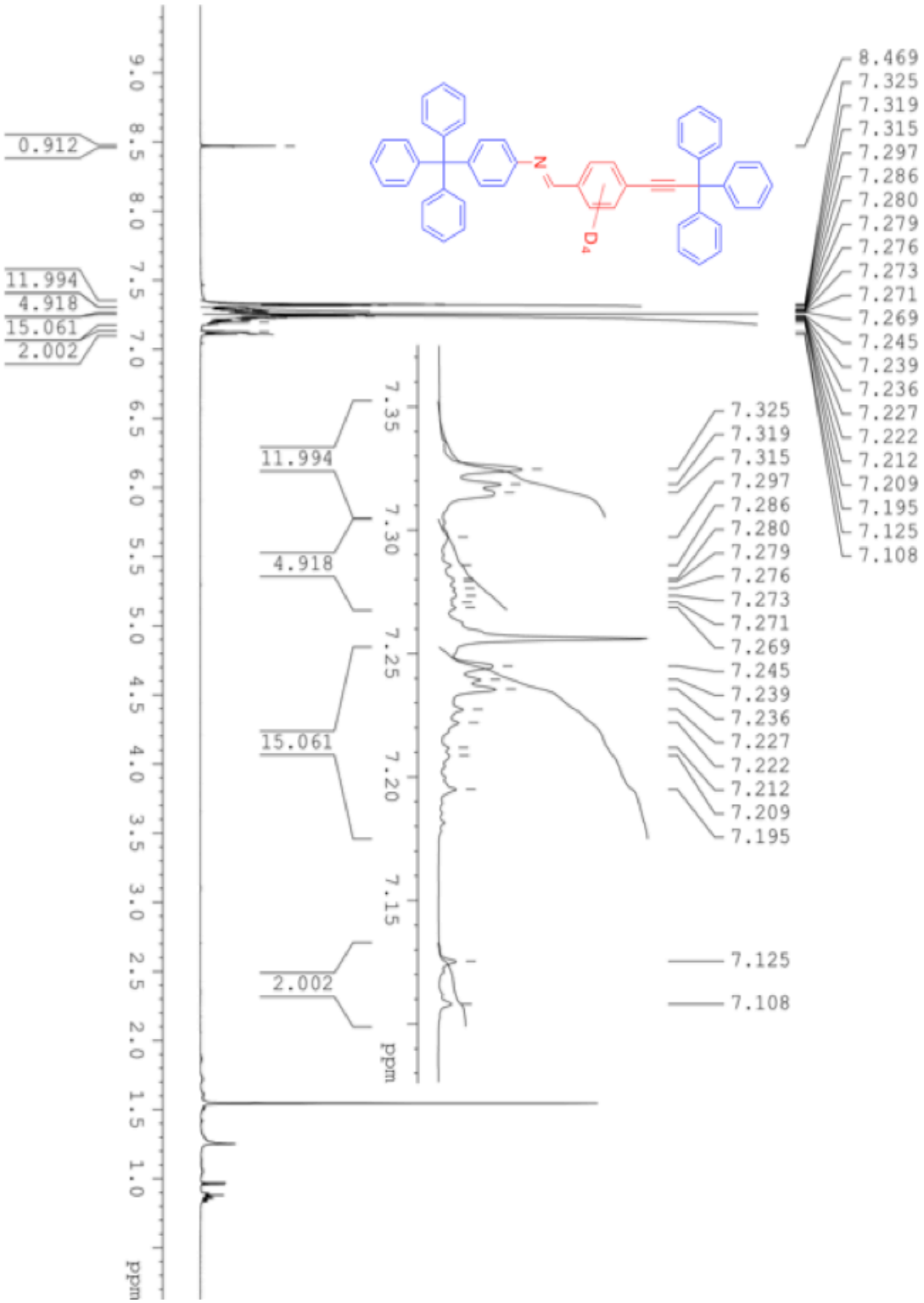

Figure S17. ^{1}H NMR of d_4-Imine Full Rotor **10**
500 MHz ^{1}H NMR spectrum of compound **10** in $CDCl_3$

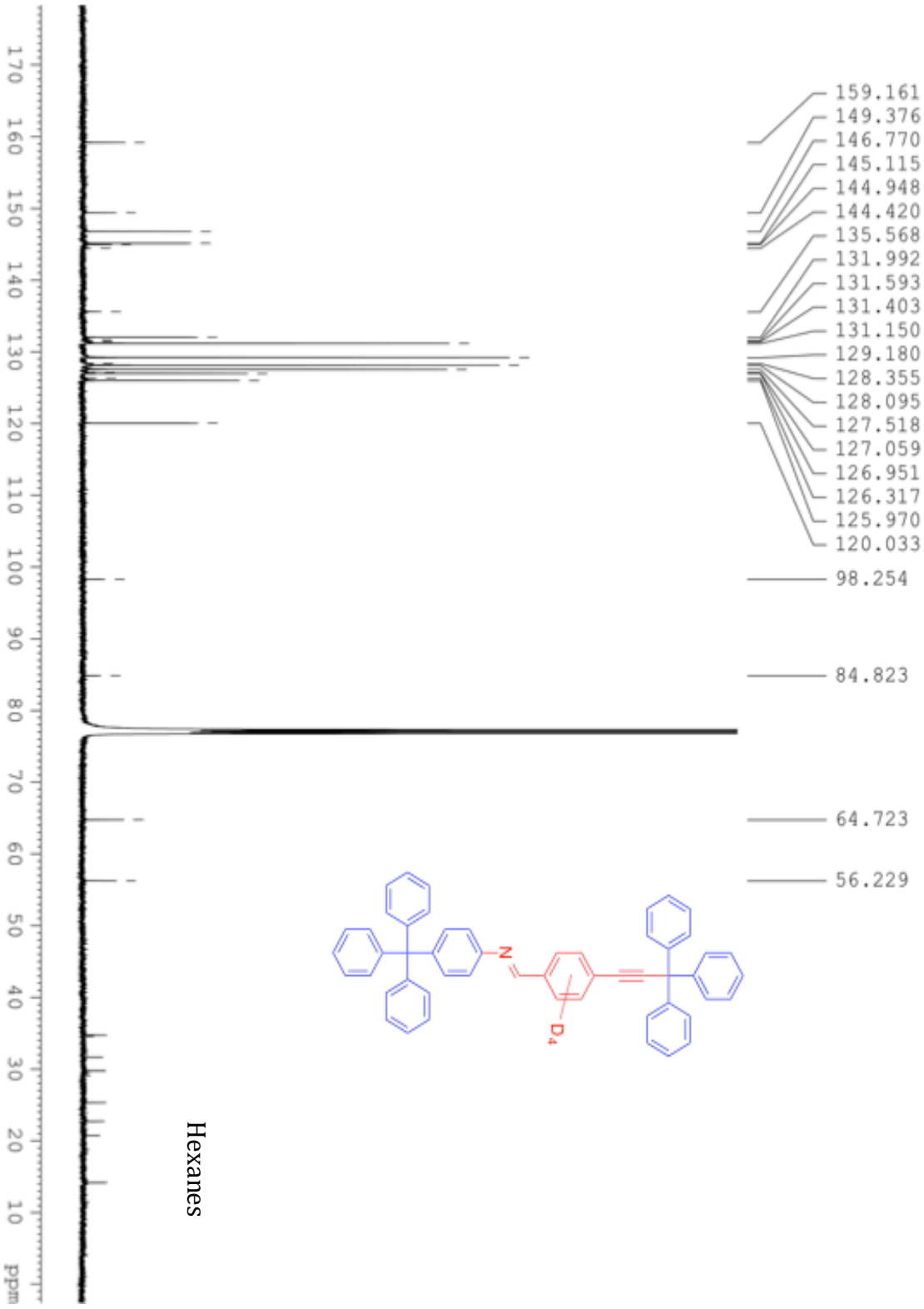

Figure S18. ^{13}C NMR of d_4-Imine Full Rotor **10**
125 MHz ^{13}C NMR spectrum of compound **10** in $CDCl_3$

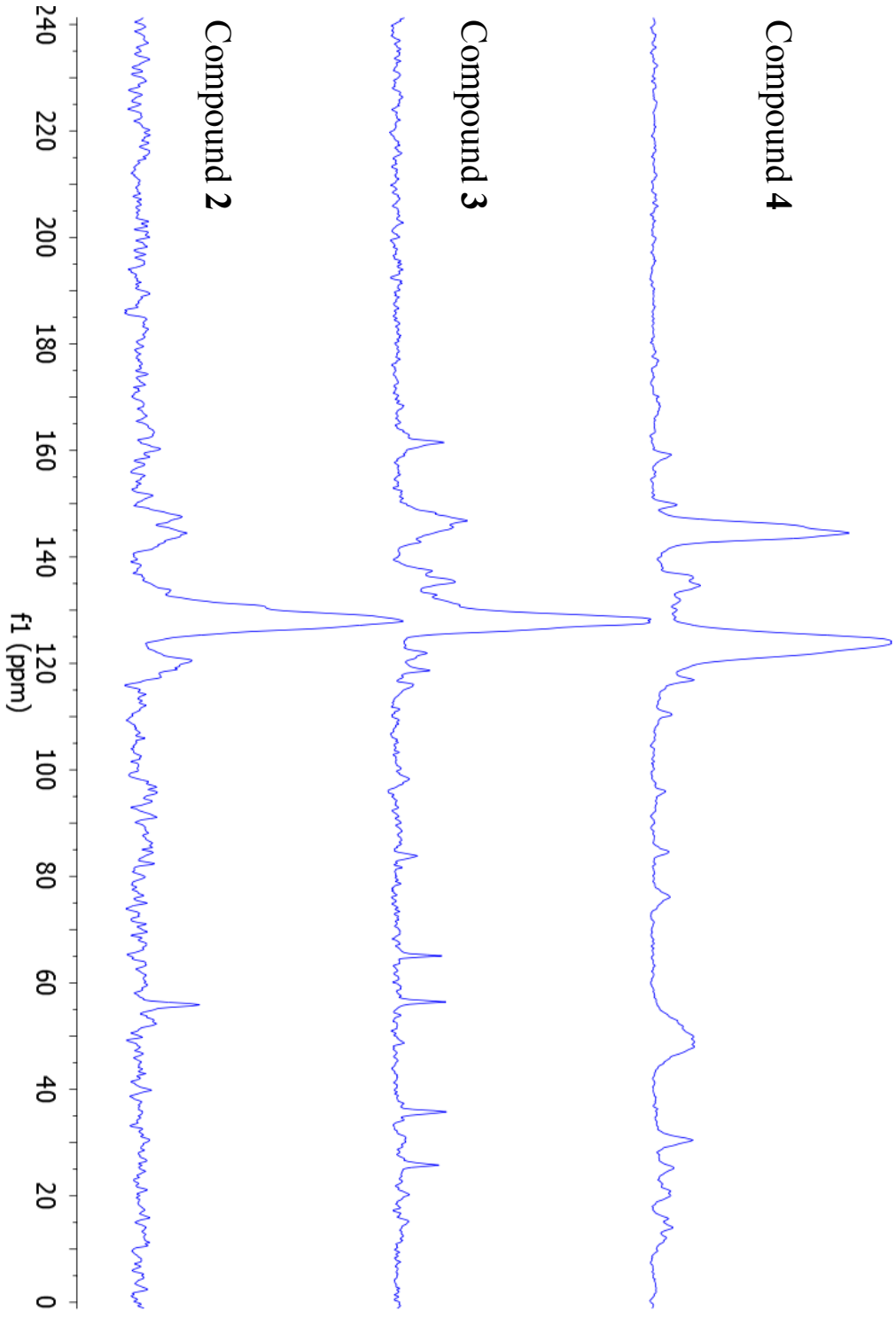

Figure S19.CPMAS of Compounds **2-4**
75 MHz ^{13}C NMR spectra of compounds **2-4**

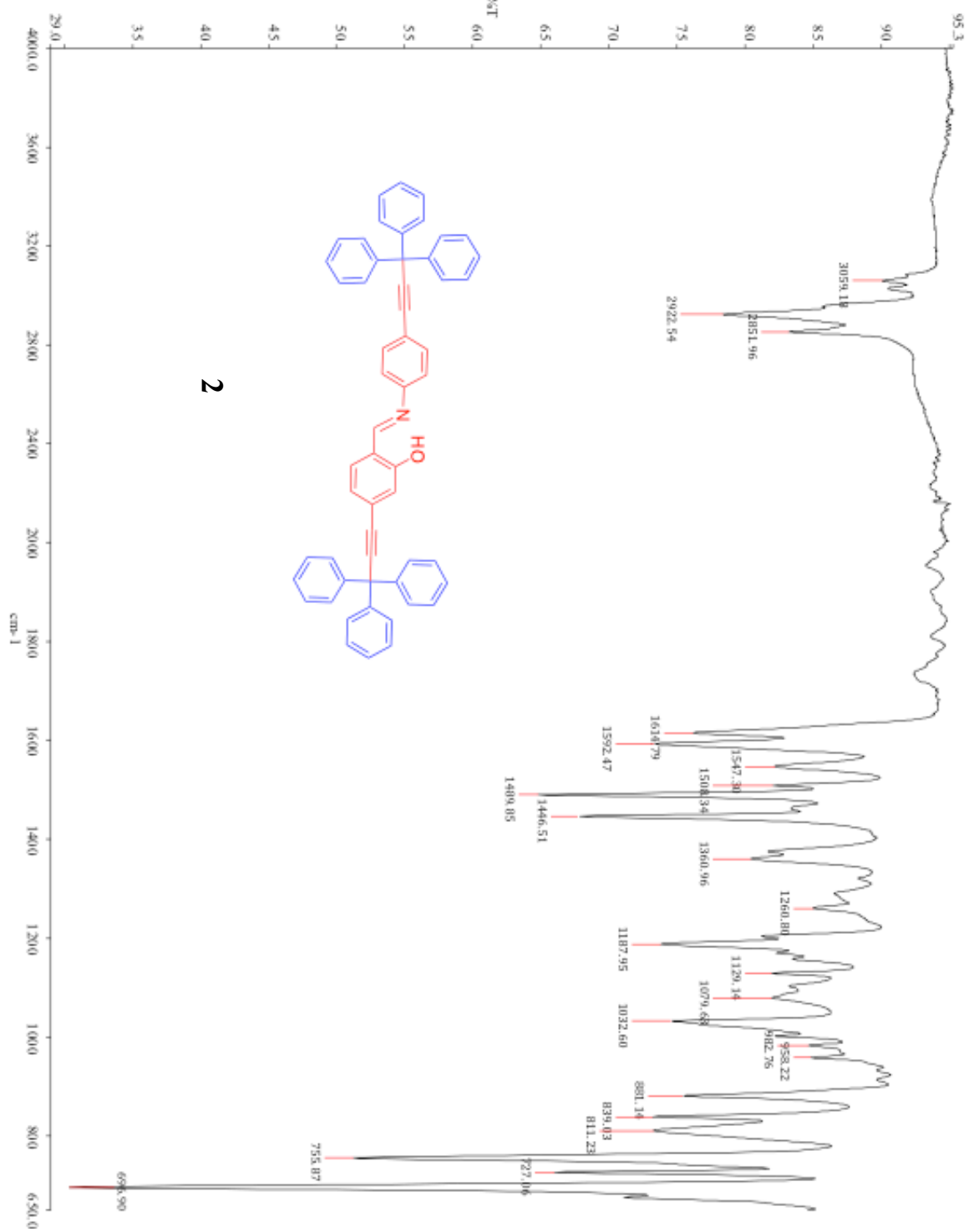

Figure S20. ATR FTIR Spectrum of Salicylidine Aniline Rotor **2** in the solid state

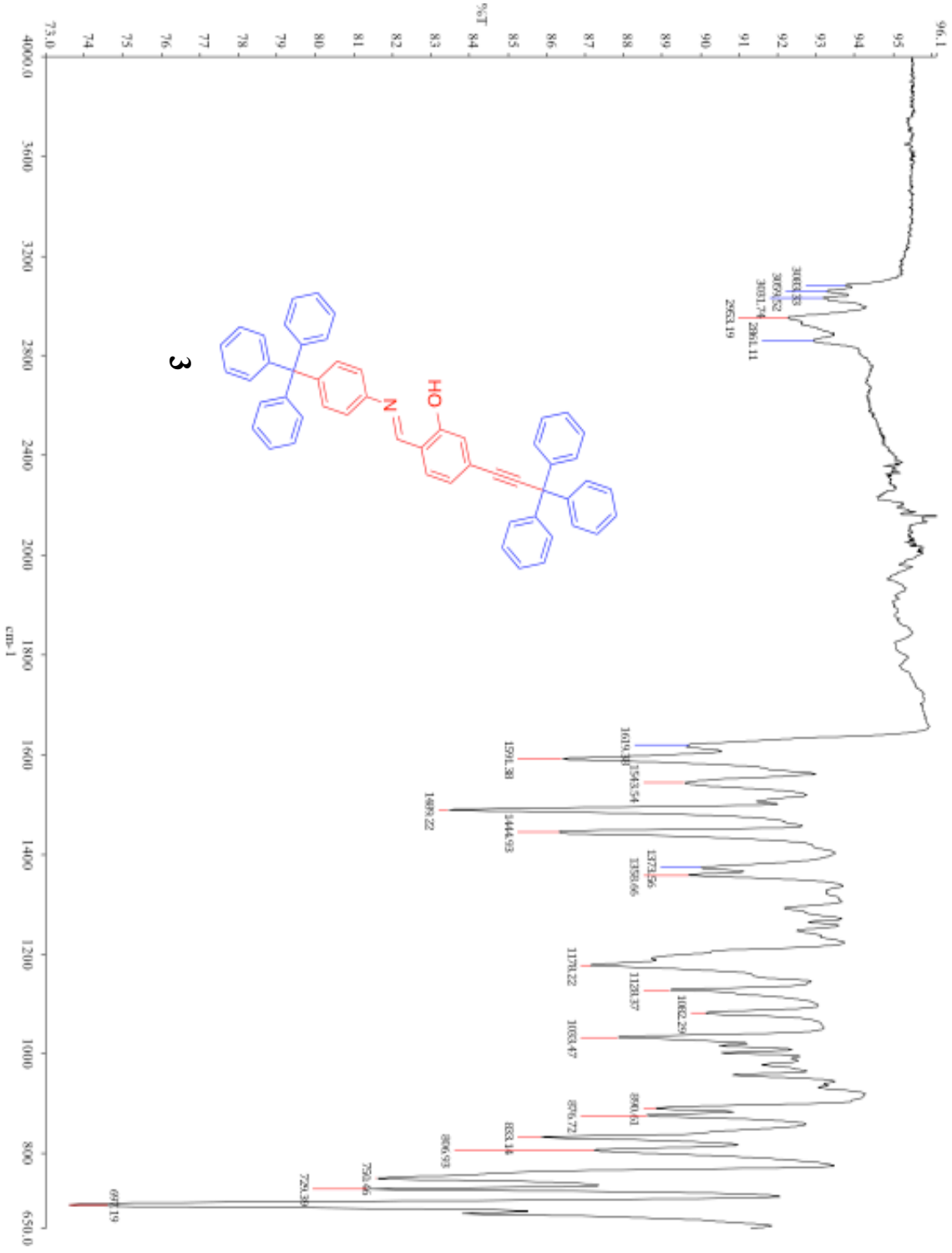

Figure S21. ATR FTIR Spectrum of Salicylidine Aniline Rotor **3** in the solid state

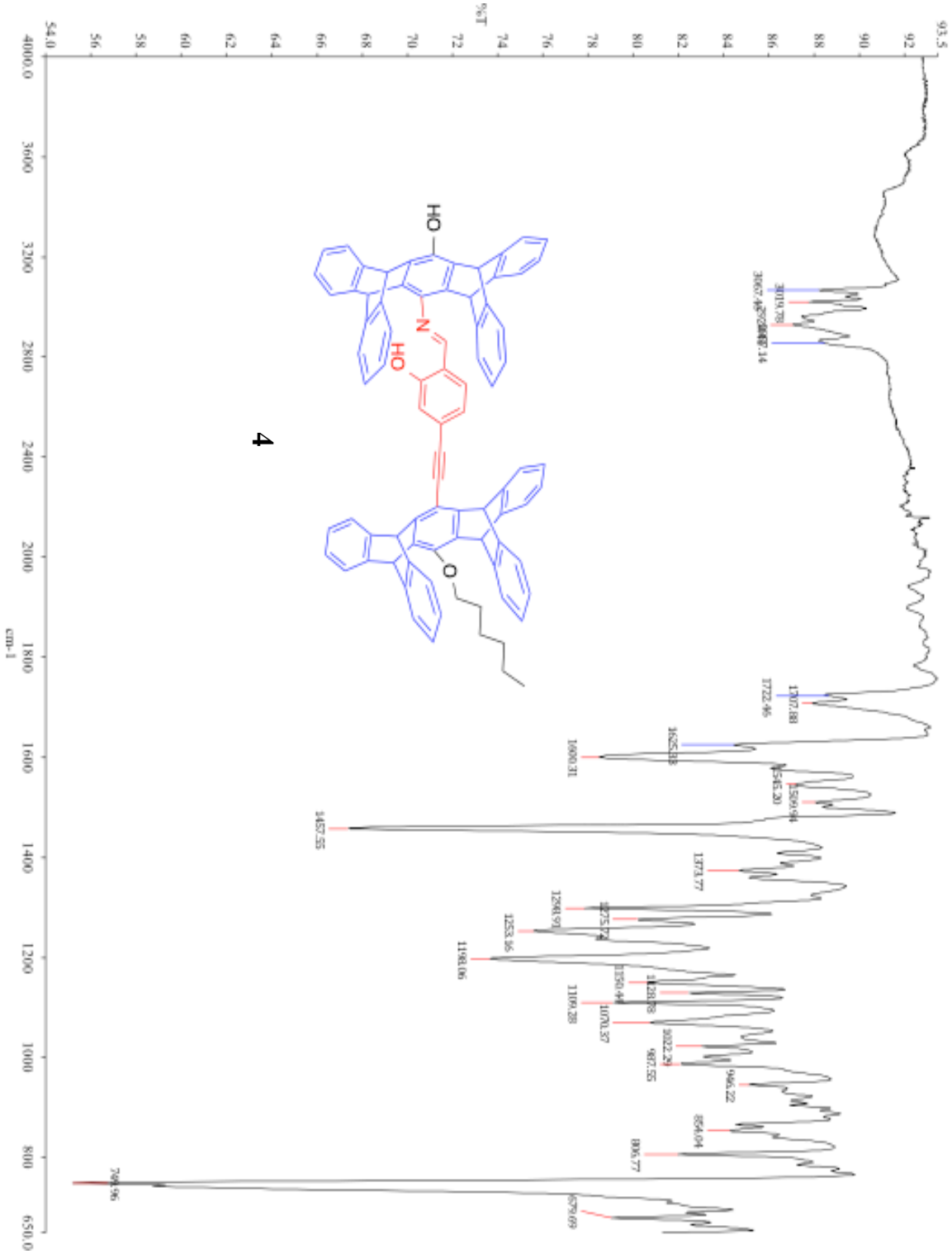

Figure S22. ATR FTIR Spectrum of Pentiptycene Salicylidine Aniline Rotor **4** in the solid state

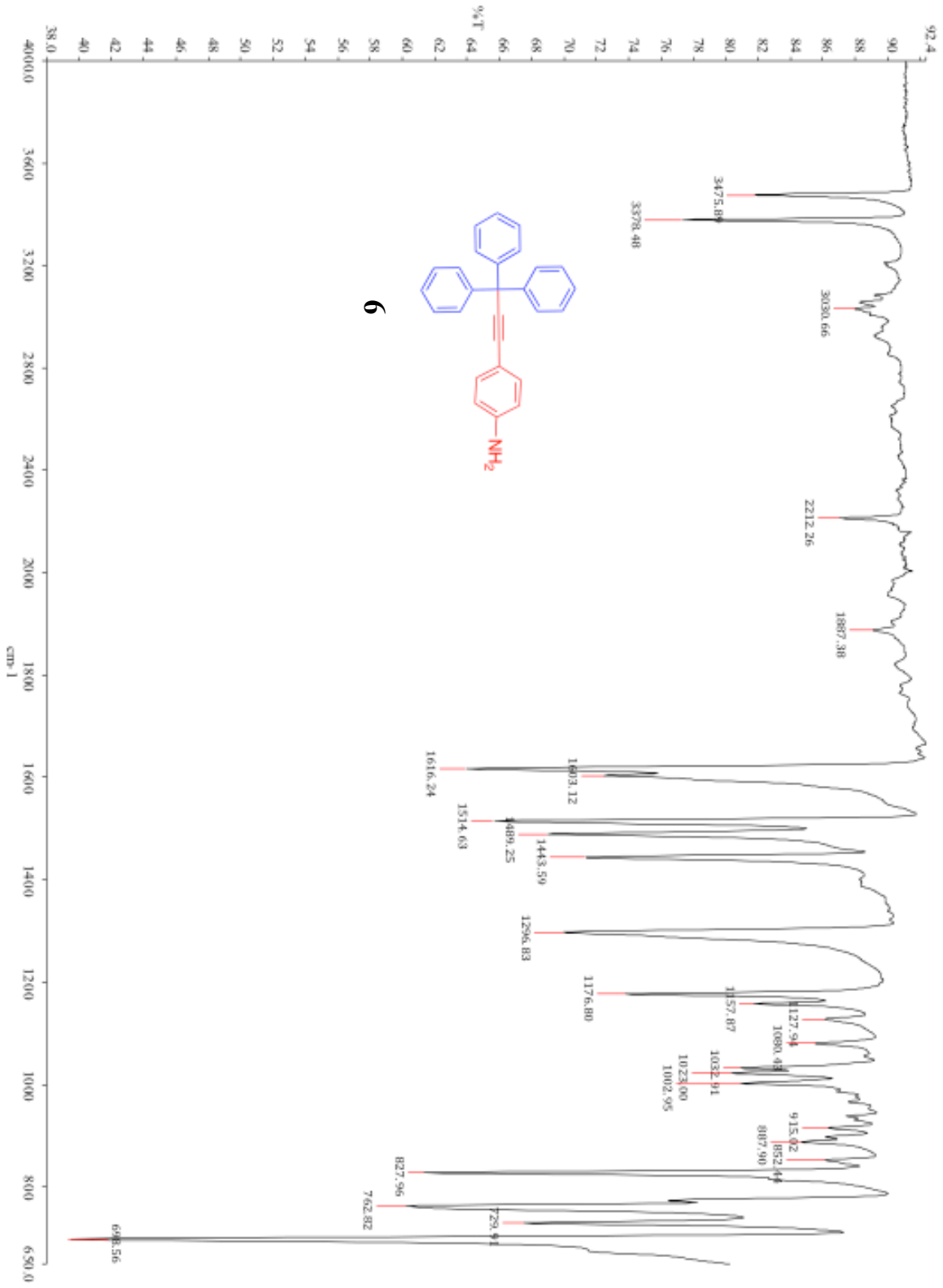

Figure S23. ATR FTIR Spectrum of Aniline Trityl Alkyne **6** in the solid state

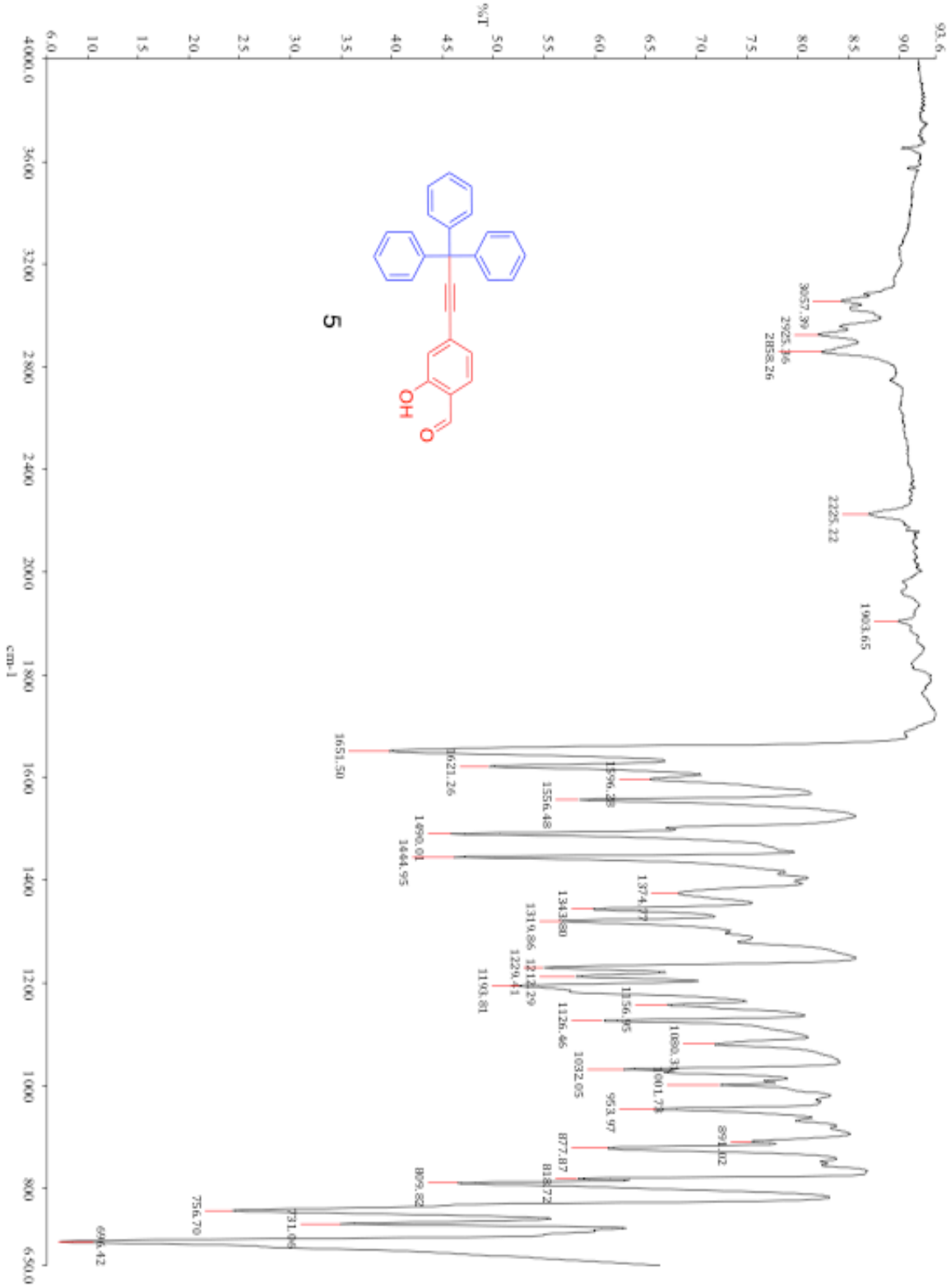

Figure S24. ATR FTIR Spectrum of Salicylaldehyde Trityl Alkyne **5** in the solid state

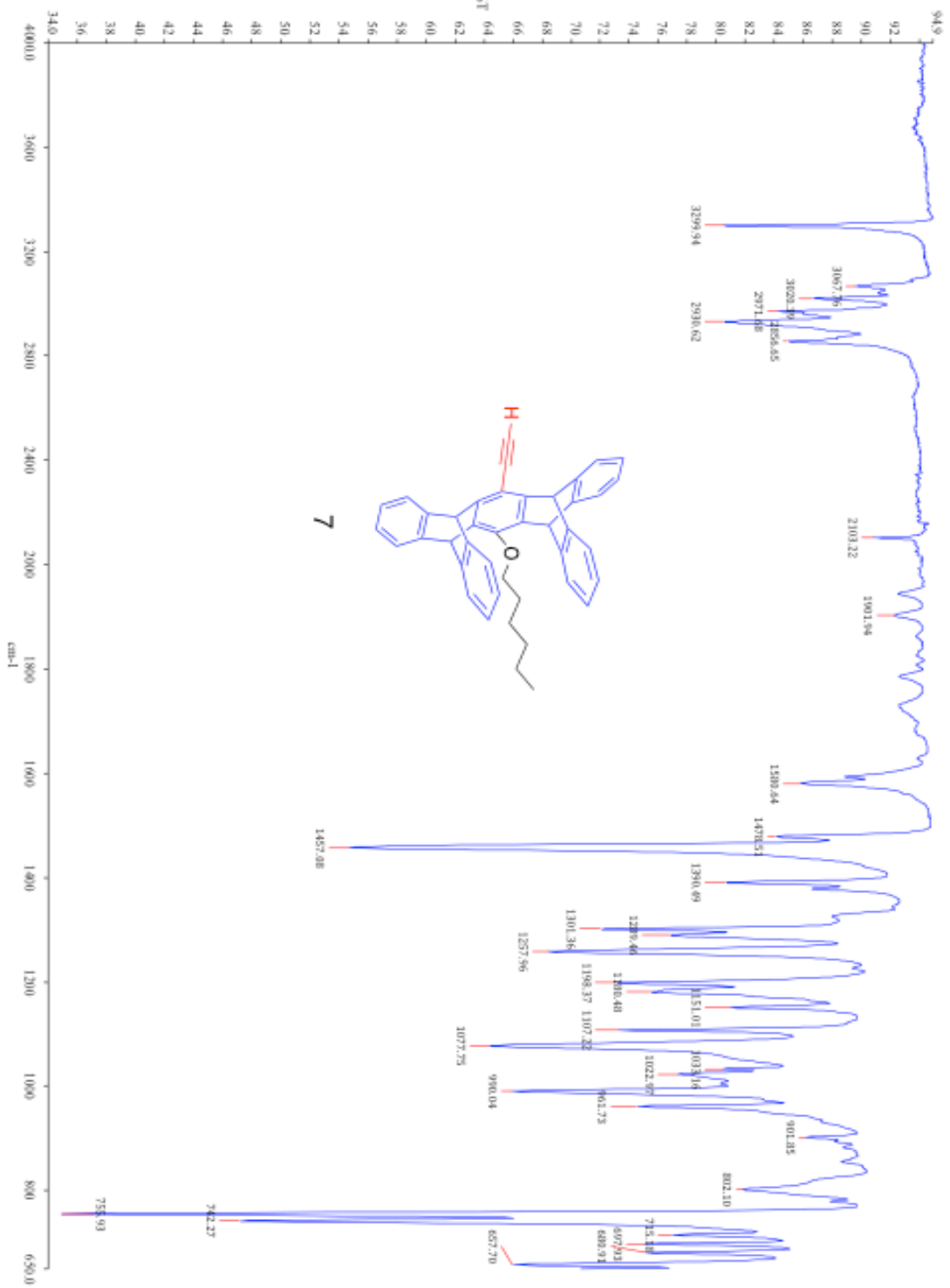

Figure S25. ATR FTIR Spectrum of Hexyl Pentiptycene Alkyne **7** in the solid state

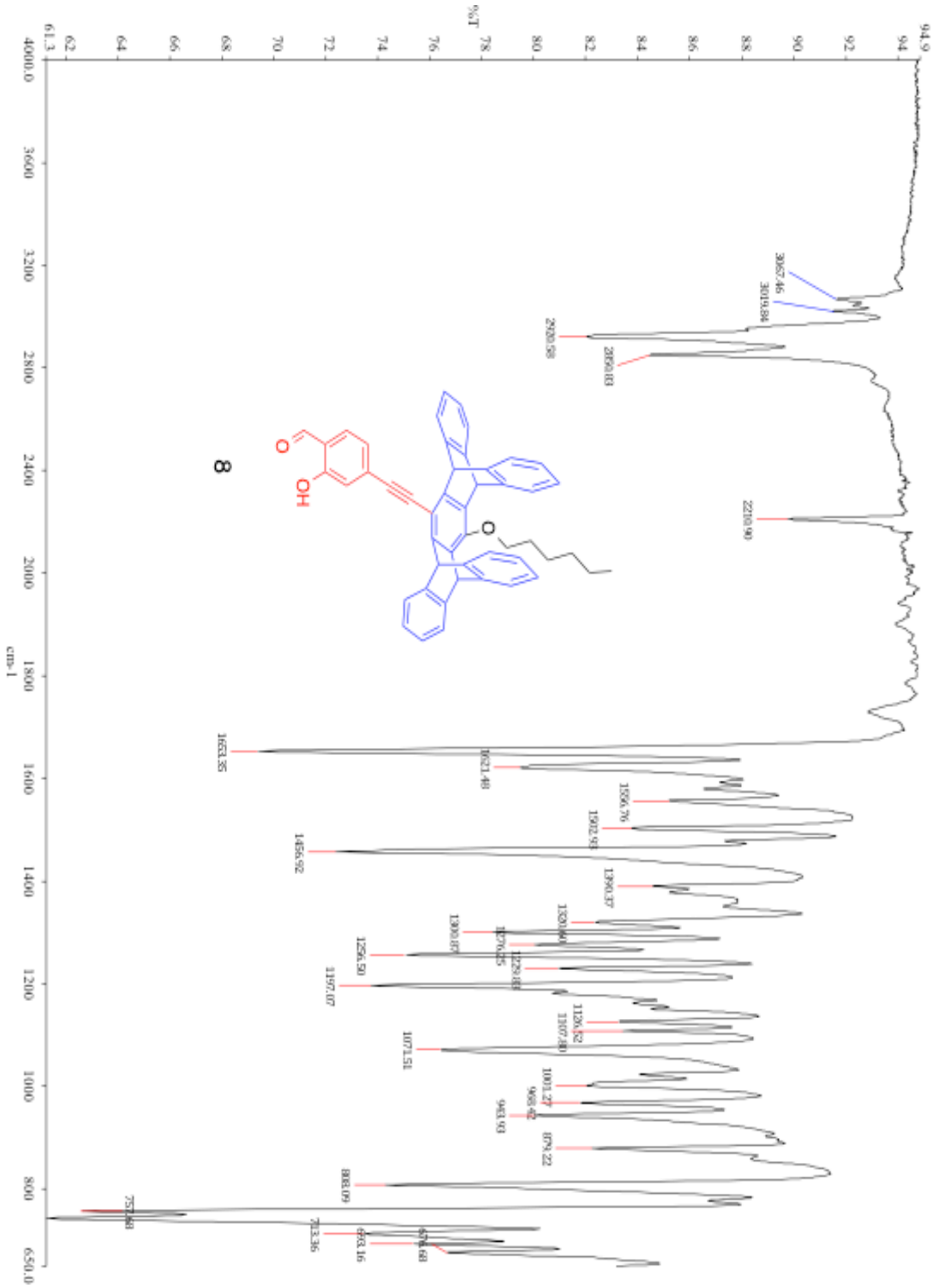

Figure S26. ATR FTIR Spectrum of Salicylaldehyde Hexyl Pentiptycene Alkyne **8** in the solid state

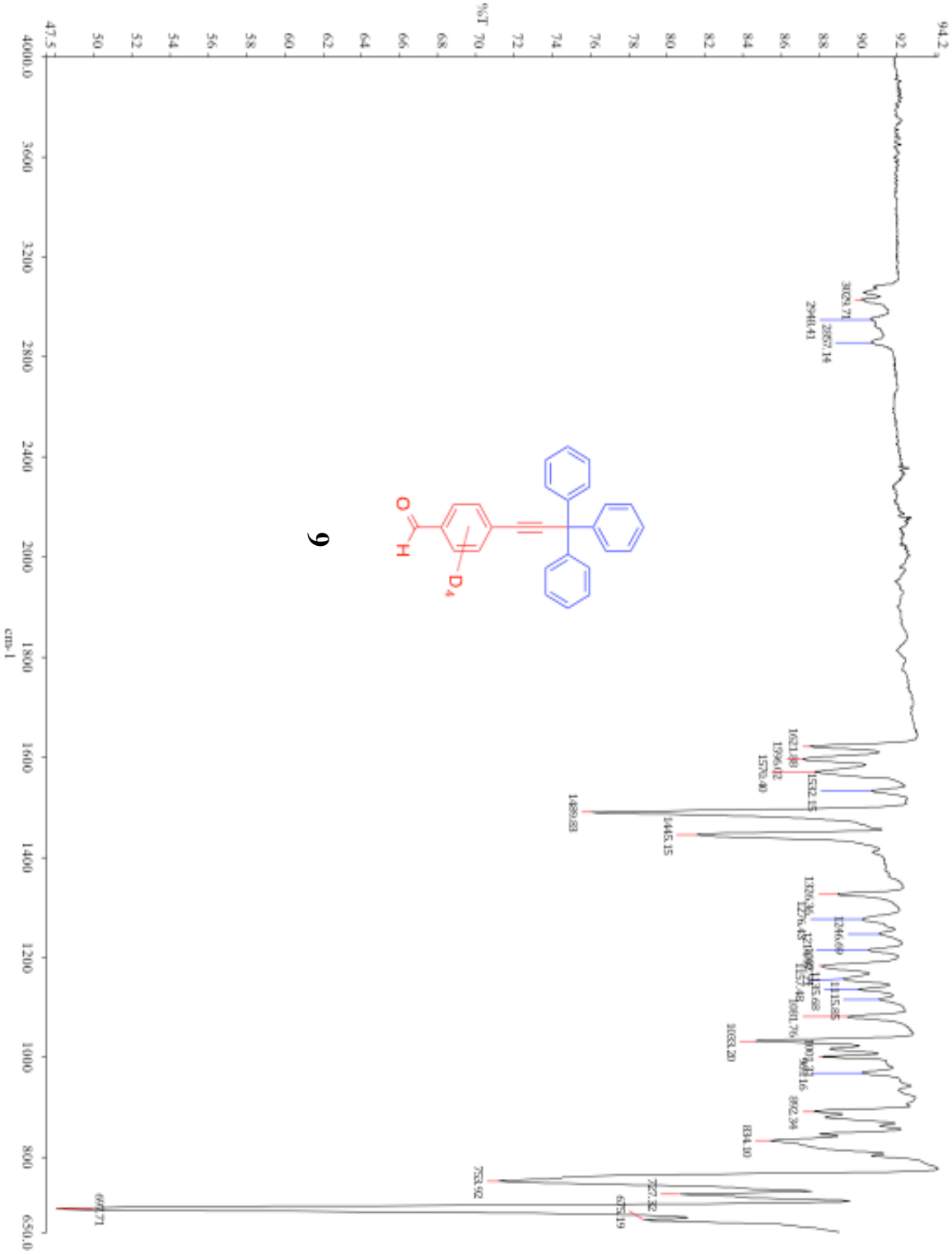

Figure S27. ATR FTIR Spectrum of d_4-Benzaldehyde Trityl Alkyne **9** in the solid state

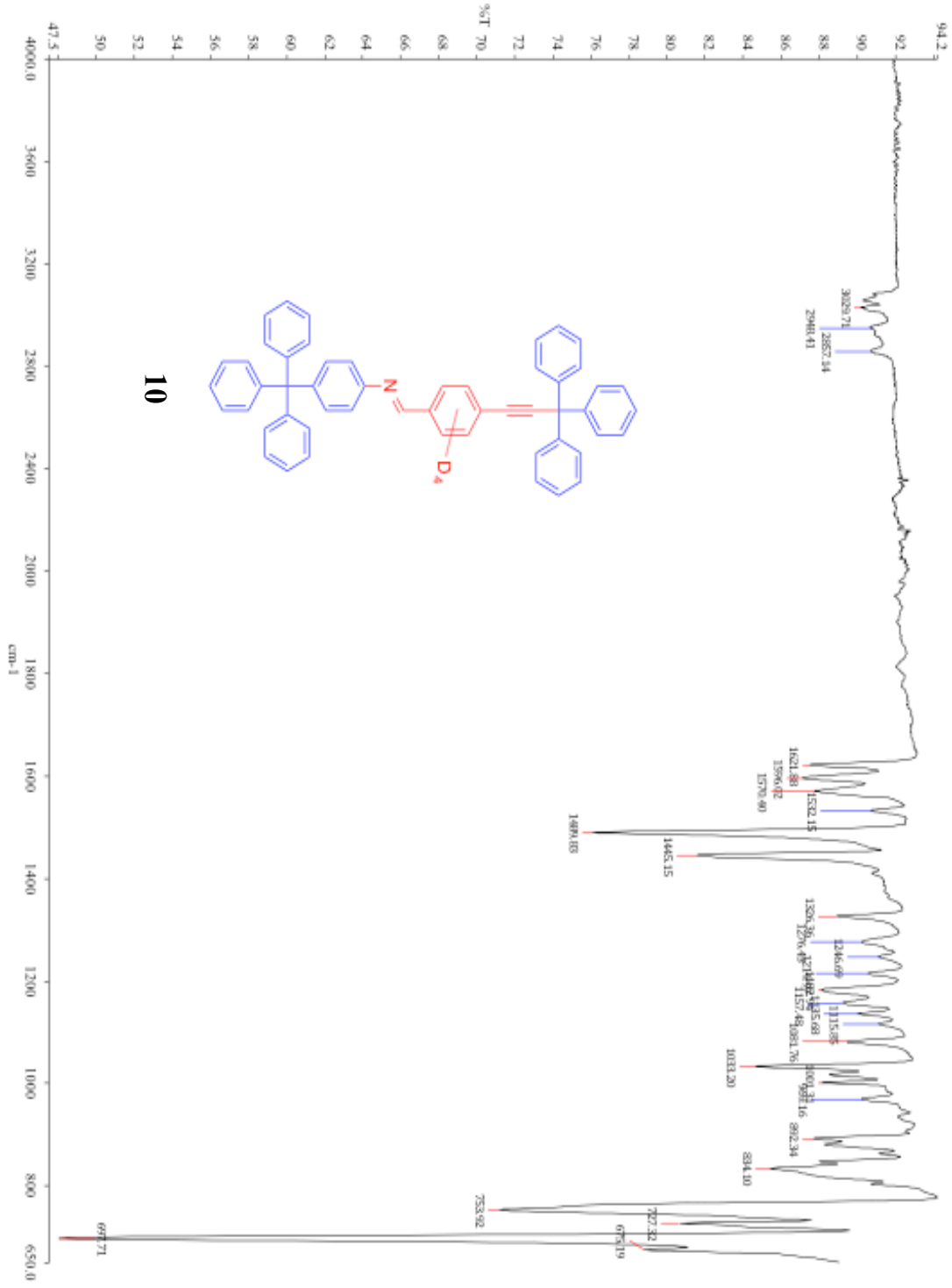

Figure S28. ATR FTIR spectrum of d_4-Imine Full Rotor **10** in the solid state

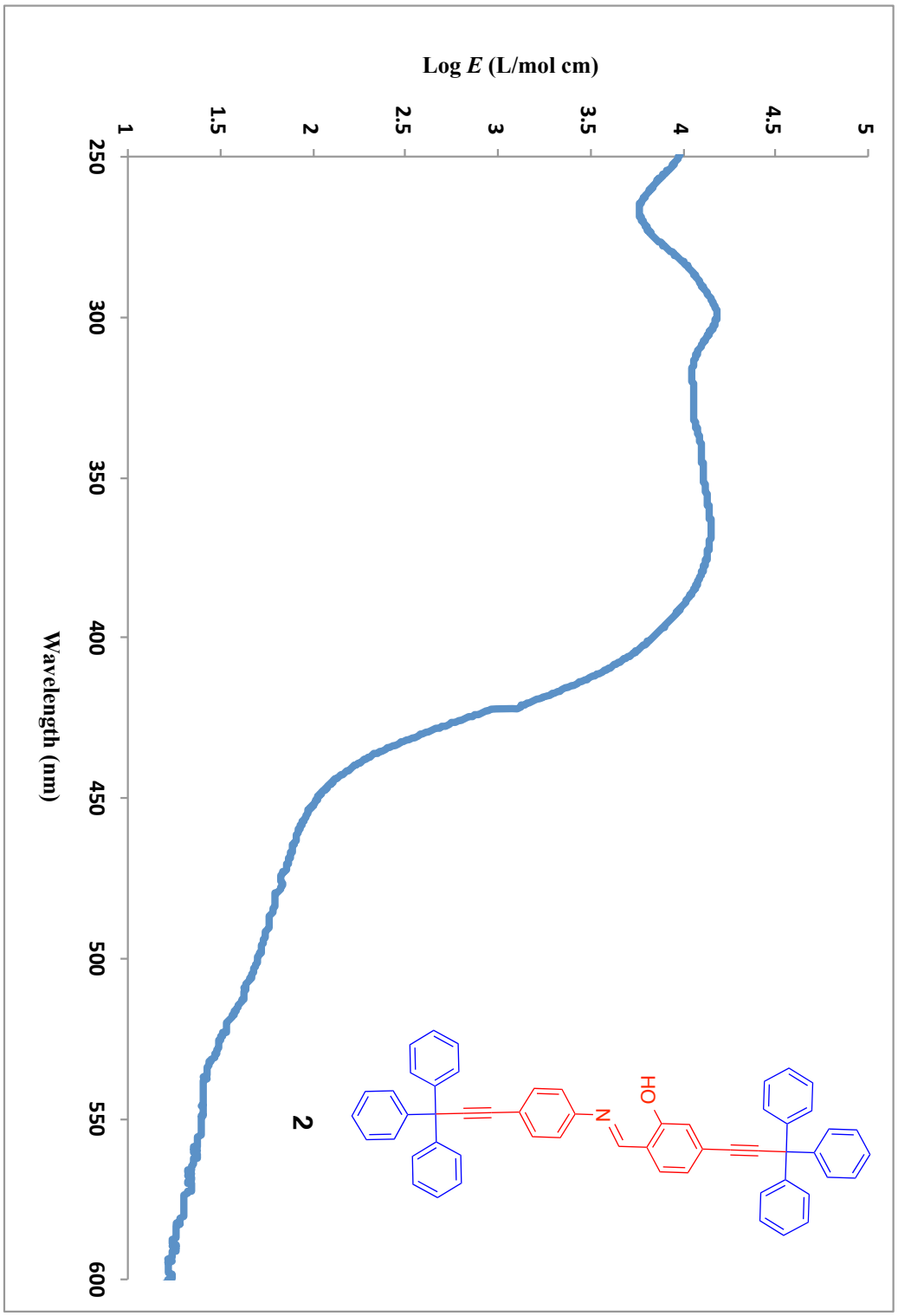

Figure S29. UV-Vis profile of Salicylidine Aniline Rotor **2** in dichloromethane

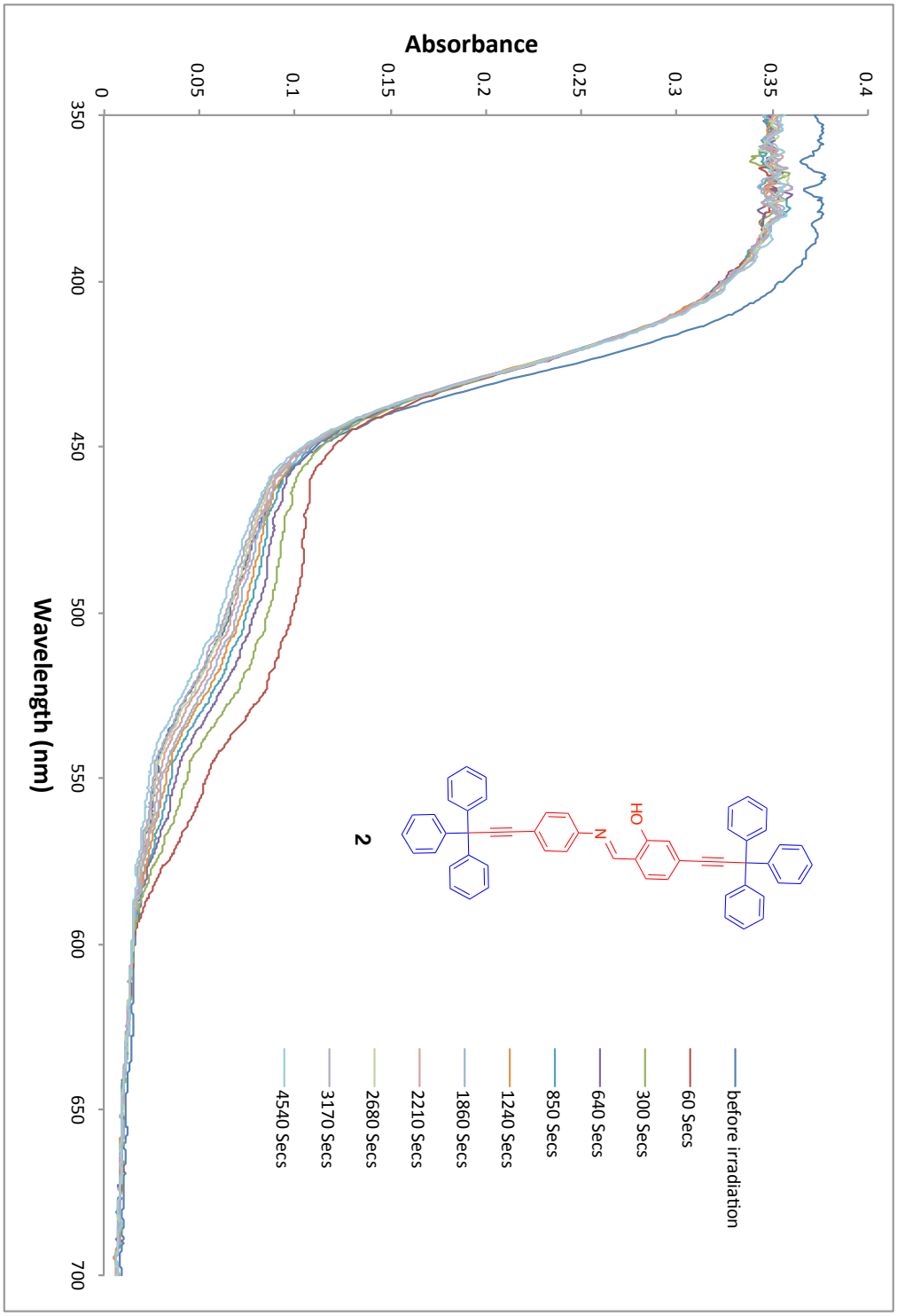

Figure S30. Diffuse Reflectance of Salicylidine Aniline Rotor **2**

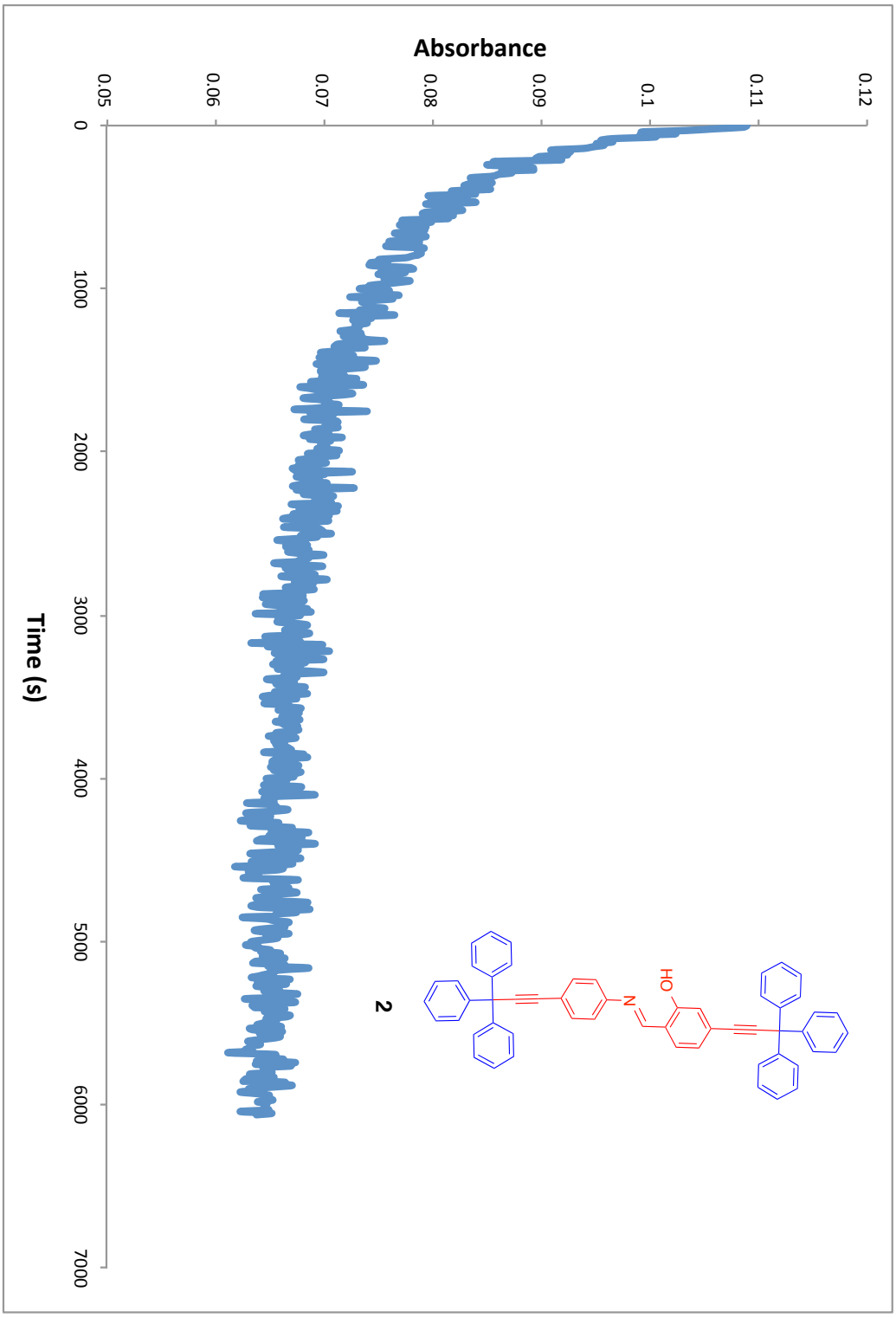

Figure S31. Diffuse Reflectance Lifetime of Salicylidine Aniline Rotor **2**

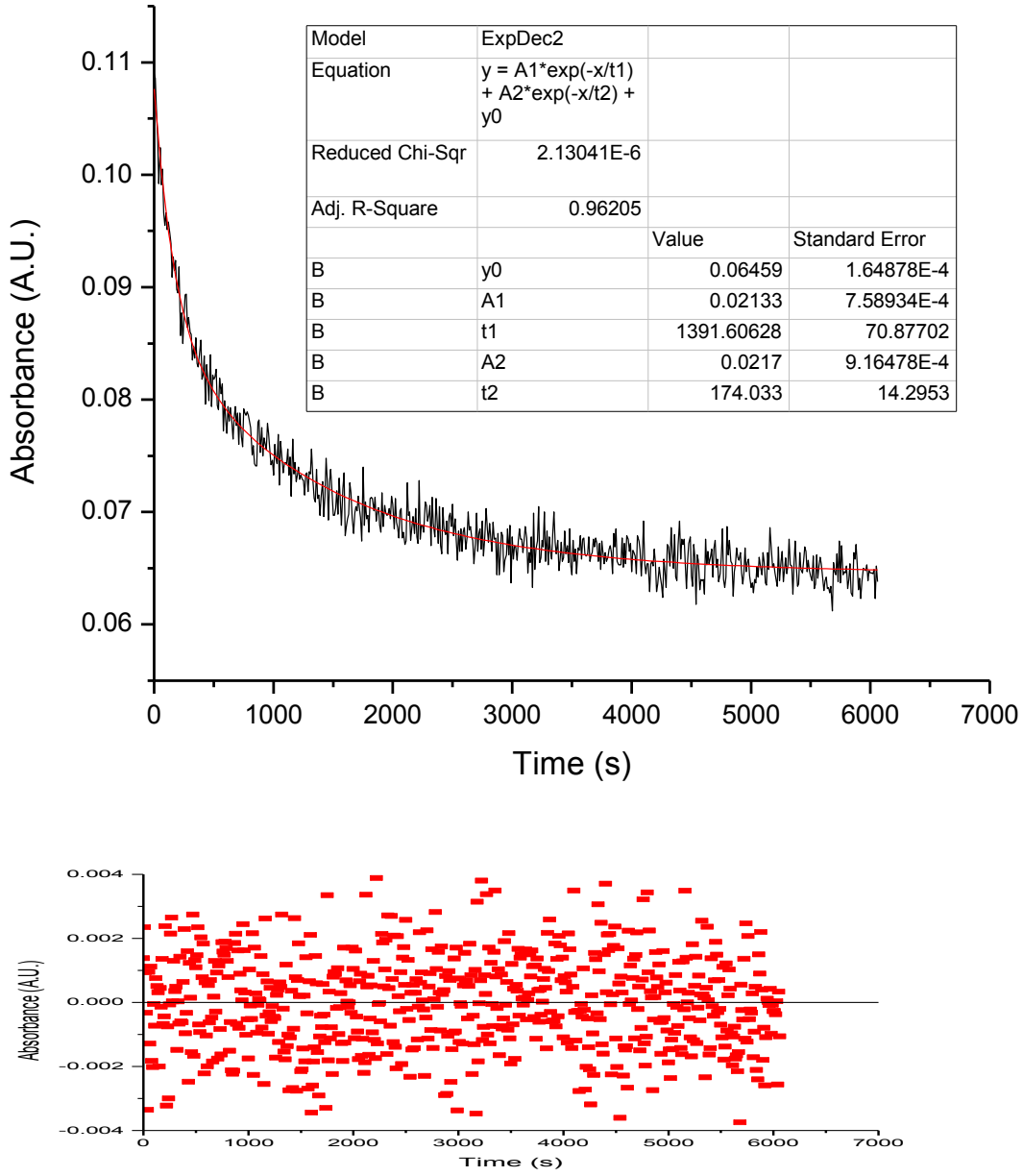

Figure S32. Diffuse Reflectance Lifetime of Salicylidine Aniline Rotor **2**

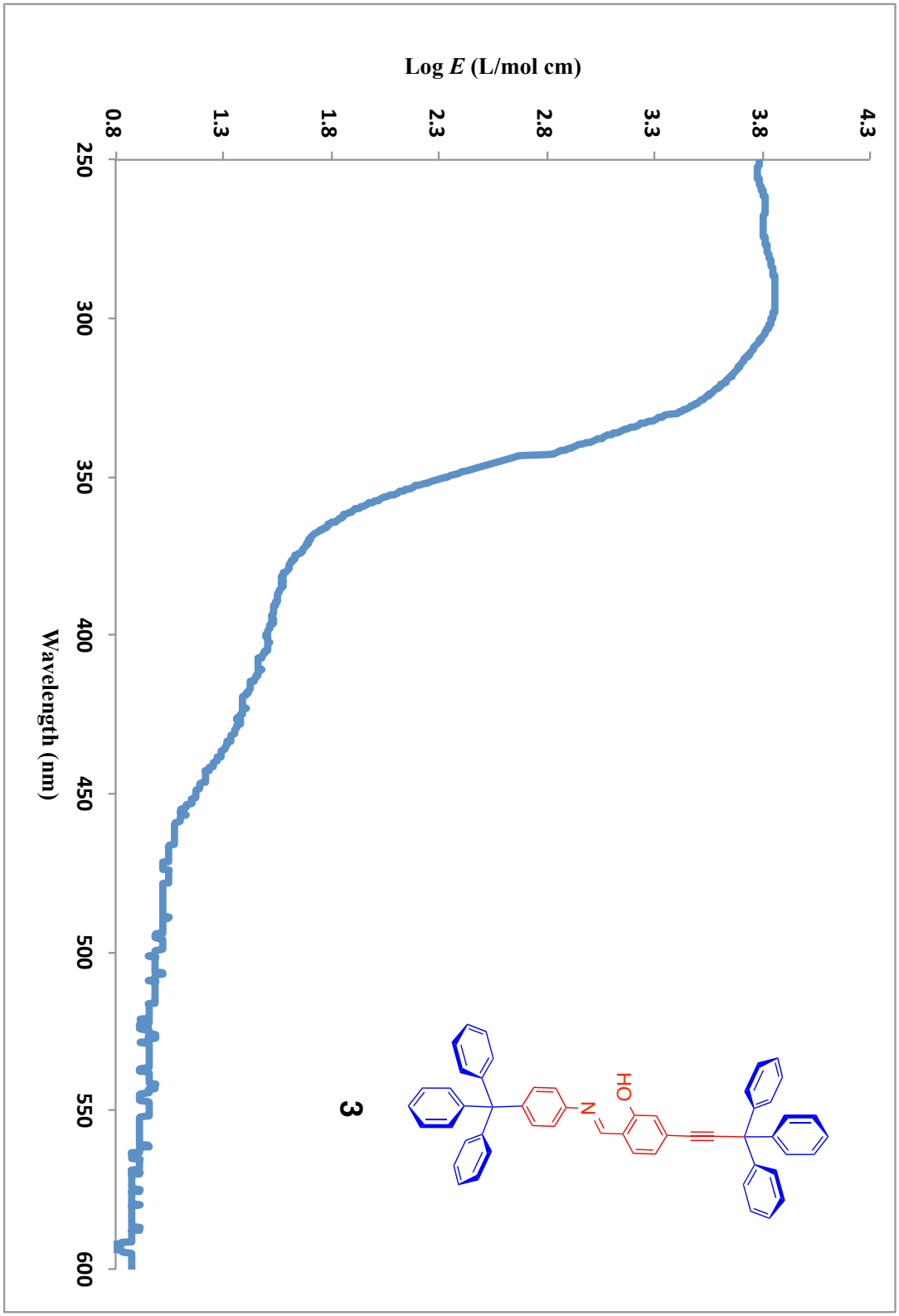

Figure S33. UV-Vis profile of Salicylidine Aniline Rotor **3** in dichloromethane

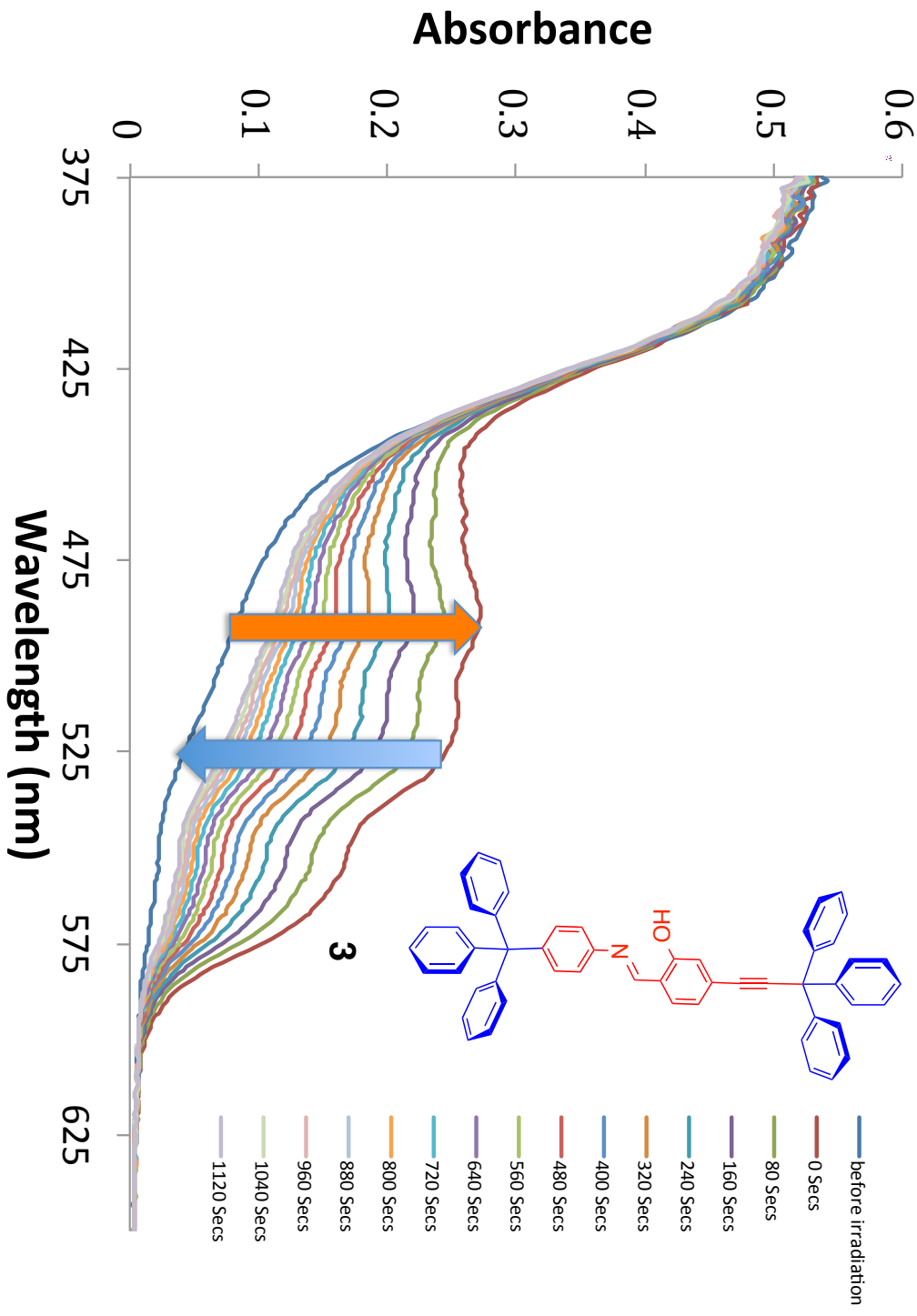

Figure S34. Diffuse Reflectance of Salicylidine Aniline Rotor **3**

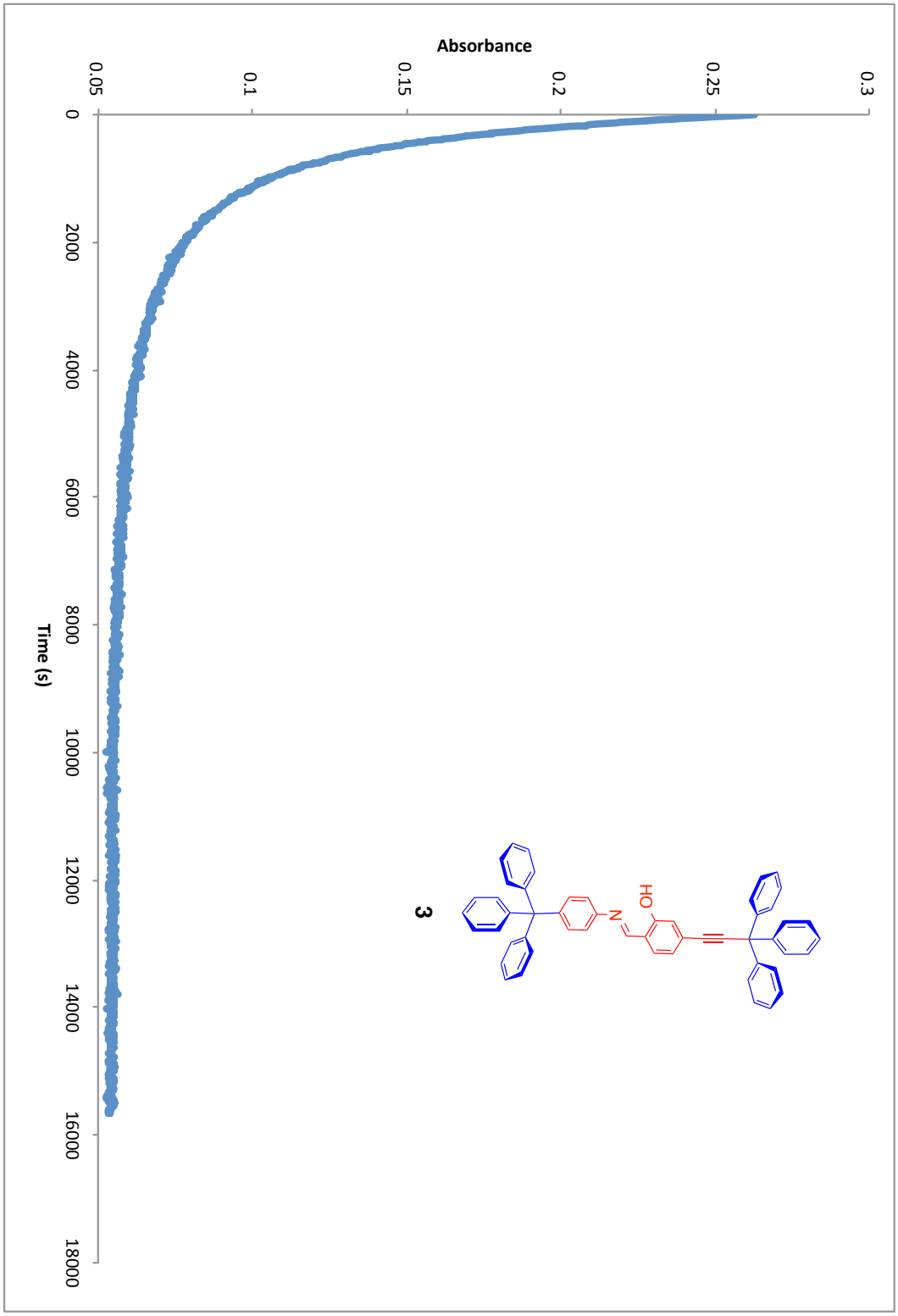

Figure S35. Diffuse Reflectance Lifetime of Salicylidine Aniline Rotor **3**

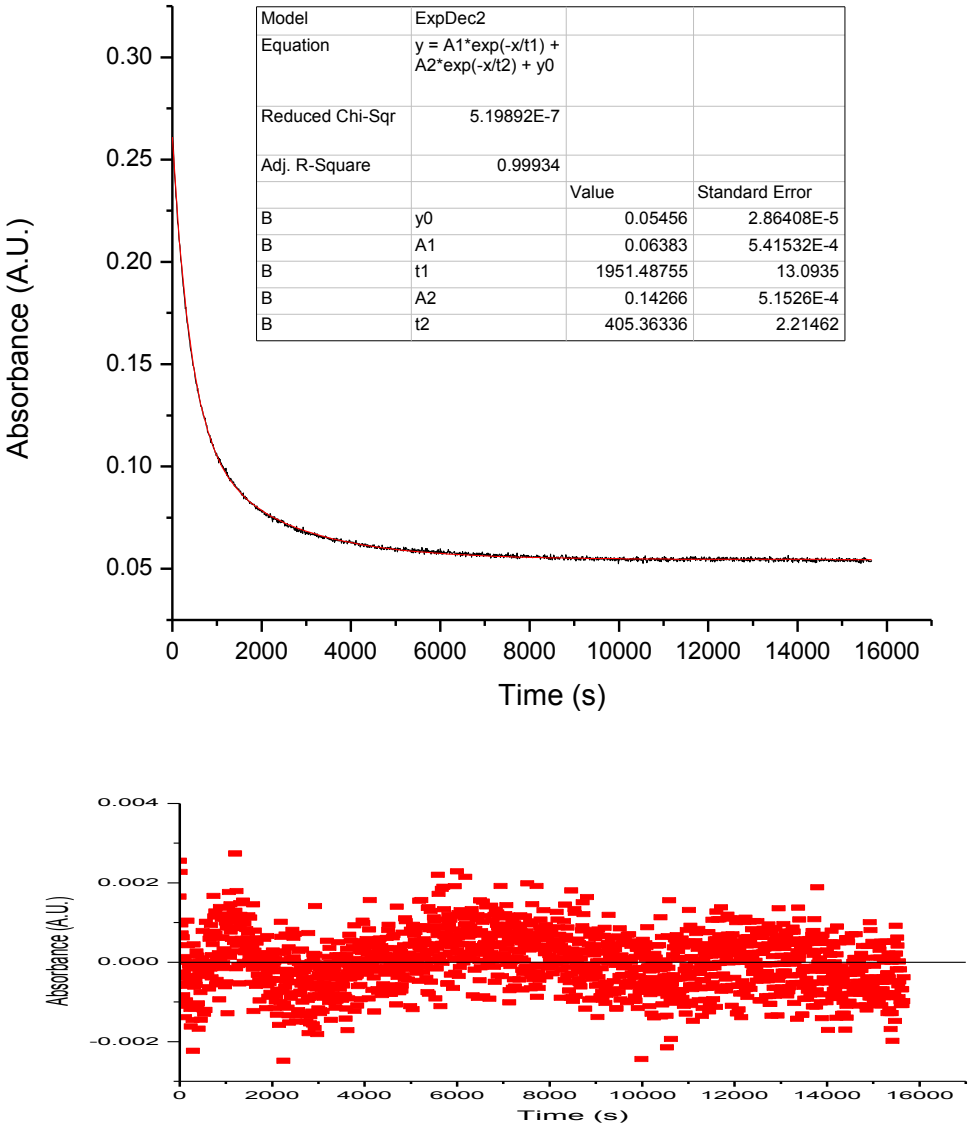

Figure S36. Diffuse Reflectance Lifetime of Salicylidine Aniline Rotor **3**

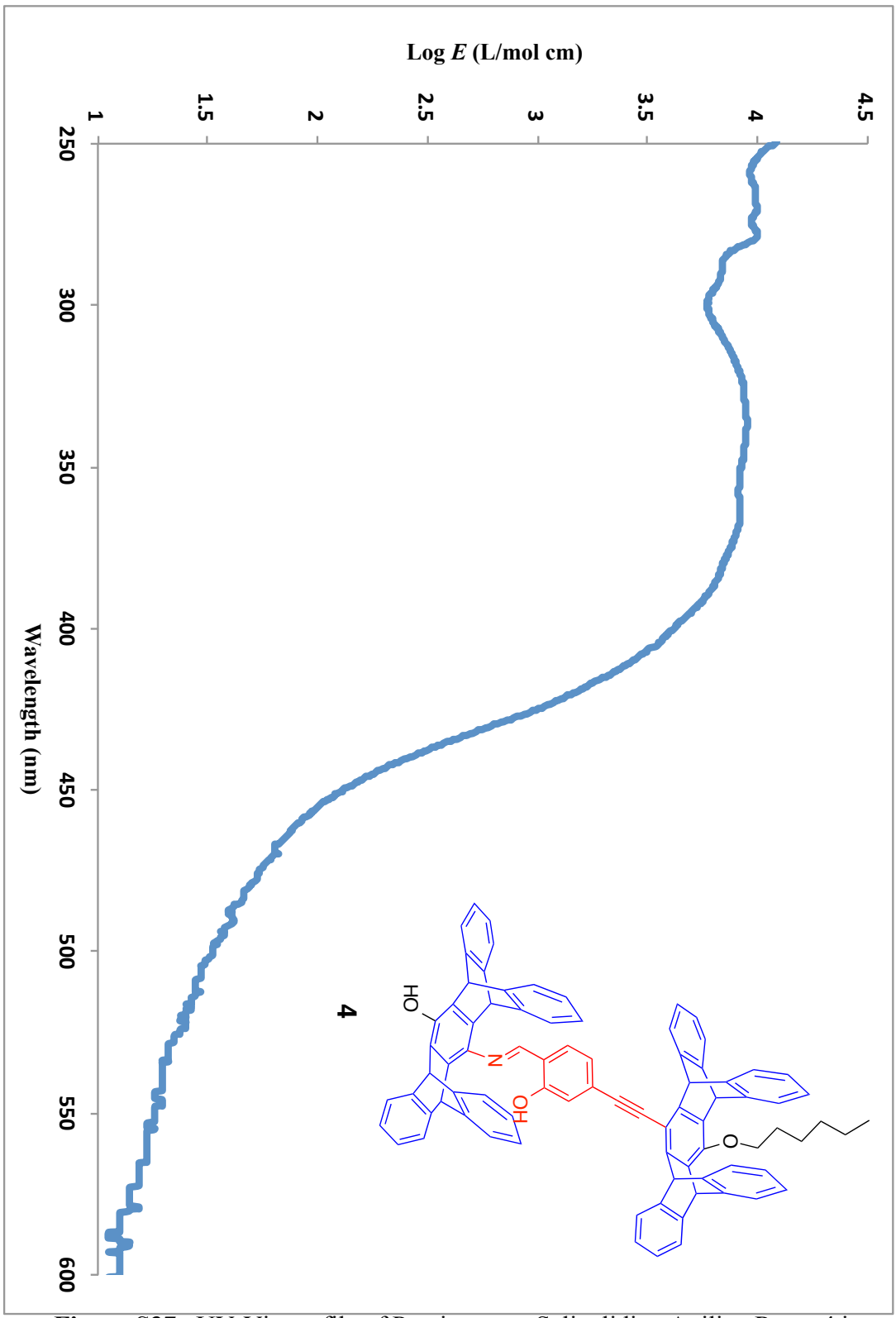

Figure S37. UV-Vis profile of Pentiptycene Salicylidine Aniline Rotor **4** in dichloromethane

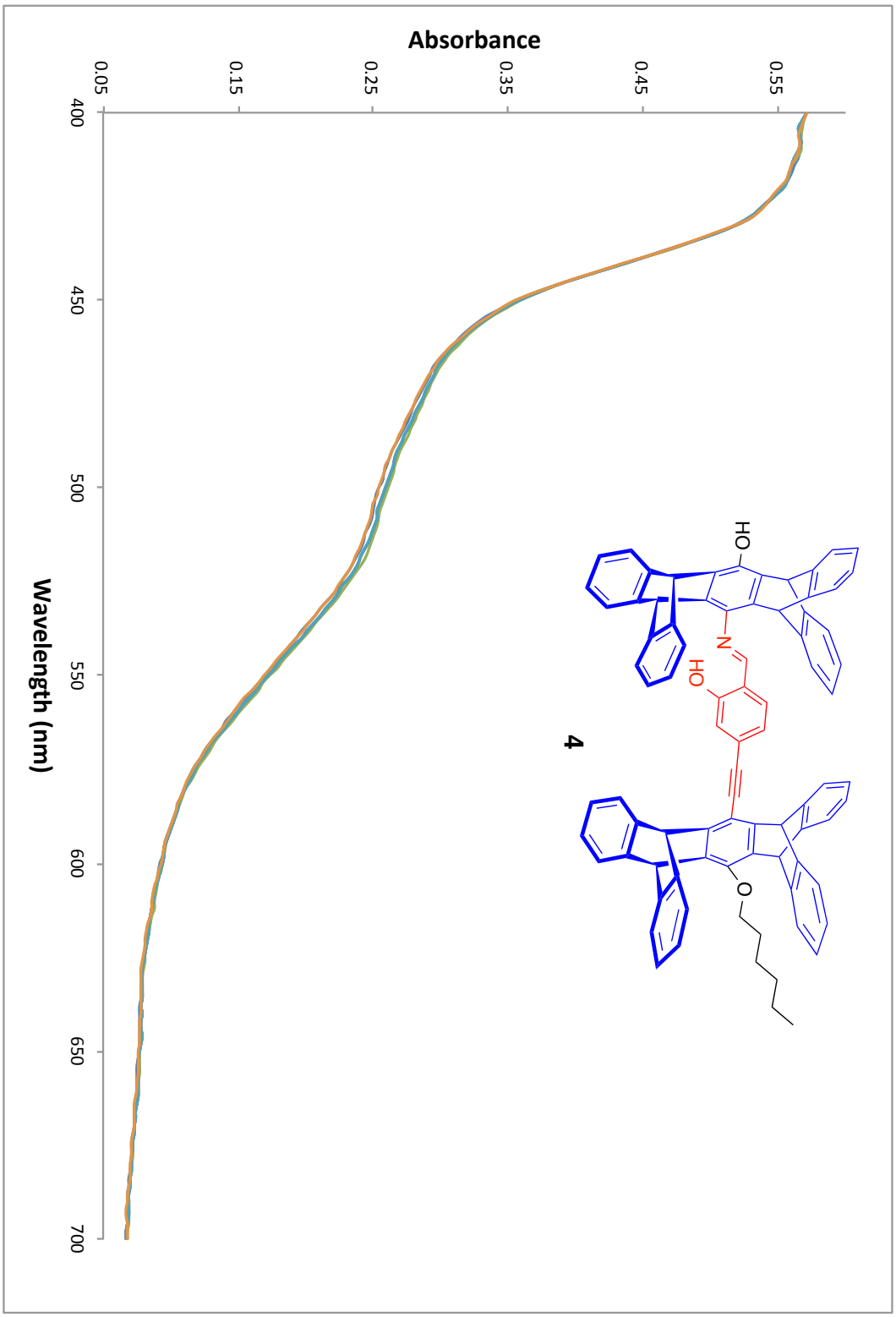

Figure S38. Diffuse Reflectance of Pentiptycene Salicylidine Aniline Rotor **4**

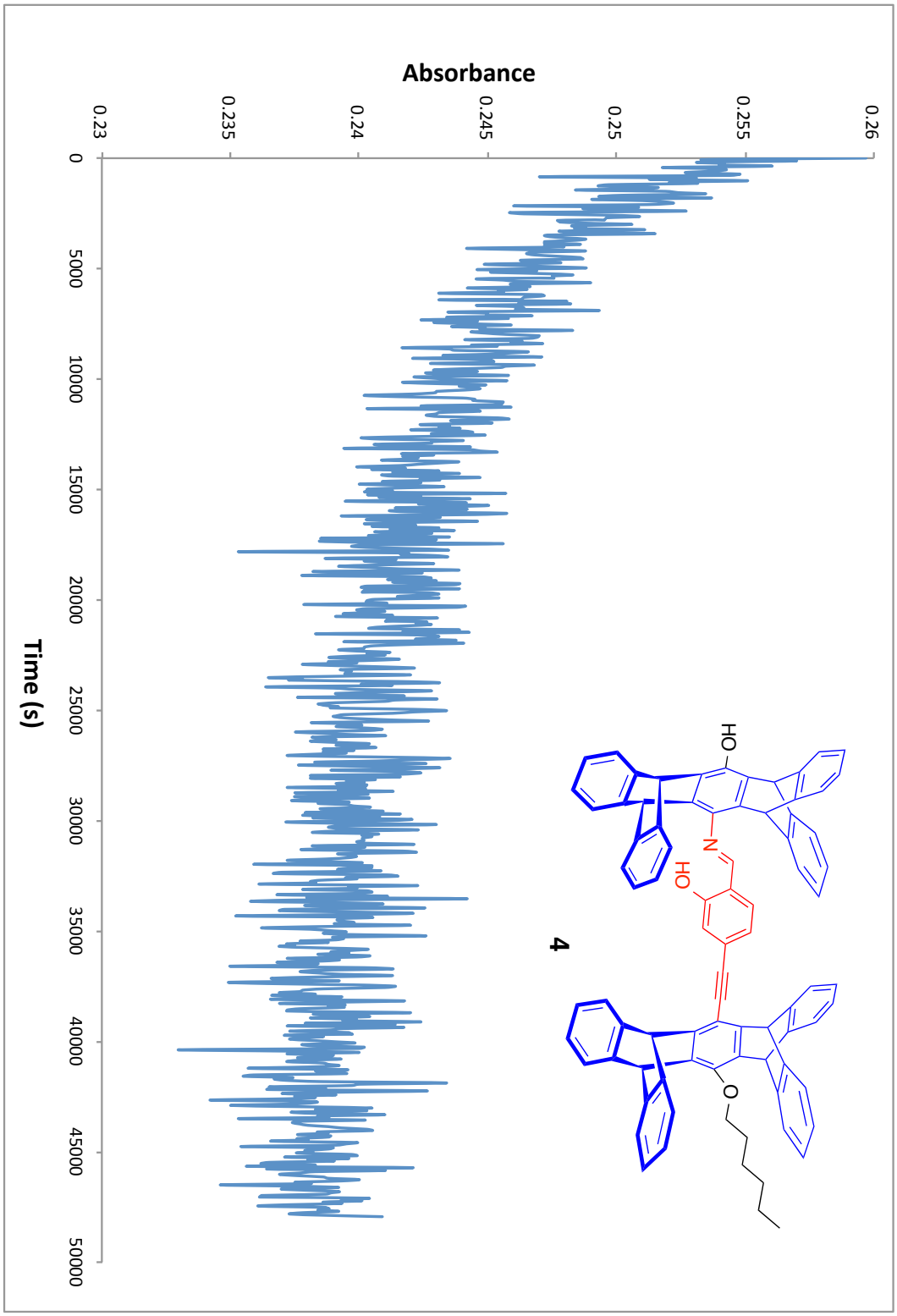

Figure S39. Diffuse Reflectance Lifetime of Pentiptycene Salicylidine Aniline Rotor **4**

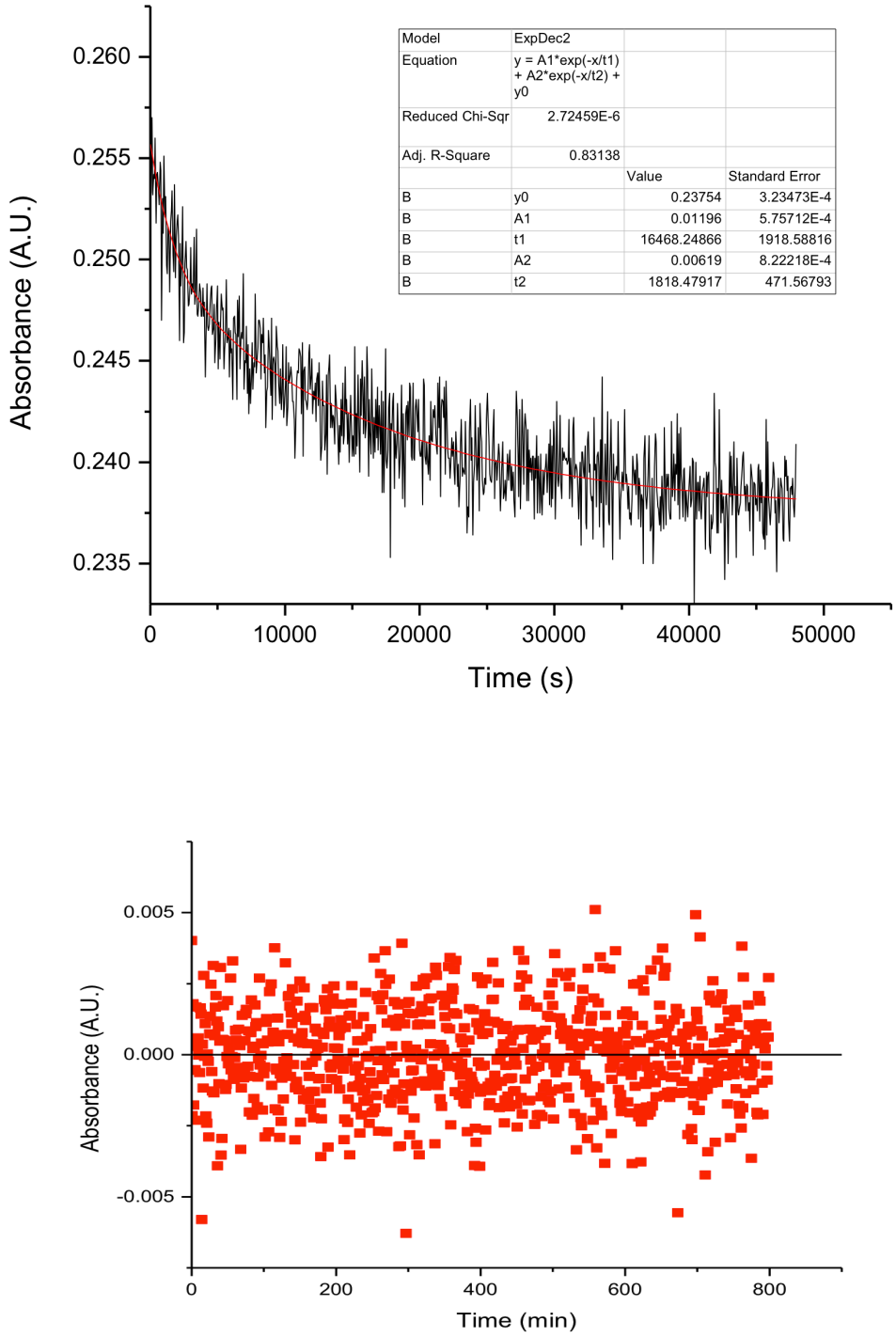

Figure S40. Diffuse Reflectance Lifetime of Pentiptycene Salicylidine Aniline Rotor **4**

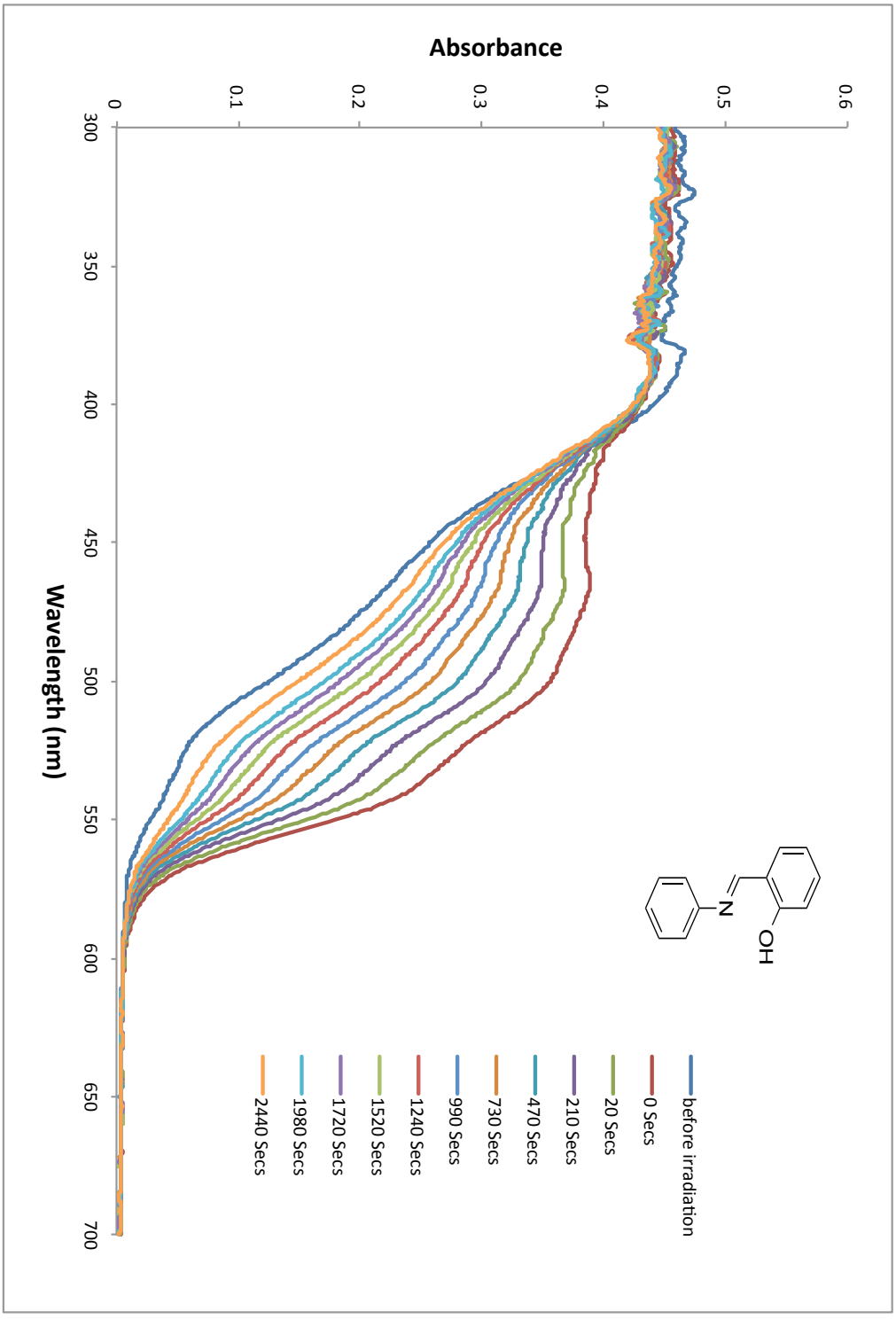

Figure S41. Diffuse Reflectance of Salicylideneaniline

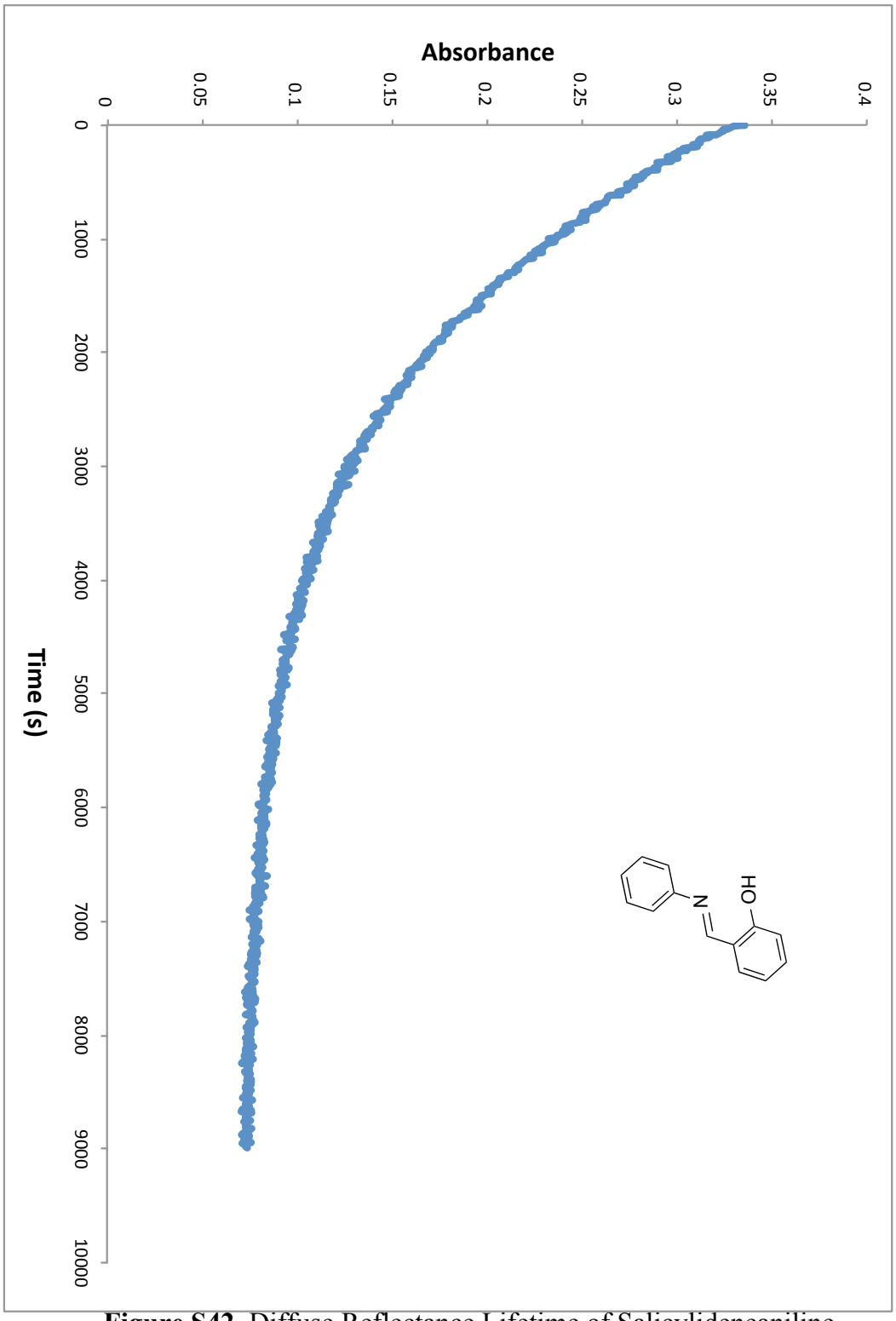

Figure S42. Diffuse Reflectance Lifetime of Salicylideneaniline

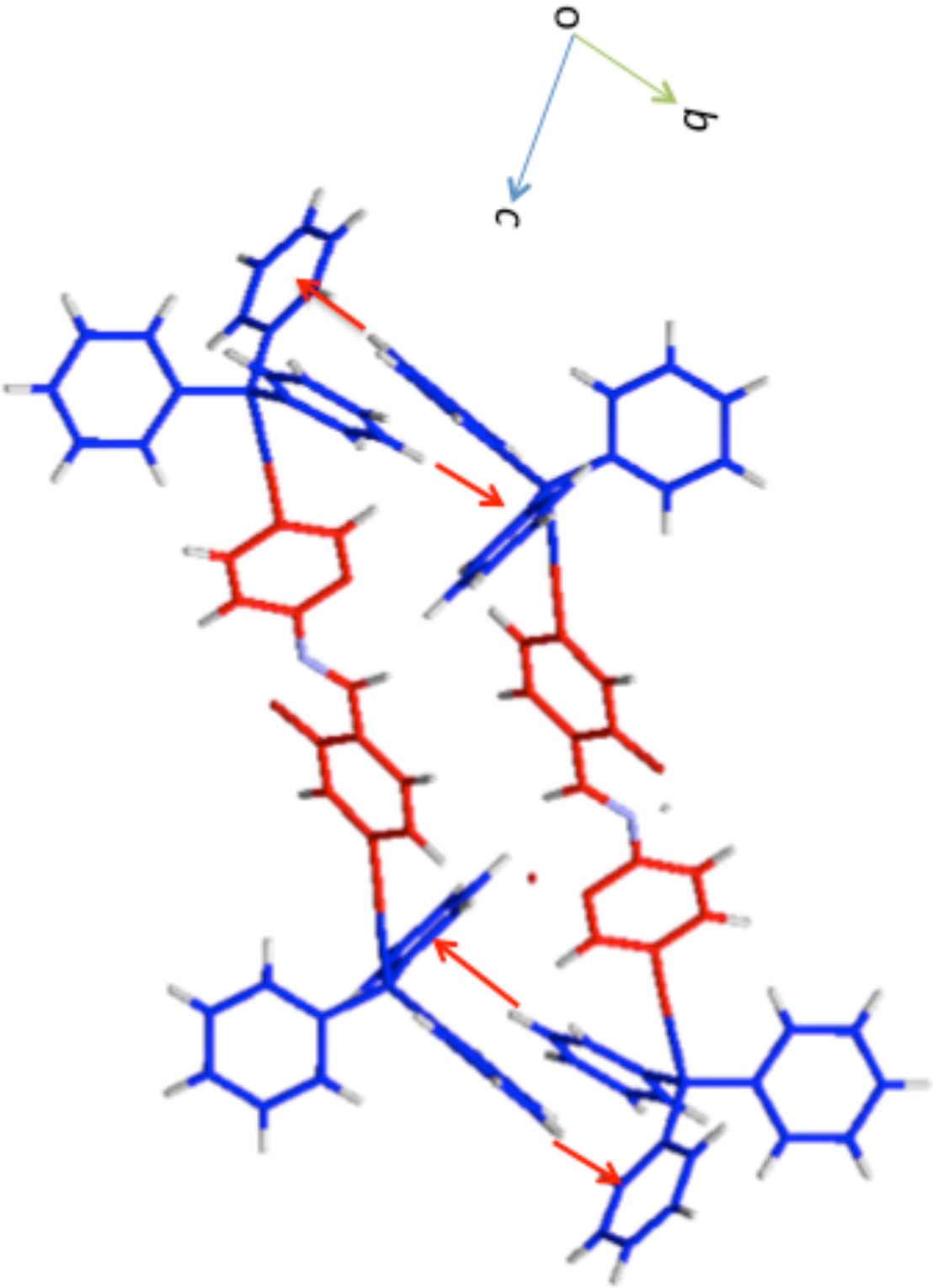

Figure S43. Crystal Structure of Salicylidine Aniline Rotor **2**

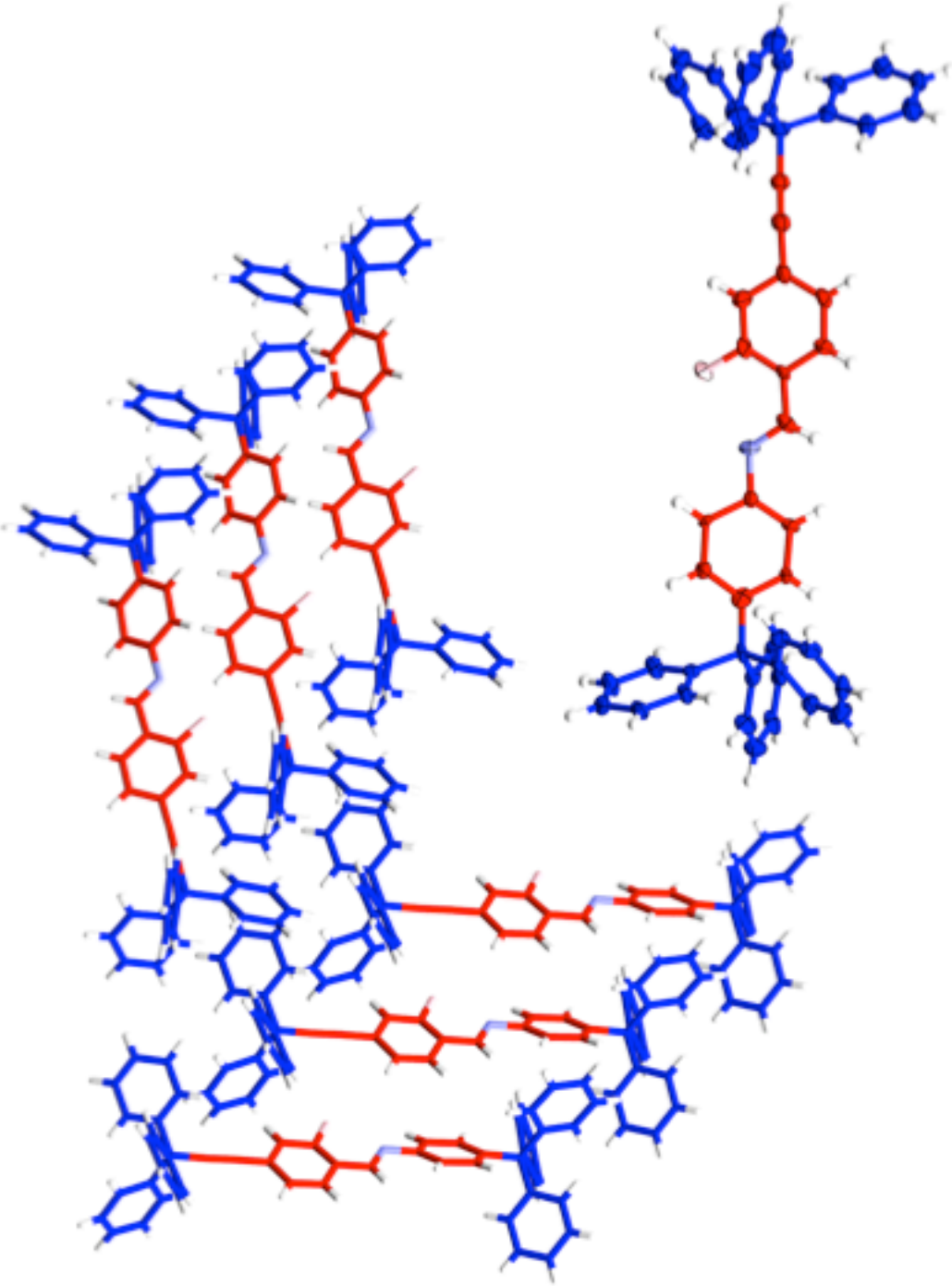

Figure S44. Crystal Structure for the Salicylidine Aniline Rotor **3**

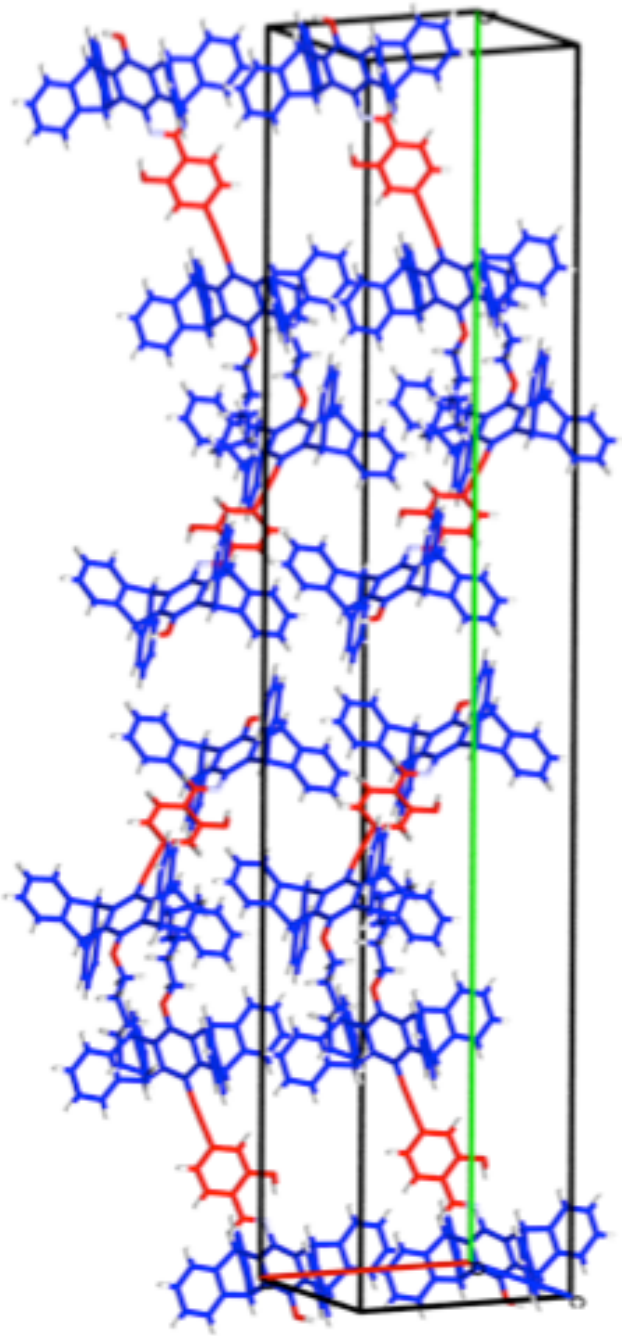

Figure S45. Crystal Structure for the Pentiptycene Salicylidine Aniline Rotor **4**

Table 1. Crystallographic parameters for the photochromic rotors.

	Compound 2	***Compound 3***	***Compound 4***
Emp. Formula	$C_{55}H_{38}NO$, CH_2Cl_2	$C_{53}H_{38}NO$, C_6H_{12}	$C_{83}H_{59}NO_3$, $5(C_2H_3N)$
Formula Wt.	813.79	789.00	1323.58
Crystal system	Triclinic	Monoclinic	Monoclinic
Space group	*P*-1	*C*2	$P2_1/c$
Z	2	4	4
Habit	platelet	needle	platelet
Crystal size [mm]	0.4x0.3x0.2	0.5x0.06x0.02	0.3x0.2x0.07
Temp [K]	100(2)	100(2)	100(2)
a [Å]	9.5933(5)	16.274(10)	11.7103(3)
b [Å]	9.7950(5)	7.323(5)	67.481(2)
c [Å]	23.4843(13)	36.49(2)	9.4377(3)
α [°]	99.6520(10)	90	90
β [°]	94.1840(10)	94.220(8)	104.188(2)
γ [°]	100.5880(11)	90	90
V [$Å^3$]	2126.2(2)	4336.86	7230.4(4)
ρ [Mg m^{-3}]	1.271	1.208	1.216
F(000)	850	1676	2792
Total reflections	12027	4811	12750
Indep. reflections	9820	3193	10590
$R_{(int)}$	0.0575	0.1385	0.0773
R_1 [I>2σ(I)]	0.0449	0.0943	0.0654
wR_2 (all data)	0.1181	0.2398	0.1793
Largest diff. peak/hole [e $Å^{-3}$]	0.347/-0.361	0.700/-0.341	0.587/-0.447

Listed below are the neighboring values corresponding to Table 1 from the paper.

Neighbors in Compound **2**

	(4) Schiff-base molecules	(1) Solvent
Contacts (Å):	2.943	2.555
	2.929	2.509
	2.832	
	2.693	
	2.453	
	2.297	

Neighbors in Compound **3** -Major conformer

	(2) Schiff-base molecules	(1) Solvent
Contacts (Å):	2.847	2.847
	2.725	2.346
	2.459	
	2.346	
	2.314	

Neighbors in Compound **4**

	(1) molecule (alkyl chain)	(4) Solvent
Contacts (Å):	2.765	2.899
	2.729	2.742
		2.721
		2.555
		2.370

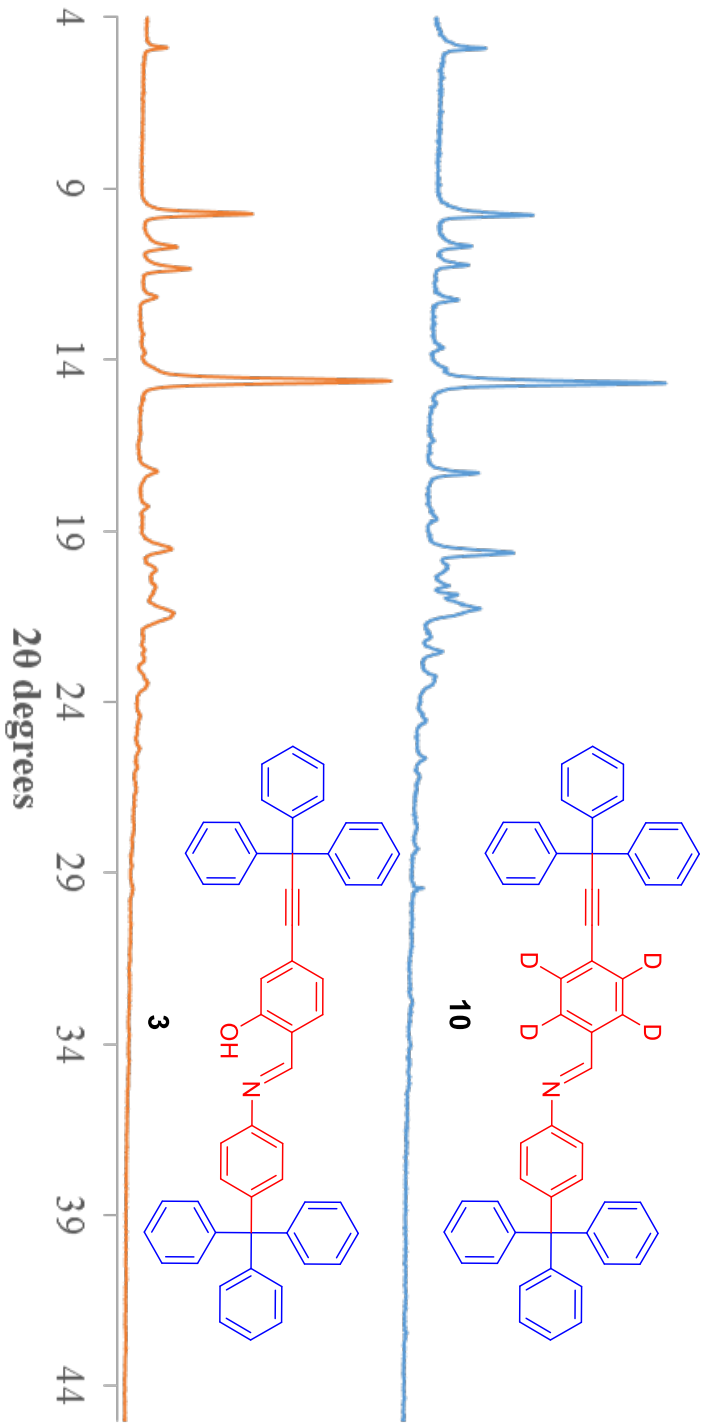

Figure S46. PXRD comparing **10** to **3** indicating isomorphic crystals

2.9. References

[1] a) Hadjoudis, E.; Mavridis, I. M. *Chem. Soc. Rev.* **2004**, *33*, 579. b) Irie, M. *Chem. Rev.* **2000**, *100*, 1683; c) Heinz Dürr, H.; Bouas-Laurent, H., Eds., Photochromism: Molecules and Systems, Elsevier, Amsterdam, 2003

[2] a) Castet, F.; Rodriguez, V.; Pozzo, J.-L.; Ducasse, L.; Plaquet, A.; Champagne, B. *Acc. Chem. Res.* **2013**, *46*, 2656. b) Safin, D. A.; Robeyns, K.; Garcia, Y. *Cryst. Eng. Comm.* 2012, *14*, 5523. c)Delaire, J. A.; Nakatani, K. *Chem. Rev.* **2000**, *100*, 1817.

[3] a) Moorthy, J. N.; Mandal, S.; Mukhopadhyay, A.; Samanta, S. *J. Am. Chem. Soc.* **2013**, *135*, 6872. b) Bruder, F.-K.; Hagen, R.; Rolle, T.; Weiser, M.-S.; Facke, T. *Angew. Chem. Int. Ed.* **2011,** *50,* 4552. c) Feringa, B. L.; Jager, W. F.; Lange, B. De. *Tetrahedron* **1993**, *49*, 8267.

[4] a) Zhang, J.; Zou, Q.; Tian, H. *Adv. Mater.* **2013**, *25*, 378. b) Natali, M.; Giordani, S. *Chem. Soc. Rev.* **2012**, *41*, 4010. c) Byrne, R. J.; Stitzel, S. E.;Diamond, D. *J. Mater. Chem.* **2006**, *16*, 1332.

[5] a) Yamada, M.; Kondo, M.; Mamiya, J. I.; Yu, Y. L.; Kinoshita, M.; Barrett, C. J.; Ikeda, T. *Angew. Chem., Int. Ed*., **2008**, *47*, 4986. b) Commins, P.; Garcia-Garibay, M. A. *J. Org. Chem.* **2014**, 1611.

[6] a) Terao, F.; Morimoto, M.; Irie, M. *Angew. Chem. Int. Ed.* **2012**, *51*, 901. b) Uno, K.; Niikura, H.; Morimoto, M.; Ishibashi, Y.; Miyasaka, H.; Irie, M. *J. Am. Chem. Soc.* **2011**, *133*, 13558. c) Fukaminato, T.; Doi, T.; Tamaoki, N.; Okuno, K.; Ishibashi, Y.; Miyasaka, H.; Irie, M. *J. Am. Chem. Soc.* **2011**, *133*, 4984.

[7] a) Klajn, R. *Chem. Soc. Rev.* **2014**, *43*, 148. b) Liu, F.; Morokuma, K. *J. Am. Chem. Soc.* **2013**, *135*, 10693. c) Harada, J.; Kawazoe, Y.; Ogawa, K. *Chem. Commun.* **2010**, *46*, 2593.

[8] a) Bushuyev, O. S.; Tomberg, A.; Fris, T.; Barrett, C. J. *J. Am. Chem. Soc.* **2013**, 135, 12556. b) Kolpak, A. M.; Grossman, J. C. *Nano Lett.* **2011**, *11*, 3156.

[9] a) Koshima, H.; Matsuo, R.; Matsudomi, M.; Uemura, Y.; Shiro, M. *Cryst. Growth Des,* .**2013**, *13*, 4330. b) Harada, J.; Nakajima, R.; Ogawa, K. *J. Am. Chem. Soc.* **2008**, *130*, 7085. c) Amimoto, K.; Kawato, T. *J. Photochem. Photobiol. C Photochem. Rev.* **2005**, *6*, 207.

[10] Johmoto, K.; Sekine, A.; Uekusa, H. *Cryst. Growth Des.* **2012**, *12*, 4779.

[11] Johmoto, K.; Sekine, A.; Uekusa, H.; Ohashi, Y. *Bull. Chem. Soc. Jpn.* **2009**, *82*, 50.

[12] (a) Flynn, C. R.; Michl, J. *J. Am. Chem. Soc.* **1974**, *96*, 3280. (b) Migirdicyan, E.; Baudet, J. J. Am. Chem. Soc. **1975**, *97*, 7400.

[13] (a) Cohen, M. D.; Schmidt, G. M. J.; Flavian, S. *J. Chem. Soc.*, **1964**, 2041. (b) Bregman, J.; Leiserowitz, L.; Osaki, K. *J. Chem. Soc*. **1964**, 2086.

[14] a) Harada, J.; Uekusa, H.; Ohashi, Y. *J. Am. Chem. Soc*., **1999**, *121*, 5809. b) Harada, J.; Ogawa, K. *J. Am. Chem. Soc.,* **2001**, *123*, 10884.

[15] a) Kawato, T.; Koyama, H.; Kanatomi, H.; Tagawa, H; Iga, T. *J. Photochem.***1994**, *78*, 71. b) Kawato, T.; Kanatomi, H.; Koyama, H.; Igarashi, T. *J. Photochem.***1986**, *33*, 199. c) Kawato, T.; Koyama, H.; Kanatomi, H.; Isshiki, M. *J. Photochem.* **1985**, *28*, 103.

[16] a) Vogelsberg C S.; Garcia-Garibay, M.A. *Chem. Soc. Rev*., **2012**, *41*, 1892. b) Karlen, S.D.; Reyes, H.; Taylor, R.E.; Khan, S.I.; Hawthorne, M.F.; Garcia-Garibay, M.A. *Proc. Nat. Acad. Sci.*, **2010**, *107*, 14973. c) Khuong, T.-A.V.; Nuñez, J.E.; Godinez, C.E.; Garcia-

Garibay, M.A. *Acc. Chem. Res*. **2006**, *39*, 413-422. d) Garcia-Garibay, M.A. *Proc. Natl. Acad. of Sci*. **2005**, *102*, 10793

[17] a) Dominguez, Z.; Dang, H.; Strouse, M.J.; Garcia-Garibay, M.A. *J. Am. Chem. Soc*. **2002**, *124*, 2398. b) Dominguez, Z.; Dang, H.; Strouse, J.M.; Garcia-Garibay, M.A. *J. Am. Chem. Soc.* **2002**, *124*, 7719.

[18] Chinchilla, R.; Nájera, C. *Chem. Soc. Rev*., **2011**, 40, 5084.

[19] These samples were checked before and after irradiation however no additional IR stretches were observed.

[20] Yang, J.; Ko, C. *J. Org. Chem.* **2006**, *71*, 844.

[21] Long, T. M.; Swager, T. M. *J. Mater. Chem.* **2002**, *12*, 3407

[22] Johmoto, K.; Ishida, T.; Sekine, A.; Uekusa, H.; Ohashi, Y. *Acta Crystallogr. B* **2012**, *68*, 297.

[23] (a) Scudder, M.; Dance, I. *J. Chem. Soc., Dalton Trans.* **1998**, 329-344. (b) Scudder, M.; Dance, I. *Dalton* **2000**, 2909. (c) Dance, I.; Scudder, M. *New Journal of Chemistry* **1998**, *22*, 481. (d) Lacour, J.; Bernardinelli, G.; Russell, V.; Dance, I. *Cryst. Eng. Comm.* **2002**, 4, 165. (e) Stopin, A.; Garcia-Garibay, M. A. *Cryst. Growth Des.* **2012,** *12,* 3792.

[24] Mosca, L.; Koutník, P.; Lynch, V. M.; Zyryanov, G. V.; Esipenko, N. A.; Anzenbacher, P. *Cryst. Growth Des.* **2012** *12*, 6104.

[25] Although the thermochromism of **2**, **3** and **4** were not analyzed in detail, visual inspection of the three samples in this study displayed changes in color when the temperature is close to the melting point. Compounds **2** and **3** turned orange at ca. 200^{o}C and orange/red above 250^{o}C. Compound **4** is the orange/yellow at room temperature and develops a deeper red above 200^{o}C.

[26] Liang, Z.; Liu, Z.; Gao, Y. *Spectrochimica Acta A*, **2007**, *68*, 1231.

[27] (a) Robert, F.; Naik, A.D.; Tinant, B.; Robiette, R.; Garcia, Y. *Chem. Eur. J*. **2009**, *15*, 4327. (b) Kawato, T.; Kanaotim, H.; Amimoto, K.; Koyoma, H.; Shigemizu, H. *Chem. Letters*, ***1999***, 47.

[28] (a) Duer, M. J. Introduction to Solid-State NMR Spectroscopy, Blackwell Publishing, Oxford, 2004. (b) Hoatson, G.L.; Vold, R.L. *NMR Basic Princ. and Prog*., **1994**, *32*, 1. (c) Mantsch, H.H.; Saito, H. Smith, I.C.P. *Progr. NMR Spect*. **1977**, *11*, 211.

[29] Karlen, S.D.; Garcia-Garibay, M.A. *Topics Curr. Chem*. **2006**, *262*, 179.

[30] Macho, V.; Brombacher, L.; Spiess: H. W. *Appl. Magn. Reson.* **2001,** *20*, 405.

[31] Website accessed March 22, 2014: http://weblab.mpip-mainz.mpg.de/cgi-bin/weblab45/weblab.pl?weblab=init&version=4.5

[32] (a) Schmidt, C.; Kuhn, J.; Spiess, H. W. *Progr. Colloid Polymer Sci.* **1985**, *71*, 71. (b) Fischer, E. W. Hellmann, G. P.; Spiess, H. W.; Hörth, F. J.; Gearius, U.; Wehrle, M. *Makromol. Chem. Suppl.* **1985**, *12*, 189.

[33] Very large pre-exponential factors for rotation have been observed also for glassy samples above the glass transition temperature: Vogelsberg, C.S.; Bracco, S.; Beretta, M.; Comotti, C.; Sozzani, P.; Garcia-Garibay, M.A. *J. Phys. Chem. B*., **2012**, *116*, 1623.

[34] Cohen, M.D. *Angew. Chem. Int. Ed*. **1975**, *14*, 386.

[35] The structural similarities between the *cis*-enol and the *trans*-keto form obtained by either ring rotation of bicycle pedal motion were determined by comparing the RMSD measurements of the structures for each pair using Mercury 3.3.

[36] Katritzky, A. R.; Akhmedov, N. G.; Güven, A.; Doskocz, J.; Akhmedova, R. G.; Majumder, S.; Dennis Hall, C. *J. Mol. Struct.* **2006**, *787*, 131–147

Chapter 3

Advances in the Functionalization of Crystalline Rotors with Photoresponsive Properties as Potential Molecular Brakes: Amino Rotors

3.1. Introduction

Artificial molecular machines have drawn the interest of chemists for the last 20 years. In particular, some research groups focus on the design and synthesis of molecules that can be switched from one state to another with suitable external stimuli in order to display function.[1] Research in our group has focused on the synthesis of "amphidynamic crystals,"[2] which are designed to have motion in a highly anisotropic manner and within a well-defined frame of reference, which should be ideal for the development of artificial molecular machines. Our group thus focuses on molecular gyroscopes, which possess these characteristics on the molecular level and act as amphidynamic crystals when in a crystalline array. These compounds emulate macroscopic molecular rotors and are composed of three components.

A rotator is the rotating component or the component with the smallest moment of inertia, which is generally a 1,4-substituted phenylene, on the molecular level. The stator is the static portion or the component with the largest moment of inertia, which is generally a triarylmethyl, on the molecular level. Lastly, the axle[3] is the component that links the rotator to the stator and is emulated using two alkynyl linkages on the molecular level. Recently, our group tried to introduce further functionality into the molecular rotor framework.[4,5] Photoresponsive bridged molecular rotors were synthesized and were shown to impede the rotation of the rotator, with visible light acting as a simple molecular brake.[4] As previously shown in Chapter 2, Salicylideneanilines (SA) were introduced into the rotator. In this

respect, we decided to synthesize and study how the introduction of SAs on the stator portion of the gyroscope could affect the rotation of the compound. The ability to modify the rotational dynamics of the molecule with an external stimulus might allow for further functionalization into advanced material applications.[5] Figure 1a illustrates a simplified SA modified rotor and the three tautomeric forms that it can explore, with the *trans*-keto potentially acting as a molecular brake to inhibit rotation of the central phenylene in the solid state.

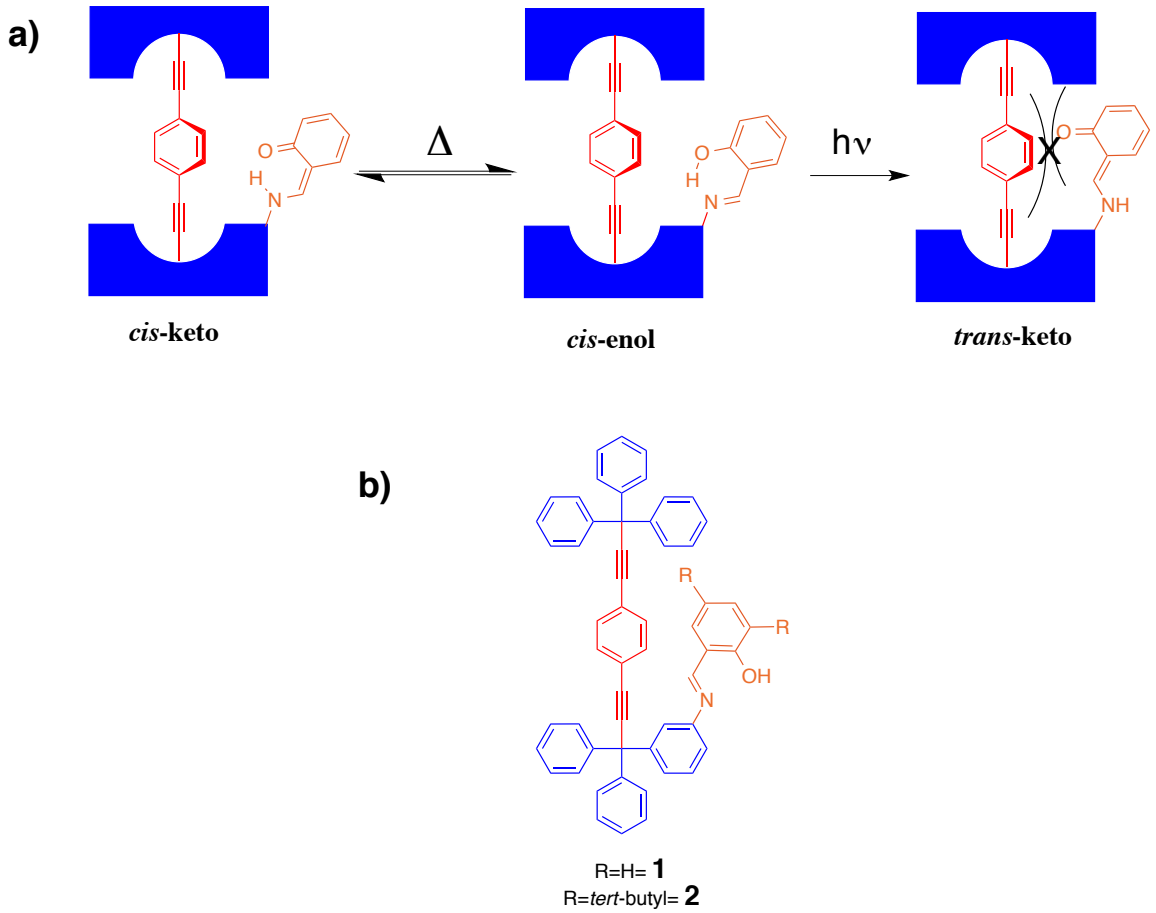

Figure 1. a) Simplified molecular rotor functionalized with a photoresponsive moiety, which upon irradiation may impede the rotation of the central phenylene in the crystalline state. b) Functionalized SA rotors **1** and **2**.

We report here the synthesis, characterization, crystallization and photochromic behavior of two molecular rotors with SA[6]-functionalized stators **1** and **2,** illustrated in Figure 1b.

3.2. Synthesis and Characterization

The synthesis of salicylideneaniline rotors **1** and **2** was achieved using a common intermediate rotor amine **5**. In order to synthesize **5,** we started from the previously reported monohydroxy substituted rotor,[7] which we reacted with trifluoromethanesulfonic anhydride and pyridine in dichloromethane for 12 h to afford monotriflate rotor **3** in a 90% yield, shown in Scheme 1.

Scheme 1.

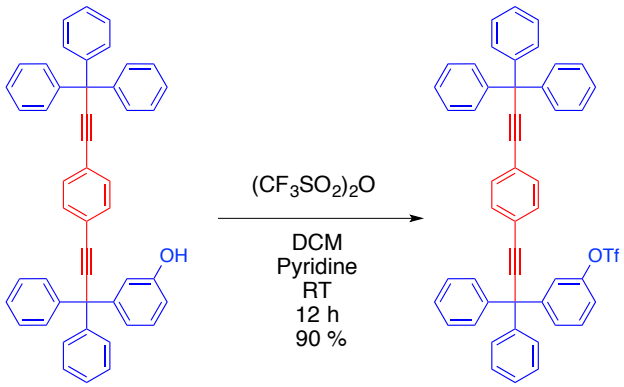

3

Rotor **3** was then coupled using Buchwald-Hartwig amination[8] conditions. These conditions utilize benzophenoneimine as the amine source along with palladium (II) acetate, BINAP, and cesium carbonate in tetrahydrofuran for 24 h at reflux to afford mono-benzophenoneimine rotor **4** in 55% yield. Rotor **4** was not purified and was submitted to sodium acetate, hydroxylamine hydrochloride in methanol at room temperature for 1 h to afford monoamino rotor **5** in 95% yield, shown in Scheme 2.

Scheme 2

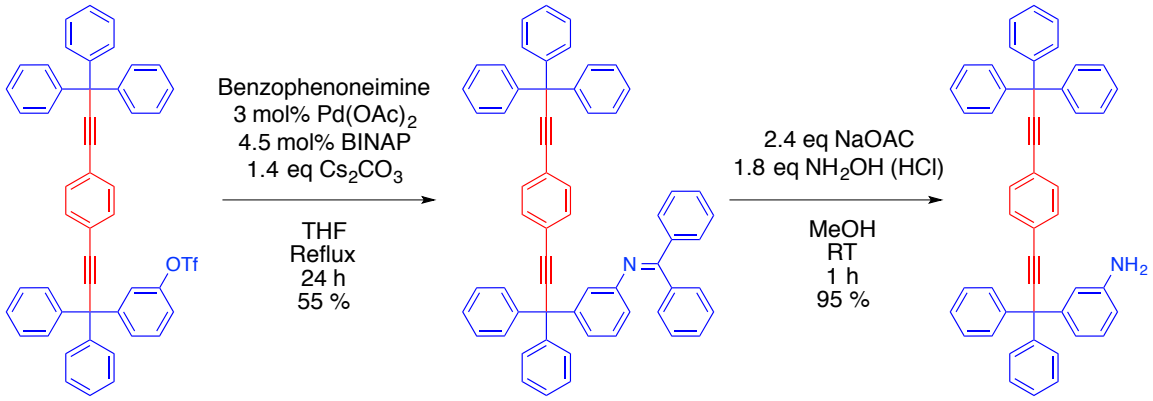

3 **4** **5**

With monoamino rotor **5** in hand, salicylaldehyde and 3,5-di-tert-butylsalicylaldehyde were selected for condensation with photochromism in the final product in mind. Salicylaldehyde and 3,5-di-tert-butylsalicylaldehyde were selected. Monoamino rotor **5** was reacted with the selected salicylaldehyde and 4 A molecular sieves to facilitate the dehydration in refluxing toluene for 24 h to afford **1** and **2** in 85% yield, as shown in Scheme 3.

Scheme 3

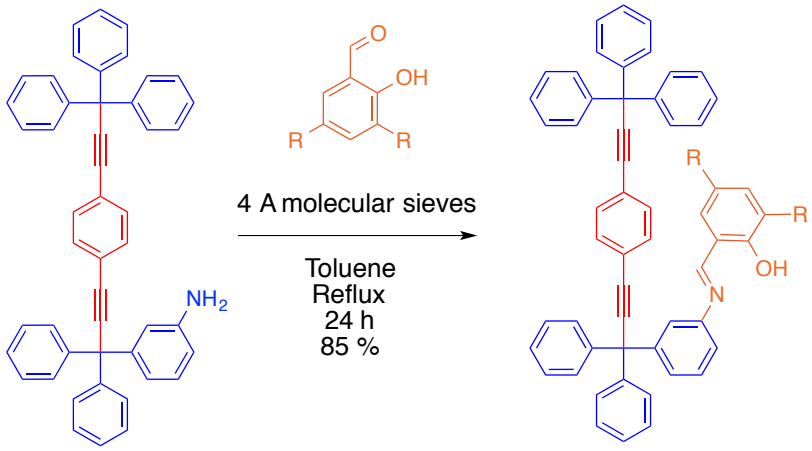

5

R=H= **1**
R=*tert*-butyl= **2**

The ^{1}H NMR spectra of **1** and **2** have the characteristic signals of the aldimine hydrogens, with chemical shifts of 8.53 ppm for **1** and 8.84 and 8.83 ppm for **2** (both integrate to one proton in relation to four protons for the central phenylene). The phenol hydrogens are located at 13.14 and 13.62 ppm for **1** and **2** respectively. The central phenylenes showed characteristic signals at 7.45 for **1** and 7.60-7.53 for **2**.

Their corresponding ^{13}C NMR spectra showed the signals of the aromatic hydroxyl-bearing carbon at 161.0 and 158.2 ppm, respectively, with the imine carbons at 163.0 and 164.1 ppm. Four signals in the range of 84 and 98 ppm, in both cases, corresponded to the two distinct alkynes in the molecules. The signal at 56.18 corresponded to the two quaternary trityl carbon atoms in the case of **1**, while the corresponding values in the case of **2** were 56.17 and 56.2 ppm. In addition to having several signals doubled, compound **2** also had two aldimine protons, which we assumed corresponded to different conformations in solution and tentatively ascribed to different rotamers.[9]

These two rotameric forms exist in equilibrium and could be confirmed by changing the polarity of the solvent, which perturbed the intensity ratio of the corresponding signals. Figure 2 illustrates three of the possible forms that we believed could be observed. Figure 2a shows the resulting rotamer from a rotation of the trityl ring bearing the salicylideneanilne. Figure 2b shows the resulting form due to a C-N bond rotation in solution. These two distinct pathways could give rise to different structures that present different aldmine protons, however, rotation of the trityl ring seemed to be more plausabile because of vastly different

environments that would be experienced with the shielding of the central phenylene, compared to no apparent shielding in solution.

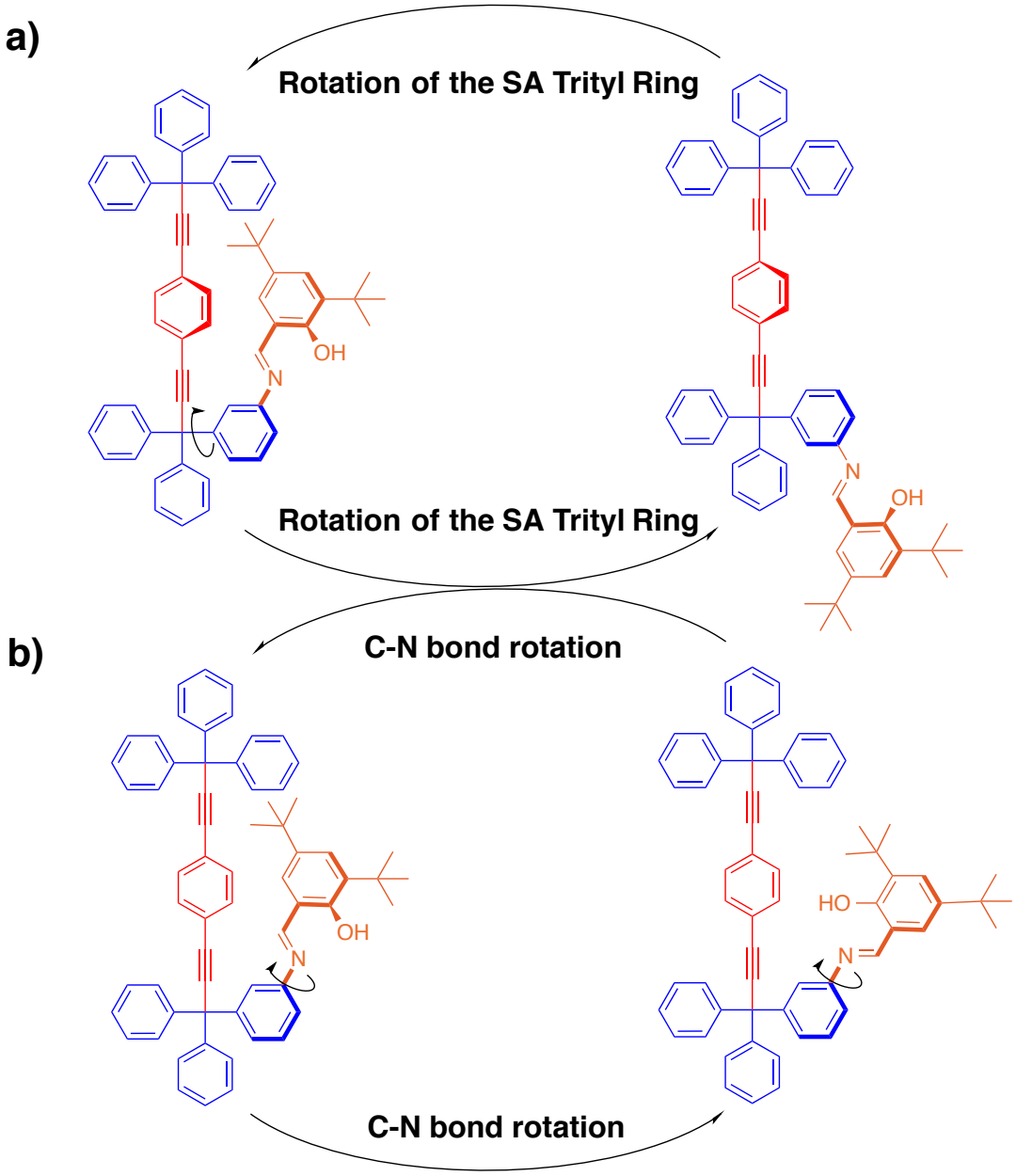

Figure 2. a) Due to two imines being seen in ^{1}H NMR and the corresponding ratios changing with polarity, it was determined that rotamers existed in solution. b) The

other potential form could be C-N bond bond rotation, resulting in two slightly different environments for the aldimine proton.

The FTIR spectra of solids **1** and **2** had a very broad signal that spanned from ca 3200-2400 $cm^{-1,}$ attributed to the O-H stretch and a signal at ca. 1664 cm^{-1} assigned to the imine stretch.

3.3. Crystallization Studies

Crystallization studies for compounds **1**-**2** were carried out at room temperature using different dry solvents and solvent mixtures. The selection of solvents was based on sample solubility and on the stability of the imine groups. Samples were soluble in chloroform, dichloromethane, toluene and xylenes, but had low solubility in acetonitrile and hexanes. Traces of water in methanol and ethanol caused the slow hydrolysis of **1** and these solvents were avoided. In a typical experiment, *ca.* 15 mg of the selected compound was placed in a small glass vial, dissolved with the appropriate solvent or solvent mixture (ca. 1 mL), and capped. Samples were monitored regularly until the first crystals appeared. Compounds **1**-**2** did not seem to give single crystals under a variety of different crystallization conditions. Instead apparent spherulitic[10] formation from slow evaporation was observed, as shown in Figure 3.

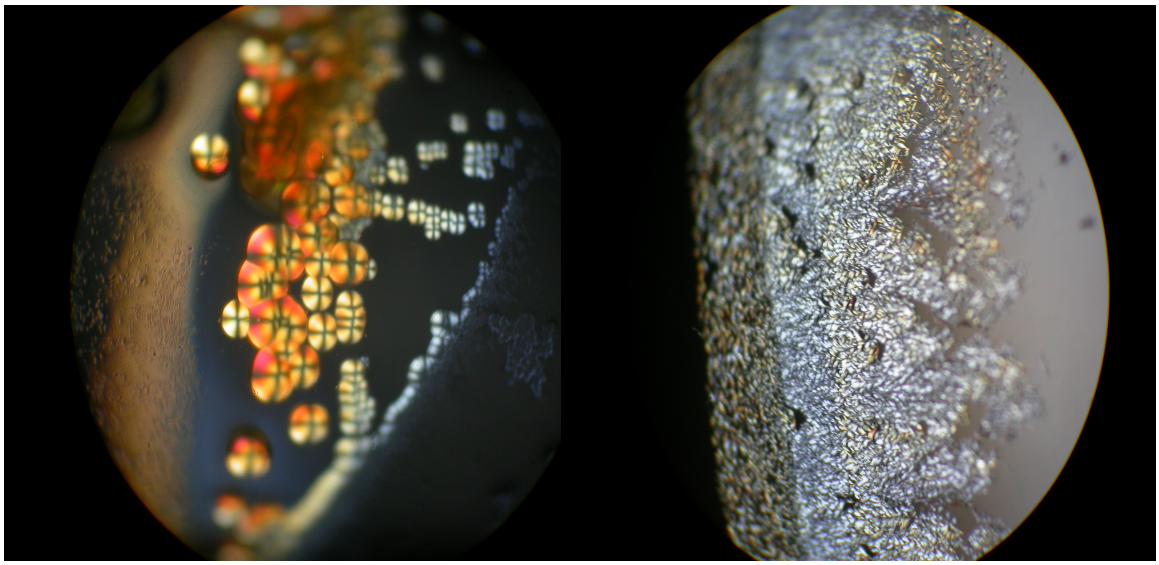

Figure 3. Compound **1** (left) showing a field of spherulites exhibiting maltese crosses under cross polarizers (black cross) grown from acetonitrile and compound **2** (right) showing what we ascribe to twisted spherulites under cross polarizers grown from $CDCl_3$.

Sphereulites formed from compound **1** appeared to have radial symmetry around a central nucleation site. Under polarized light, the spherulites of **1** exhibited a maltese cross, which in response to the rotation of polarized light rotated the cross respectively. The twisted spherulites grown from **2** tended to form three-dimensional aggregates (see appendix), which occurred during the evaporation process. Since these crystals did not diffract well enough to obtain a single crystal structure, because of their relatively small size and disorder, it was determined that their photoresponsiveness should be tested.

3.4. Solid State Photochromism

As previously mentioned above, the ^{1}H NMR, ^{13}C NMR, and IR spectra were consistent with the stable *cis*-enol as the predominant form. In order to determine the relative contributions of the *cis*-enol and *trans*-keto forms of SA molecular rotors

1-**2**, spectroscopic measurements were carried out using UV-Vis diffuse reflectance before and after exposure to UV light.

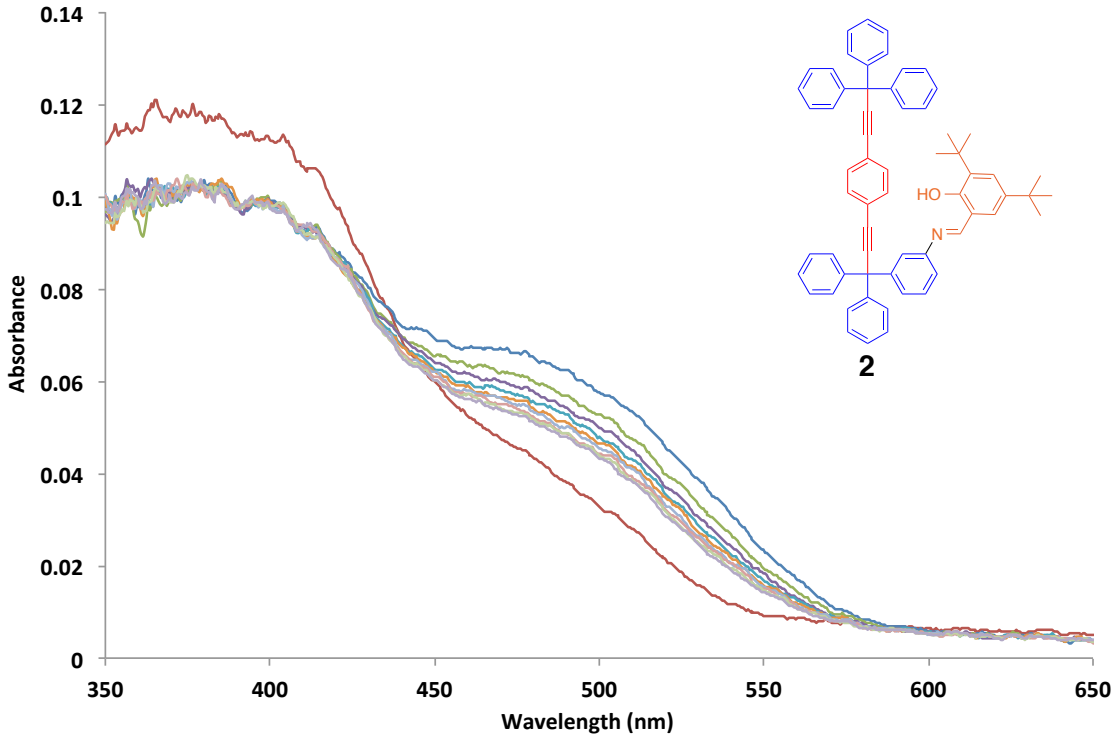

Figure 4. Optical absorption from the Kubelka-Monk function analysis of diffuse reflectance measurements of **2** obtained immediately after irradiation with hv=365 nm. Red line before irradiation and blue immediately after irradiation.

Well-characterized polycrystalline powders were placed onto a barium sulfate plate, pressed, and their diffuse reflectance measured before irradiation, with 365 nm UV light for 15 min at 300 K. After that, as illustrated in Figure 4 for the case of compound **2**, diffuse reflectance measurements of the photogenerated *trans*-keto form were carried out over time scales that ranged from 550 s (ca 10 min) to 4,500 s (ca. 1 h). The spectrum of compound **1** was characterized by an absorption band that extended from ca. 270-450 nm with a λ_{max} at ca. 380 nm that could be assigned to the *cis*-enol. A weak shoulder in the range of 450-550 was

assigned to the small equilibrium concentrations of the *cis*-keto form. Exposure to 365 nm UV light resulted in the growth of a broad band that extended up to 550 nm with a λ_{max} at ca. 500, with an absorbance increased by a factor of 1.28 from 0.039 to 0.050±0.001. This band was assigned to the *trans*-keto form, which decays thermally in a manner that can best be described by a biexponential function with components having lifetimes of 26.6±4 s and 211±25 s, respectively. The solid state spectra obtained from compound **2** (Figure 4) were similar to those of **1**. Before irradiation, the spectrum had a λ_{max} at 376 nm and a weak shoulder that extended to ca. 600 nm, which we tentatively assigned, respectively, to the *cis*-enol and the *cis*-keto forms. Exposure to UV light resulted in the growth of a new broad, vibrationally resolved absorption band between ca. 425-575 nm, with a 1.8-fold increase in absorbance from 0.033 to 0.061±0.001 at 500 nm (Figure 4). The lifetime for **2** was also fit to a biexponential function, with a fast component of 168±7 s and a slow component of 1777±57 s.

3.5. Conclusions

In conclusion, we synthesized and fully characterized two molecular rotors with salicylideneaniline stators. The photoresponsiveness in the crystal was partially explored, but, due to the lack of single crystal x-ray analysis, the interaction between the stator photochrome and the rotator could not be determined. The poor crystal quality was attributed to asymmetry in the molecule, in addition to two rotoamers of compounds **1** and **2**, which impeded single crystal growth and favored spherulitic formation. While both SA molecular rotors generated the colored *trans*-

keto tautomer upon irradiation with UV light, the extent of the photochromic reaction was significantly less then simpler SA chromophores.

3.6. Appendix

General Methods

The IR spectra were obtained with a Perkin-Elmer spectrum 100 HATR FTIR instrument. ^{1}H and ^{13}C NMR spectra were acquired on a Brüker NMR spectrometer at 400 and 100 MHz or 300 and 75 MHz, respectively, with $CDCl_3$ as the solvent. The NMR coupling constants were calculated using gNMR[11]. Mass spectra were acquired on an Applied Biosystems voyager-DE-STR MALDI-TOF. Solution UV-Vis measurements were taken on an Ocean Optics USB2000+ while solid-state diffuse reflectance measurements were taken on a UV-3101PC UV-Vis N/R Scanning Spectrophotometer. Samples for diffuse reflectance were placed on a barium sulfate plate and pressed. This was then irradiated, using a Rayonet Photochemical Reactor with 6-12 inch 8W (BLE-8T365) 365nm bulbs. A Coherent 405 nm CUBE laser was used to excite the solid in a NMR tube at both room temperature and 77K, and the subsequent emission spectra were monitored using a Princeton Instruments Roper CCD detector, which was cooled, to liquid nitrogen temperatures. The boron tribromide, trifluoromethanesulfonic, pyridine, acetyl chloride, 0.5 M ethynylmagnesium bromide in THF, benzophenone imine, Palladium (II) Acetate, BINAP, Cesium Carbonate, Sodium Acetate, Hydroxylamine Hydrochloride, diisopropylamine, CuI, bis(triphenylphosphine) palladium (II) chloride, potassium carbonate, tetra-n-butylammonium fluoride, salicylaldehyde, and 3,5-di-tert-butylsalicylaldehyde were commercially available and were used without further purification. THF and benzene were distilled from sodium and kept under argon. Toluene was distilled from calcium hydride and kept under argon.

Synthesis of Monosalicylideneaniline Rotor 1.

In a round bottom flask with a condenser adapted, under argon atmosphere, 100 mg of Monoamino Rotor **5** (0.16 mmol) powder were combined with 0.1 mL of salicylaldehyde (0.94 mmol). To the flask 4 A molecular sieves were added along with dry toluene (20 mL). The solution was then allowed to reflux 24 h. The reaction was worked up by filtering and then reduced under reduced pressure to yield a faintly yellow solid. This was then purified by column chromatography using silica gel and hexanes/dichloromethane (4:1) to afford 99 mg (85 %) of **1** as a faintly yellow solid m.p. 251-252 °C. ^{1}H NMR ($CDCl_3$) δ: 13.14 (s, 1H), 8.53 (s, 1H), 7.45 (s, 4H), 7.38–7.23 (m, 29H), 7.21 (ddd, *J* = 7.85 1.78, 1 Hz, 1H), 7.19 (ddd, *J* = 7.63, 2.13, 1 Hz, 1H), 6.99 (d, 8.5 Hz, 1H), 6.91 (td, *J* =7.75, 1 Hz, 1H). ^{13}C NMR ($CDCl_3$) δ: 163.0, 161.0, 146.9, 145.2, 144.8, 133.2, 132.3, 131.5, 131.4, 129.2, 129.1, 129.0, 128.2, 128.0, 128.0, 127.8, 127.1, 126.9, 123.4, 123.0, 122.0, 119.8, 119.1, 119.0, 117.2, 97.4, 96.9, 85.2, 84.8, 56.2. FTIR (powder, HATR, cm^{-1}): 3058, 1664, 1619, 1594, 1571, 1490, 1446, 1278. HRMS (ESI+, m/z) calculated for $C_{55}H_{39}NO$ = 729.30316, found 730.30802, error: -6.7 ppm.

Synthesis of ditertbutyl-Monosalicylideneaniline Rotor 2

In a round bottom flask with a condenser adapted, under argon atmosphere, 100 mg of Monoamino Rotor **5** (0.16 mmol) powder were combined with 100 mg of 3,5-di-tert-butylsalicylaldehyde (0.46 mmol). To the flask 4 A molecular sieves were added along with dry toluene (30 mL). The solution was then allowed to reflux 24 h. The reaction was worked up by filtering and then reduced under reduced pressure to yield a yellow solid. This was then purified by column chromatography using

silica gel and hexanes to afford 114 mg (85 %) of **2** as a yellow solid m.p. 255-256 °C. ^{1}H NMR ($CDCl_3$) δ: 13.62 (s, 1H), 8.84, 8.83 (s, 1H)(rotamers), 7.58 (ddd, $J_{Ab}=J_{A'B'}$= 8.00 Hz, $J_{AA'}=J_{BB'}$= 1.70 Hz, $J_{AB''}=J_{A'B}$=0.60 Hz 2H), 7.55 (ddd, $J_{Ab}=J_{A'B'}$= 8.00 Hz, $J_{AA'}=J_{BB'}$= 1.70 Hz, $J_{AB''}=J_{A'B}$=0.60 Hz 2H), 7.50–7.21 (m, 31H), 1.40 (s, 9H), 1.30 (s, 9H),^{13}C NMR ($CDCl_3$) δ: 164.1, 158.2, 148.8, 146.7, 145.2, 144.9, 140.6, 136.9, 131.5, 129.2, 129.1, 128.9, 128.2, 128.1, 127.3, 127.1, 126.9, 126.9, 123.3, 123.1, 122.1, 119.9, 118.2, 97.4, 97.1, 85.2, 84.8, 56.2, 56.2. FTIR (powder, HATR, cm^{-1}): 2956, 2869, 1647, 1617, 1586, 1506, 1466, 1439, 1362. HRMS (ESI+, m/z) calculated for $C_{63}H_{55}NO$ =841.42837, found 842.43122, error: -3.4 ppm.

Synthesis of Monotriflate Rotor 3.

In a round bottom flask, under argon atmosphere, 250 mg of monohydroxy rotor (0.4 mmol) was dissolved in 50 mL of dichloromethane. To this solution 141 mg of trifluoromethanesulfonicanhydirde (0.5 mmol) was added along with 3 mLs of pyridine. The resulting solution was allowed to stir for 12h. It was then worked up with (10 mL) of water, followed by (10 mL) of 1 M HCl, followed by (20 mL) of saturated sodium bircarbonate. This was then rinsed with (20 mL) of brine and separated and reduced under pressure. This was then purified by column chromatography using silica gel and hexanes:DCM (1:1) to afford 273 mg (90 %) of **3** as an off white solid m.p. 211-213 °C ^{1}H NMR ($CDCl_3$) δ: 7.46 (ddd, $J_{Ab}=J_{A'B'}$= 7.80 Hz, $J_{AA'}=J_{BB'}$= 1.70 Hz, $J_{AB''}=J_{A'B}$=0.50 Hz 2H), 7.44 (ddd, $J_{Ab}=J_{A'B'}$= 7.80 Hz, $J_{AA'}=J_{BB'}$= 1.70 Hz, $J_{AB''}=J_{A'B}$=0.50 Hz 2H) 7.41-7.15 (m, 27H).^{13}C NMR ($CDCl_3$) δ: 149.0, 148.2, 145.2, 144.1, 131.6, 129.7, 129.3, 129.2, 129.1, 129.0, 128.6, 128.3, 128.0, 127.4, 126.9, 123.6, 122.6, 122.3, 120.0, 119.9, 97.6, 95.9, 85.6, 84.7, 56.2, 56.0. FTIR

(powder, HATR, cm^{-1}): 3065, 3033, 1598, 1579, 1490, 1445, 1422, 1251. HRMS (ESI+, m/z) calculated for $C_{49}H_{33}F_3O_3S$ =758.21025, found 759.21413, error: -5.1 ppm.

Synthesis of Monoamino Rotor 5

In a round bottom flask, under argon atmosphere, 250 mg of full rotor triflate **3** (0.33 mmol) was dissolved in 50 mL of THF. To this solution 3 mol% $Pd(OAc)_2$, 4.5 mol% BINAP and 1.4 equivs of cesium carbonate were added. These were allowed to solubilize prior to the addition of 0.1 mL of benzophenone imine (0.60 mmol). The resulting solution was then heated to reflux for 24 h. The reaction was allowed to cool and worked up with (20 mL) of saturated ammonium chloride solution then isolated under reduced pressure to yield an off yellow solid. This solid was then taken onto the next step without further purification. The resulting solid was solubilized in 30 mL of MeOH and to the resulting solution 2.4 equivs. of sodium acetate and 1.8 equivs. of hydroxylamine hydrochloride. This was then allowed to stir for 1 h and worked up using (20 mL) of 0.1 M NaOH followed by (25 mL x 3) extractions with DCM. The resulting solution was dried over sodium sulfate, filtered and then isolated under reduced pressure. This was then purified by column chromatography using silica gel and hexanes:DCM (2:1) to afford 108 mg (52.3 %) of **5** as an off yellow solid over two steps m.p. 269-271 °C (decomposition) ^1H NMR ($CDCl_3$) δ: 7.44 (s, 4H), 7.38-7.22 (m, XH), 7.09 (ddd, *J* = 8.00, 0.80, 0.40 Hz, 1H), 6.67 ((ddd, *J* = 8.00, 1.80, 0.80 Hz, 1H) 6.66(ddd, *J* = 2.30, 1.80, 0.40 Hz, 1H), 6.59 (ddd, *J* = 2.30, 1.80, 0.40 Hz, 1H) 3.60 (s, 2H), ^{13}C NMR ($CDCl_3$) δ: 146.3, 146.0, 145.1, 145.1, 131.4, 131.3, 129.1, 129.1, 128.8, 128.0, 127.9, 126.8, 126.7, 123.2, 123.1, 119.7,

116.1, 113.6, 97.4, 97.2, 84.8, 84.6, 56.1, 53.3. FTIR (powder, HATR, cm^{-1}): 3029, 2960, 2921, 2856, 2366, 1725, 1683, 1549, 1445. HRMS (ESI+, m/z) calculated for $C_{48}H_{35}N$ =625.27695, found 626.28144, error: -7.1 ppm.

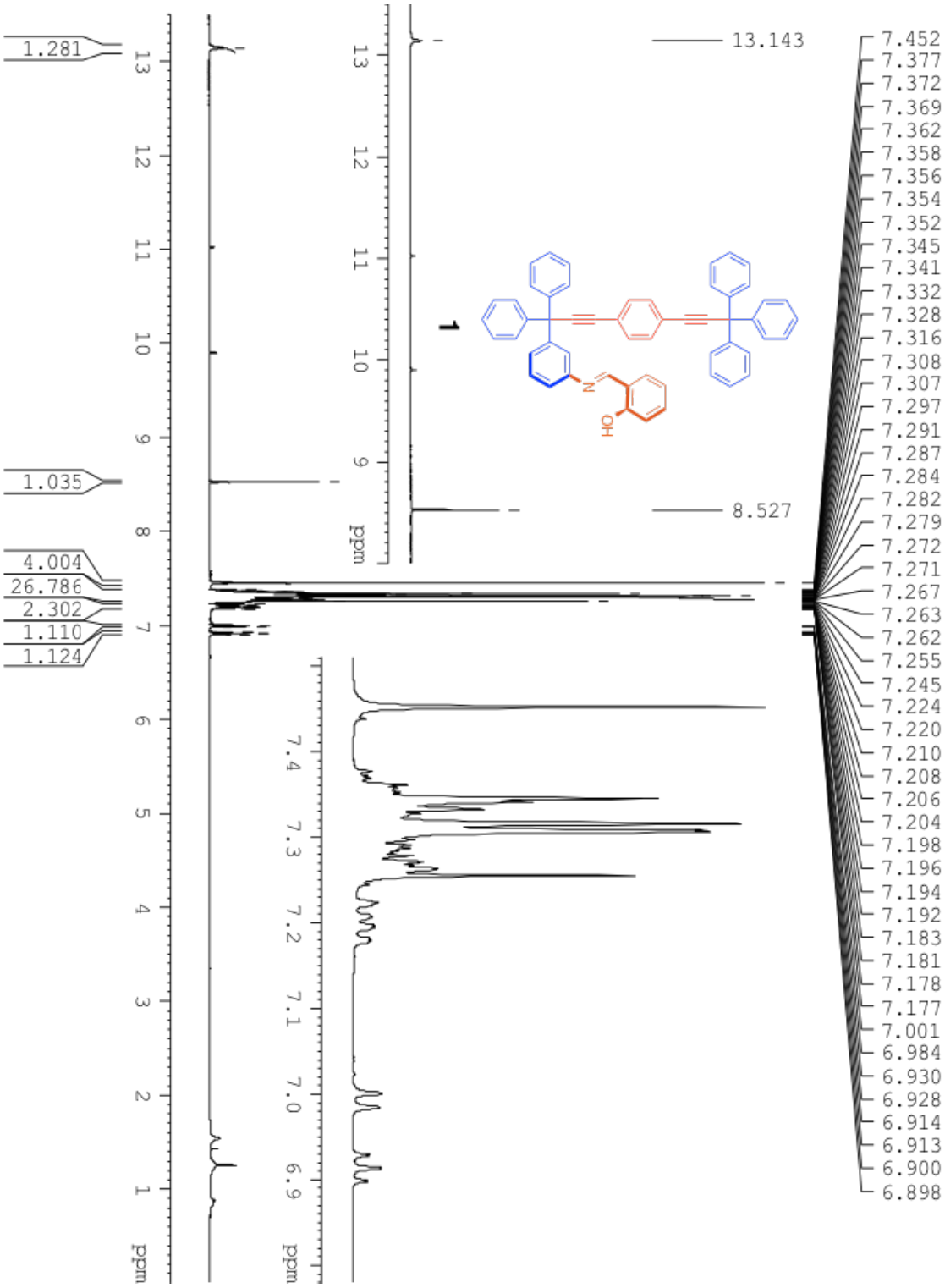

Figure S1. ^{1}H NMR of Monosalicylideneaniline Rotor **1**
500 MHz ^{1}H NMR spectrum of compound **1** in $CDCl_3$

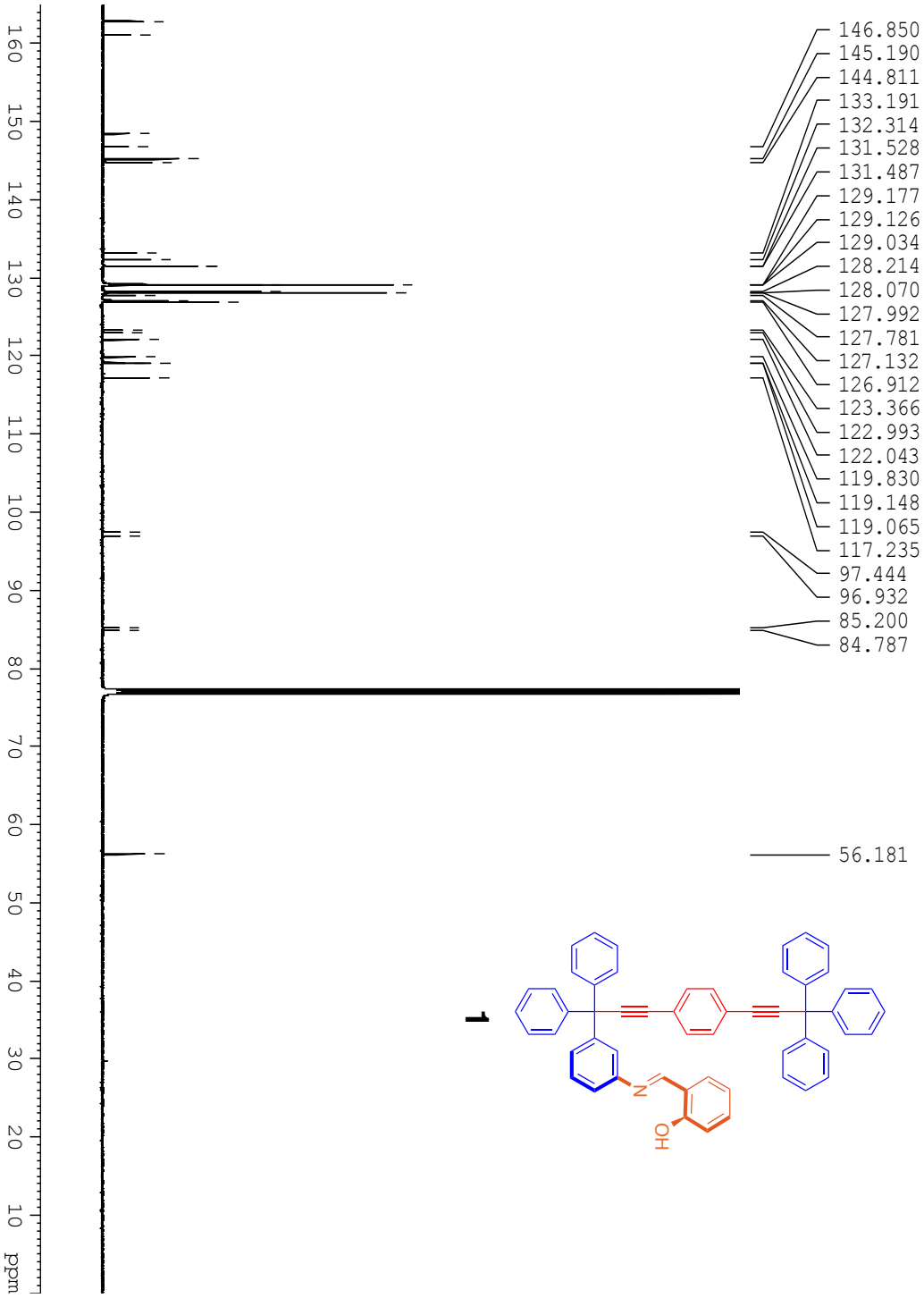

Figure S2. ^{13}C NMR of Monosalicylideneaniline Rotor **1**
125 MHz ^{13}C NMR spectrum of compound **1** in $CDCl_3$

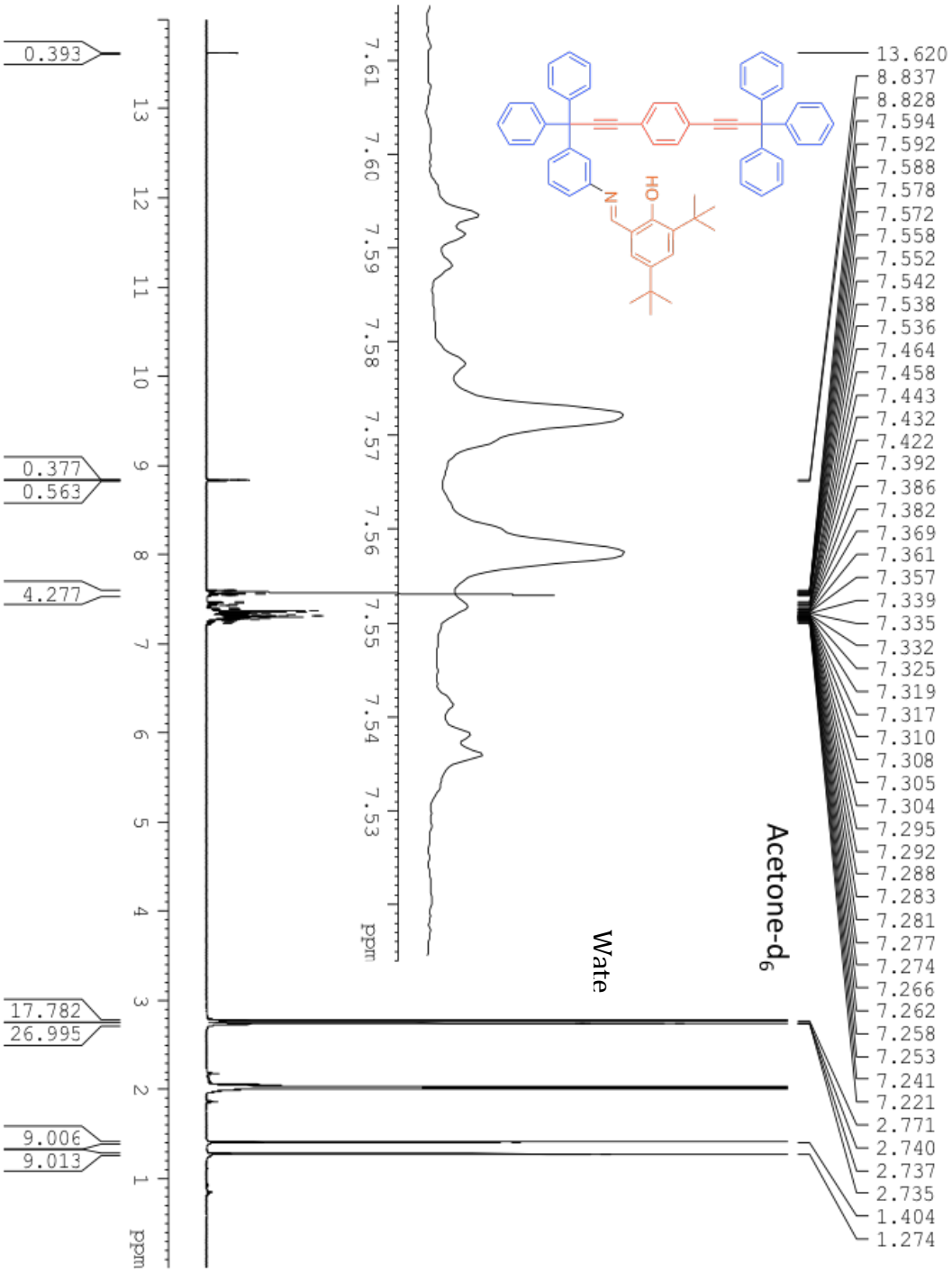

Figure S3. ^{1}H NMR of ditertbutyl-Monosalicylideneaniline Rotor **2**
500 MHz ^{1}H NMR spectrum of compound **2** in Acetone-d_6

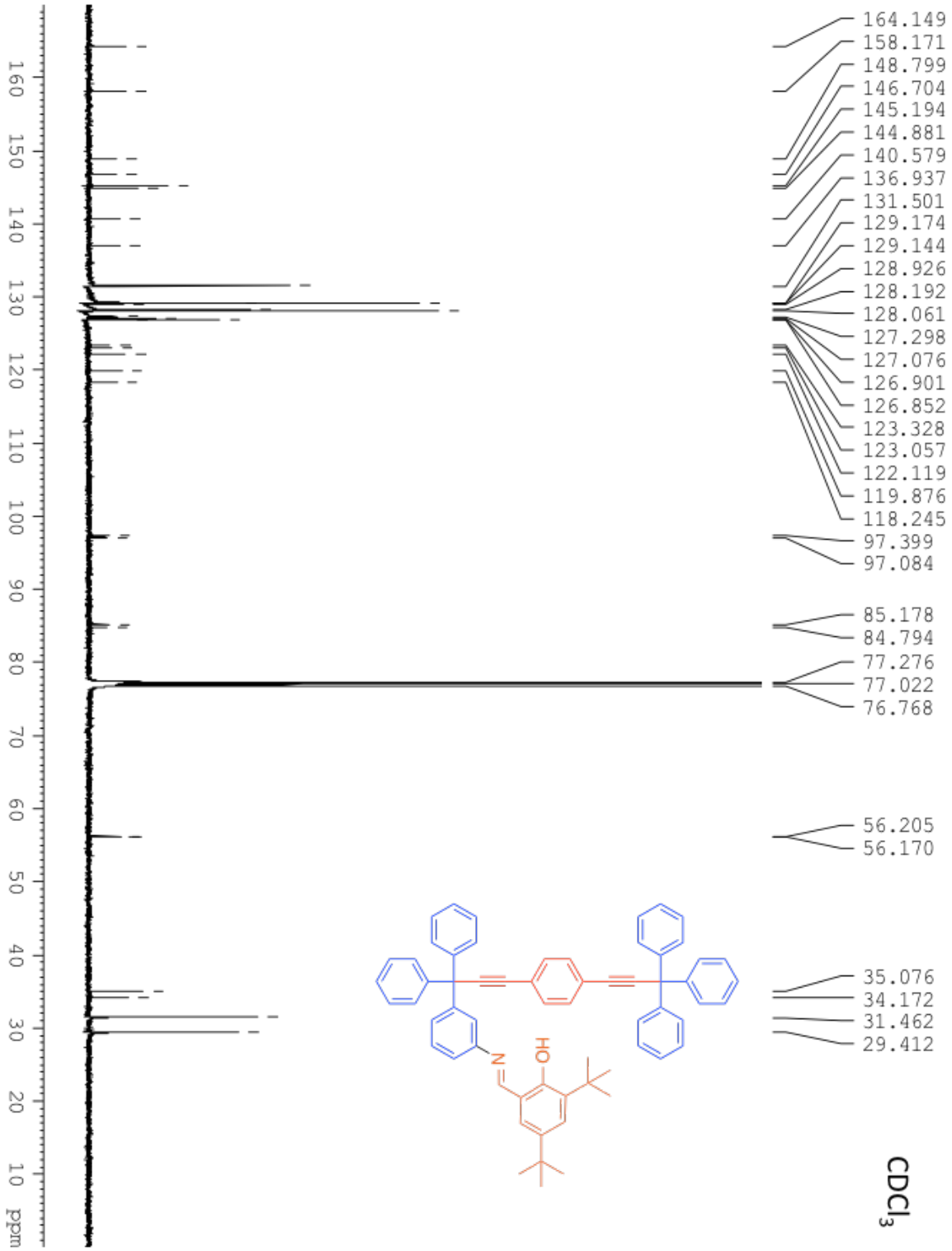

Figure S4. ^{13}C NMR of ditertbutyl-Monosalicylideneaniline Rotor **2**
125 MHz ^{13}C NMR spectrum of compound **2** in $CDCl_3$

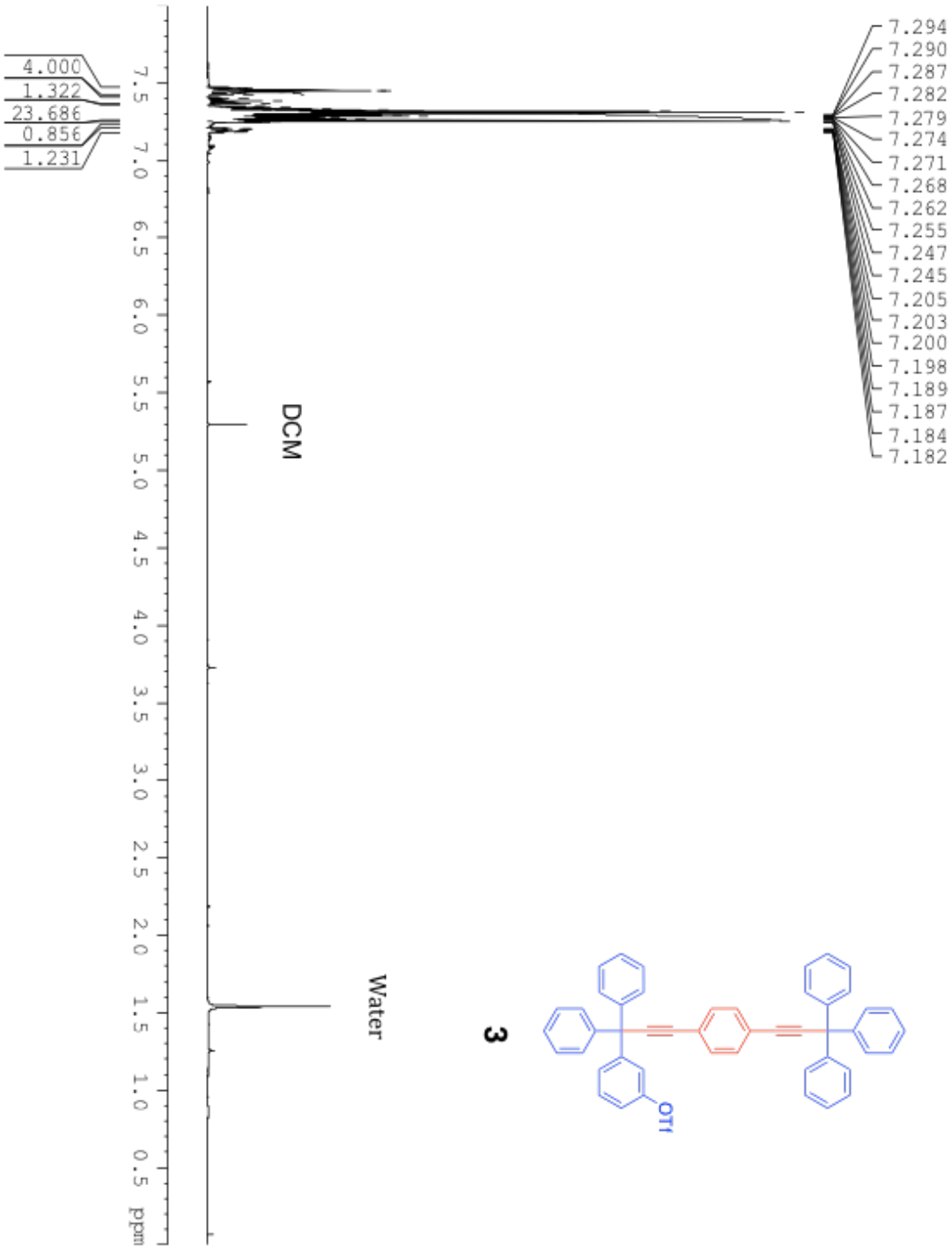

Figure S5. ^{1}H NMR of Monotriflate Rotor **3**
500 MHz ^{1}H NMR spectrum of compound **3** in $CDCl_3$

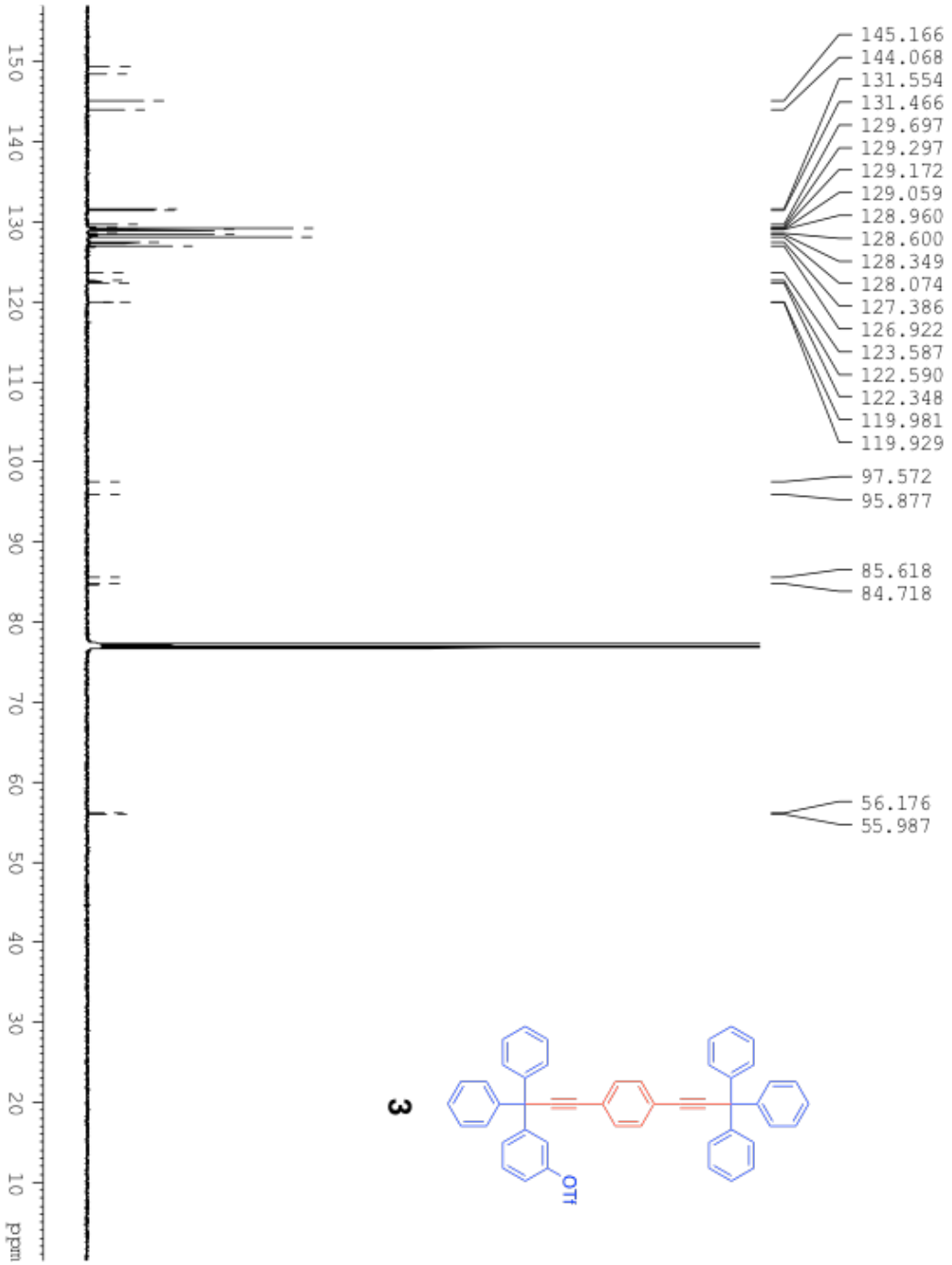

Figure S6. ^{13}C NMR of Monotriflate Rotor **3**
125 MHz ^{13}C NMR spectrum of compound **3** in $CDCl_3$

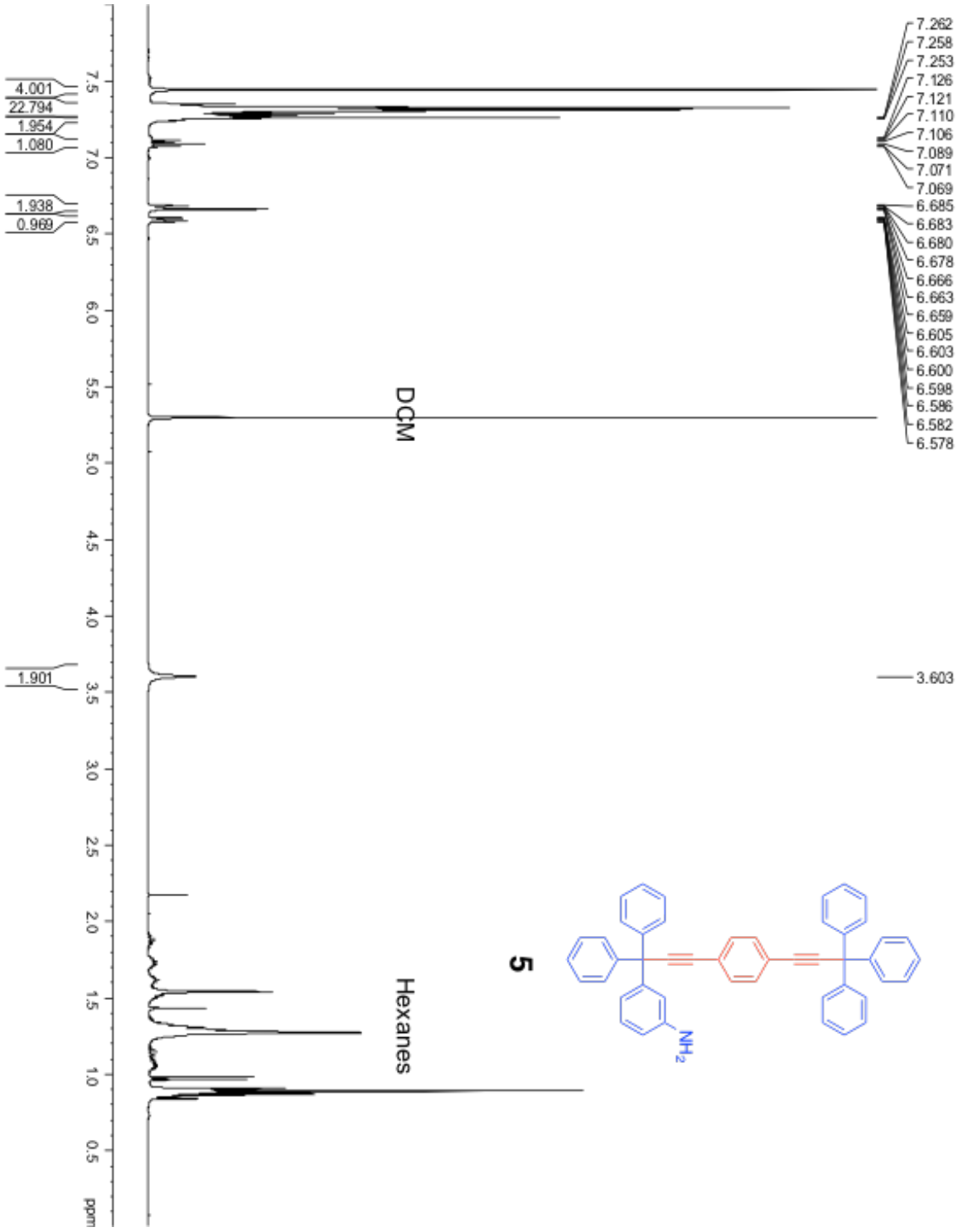

Figure S7. ^{1}H NMR of Monoamino Rotor **5**
500 MHz ^{1}H NMR spectrum of compound **5** in $CDCl_3$

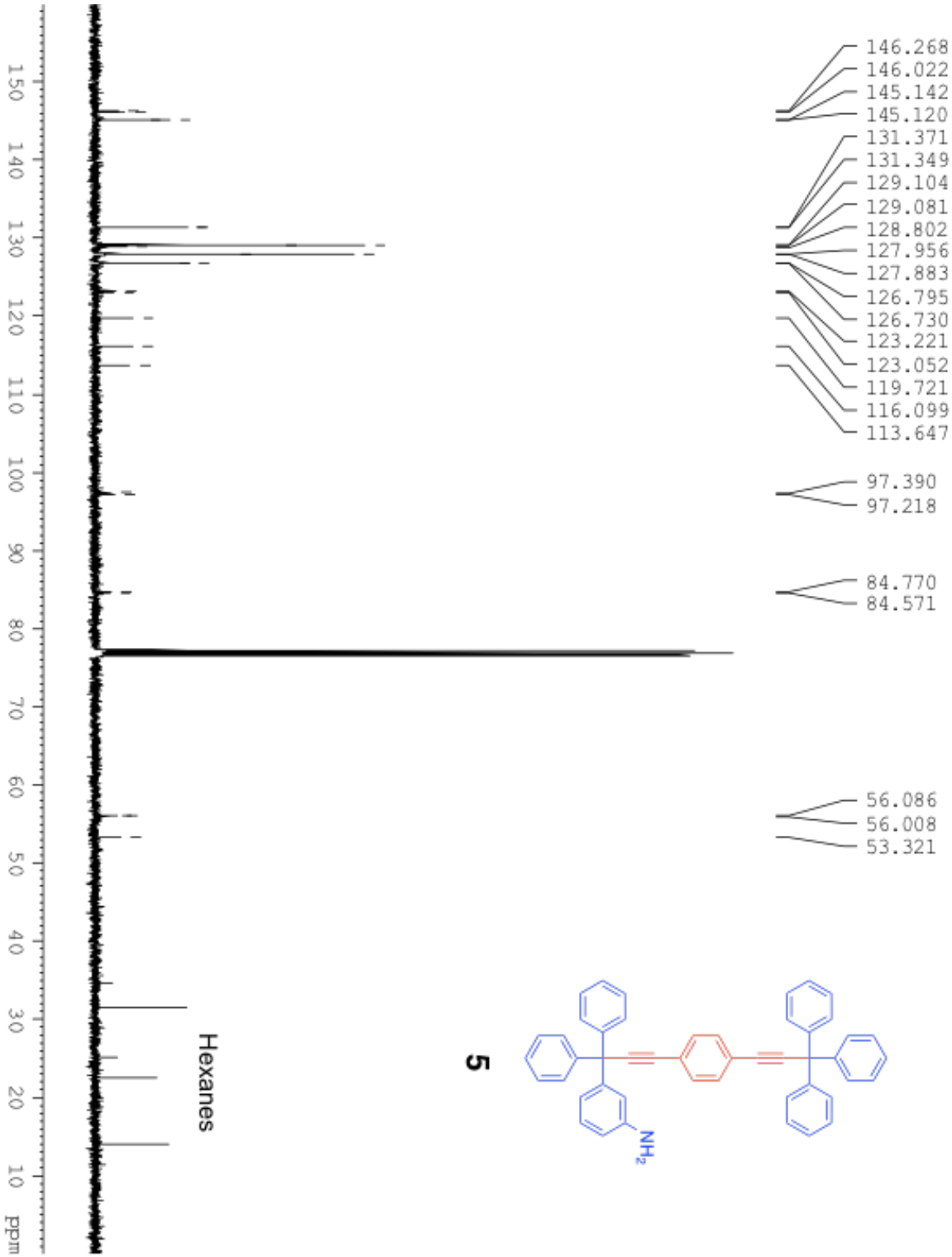

Figure S8. ^{13}C NMR of Monoamino Rotor **5**
125 MHz ^{13}C NMR spectrum of compound **5** in $CDCl_3$

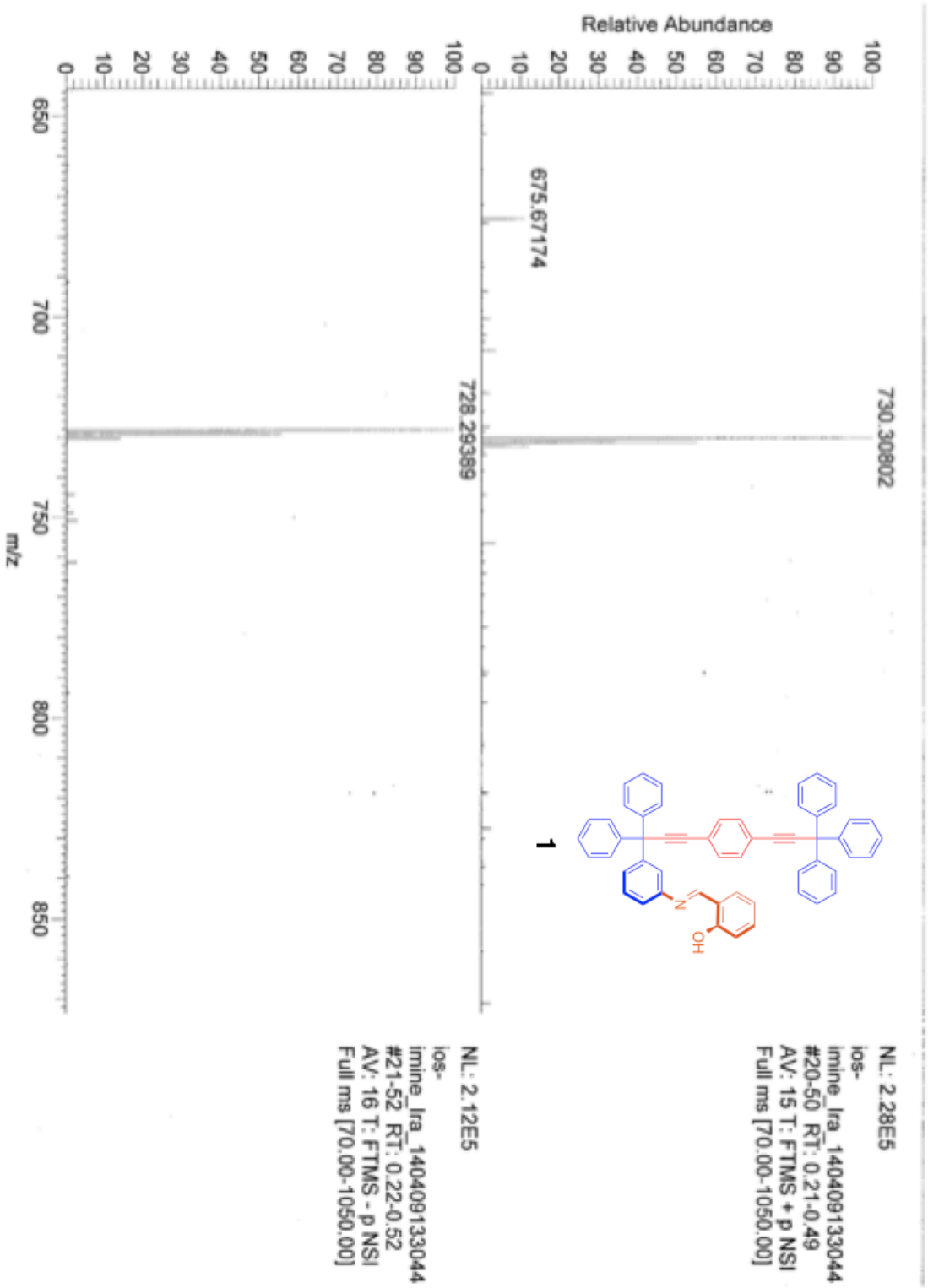

Figure S9. ESI+ of Monosalicylideneaniline Rotor **1**

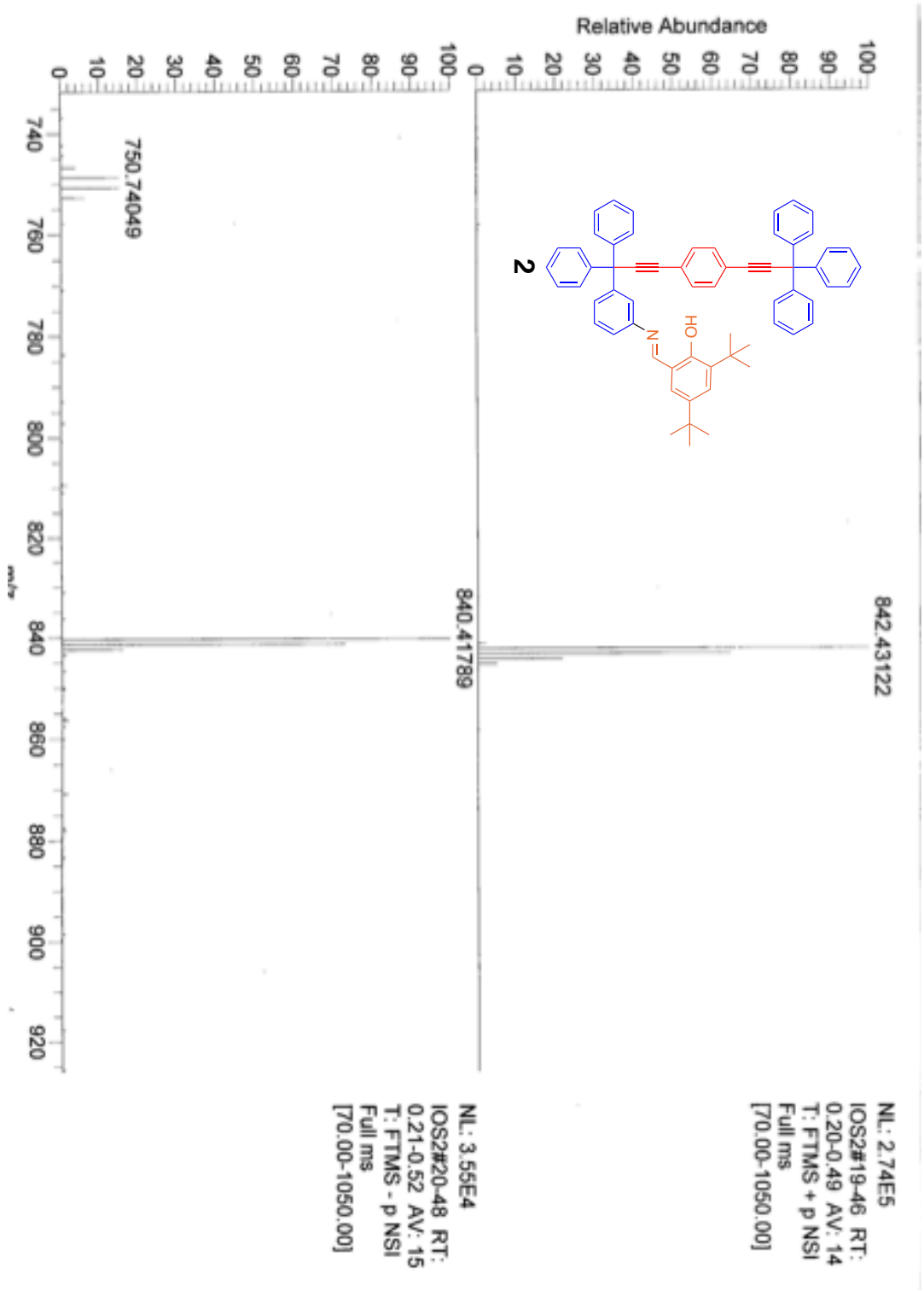

Figure S10. ESI+ of ditertbutyl-Monosalicylideneaniline Rotor **2**

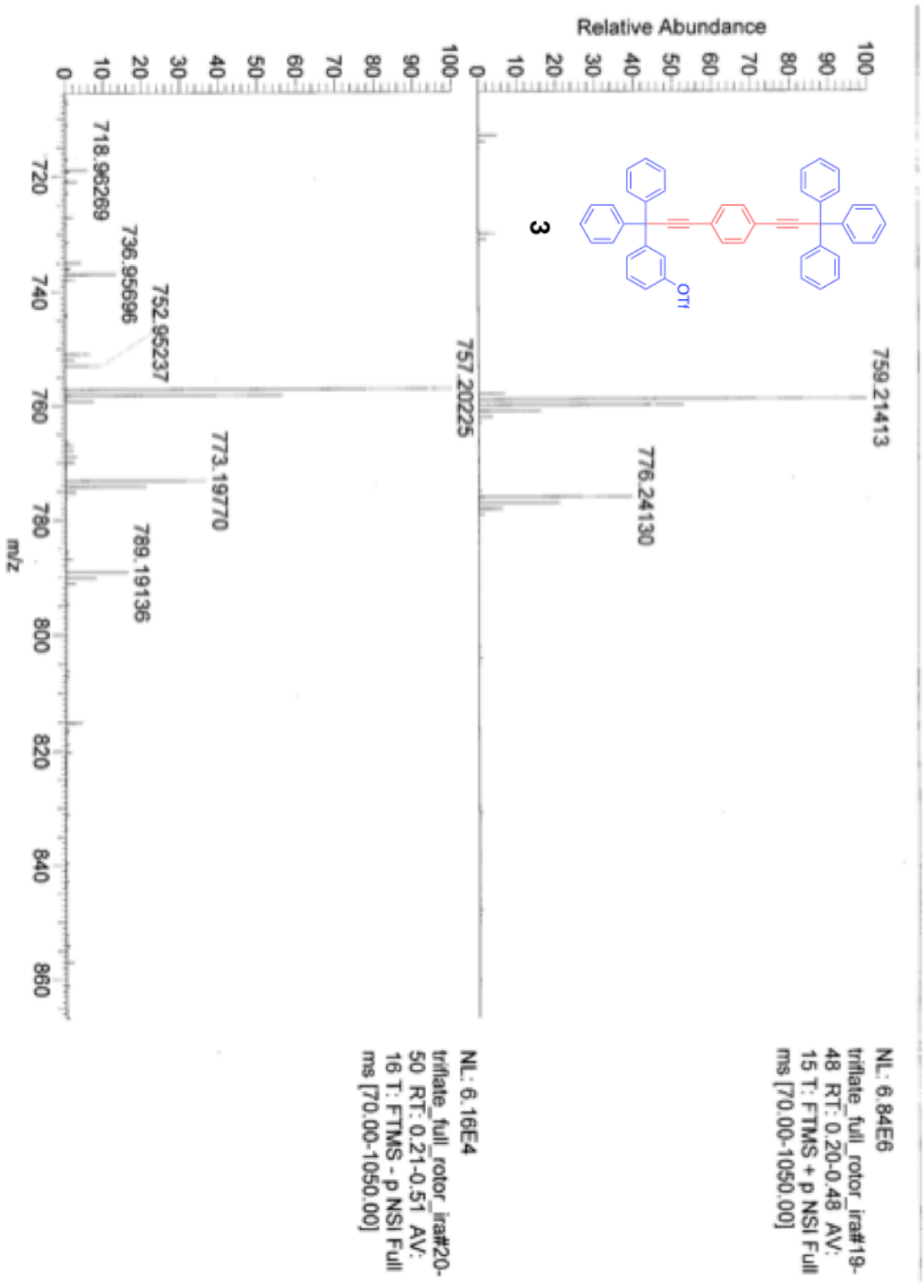

Figure S11. ESI+ of Monotriflate Rotor **3**

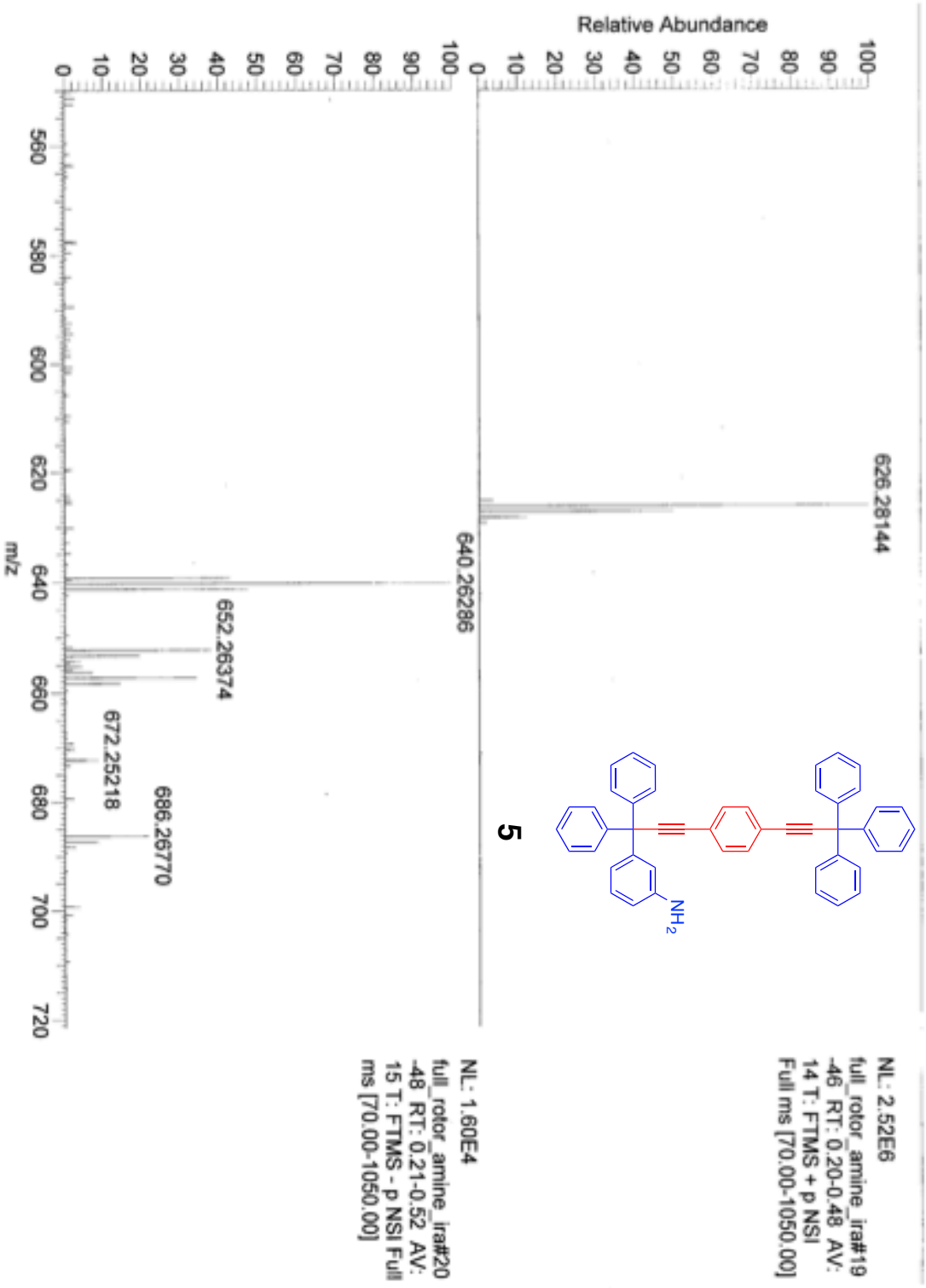

Figure S12. ESI+ of Monoamino Rotor **5**

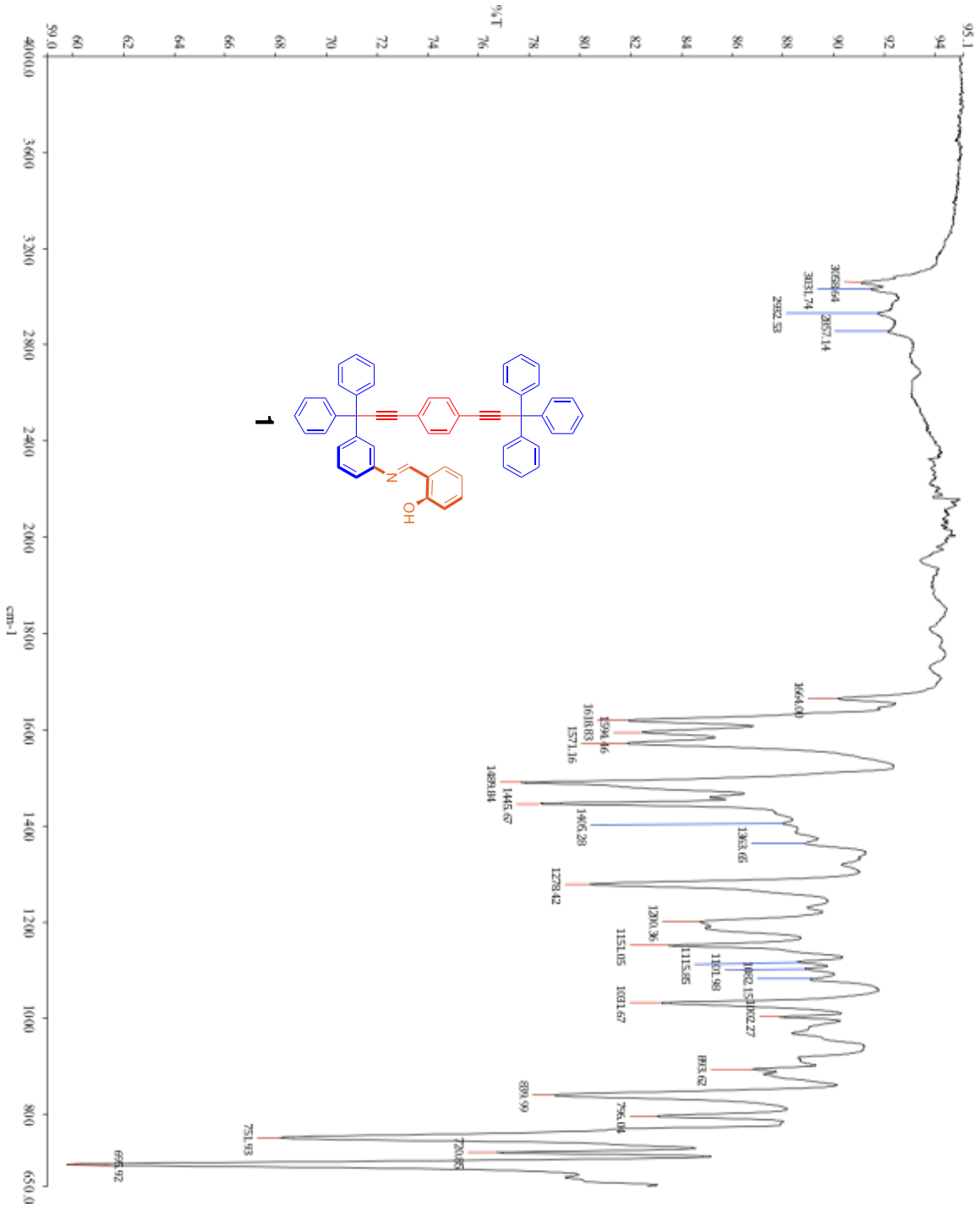

Figure S13. ATR FTIR Spectrum of Monosalicylideneaniline Rotor **1** in the solid state

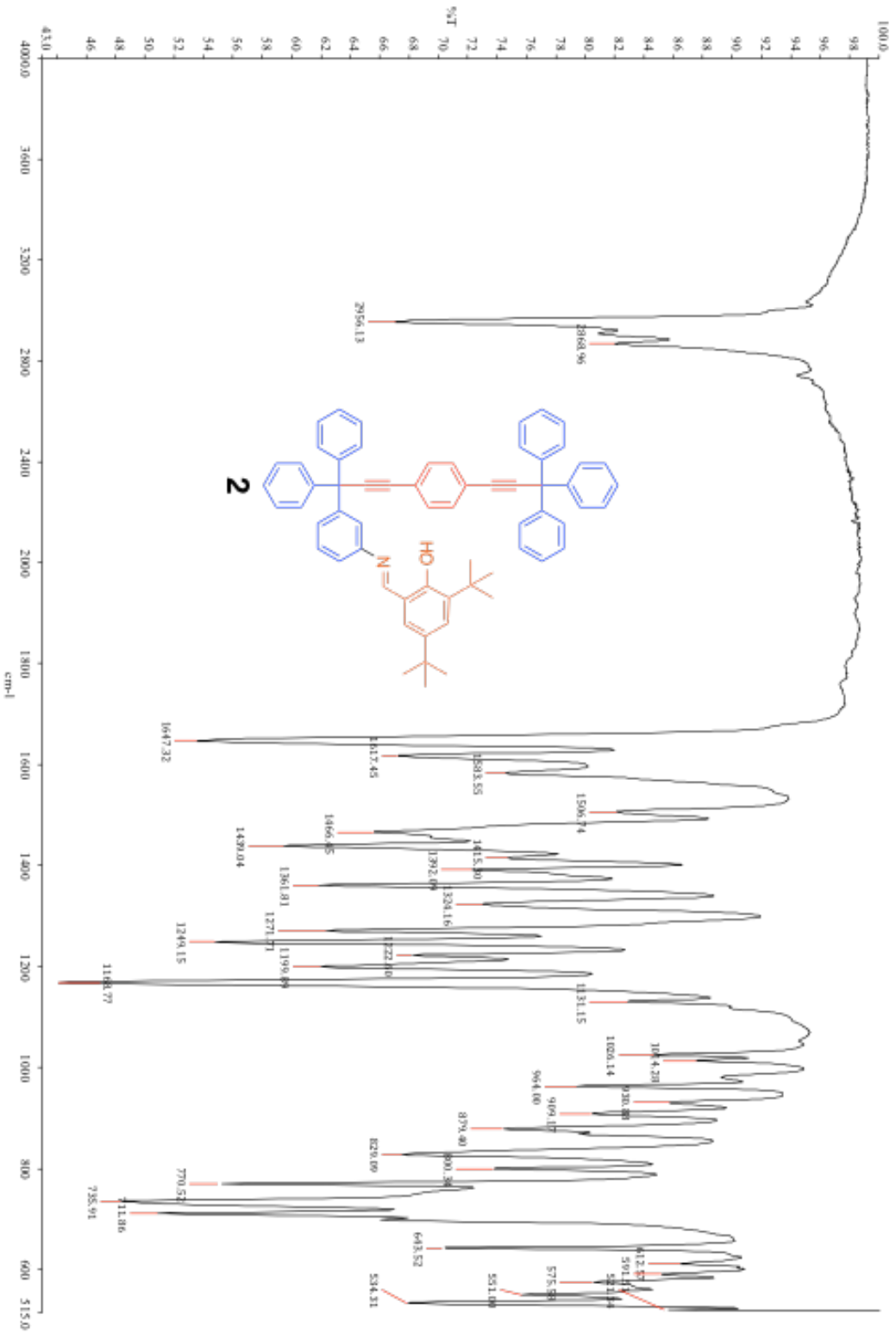

Figure S14. ATR FTIR Spectrum of ditertbutyl-Monosalicylideneaniline Rotor **2** in the solid state

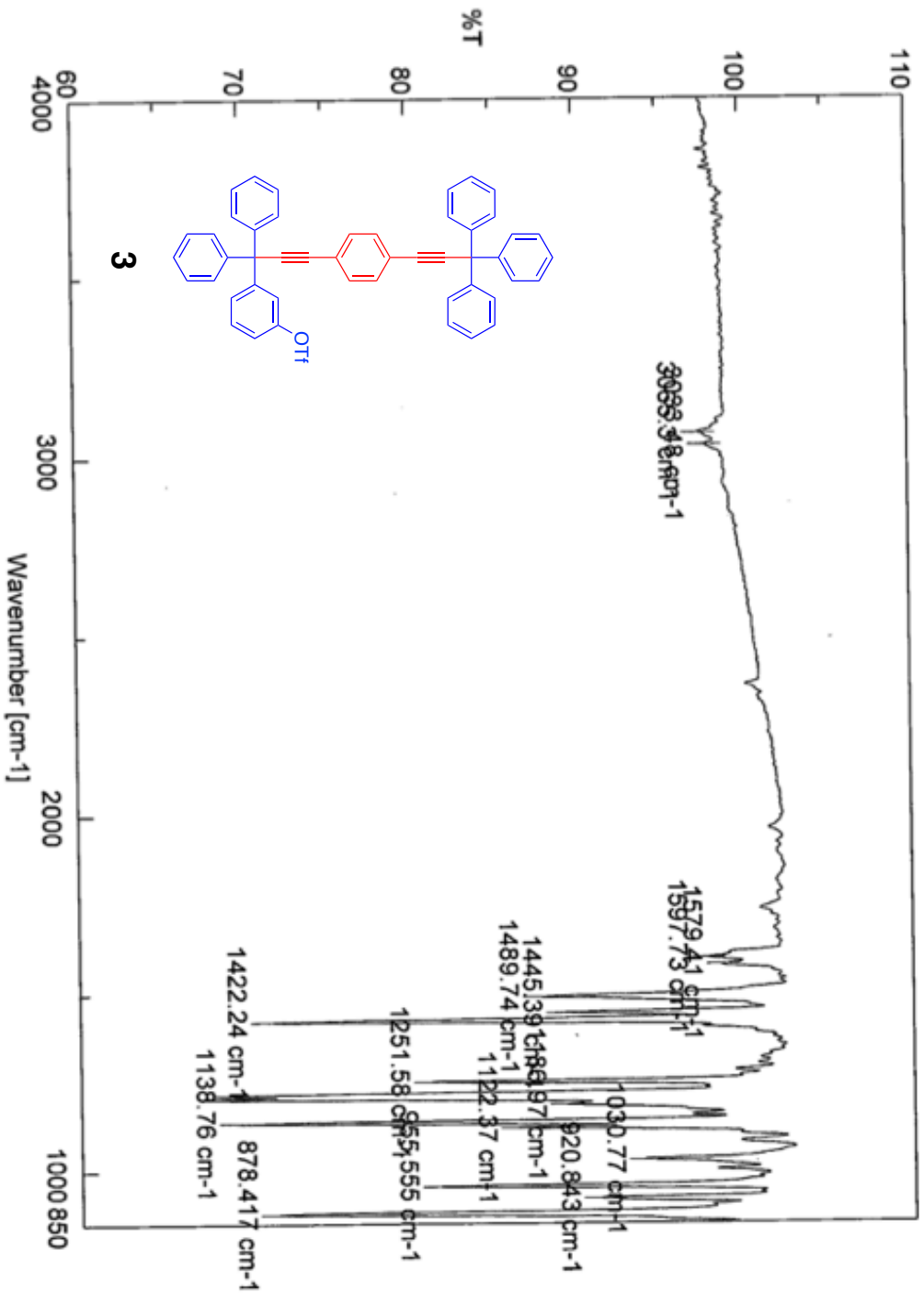

Figure S15. ATR FTIR Spectrum of Monotriflate Rotor **3** in the solid state

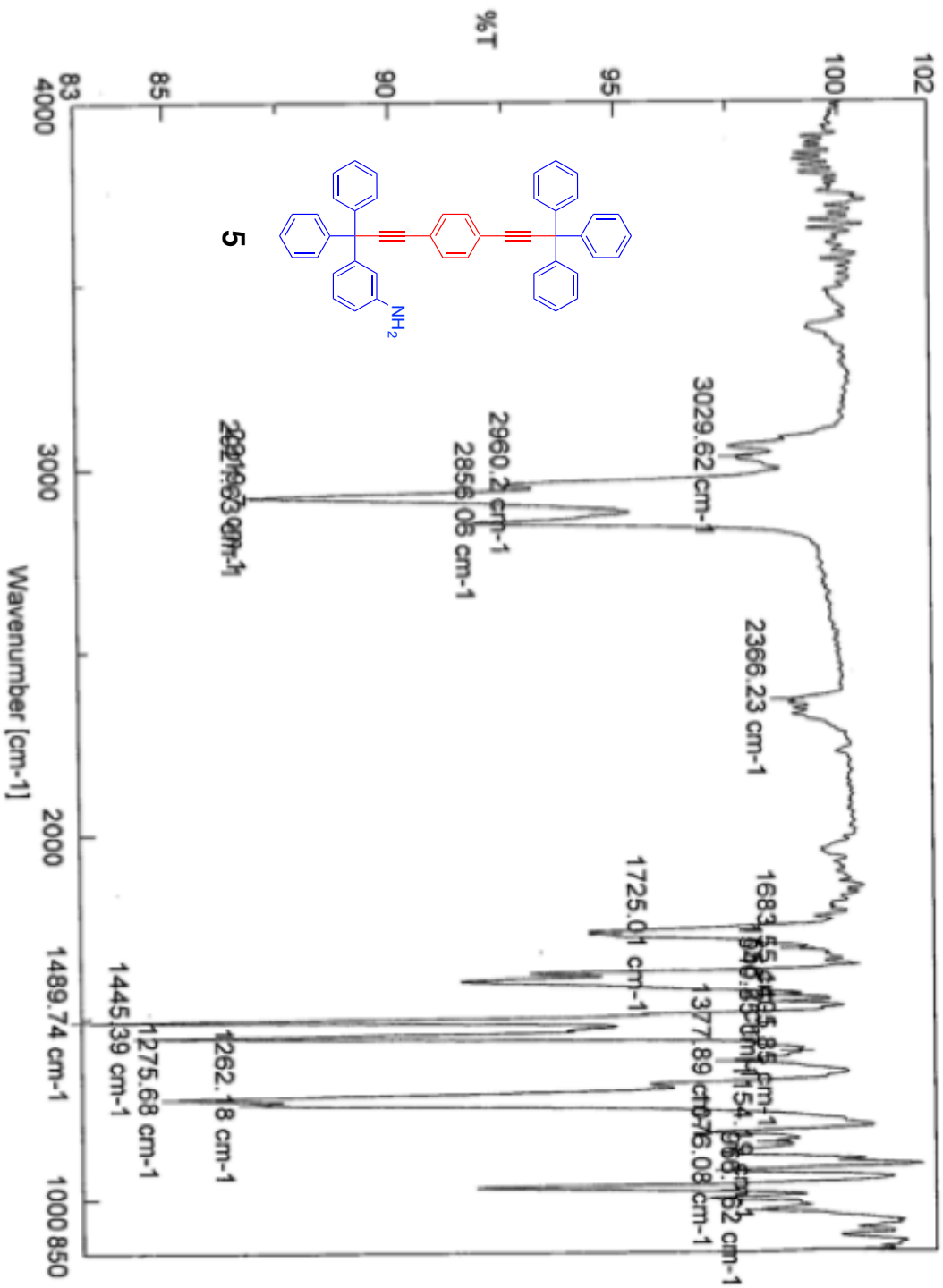

Figure S16. ATR FTIR Spectrum of Monoamino Rotor **5** in the solid state

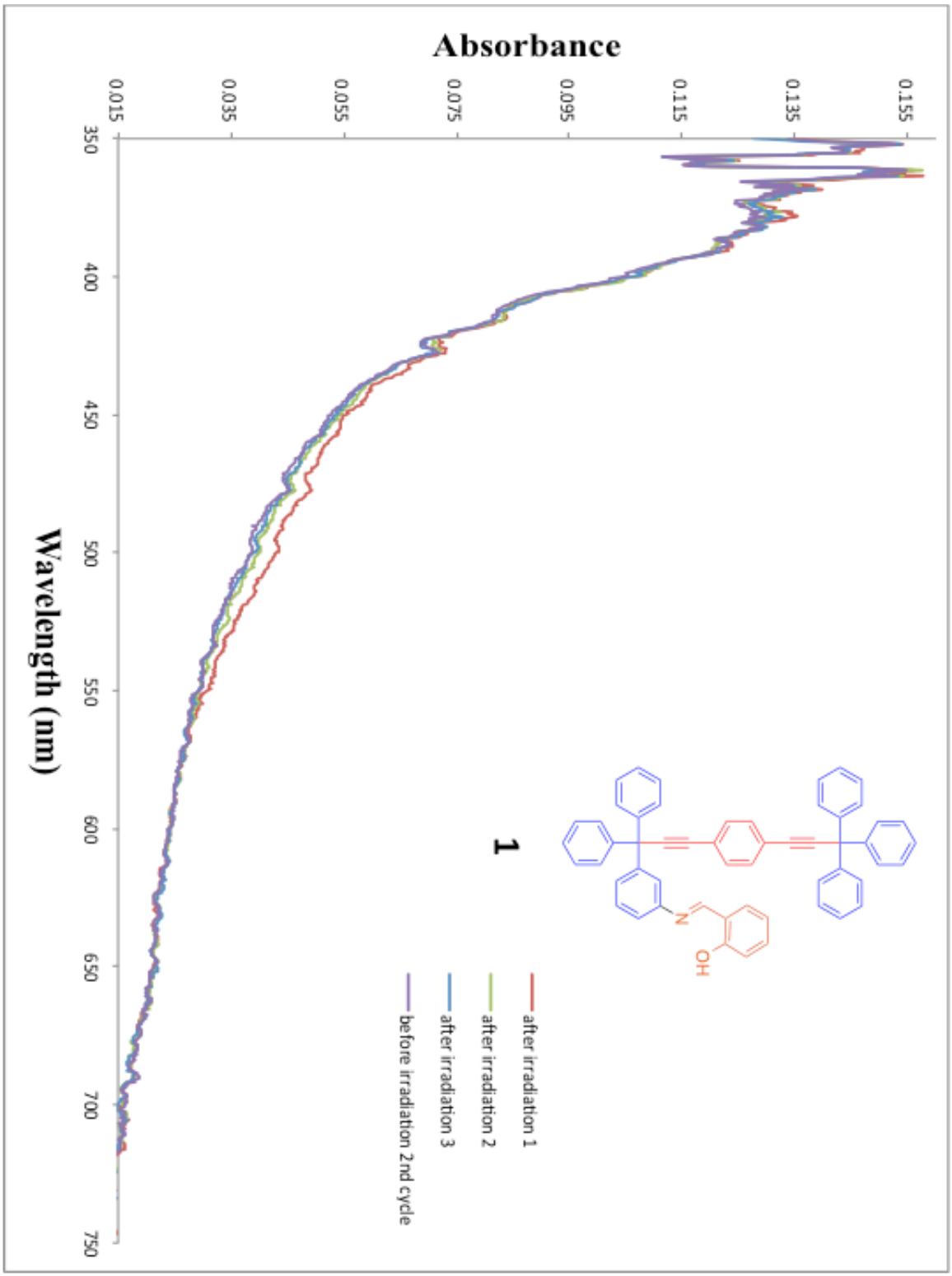

Figure S17. Diffuse Reflectance of Monosalicylideneaniline Rotor **1** in the solid state

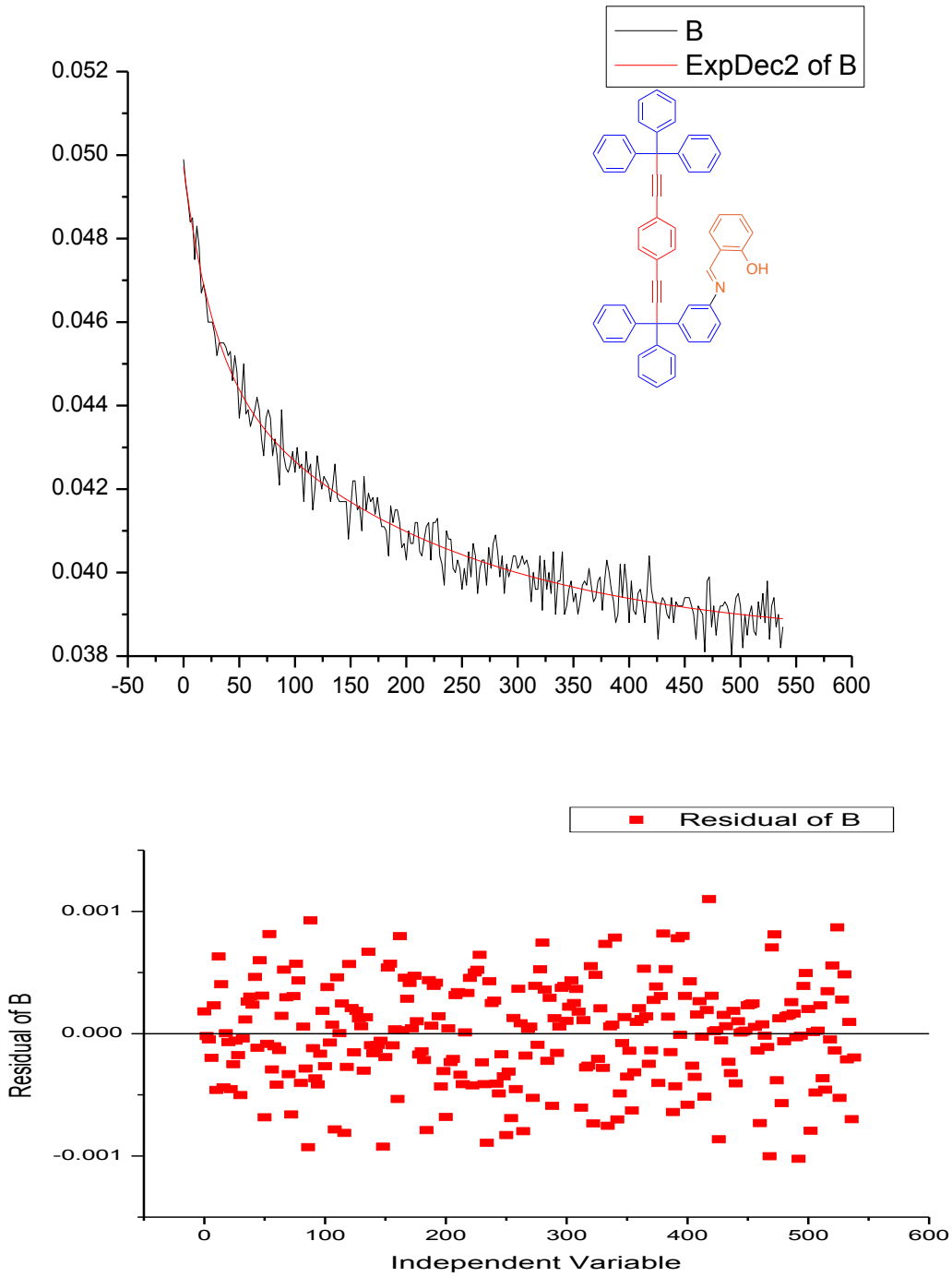

Figure S18. Diffuse Reflectance Lifetime of Monosalicylideneaniline Rotor **1** in the solid state

		Value	Standard Error B
	y0	0.03837	1.99212E-4
B	A1	0.00672	2.85234E-4
B	t1	211.58753	24.9042
B	A2	0.00463	4.08351E-4
B	t2	26.64903	4.05656

	B
Number of Points	270
Degrees of Freedom	265
Reduced Chi-Sqr	1.72926E-7
Residual Sum of Squares	4.58254E-5
Adj. R-Square	0.96749
Fit Status	Succeeded(100)

Figure S19. Fitting parameters for Diffuse Reflectance Lifetime of Monosalicylideneaniline Rotor **1** in the solid state

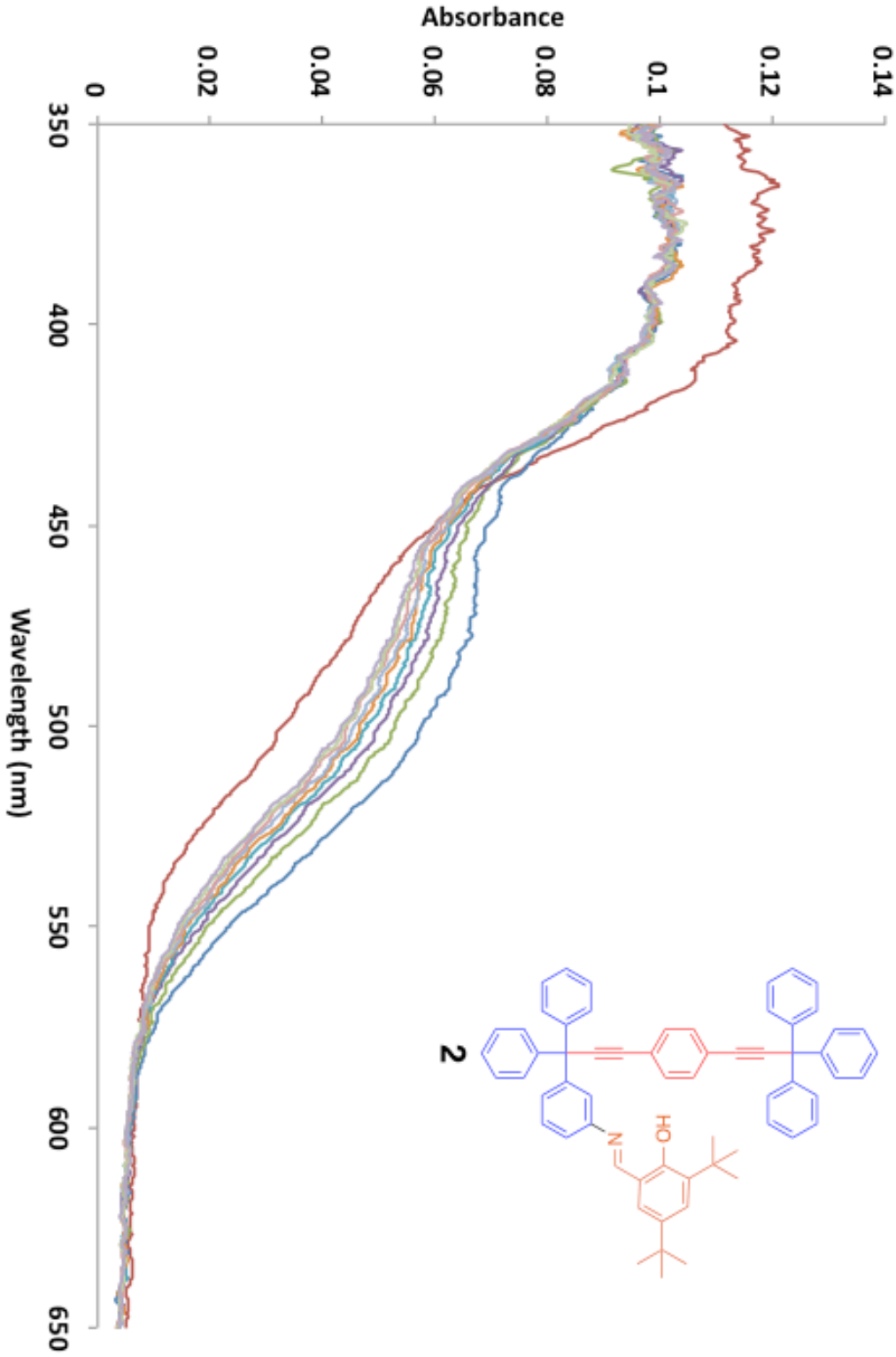

Figure S20. Diffuse Reflectance of ditertbutyl-Monosalicylideneaniline Rotor **2**

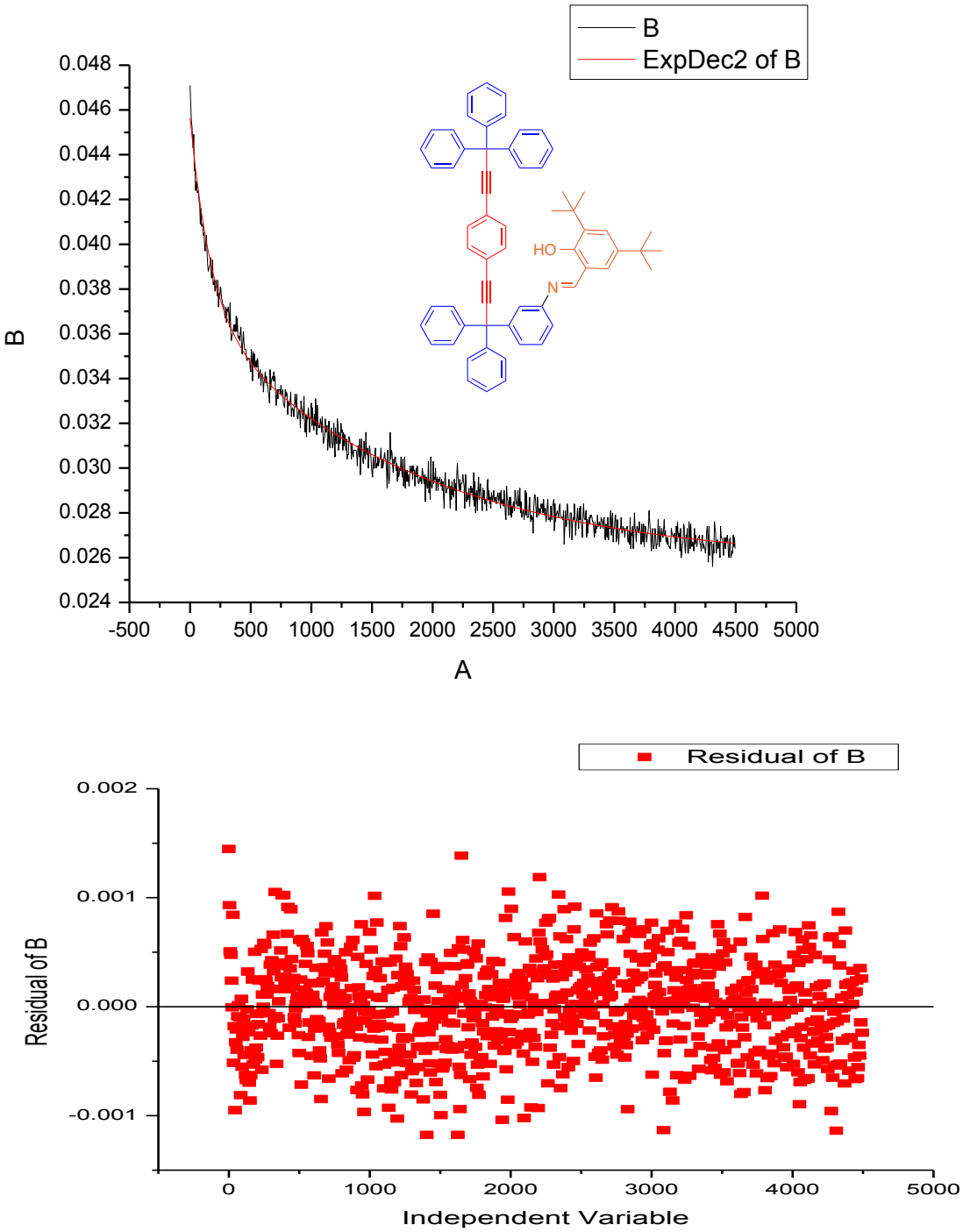

Figure S21. Diffuse Reflectance Lifetime of ditertbutyl-Monosalicylideneaniline Rotor **2**

		Value	Standard Error
B	y0	0.02574	1.00231E-4
B	A1	0.01133	1.09739E-4
B	t1	1776.60122	57.17274
B	A2	0.00858	1.87629E-4
B	t2	167.71911	7.35919

	B
Number of Points	900
Degrees of Freedom	895
Reduced Chi-Sqr	1.83729E-7
Residual Sum of Squares	1.64438E-4
Adj. R-Square	0.9867
Fit Status	Succeeded(100)

Figure S22. Fitting parameters for Diffuse Reflectance Lifetime of ditertbutyl-Monosalicylideneaniline Rotor **2** in the solid state

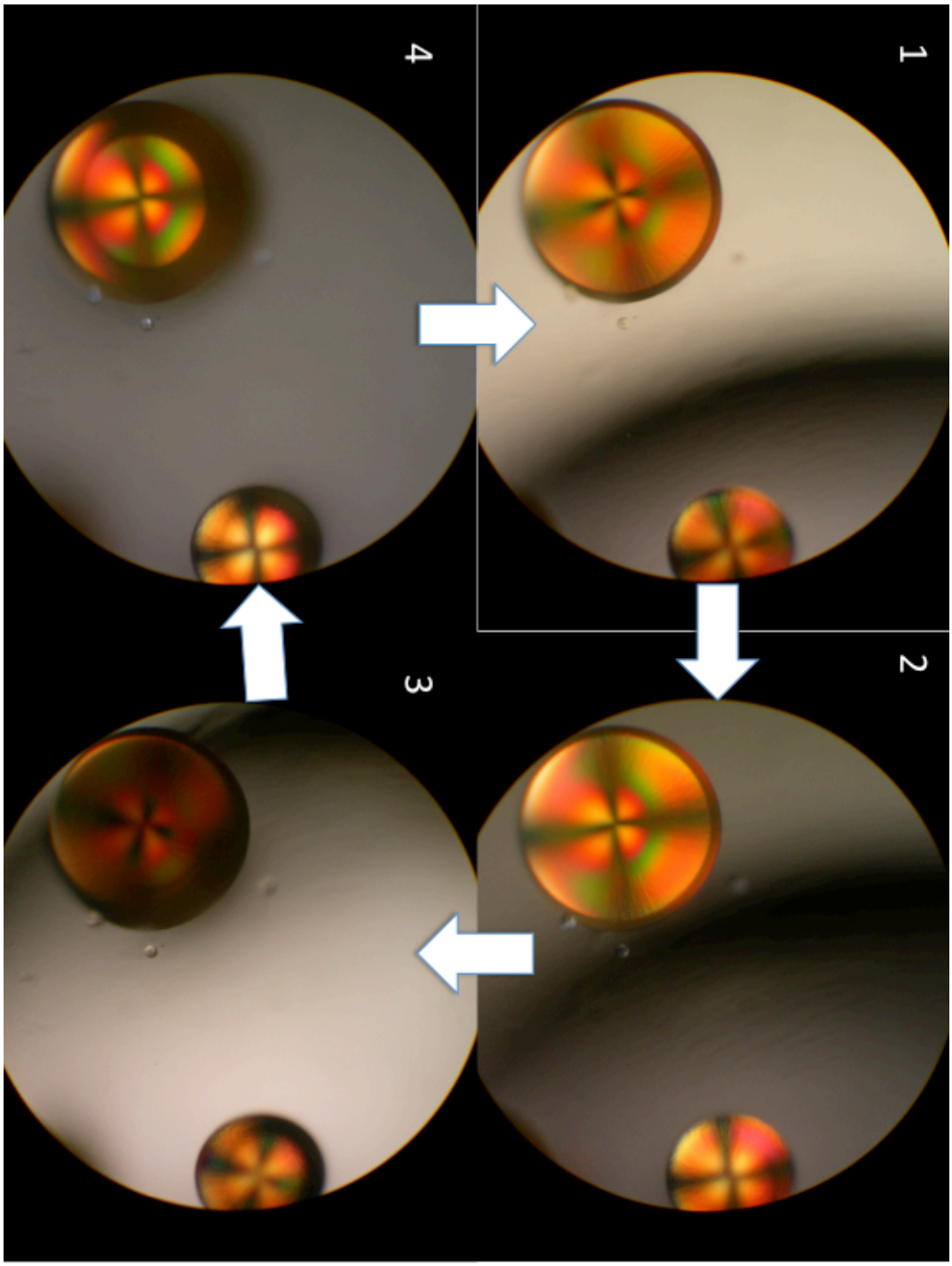

Figure S23. Spherulitic crystals of **1** showing the maltese changing orientation with respect to the polarized light.

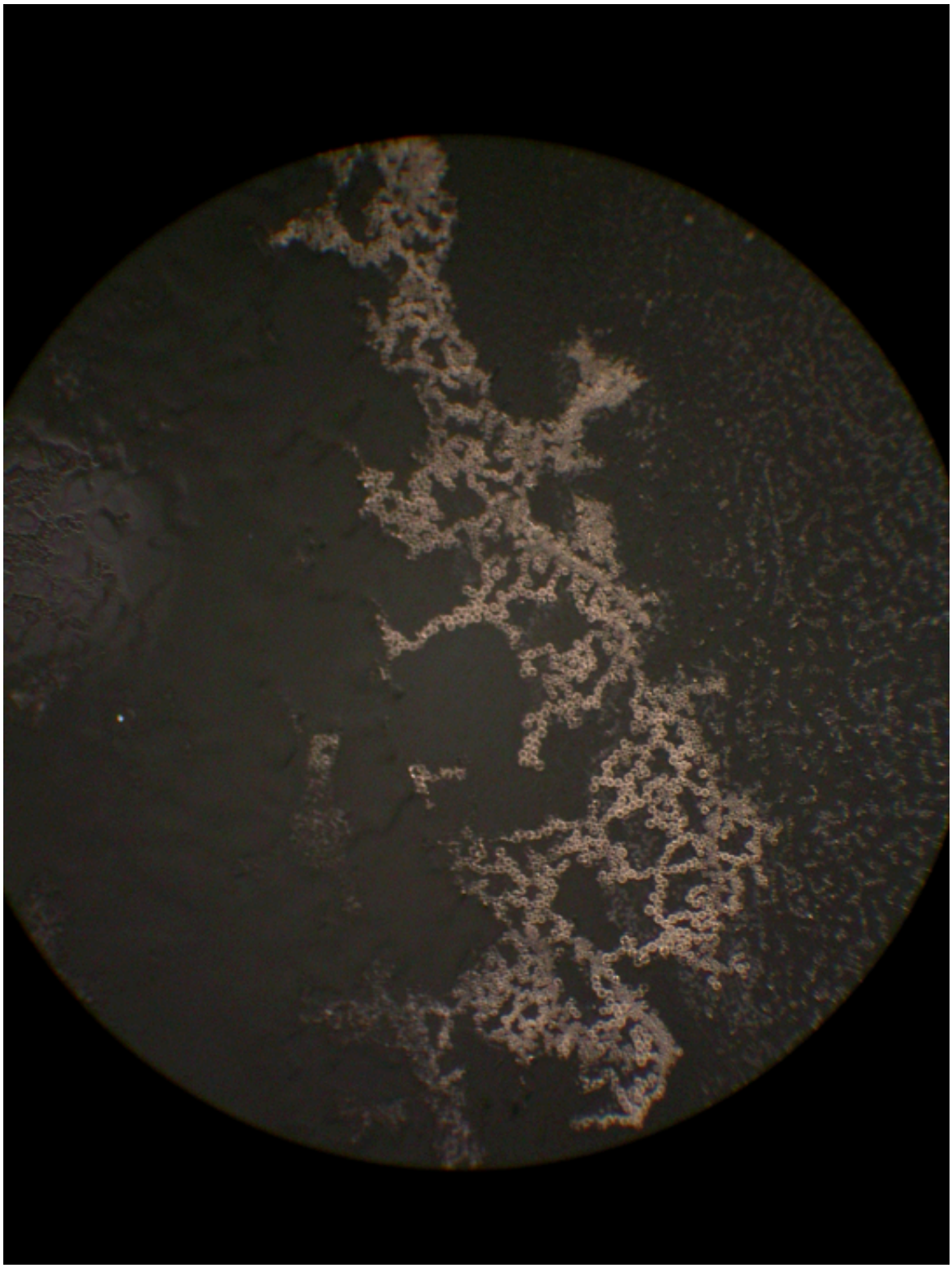

Figure S24. Spherulitic crystals of **1** from fast evaporation from a drop of DCM to determine if formation was thermally or kinetically driven.

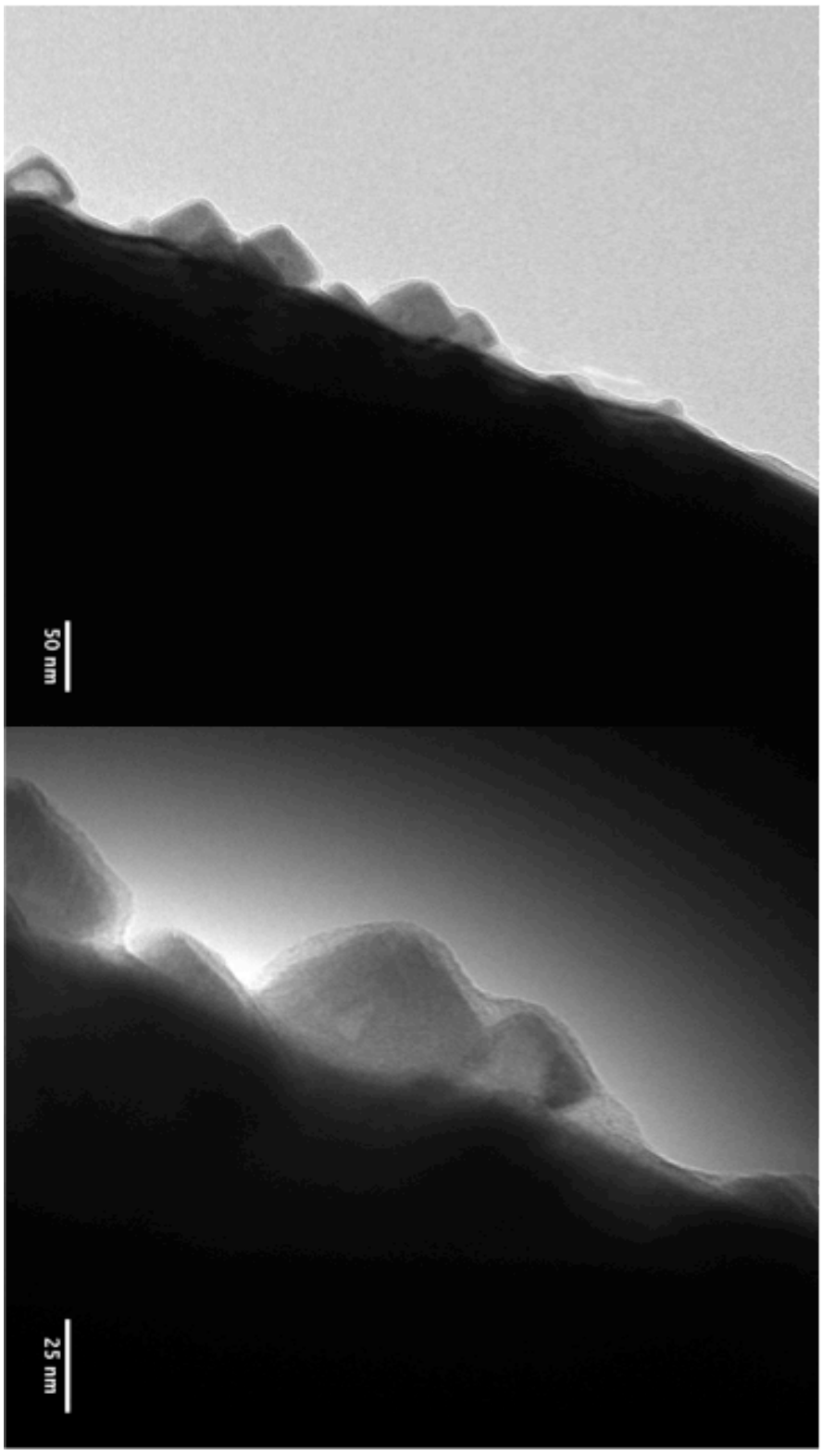

Figure S25. TEM images of **1** to determine if spherulites would form on the nanoscale size.

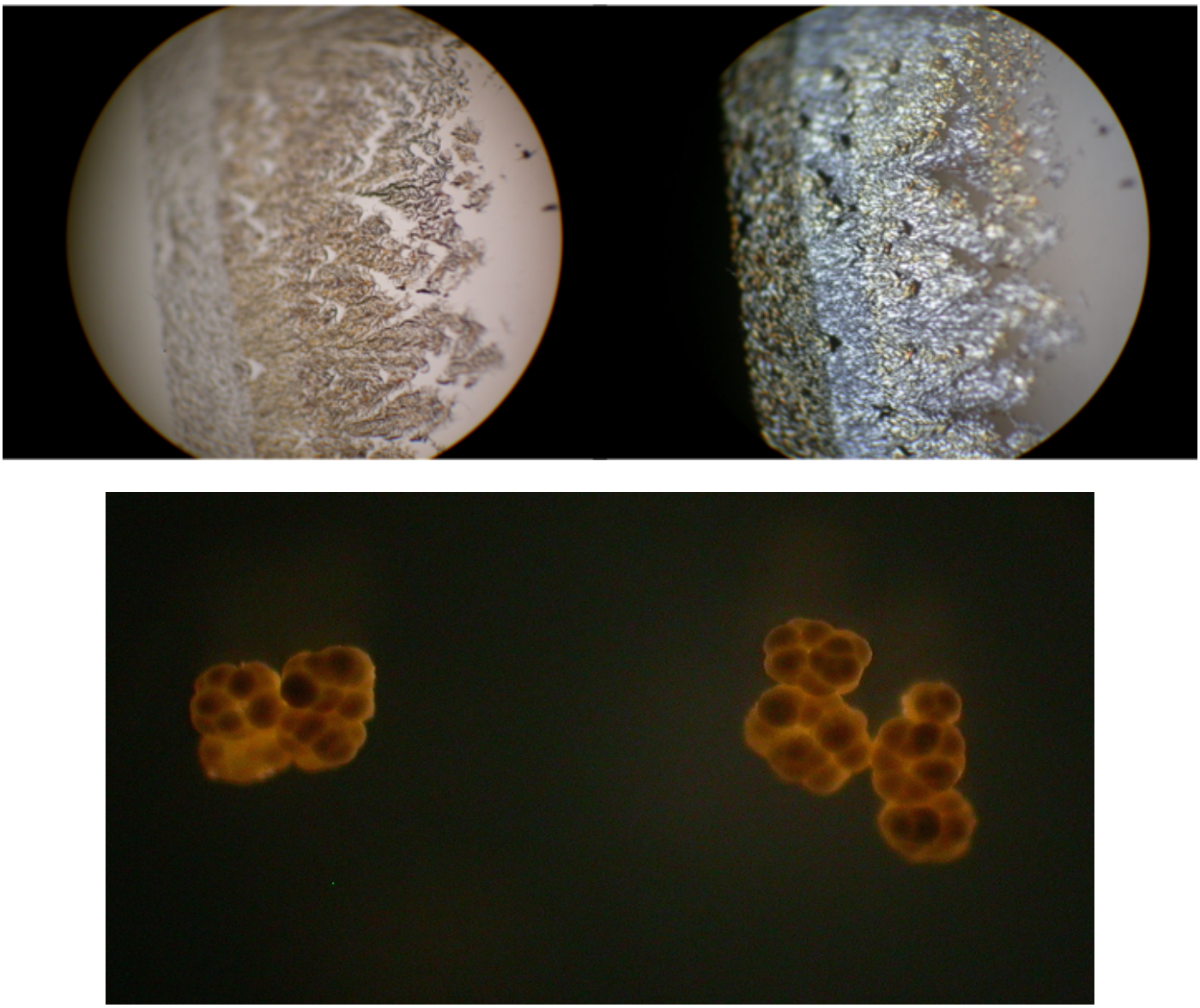

Figure S26. Spherulitic crystals of **2** (top) showing strained spherulites that generate curved crystals. Aggregates generated from solution concentrated down resulting in a three dimensional structure that is crystalline under polarized light (bottom)

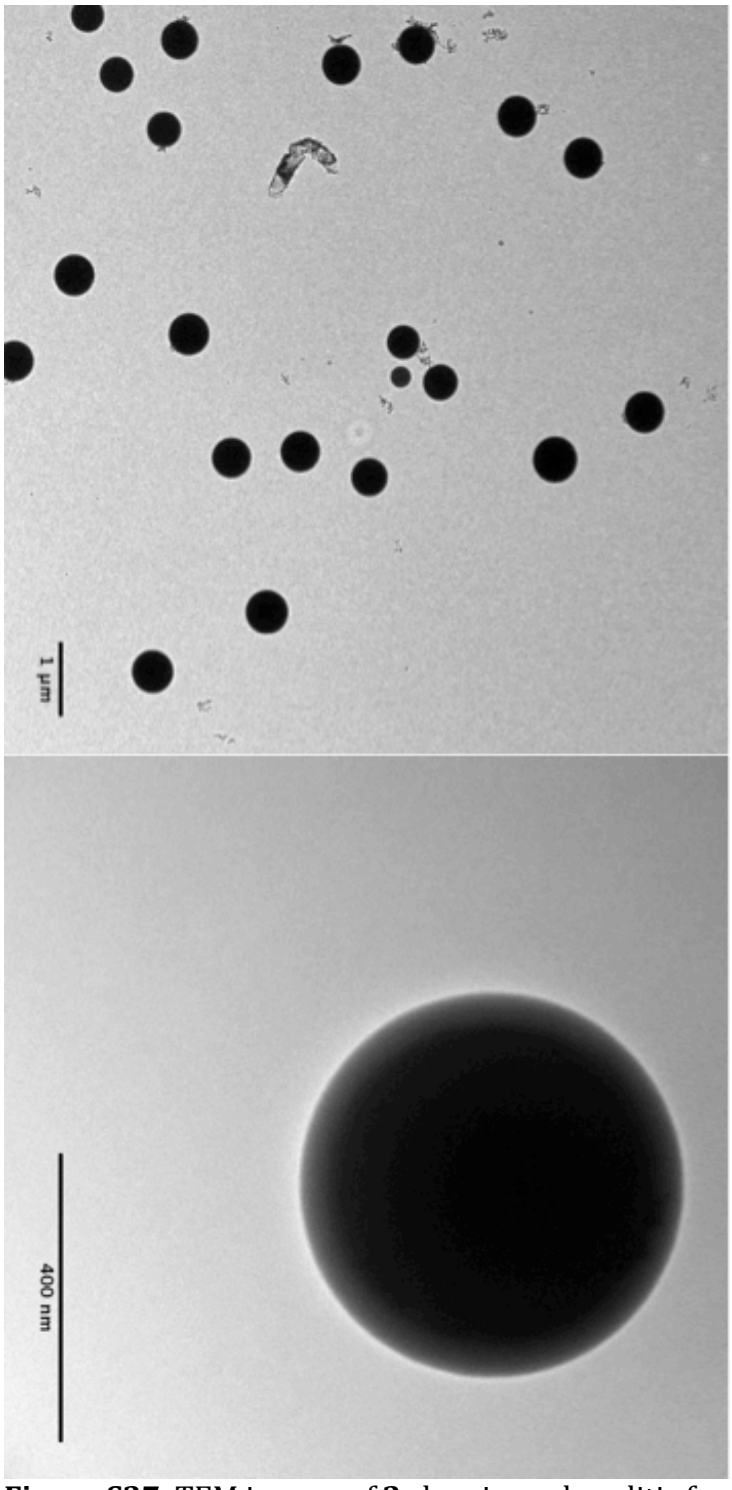

Figure S27. TEM images of **2** showing spherulitic formation on the nanoscale size.

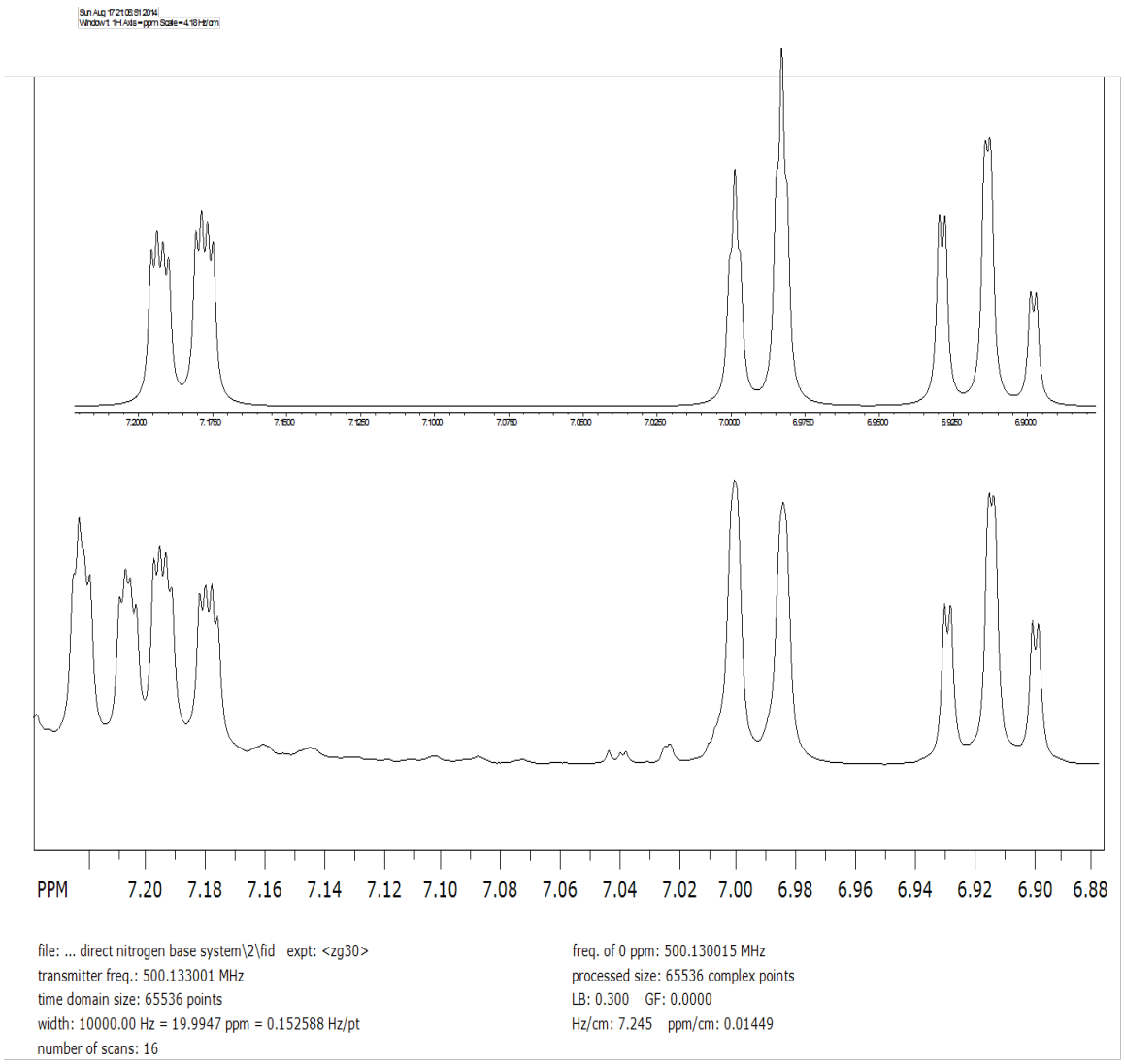

Figure S28. gNMR fitting of aromatic region of **1** simulated (top) experimental (bottom)

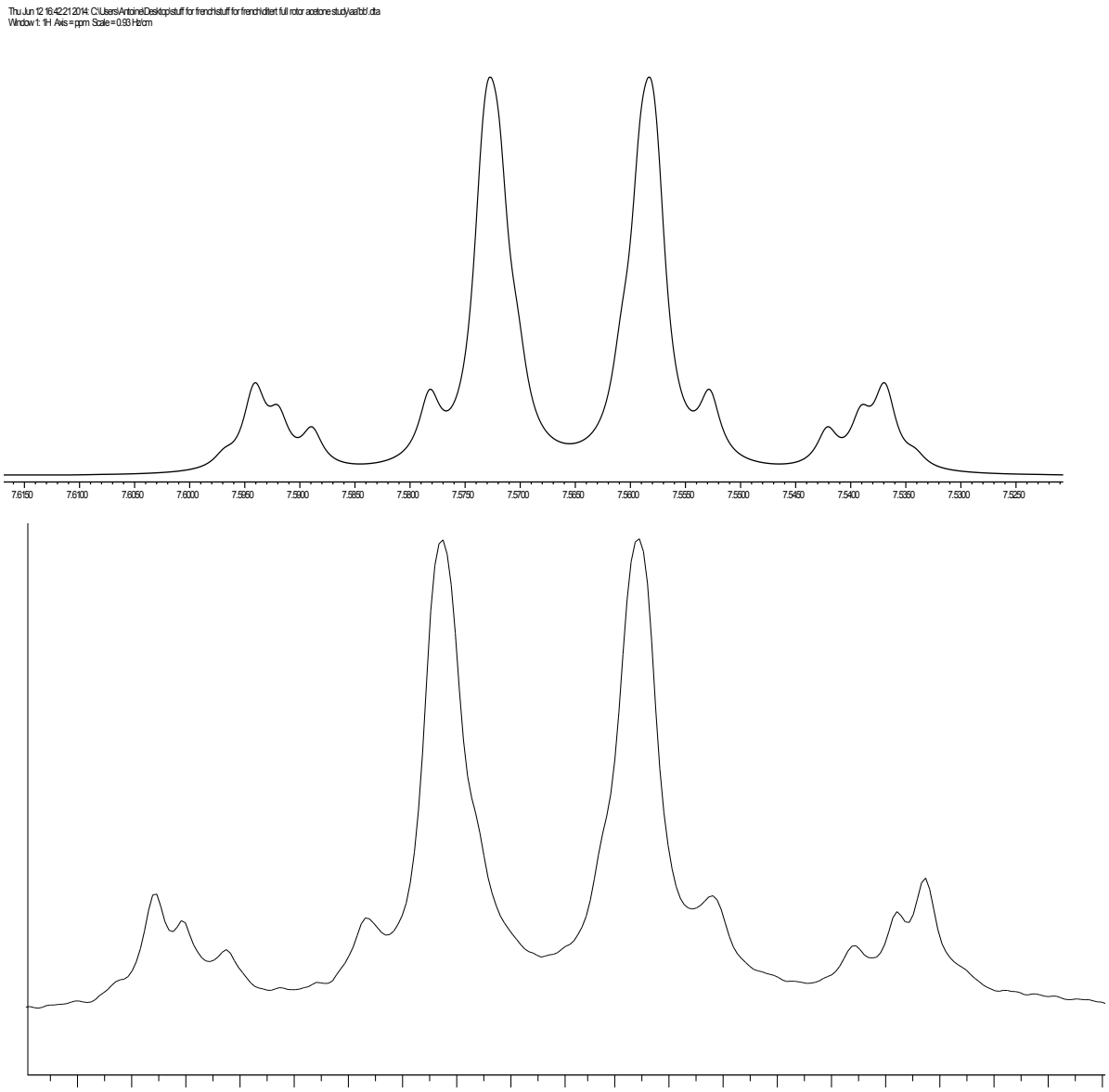

Figure S29. gNMR fitting of central phenylene of **2** simulated (top) experimental (bottom)

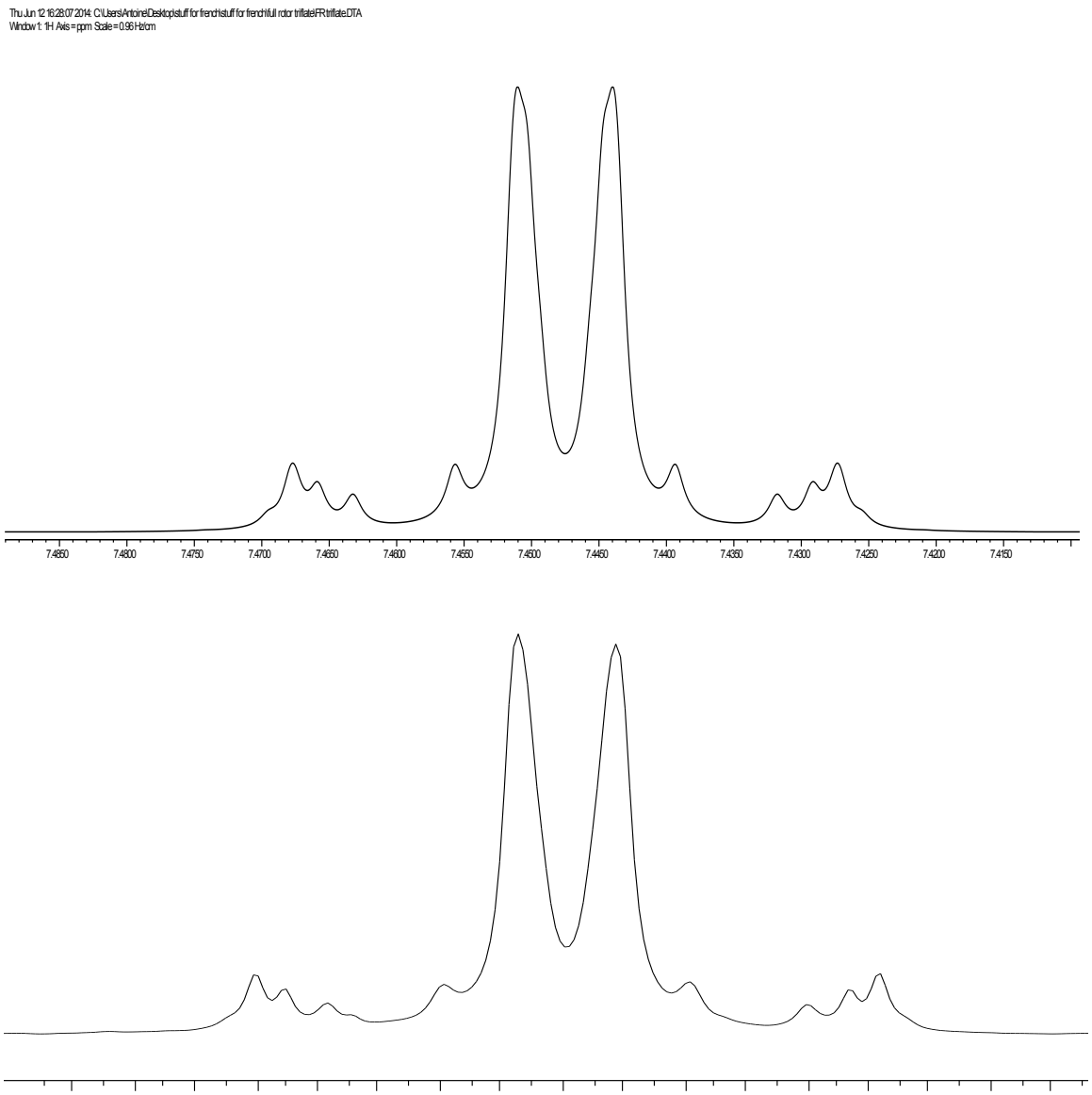

Figure S30. gNMR fitting of central phenylene of **3** simulated (top) experimental (bottom)

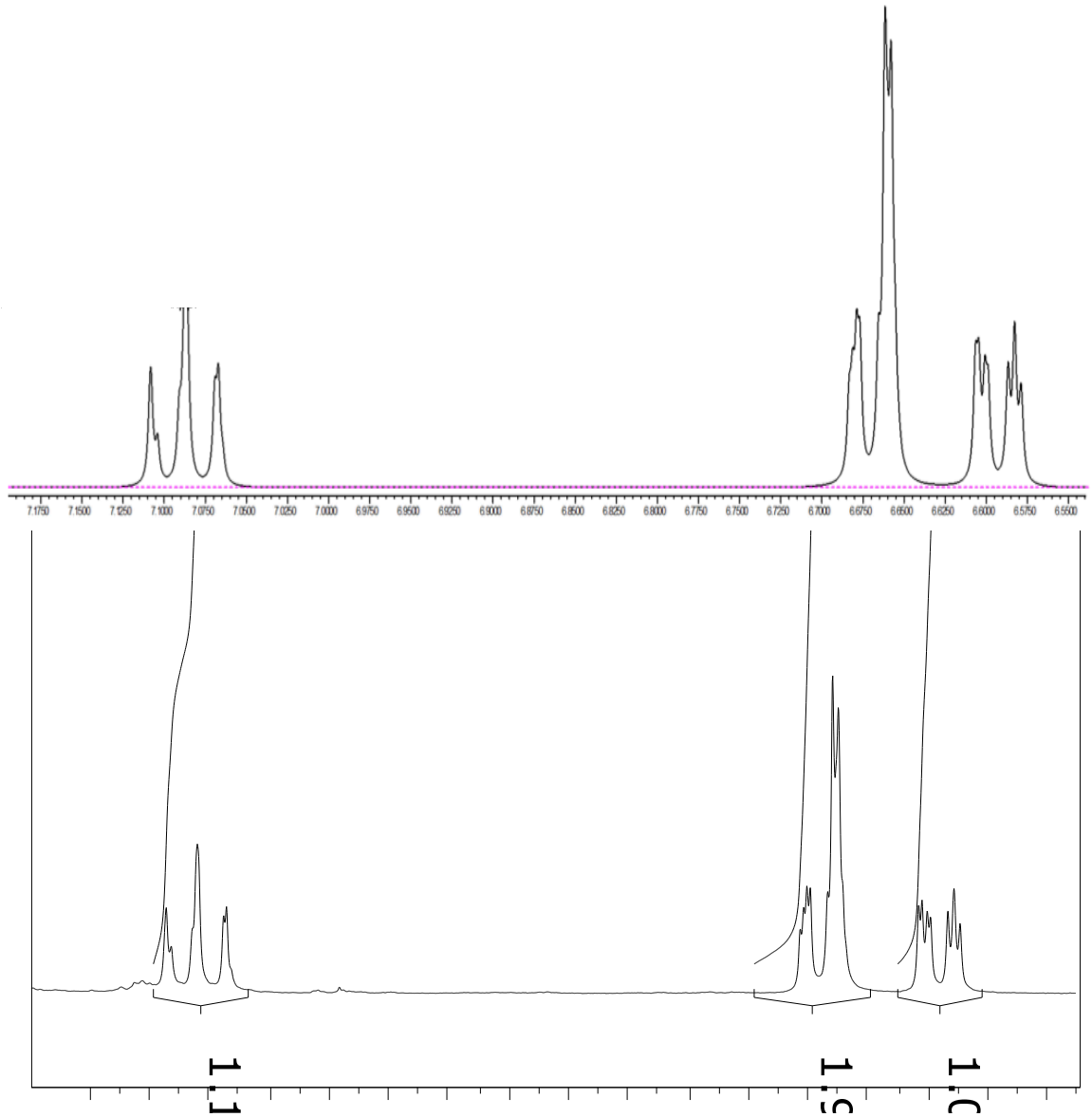

Figure S31. gNMR fitting of aromatic region of **4** simulated (top) experimental (bottom)

3.7. References

[1] a) Koumura, N.; Zijlstra, R.; Delden, R.; Harada, N.; Feringa, B. *Nature,* **1999**, *401*, 152. b) Balzani, V.; Credi, A.; Raymo, F.; Stoddart, F. *Angew. Chem., Int. Ed.,* **2000**, *39*, 3348. c) Kelly, T. R.; De Silva, H.; Silva, R. A. *Nature* **1999**, *401*, 150. d) Karim, A. R.; Linden, A.; Baldridge, K. K.; Siegel, J. S. *Chemical Science* **2010**, *1*, 102. e) Muraoka, T.; Kinbara, K.; Aida, T. *Nature* **2006**, *440*, 512. f) Coskun, A.; Banaszak, M.; Astumian, D. R.; Stoddart, J. F.; Grzybowski, B. A. *Chem. Soc. Rev.* **2012**, *41*, 19. g) Browne, W. R.; Feringa, B. L. *Nat. Nanotechnol.* **2006**, *1*, 25. h) Michl, J.; Sykes, E. C. H. *ACS Nano* **2009**, *3*, 1042.

[2] a) Khuong, T.-A. V.; Nuñez, J. E.; Godinez, C. E.; Garcia-Garibay, M. A. *Acc. Chem. Res.* **2006**, *39*, 413. b) Karlen, S. D.; Garcia-Garibay, M. A. *Top. Curr. Chem.* **2006**, *262*, 179. c) Vogelsberg, C. S.; Garcia-Garibay, M. A. *Chem. Soc. Rev.* **2012**, *41*, 1892.

[3] Saebo, S.; Almolof, J.; Boggs, J. E.; Stark, J. G. *J. Mol. Struct. (Theochem)* **1989**, *200*, 361.

[4] Commins, P.; Garcia-Garibay, M. A. *J. Org. Chem.* **2014**, *79*, 1611-1619.

[5] a) G. S. Kottas; L. I. Clarke, D. Horinek and J. Michl, *Chem. Rev.*, **2005**, *105*, 1281; b) B. L. Feringa, *Acc. Chem. Res.*, **2001**, *34*, 504. c) D. Horinek and J. Michl, *Proc. Natl. Acad. Sci. U. S. A.*, **2005**, *102*, 14175.

[6] a) Koshima, H.; Matsuo, R.; Matsudomi, M.; Uemura, Y.; Shiro, M. *Cryst. Growth Des.,* **2013**, *13*, 4330. b) Harada, J.; Nakajima, R.; Ogawa, K. *J. Am. Chem. Soc.* **2008**, *130*, 7085. c) Amimoto, K.; Kawato, T. *J. Photochem. Photobiol. C Photochem. Rev.* **2005**, *6*, 207.

[7] Commins, P.; Nuñez, J. E.; Garcia-Garibay, M. A. *J. Org. Chem.* **2011**, *76*, 8355–8363

[8] Wolfe, J. P.; Ahman, J.; Sadighi, J. P.; Singer, R. A.; Buchwald, S. L. *Tett. Lett.* **1997**, *38*, 6367.

[9] Kraszni, M.; Szakacs, Z.; Noszal, B. *Anal. Bioanal. Chem.* **2004**, *378*, 1449.

[10] Shtukenberg, A. G.; Punin, Y. O.; Gunn, E.; Kahr, B. *Chem. Rev.* **2012**, *112*, 1805.

[11] Katritzky, A. R.; Akhmedov, N. G.; Güven, A.; Doskocz, J.; Akhmedova, R. G.; Majumder, S.; Dennis Hall, C. *J. Mol. Struct.* **2006**, *787*, 131–147

Chapter 4

Advances in the Functionalization of Crystalline Molecular Rotors with Photoresponsive Properties as Potential Molecular Brakes with Ester-Linked Photochromic Salicylideneanilines

4.1. Introduction

As previously mentioned, artificial molecular machines have drawn the interest of chemists to explore these peculiar molecules for the last 20 years. In particular, some research groups focus on the design and synthesis of molecules that can be switched from one state to another with suitable external stimuli in order to display function.[1] Research in our group has focused on the synthesis of "amphidynamic crystals," [2] which are designed to have motion in a highly anisotropic manner and within a well-defined frame of reference, which should be ideal for the development of artificial molecular machines. Our group thus focuses on the design of crystalline molecular gyroscopes, which have the potential of possessing these characteristics and act as amphidynamic crystals. These compounds emulate macroscopic gyroscopes and are composed of three components, as shown in Figure 1. A rotator is the rotating component or the component with the smallest moment of inertia, which is commonly a 1,4-disubstituted phenylene. The stator is the static portion or the component with the largest moment of inertia, and most often it consists of two triarylmethyl groups at the two ends of the molecular rotor. Lastly, the axle[3] is the component that links the rotator to the components of the stator and is emulated by two alkynyl linkages.

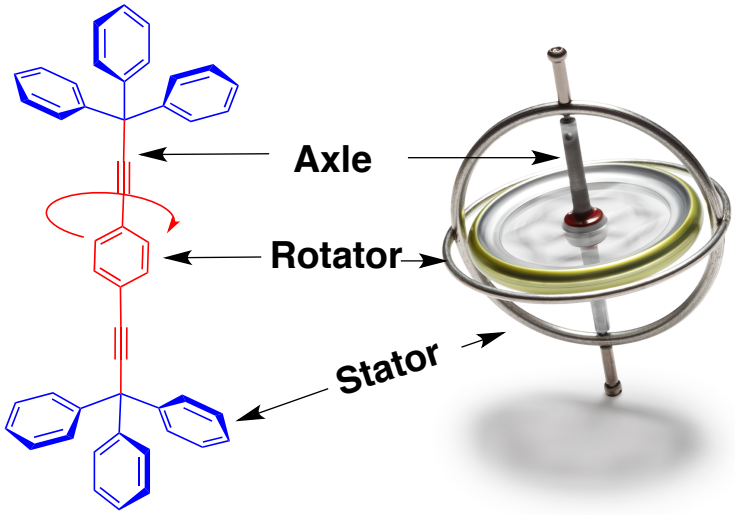

Figure 1. A simplified molecular rotor composed of the three essential components: a rotator, an axle, and a stator alongside the macroscale analog of a gyroscope modified from reference 2d.

The inspiration for the field of artificial molecular machines is derived from biomolecular systems. The membrane-bound flagellar motor displayed in Figure 2 is a complex biomolecular machine that contains over 30 different proteins assembled together to form the components that enable its function.[4] This two-state device functions by switching between left and right handed supercoiled forms that differ in protofilament distance by only 0.8 A.[5a] The structure and function of the flagellum must function with exact, even sub-Angstrom precision in order to execute sophisticated tasks on the molecular scale.

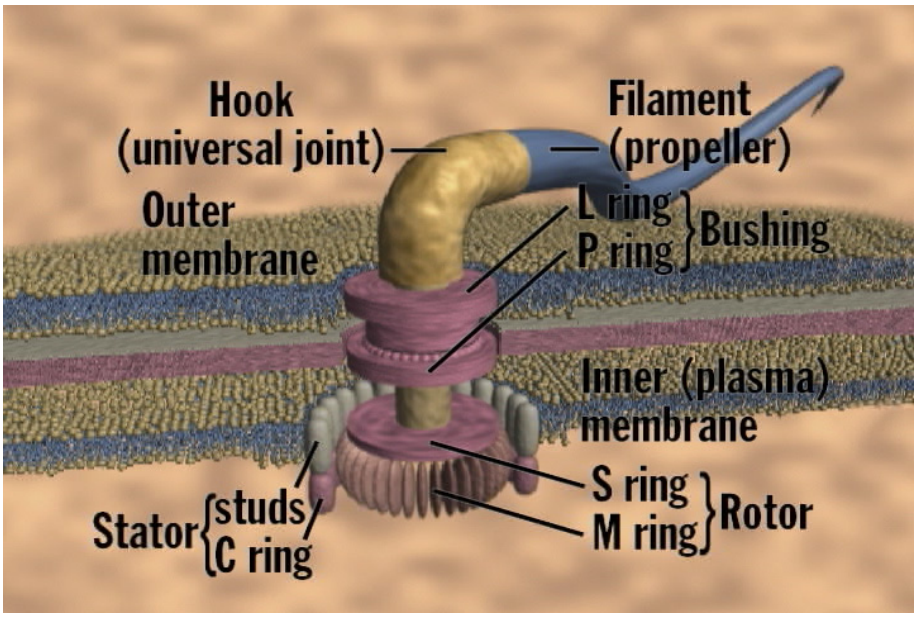

Figure 2. Computer rendering depicting a bacteria flagellum comprised of a stator bound in the plasma membrane and a rotor, which facilitates the motion of the propeller from reference 5c.

In order to generate a system equally complex to these biological counterparts we need to be able to switch the system between two or more states on command. One of the most promising ways to facilitate this is with photochromic molecules. Photochromism generally entails changes in bonding patterns and the extent of conjugation resulting from electrocyclic reactions, proton transfer, and tautomerism, as well as *trans*-to-*cis* double bond isomerizations.[6] In the specific case of salicylideneanilines (SAs), they exist in thermal equilibrium between *cis*-enol and *cis*-keto tautomeric forms, as shown in Figure 3, with the aromatic hydroxyl-bearing tautomer being the most stable.

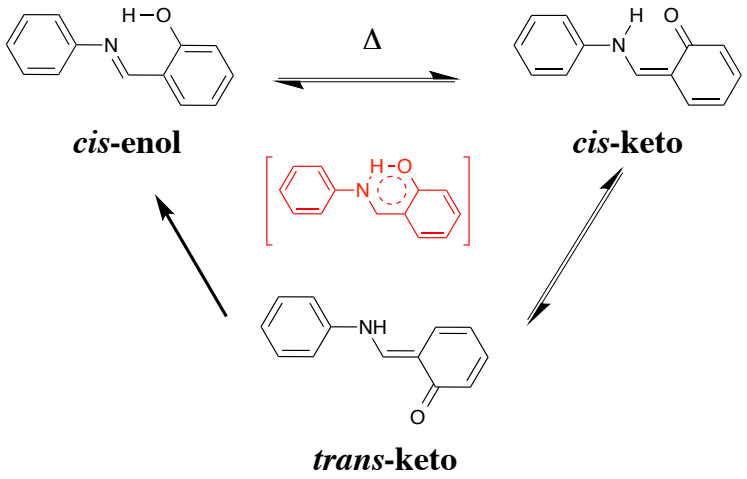

Figure 3. Three tautomeric forms of salicyladeneaniline with the most stable being the *cis*-enol with a small steady state concentration of the *cis*-keto. Upon excitation the *trans*-keto is generated which thermally relaxes back to the ground state.

As indicated in reference 5b, "Photochromism in these molecules occurs upon electronic excitation of the stable *cis*-enol followed by an adiabatic oxygen-to-nitrogen proton transfer reaction and an isomerization process that positions the N-H group opposite to the carbonyl oxygen to form the longer-lived, *trans*-keto species,[6a] which has a red colored *ortho*-quino-dimethane chromophore[7]" (Figure 3). As previously shown in Chapter 2, salicylideneanilines (SA) have been introduced into the rotator. In this respect, we decided to synthesize and study how the introduction of SAs on the stator portion of the gyroscope could affect the rotation of the compounds. The rotator and stator functionalized rotors are illustrated in Figure 4.

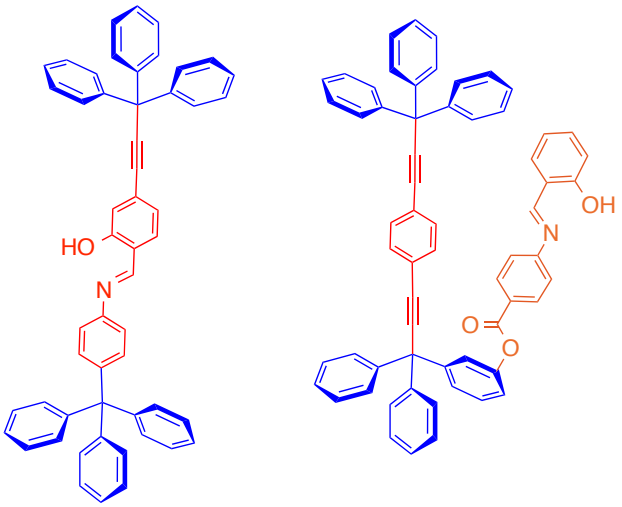

Figure 4. On the left is the SA functionalized rotator while on the right is proposed ester SA functionalized molecular rotor.

We report here the synthesis, characterization, and attempted crystallization of an ester linked molecular rotor with a SA[8]-functionalized stator**,** illustrated in Figure 4.

4.2. Synthesis and Characterization

The synthesis of salicylideneaniline ester linked rotor **3** was achieved over two steps starting from previously reported monohydroxy substituted rotor.[9] Monohydroxy substituted rotor was reacted with boc-p-aminobenzoic acid, N,N'-diisopropylcarbodiimide, and dimethylaminopyridine in a dichloromethane/dimethylformamide (1:1) for 3 h at 0 ^{o}C, after this time the reaction was allowed to warm up to room temperature and stirred for an additional 48 h to afford PABA-boc ester linked rotor **1** in a 45% yield, shown in Scheme 1. Rotor **1** was then deprotected, using trifluoroacetic acid (50% by volume) in dichloromethane for 1 h at 0 ^{o}C to afford amino ester linked rotor **2** in 81% yield.

Scheme 1.

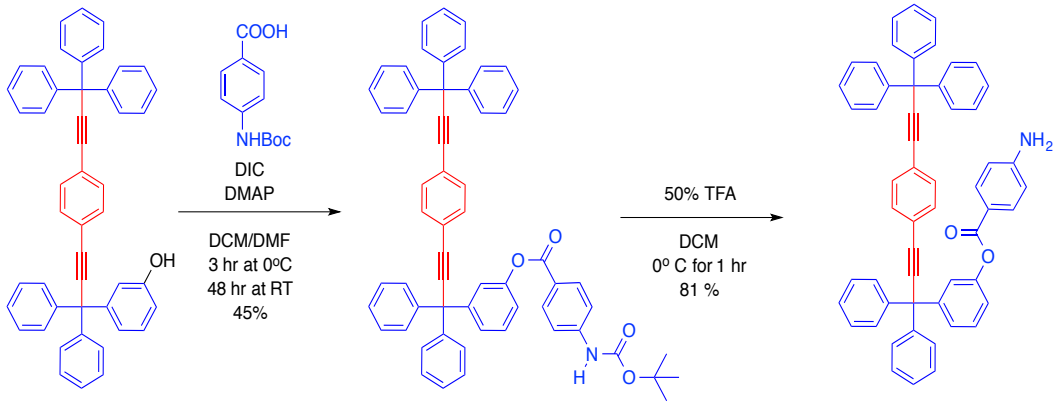

With amino ester linked rotor **2** in hand, it was reacted with salicylaldehyde and 4 Å molecular sieves to facilitate the dehydration in refluxing toluene for 20 h to afford **3** in 37% yield, shown in Scheme 2.

Scheme 2.

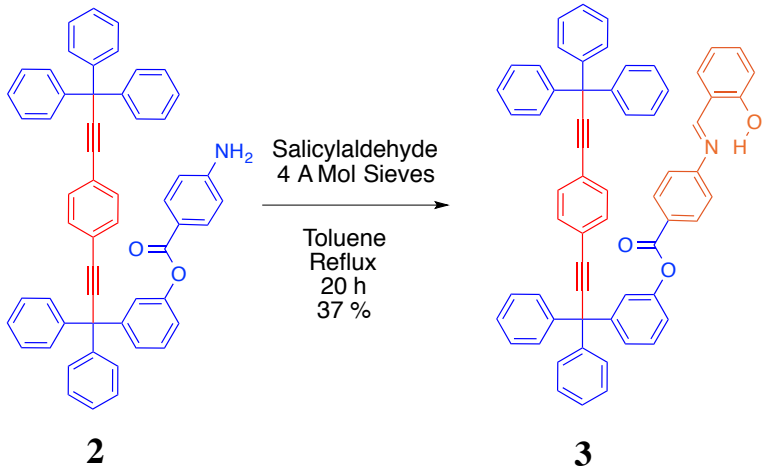

The ^{1}H NMR spectra of **1** and **2** have characteristic signals for the central phenlyene, along with the AA'BB' coupling of the extended portion of the stator. The extended portion of the stator showed two doublets at 8.08 and 7.46 ppm for **1,** and 7.96 and 6.67 ppm for **2**. This corresponded well to the different environments felt by the AA'BB' ring system between **1** (pull-pull) and **2** (pull-push). The central

phenylene showed a characteristic signal at 7.44 ppm and corresponds to four protons. Additionally **1** had a characteristic signal at 1.54, corresponding to the *tert*-butyl protons.

Compound **3** had a phenol hydrogen located at 12.80 ppm, in addition to an aldimine hydrogen at 8.64 ppm. The AA'BB' system was still observed as two doublets, however it shifted to 8.22 and 6.95 ppm. The central phenylene shifted to 7.46 ppm, indicating a minor change in shielding. The ^{13}C NMR spectra showed several characteristic signals for compounds **1**-**3**. The carbonyl carbon for **1** was located at 164.6 ppm, while the carbonyl of **2** was located at 165.0 ppm and the carbonyl of **3** was located at 164.6 ppm. Unique to **3** was the hydroxyl bearing carbon located at 161.6 ppm.

Due to the asymmetry in the molecule, the alkyne carbons correlated to four distinct signals. In compound **1,** these signals corresponded to 97.3, 96.9, 85.1 and 84.8 ppm. The alkynes for compound **2** were observed at 97.3, 96.9, 85.0, and 84.8 ppm. In compound **3,** these signals corresponded to 97.6, 97.0, 85.4 and 85.0 ppm. The signal at 56.1 ppm corresponded to the quaternary trityl carbon atom, in the case of **1** and **2,** and 56.4 ppm, in the case of **3**. The FT-IR spectra of **1** had a broad signal that spanned from 3700-3000 cm^{-1} , which was attributed to the N-H stretch. Additionally the signals at 1728 and 1704 cm^{-1} were attributed to the C=O ester stretch, while the signals at 1670 and 1642 cm^{-1} were attributed to the C=O amide stretch. The spectra of **2** had two sharp signals at 3487 and 3382 cm^{-1} ,attributed to the N-H protons. The signals at 1723 and 1713 cm^{-1} were attributed to the C=O ester stretch. Compound **3** had a broad signal that spanned from 3600-2800,

attributed to the O-H stretch. Characteristic imine stretches were observed at 1661 and 1644 cm^{-1} ,corresponding to the SA formation.

4.3. Crystallization Study

Crystallization studies for compound **3** were carried out at room temperature, using different dry solvents and solvent mixtures. Based on previously reported crystallization conditions[10] , it was determined that we should try to crystallize this system from methanol. In a typical experiment, ca. 15 mg of the selected compound was placed in a small glass vial, dissolved with the appropriate solvent or solvent mixture (ca. 1 mL), and capped. Samples were monitored regularly until the first crystal appeared. Although single crystals were obtained, the X-ray crystal structure solution revealed that they were formed with compound **2**. This was attributed to the hydrolysis of the salicylaldehyde group during the crystallization, because of traces of water. However, after various crystallization attempts with numerous solvents, no other solvent produced single crystals. The X-ray determined structure of compound **2** can be viewed in Figure 5.

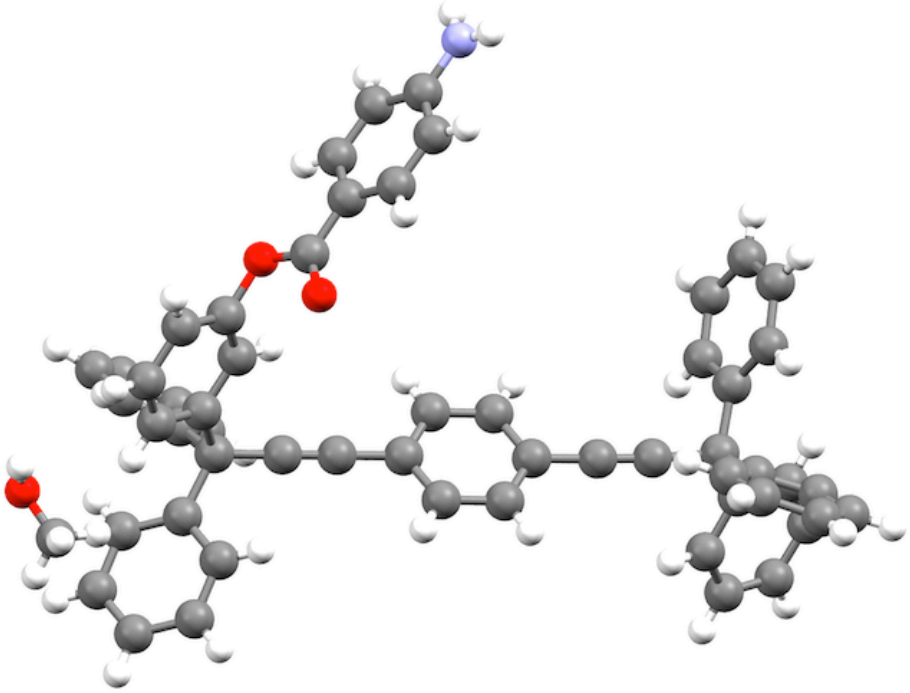

Figure 5. Low quality single crystal which shows the connectivity of **2** with one methanol molecule in the lattice and one disordered phenyl ring in the stator, which was removed, belonging to the space group C2/c.

4.4. Solid-State NMR

Spectroscopic determination of the *cis*-keto and *trans*-keto forms of salicylideneanilines by ^{13}C CPMAS NMR has been well documented.[11] Variable temperature ^{13}C CPMAS NMR measurements were taken of two standard compounds, along with **3**. The first standard was a methylated salicylideneaniline; the spectra for this sample was collected before and after irradiation at 365 nm light for 15 minutes and is shown in Figure 6.

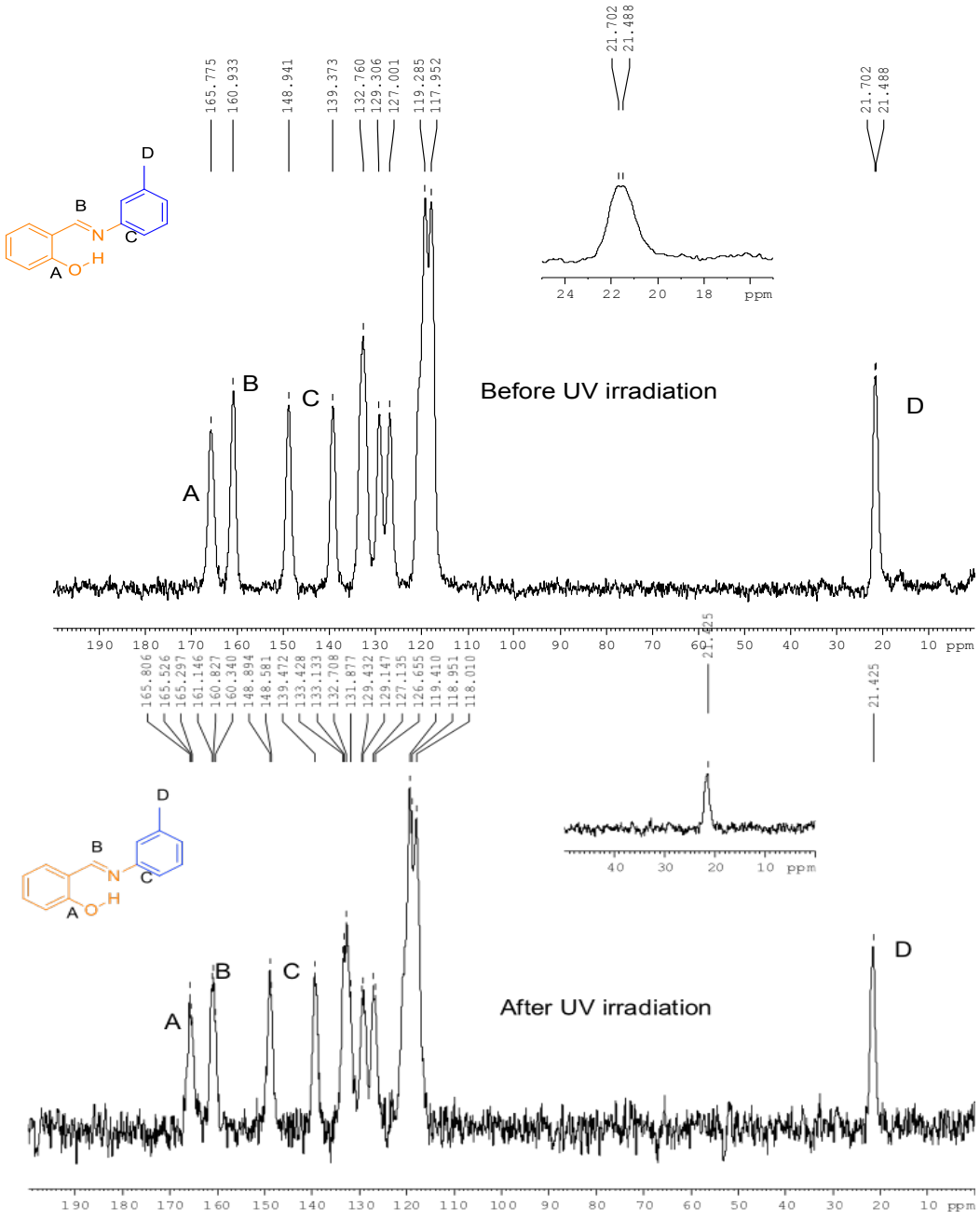

Figure 6. Methylated salicylideneaniline by ^{13}C CPMAS before irradiation (top) compared to the same sample after 15 minutes of irradiation (bottom). Peak assignments are labeled.

Four characteristic signals were observed at 165.8 ppm ascribed to the phenolic carbon, at 160.9 ppm ascribed to the imine carbon, at 148.9 ppm ascribed to the amino carbon, and, lastly, at 139.4 ppm ascribed to the methylated phenyl

carbon. Minimal changes were observed with the spectra, however, the sample color was visibly photoresponsive, going from a yellow color to a deep orange. This suggested that the photoirradiation did not penetrate past the surface layer, resulting in a minimal change in the overall sample composition. Complementarily, a second standard, ester linked salicylideneaniline, was monitored using variable temperature ^{13}C CPMAS NMR, with the aim of documenting the thermochromic properties from -100 ^{o}C to 100 ^{o}C. Utilizing the thermochromic properties, a homogenous sample mixture was obtained, rather than just the surface layer, as in the case of the photoresponsive case, providing improved signal to noise. No new chemical shifts were observed over a 200^{o} C temperature range, as shown in Figure 7.

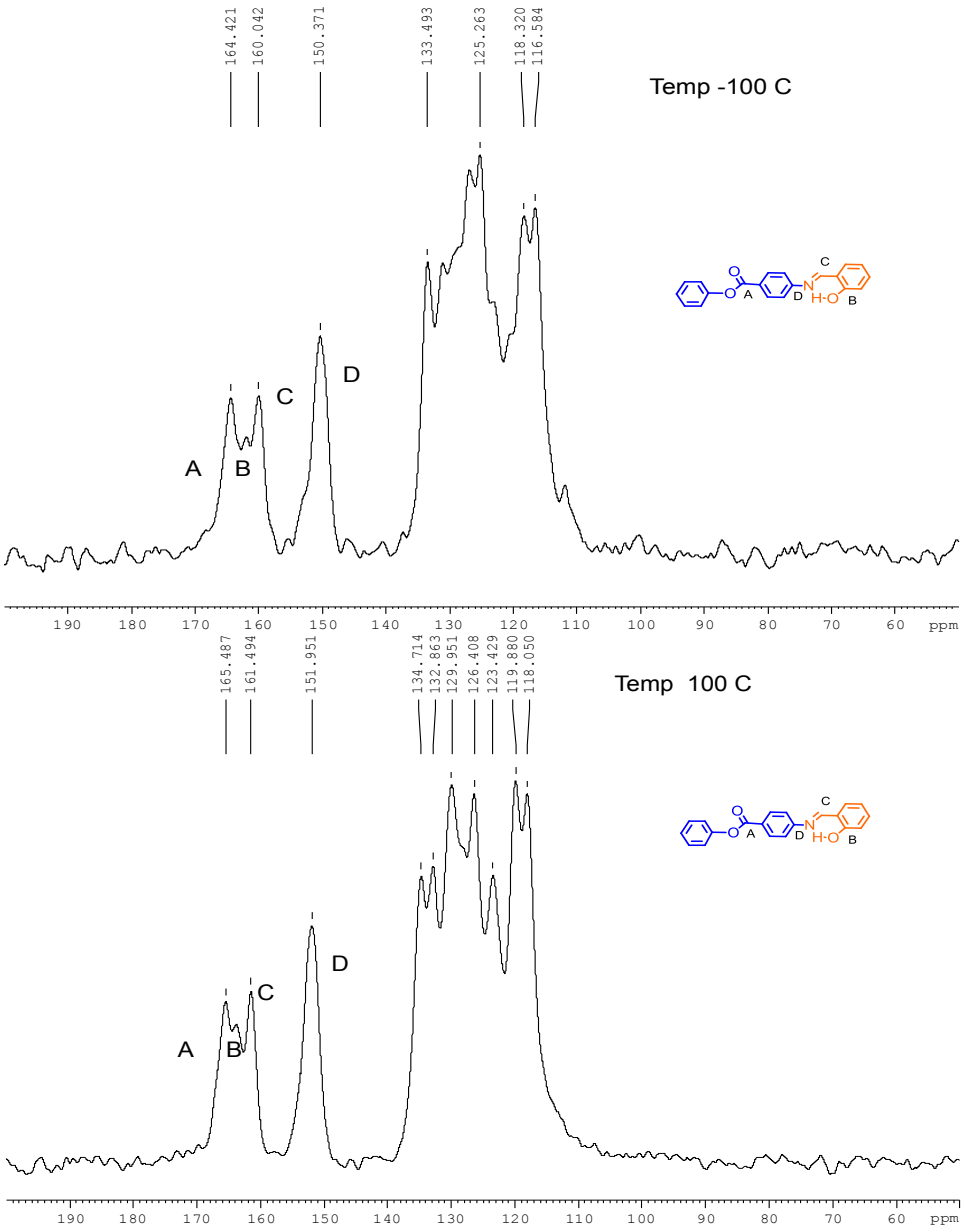

Figure 7. Ester linked salicylideneaniline by ^{13}C CPMAS at -100 ^{o}C (top) compared to the same sample at 100 ^{o}C (bottom). Peak assignments are labeled.

Similar to standard ester linked saliylideneaniline, compound **3** showed no detectable amount of the keto forms, as illustrated in Figure 8.

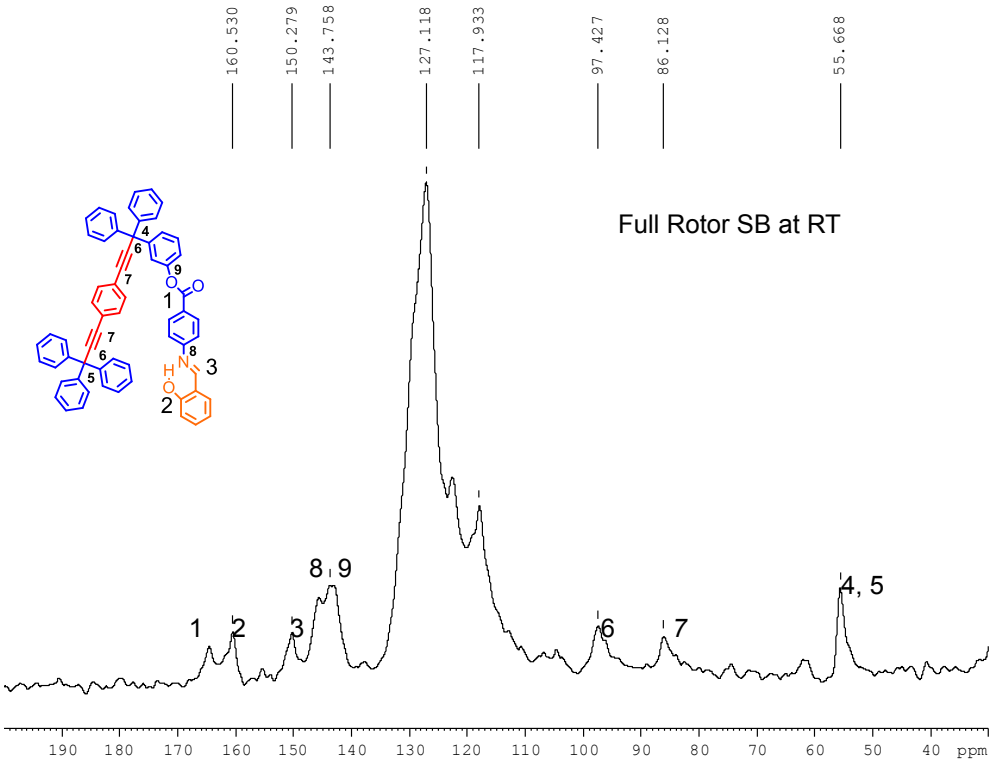

Figure 8. ^{13}C CPMAS of compound **3** at RT, however, no signals appear above 170 ppm, which would indicate *trans*- or *cis*- keto form. Peak assignments are labeled.

Based on these findings, further ^{13}C CPMAS NMR characterization was not pursued.

4.5. Conclusions

Salicyladeneaniline ester linked rotor **3** was synthesized and characterized, but single crystals could not be grown. Rapid cleavage of the salicylaldehyde ring occurred, which could be attributed to trace water. Additionally the ester linked arm possessed a high degree of conformational freedom, thus reducing the potential motion of the central phenylene by consuming some of the 3N-6 vibrational modes. It was clear that functionalization of the stator was possible, but the flexibility of the linker should be reduced in order to limit the degrees of freedom of the molecule, as it is well known that rigid molecules are more prone to crystallization. Based on the

results shown in this chapter, it can be concluded that the synthesis and exploration of analogous systems with less flexible linkers may help obtain crystalline molecular rotors with a photochromic unit. This may increase the understanding of structures capable of displaying function, which may be useful for future material applications.

4.6. APPENDIX

General Methods

The IR spectra were obtained with a Perkin-Elmer spectrum 100 HATR FT-IR instrument. The ^{1}H and ^{13}C NMR spectra were acquired on a Brüker NMR spectrometer at 400 and 100 MHz or 300 and 75 MHz, respectively, with $CDCl_3$ as the solvent. Mass spectra were acquired on an Applied Biosystems voyager-DE-STR MALDI-TOF. Samples for diffuse reflectance were placed on a barium sulfate plate and pressed. A Coherent 405 nm CUBE laser was used to excite the solid in a NMR tube at both room temperature and 77K, and the subsequent emission spectra were monitored using a Princeton Instruments Roper CCD detector, which was cooled, to liquid nitrogen temperatures. The acetyl chloride, 0.5 M ethynylmagnesium bromide in THF, diisopropylamine, CuI, bis(triphenylphosphine) palladium (II) chloride, potassium carbonate, tetra-n-butylammonium fluoride, boc-p-aminobenzoic acid, N,N'-diisopropylcarbodiimide, dimethylaminopyridine, trifluoroacetic acid, salicylaldehyde, 1 M boron tribromide in DCM, were commercially available and were used without further purification. THF and benzene were distilled from sodium and kept under argon. Toluene was distilled from calcium hydride and kept under argon.

Synthesis of PABA-boc ester linked rotor 1

In a round bottom flask, under argon atmosphere a stir bar was added, followed by 1 g of monohydroxy rotor (1.597 mmol) powder was dissolved in DMF (20 mL) and DCM (50 mL) combined with 378 mg of PABA-Boc (1.593 mmol) powder. The resulting solution was then cooled to 0 °C followed by the addition of 200 mg of DIC

(1.585 mmol) and 200 mg of DMAP (1.637 mmol). The solution was then stirred for 3 h at 0°C. After this time the solution was allowed to warm up to room temperature and then stirred for an additional 48 h. The resulting solution is rinsed with 1M HCl (2 x 20 mL) followed by saturated $NaHCO_3$ (2 x 20 mL). This solution is then dried over $MgSO_4$ and filtered. This is then reduced under reduced pressure to yield an off white solid. This was then purified by column chromatography using silica gel and hexanes/dichloromethane (1:2) to afford 607 mg (45 %) of **1** as an off white solid m.p. 235-237 °C. ^{1}H NMR ($CDCl_3$) δ: 8.08 (d, *J*= 8 Hz, 2H), 7.46 (d, *J*= 8 Hz, 2H), 7.44 (s, 4H), 7.40-7.10 (m, 29H), 6.67 (s, 1H), 1.54 (s, 9H), ^{13}C NMR (CDCl3) δ: 164.6, 150.8, 147.0, 145.2, 145.0, 144.8, 143.3, 140.9, 131.6, 131.5, 131.4, 129.2, 129.1, 128.2, 128.1, 127.1, 126.94, 126.90, 126.89, 123.6, 123.3, 123.0, 122.6, 121.7, 120.5, 117.8, 117.4, 116.4, 114.0, 106.5, 97.3, 96.9, 85.1, 84.8, 81.4, 56.1, 28.3. FT-IR (powder, HATR, cm $^{-1}$): 3339, 2976, 2932, 2242, 1728, 1704, 1671, 1643, 1598, 1530, 1490. HRMS (ESI+, m/*z*) calculated for $C_{60}H_{47}NO_4$ = 845.35051, found 846.3583, error: -9.2 ppm.

Synthesis of amino ester linked rotor 2

In a round bottom flask, under argon atmosphere a stir bar was added along with 250 mg of **1** (0.296 mmol) was dissolved in DCM (30 mL). The resulting solution was then cooled to 0 °C followed by the addition of 50% TFA/DCM by volume (5 mL). The solution was then stirred for 1 h at 0 °C. The resulting crude was allowed to warm up to room temperature and then washed with saturated Na_2CO_3 (2 x 20 mL) followed by brine (2 x 20 mL). The organic layer was dried with $MgSO_4$ and then reduced under reduced pressure to yield an off white solid. This was then

purified by column chromatography using silica gel and hexanes/dichloromethane (1:4) to afford 179 mg (81 %) of **2** as an off white solid m.p. 251-253 °C. ^{1}H NMR ($CDCl_3$) δ: 7.96 (d, *J*= 8 Hz, 2H), 7.44 (s, 4H), 7.37-7.23 (m, 27H), 7.22-7.18 (m, 2H), 7.15-7.11 (m, 2H), 6.67 (d, *J*= 8 Hz, 2H), ^{13}C NMR ($CDCl_3$) δ: 165.0, 151.0, 146.8, 145.2, 144.8, 132.3, 131.5, 131.4, 130.1, 129.1, 128.8, 128.2, 128.1, 128.0, 127.7, 127.0, 126.9, 126.40, 126.36, 123.2, 123.1, 122.6, 120.6, 118.8, 113.8, 97.3, 96.9, 85.0, 84.8, 56.1, 56.0. FTIR (powder, HATR, cm $^{-1}$):3487, 3382, 3063, 3034, 2924, 2849, 17234, 1713, 1621, 1602, 1491. HRMS (ESI+, m/*z*) calculated for $C_{55}H_{39}NO_2$ = 745.29808, found 746.3063, error: -11.0 ppm.

Synthesis of salicyladeneaniline ester linked rotor 3

In a round bottom flask with a condenser adapted, under argon atmosphere, 150 mg of amino ester linked rotor **2** (0.20 mmol) powder was combined with 5 mL of salicylaldehyde (1.00 mmol). To the flask 4 A molecular sieves were added along with dry toluene (30 mL). The solution was then allowed to reflux 20 h. The reaction was worked up by filtering and then reduced under reduced pressure to yield a yellow solid. This was then purified by column chromatography using silica gel and hexanes/dichloromethane (1:1) to afford 63 mg (37 %) of **3** as a yellow solid m.p. 192-194 °C. ^{1}H NMR ($CDCl_3$) δ: 12.80 (s, 1H), 8.64 (s, 1H), 8.22 (d, *J*= 7 Hz, 2H), 7.46 (s, 4H), 7.45-7.02 (m, 33H), 6.95(d, *J*= 7 Hz, 2H) ^{13}C NMR (CDCl3) δ: 164.6, 161.6, 153.4, 151.0, 147.4, 145.4, 145.0, 134.1, 132.8, 131.9, 131.7, 131.6, 129.4, 129.1, 128.3, 128.2, 127.9, 127.2, 127.0, 126.9, 123.6, 123.3, 122.8, 121.4, 120.6, 119.4, 119.2, 117.6, 97.6, 97.0, 85.4, 85.0, 56.4, 53.4. FT-IR (powder, HATR, cm $^{-1}$):3600-2800 very broad, 3068, 2847, 1662, 1644, 1619, 1580, 1485, 1459, 1386,

1274. HRMS (ESI+, m/z) calculated for $C_{62}H_{43}NO_3$ = 849.32429, found 850.3, error: -11.0 ppm.

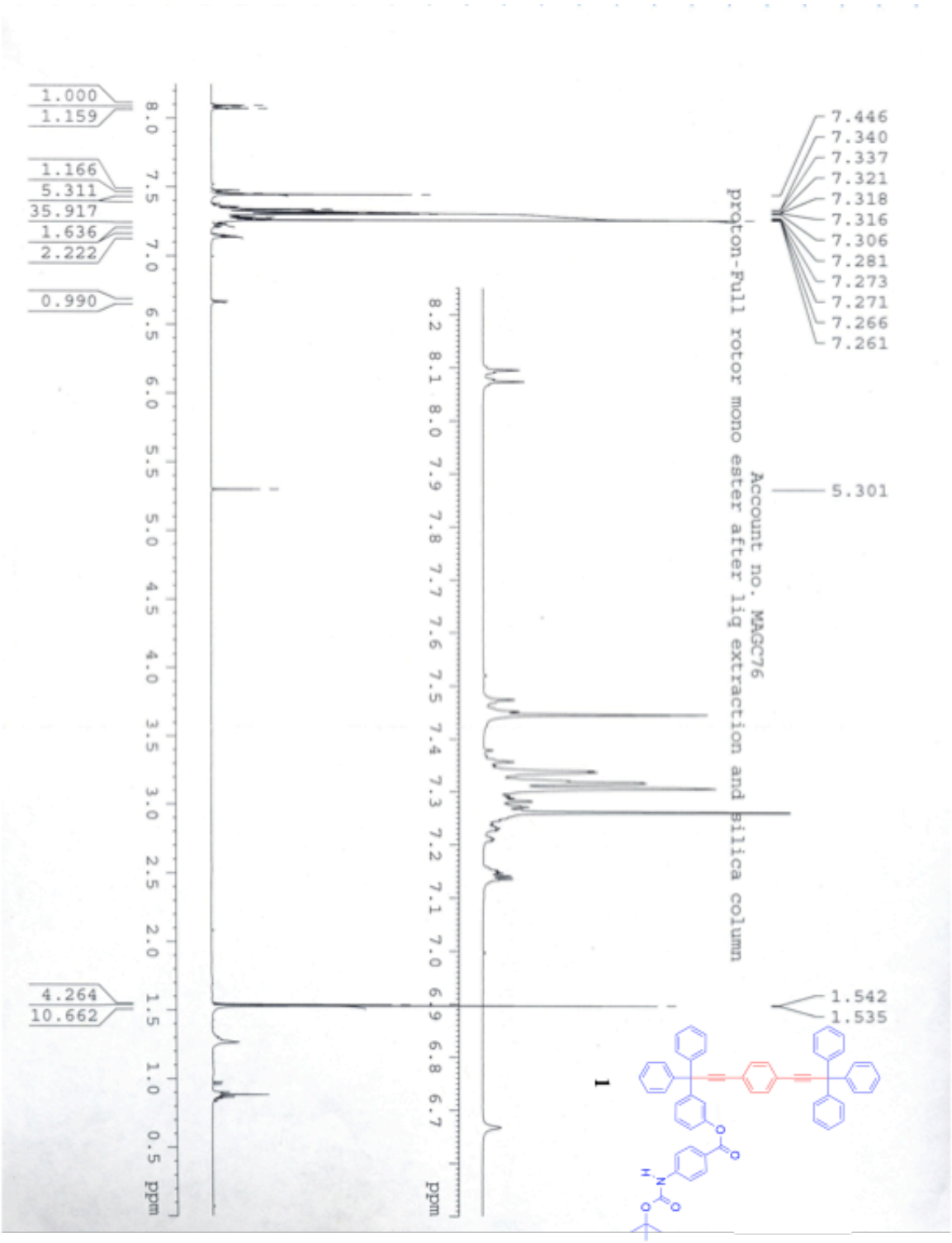

Figure S1. ^{1}H NMR of PABA-boc ester linked rotor **1**
400 MHz ^{1}H NMR spectrum of compound **1** in $CDCl_3$

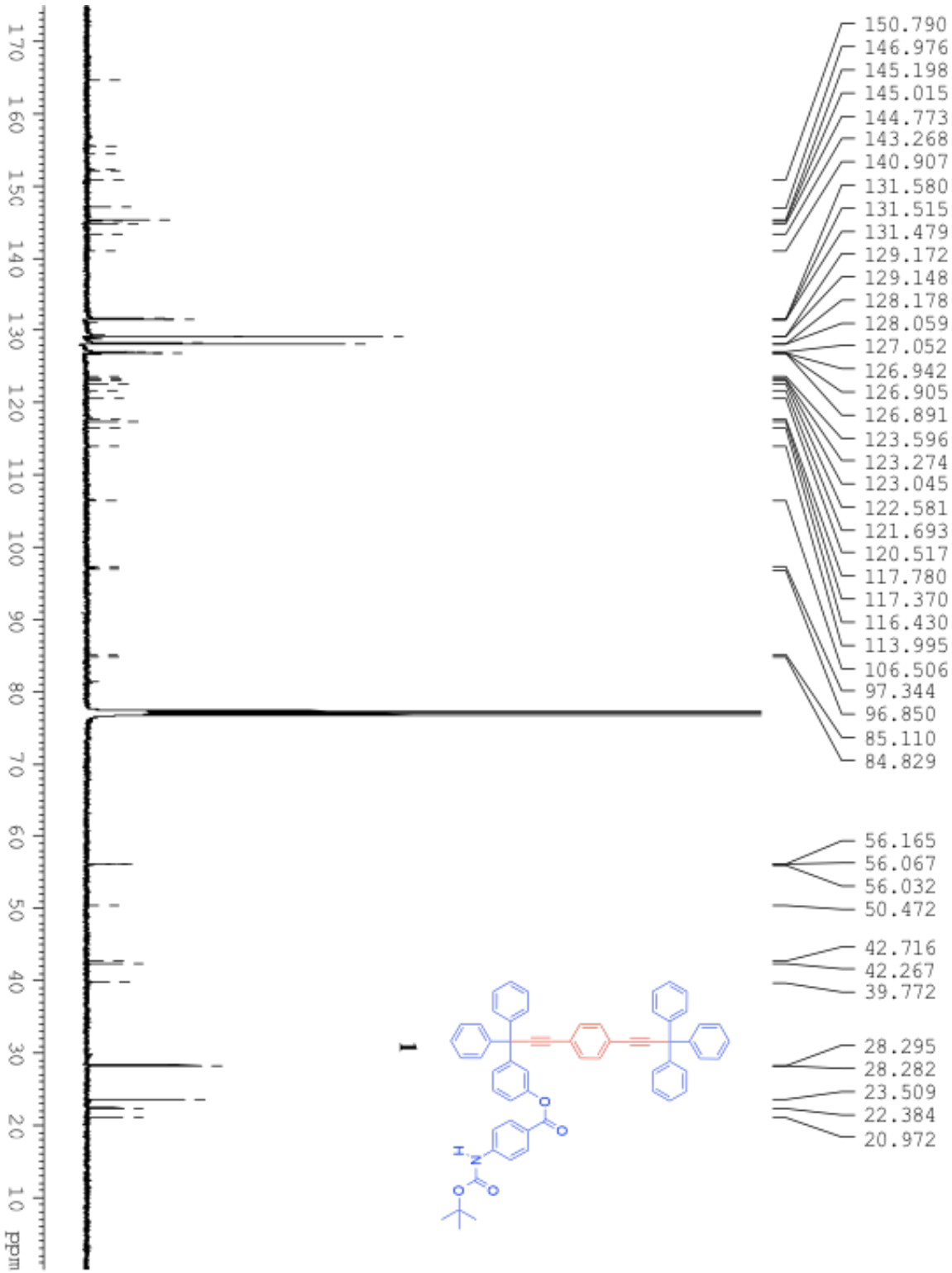

Figure S2. ^{13}C NMR of PABA-boc ester linked rotor **1**
100 MHz ^{13}C NMR spectrum of compound **1** in $CDCl_3$

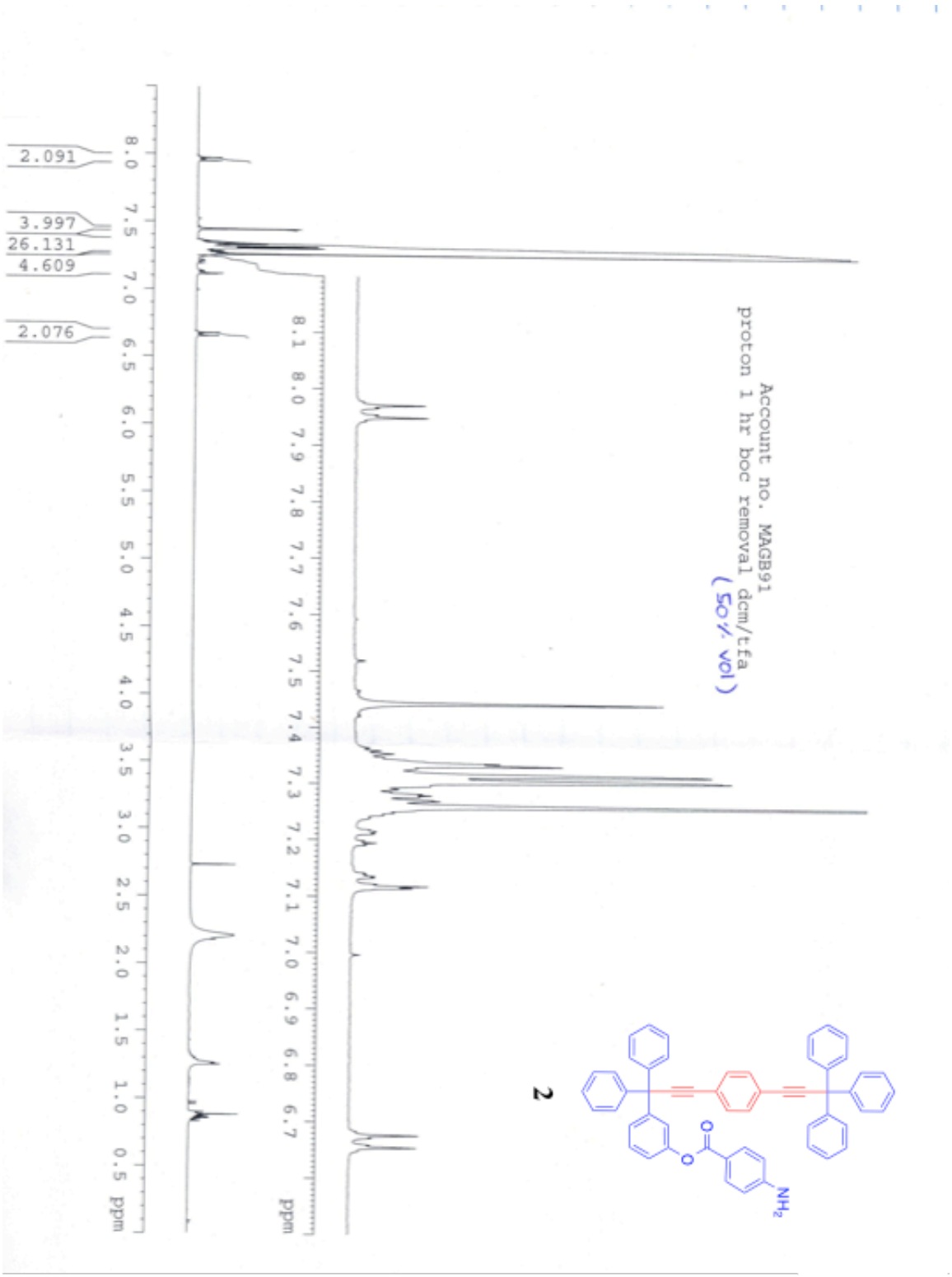

Figure S3. ^{1}H NMR of amino ester linked rotor **2**
400 MHz ^{1}H NMR spectrum of compound **2** in $CDCl_3$

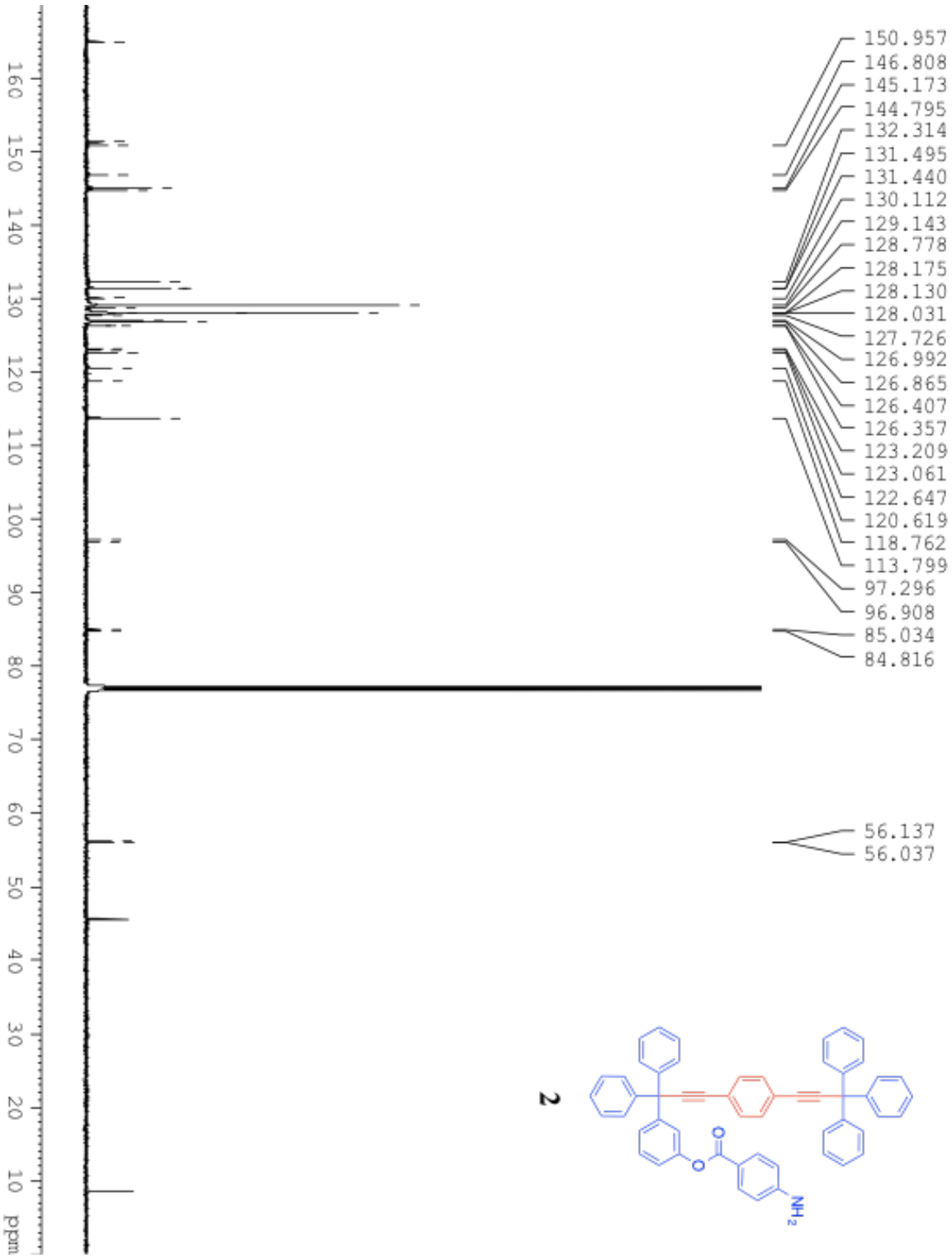

Figure S4. ^{13}C NMR of amino ester linked rotor **2**
100 MHz ^{13}C NMR spectrum of compound **2** in $CDCl_3$

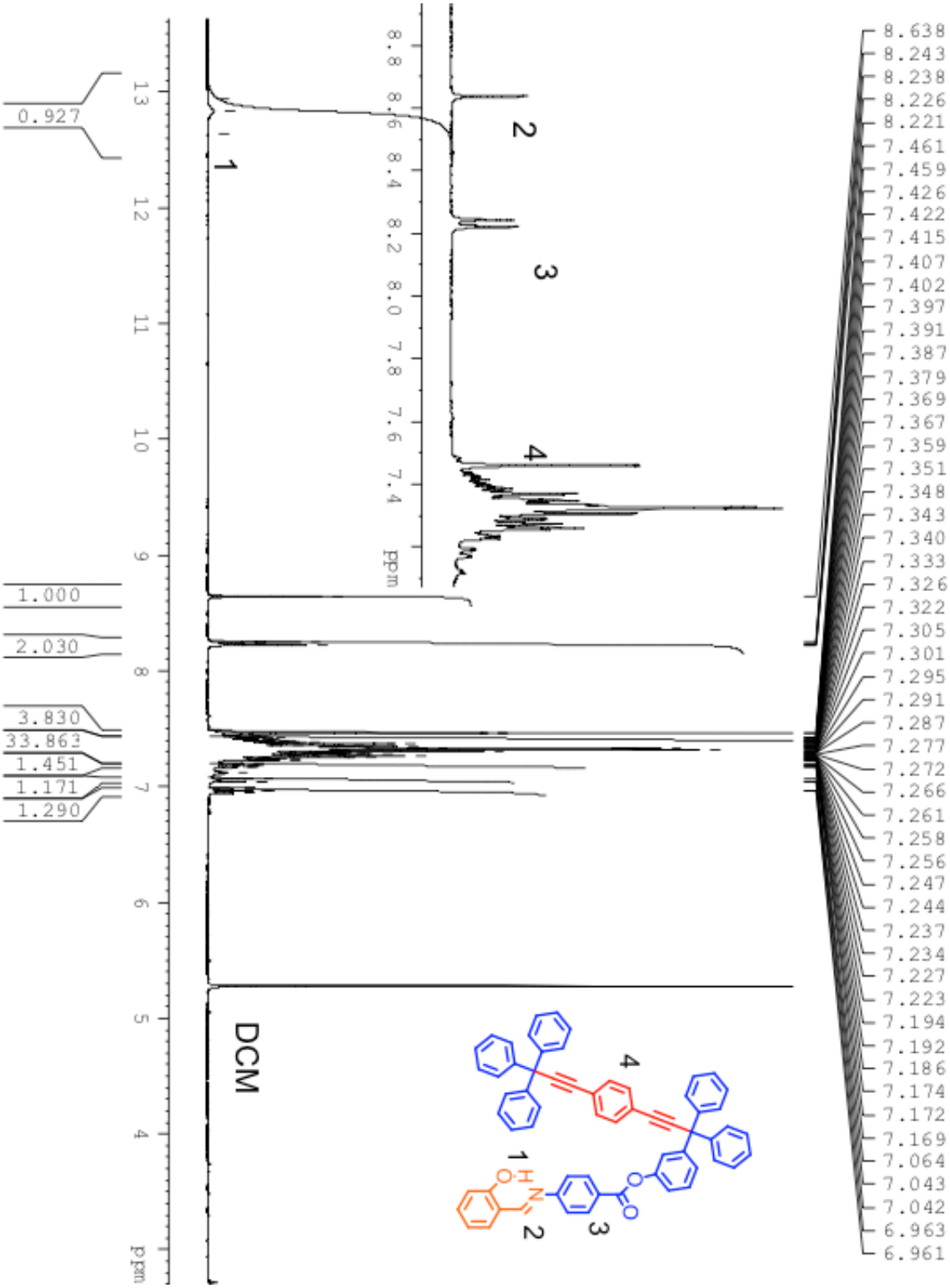

Figure S5. ^{1}H NMR of salicyladeneaniline ester linked rotor **3**
400 MHz ^{1}H NMR spectrum of compound **3** in $CDCl_3$

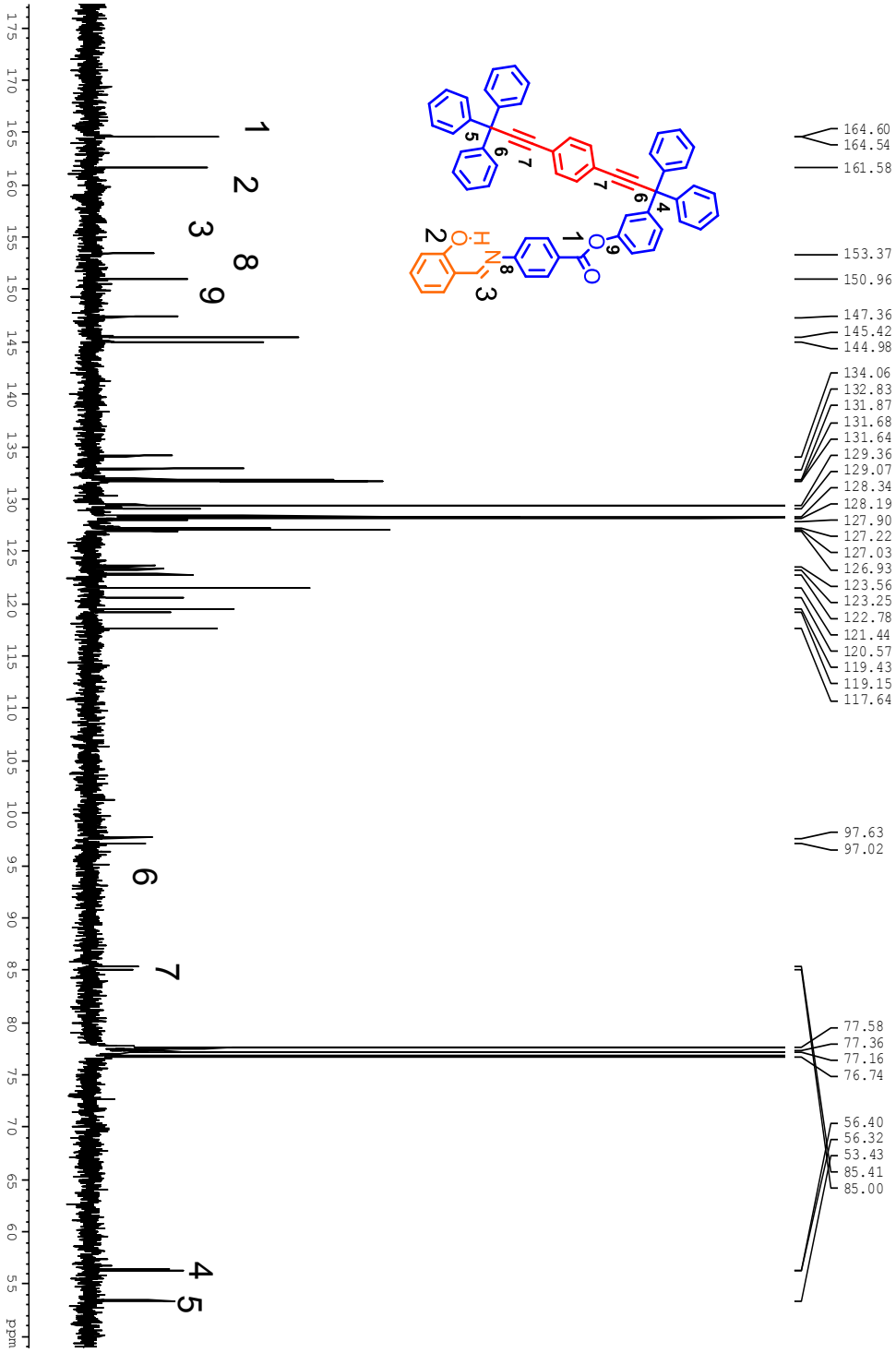

Figure S6. ^{13}C NMR of salicyladeneaniline ester linked rotor **3**
100 MHz ^{13}C NMR spectrum of compound **3** in $CDCl_3$

Figure S7. Maldi-TOF of PABA-boc ester linked rotor **1**

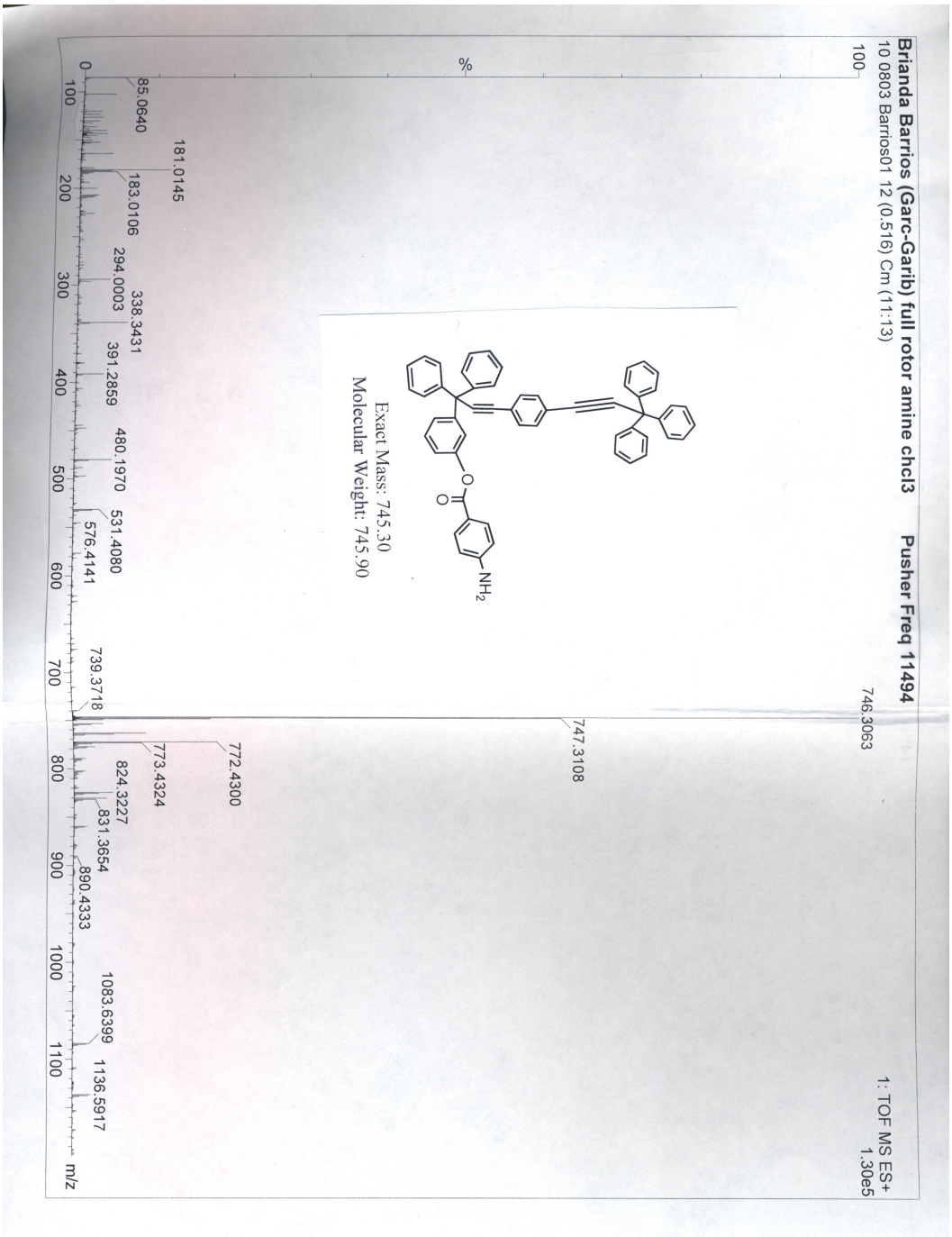

Figure S8. Maldi-TOF of amino ester linked rotor **2**

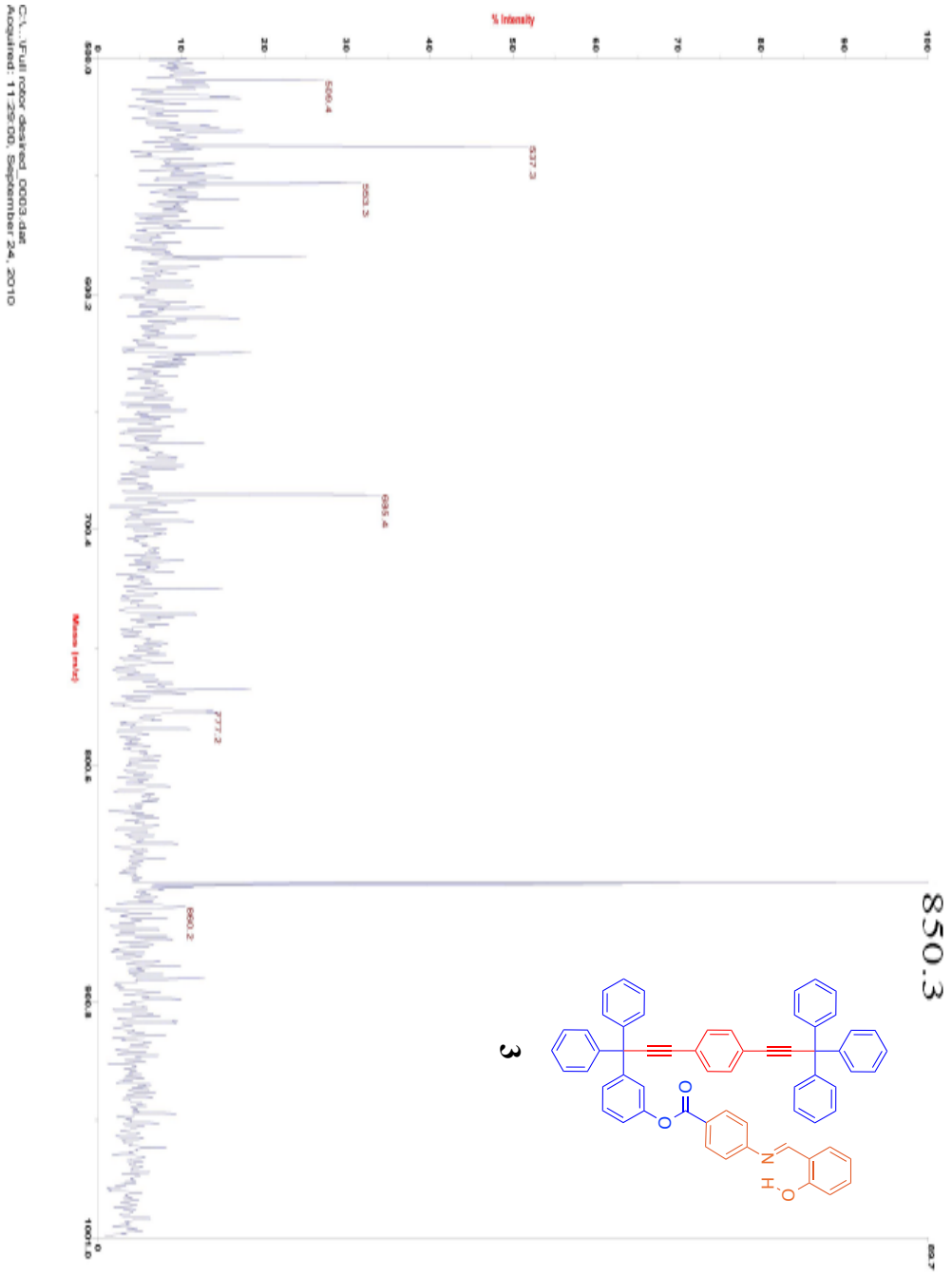

Figure S9. Maldi-TOF of salicyladeneaniline ester linked rotor **3**

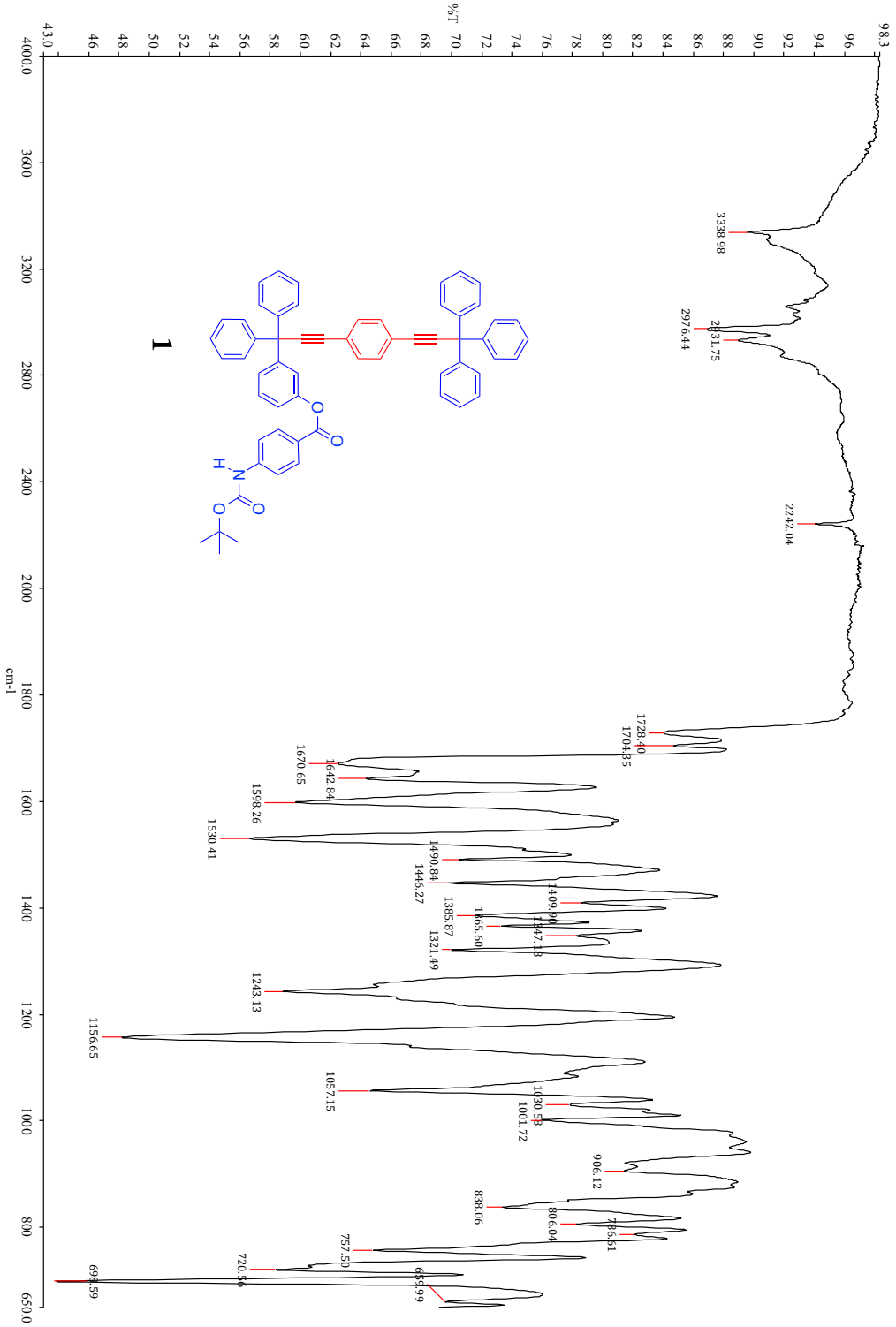

Figure S10. FT-IR of PABA-boc ester linked rotor **1**

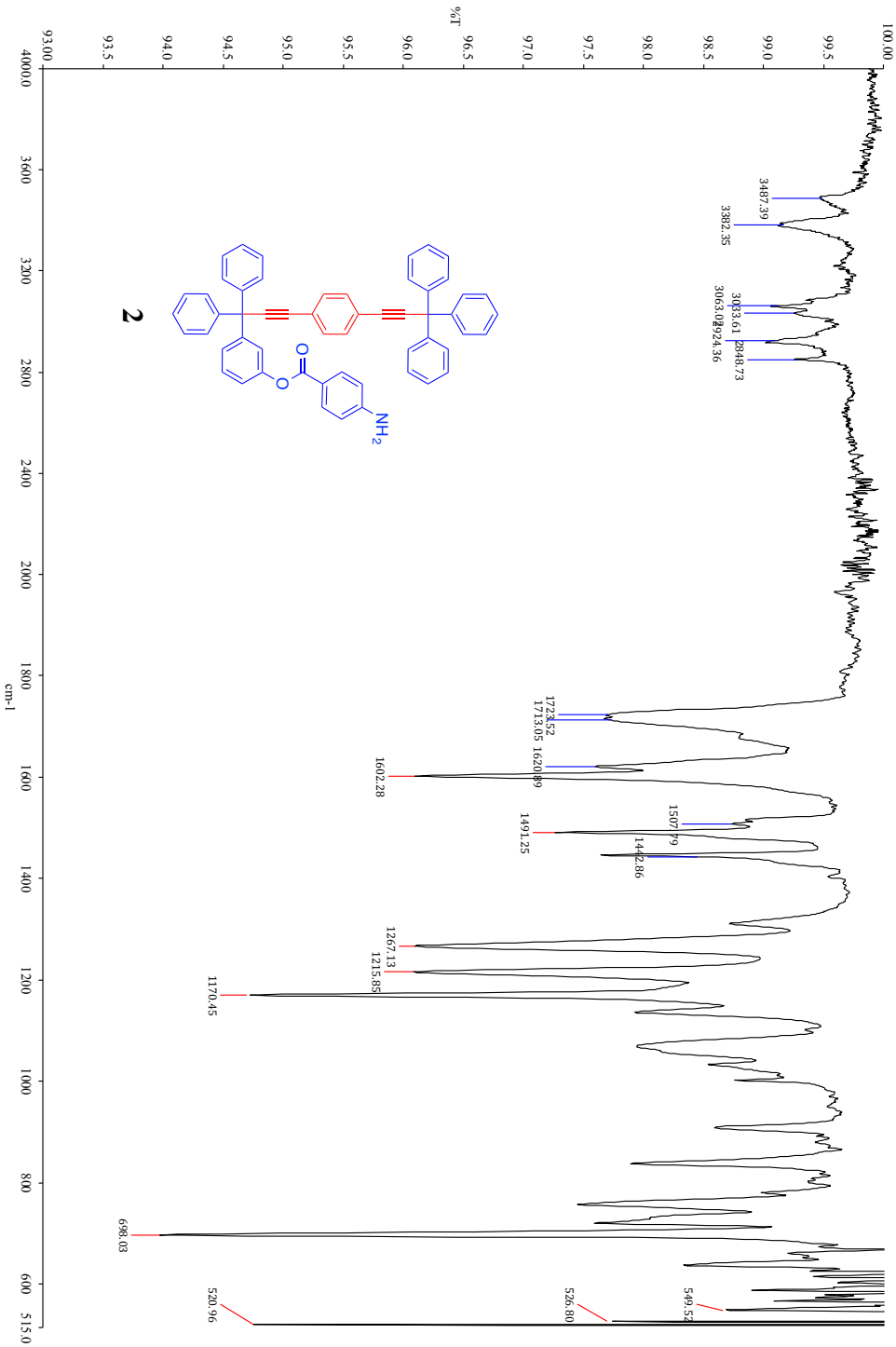

Figure S11. FT-IR of amino ester linked rotor **2**

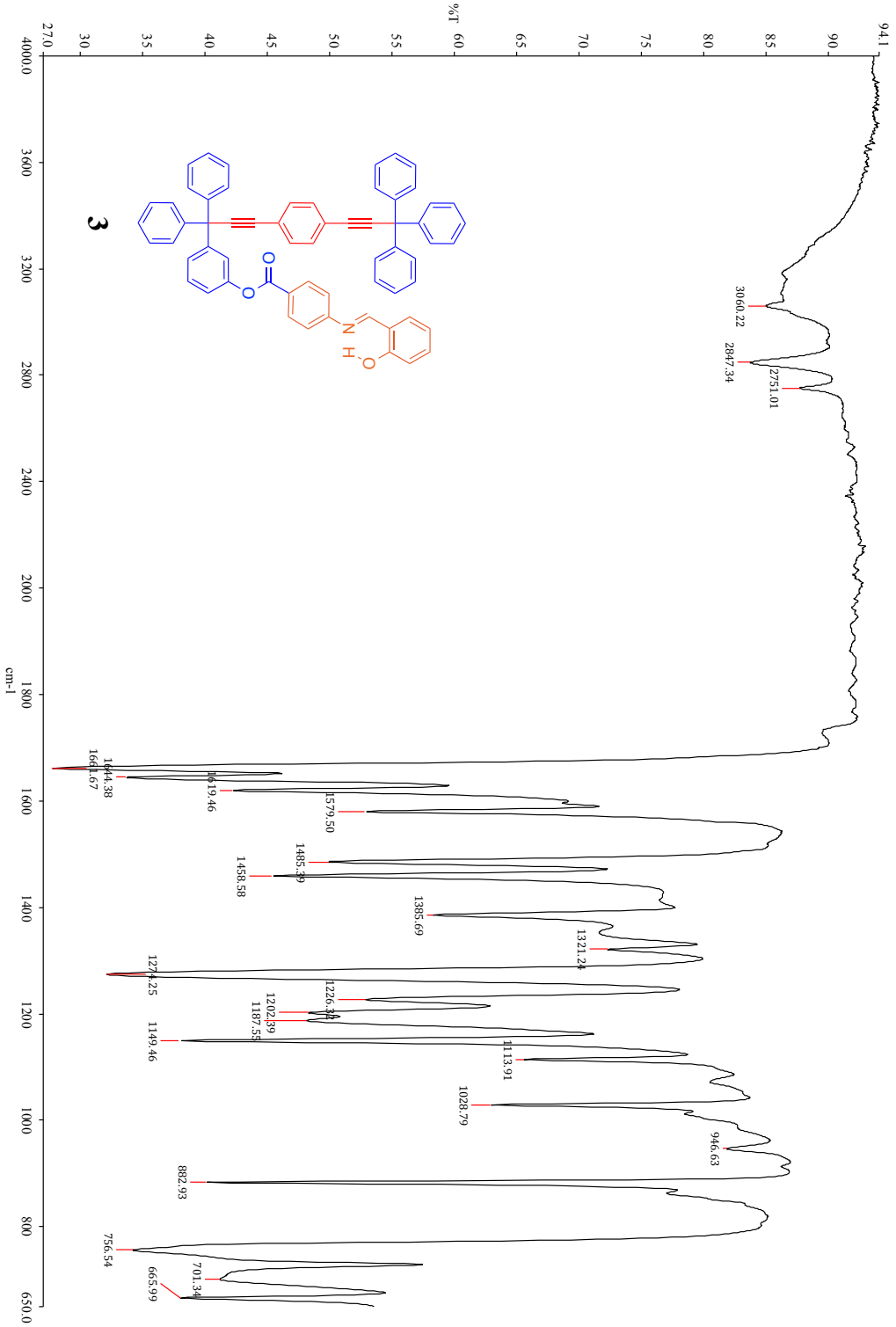

Figure S12. FT-IR of salicyladeneaniline ester linked rotor **3**

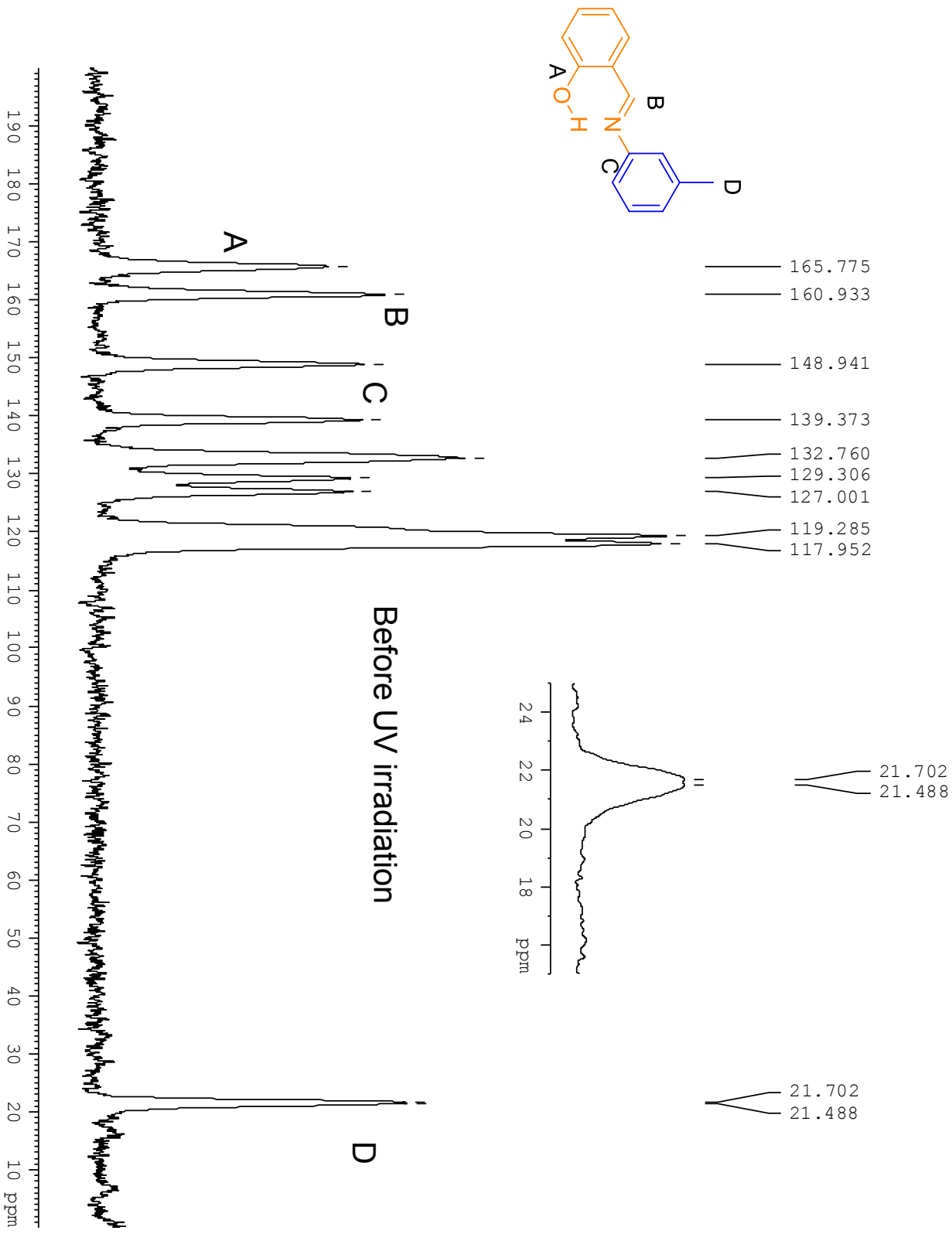

Figure S13. CPMAS of standard methyl salicyladeneaniline before irradiation with 365 nm light

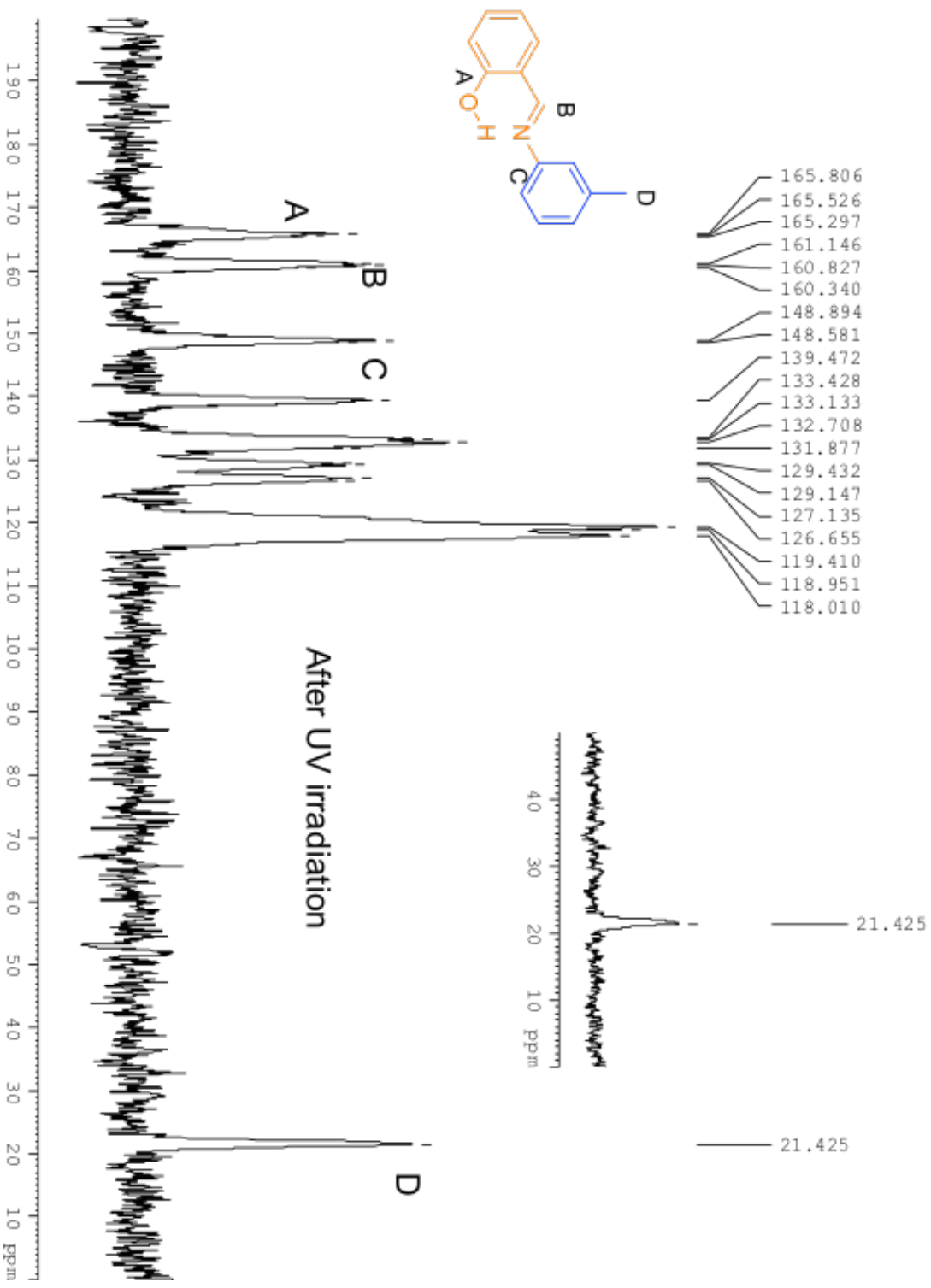

Figure S14. CPMAS of standard methyl salicyladeneaniline after irradiation with 365 nm light

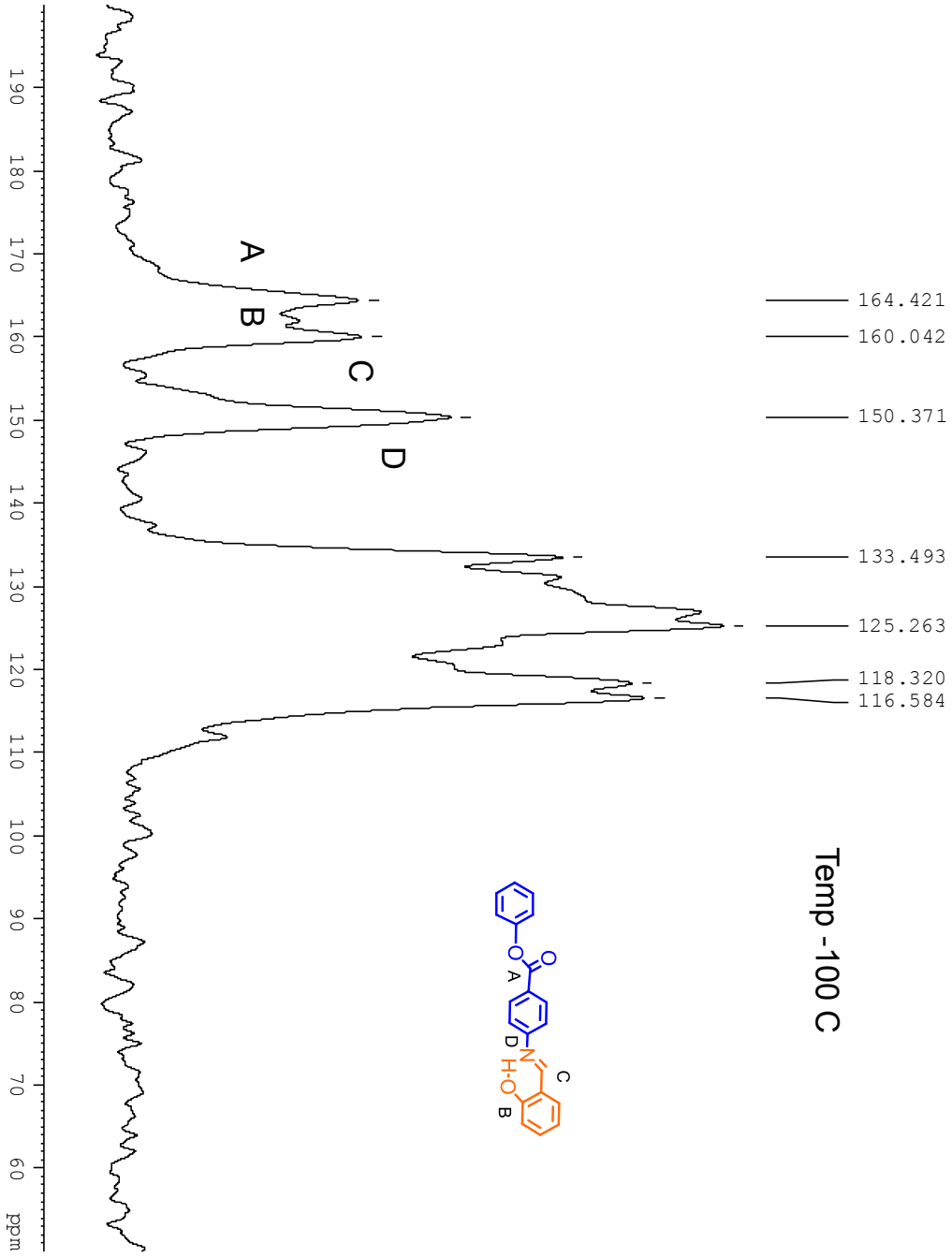

Figure S15. CPMAS of standard ester linked salicyladeneaniline at -100 °C

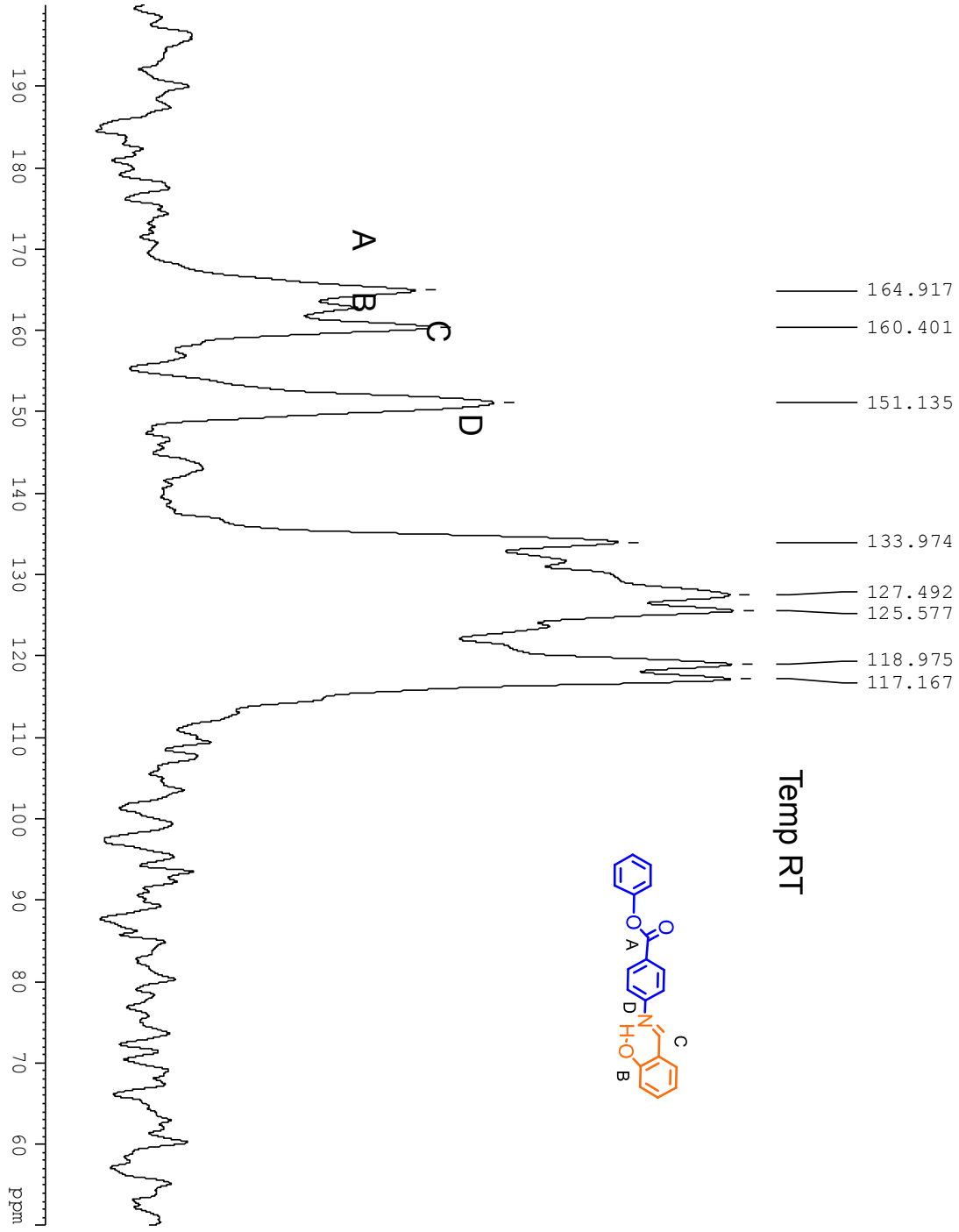

Figure S16. CPMAS of standard ester linked salicyladeneaniline at room temperature

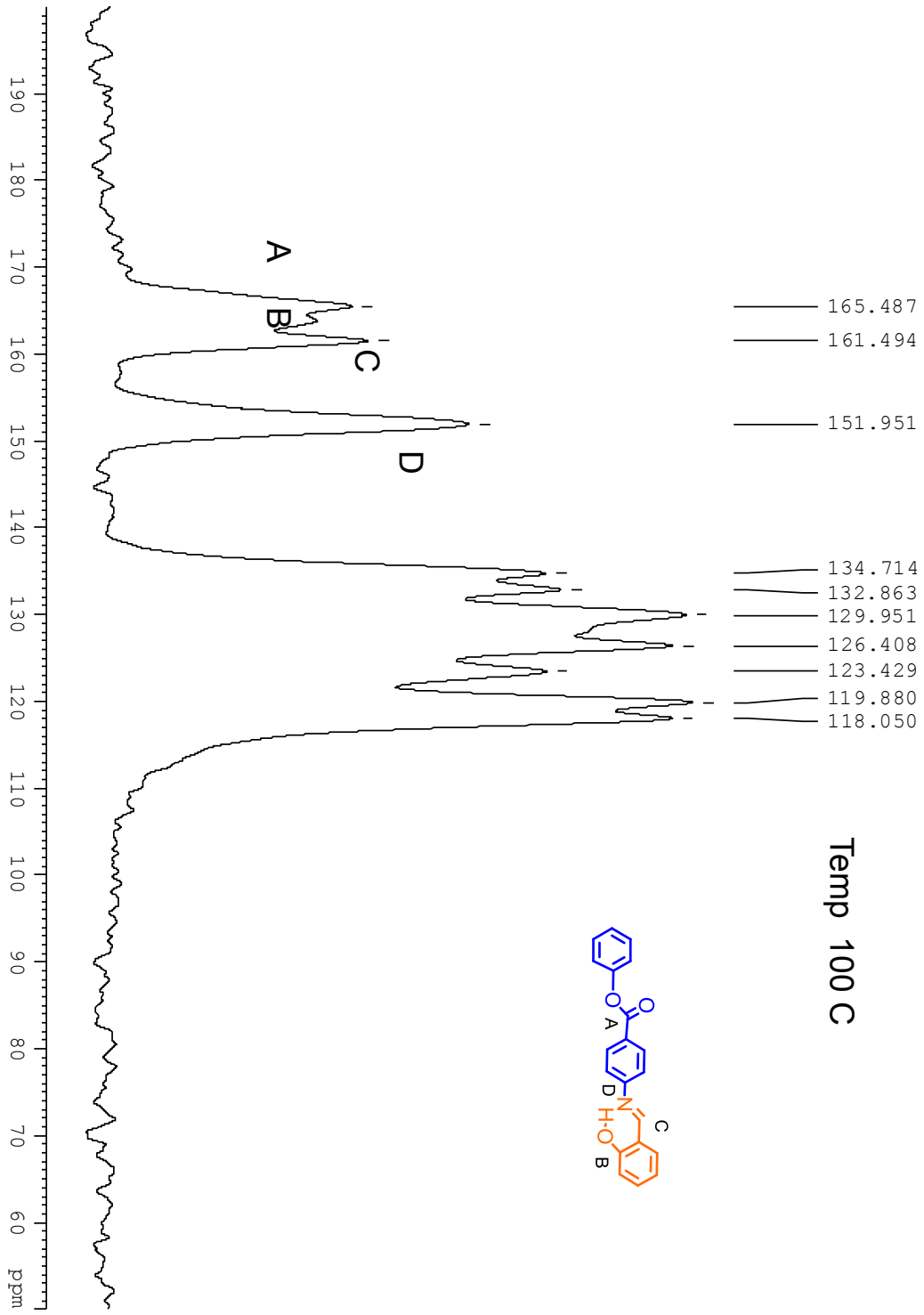

Figure S17. CPMAS of standard ester linked salicyladeneaniline at 100 °C

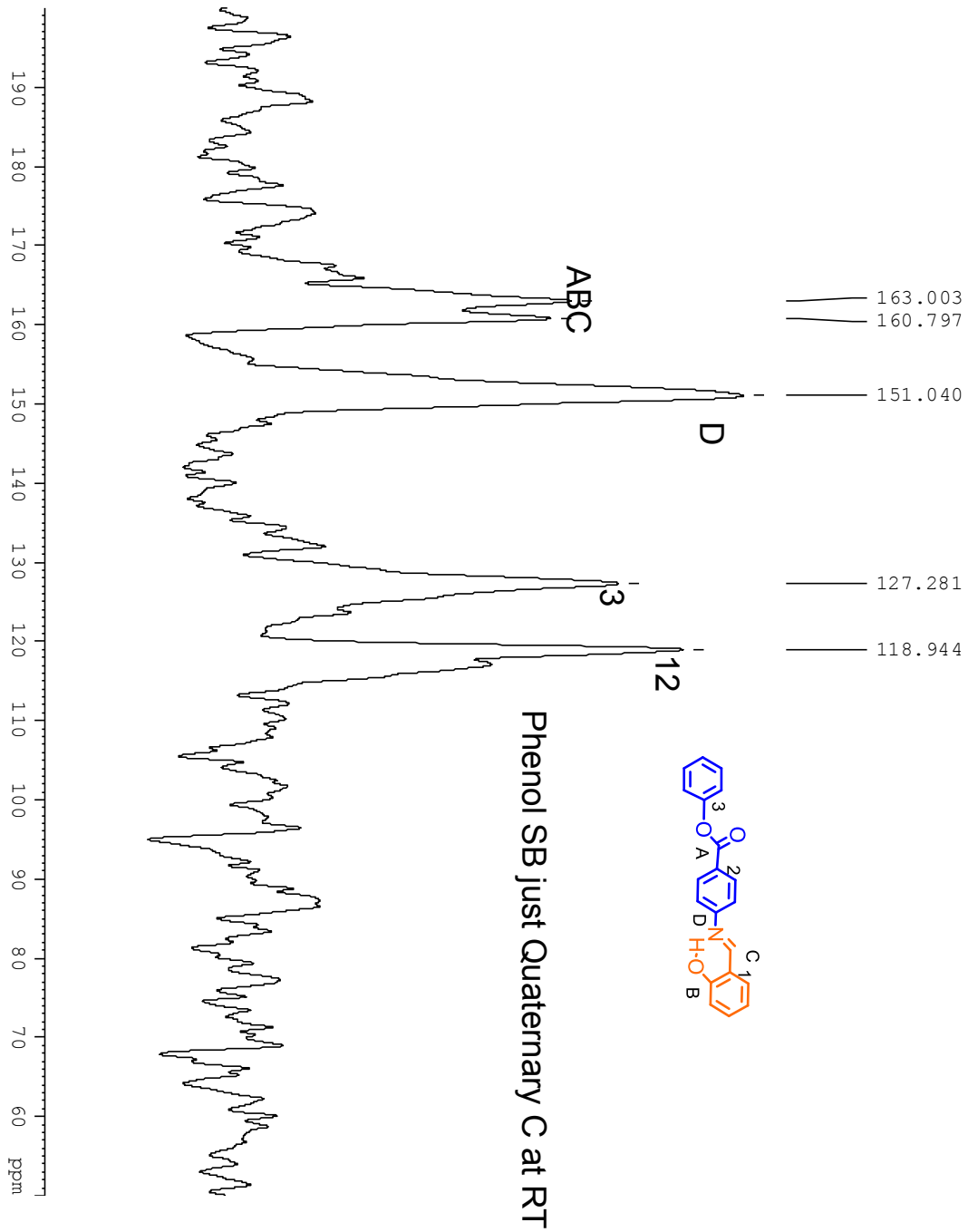

Figure S18. CPMAS of standard ester linked salicyladeneaniline showing quaternary carbons

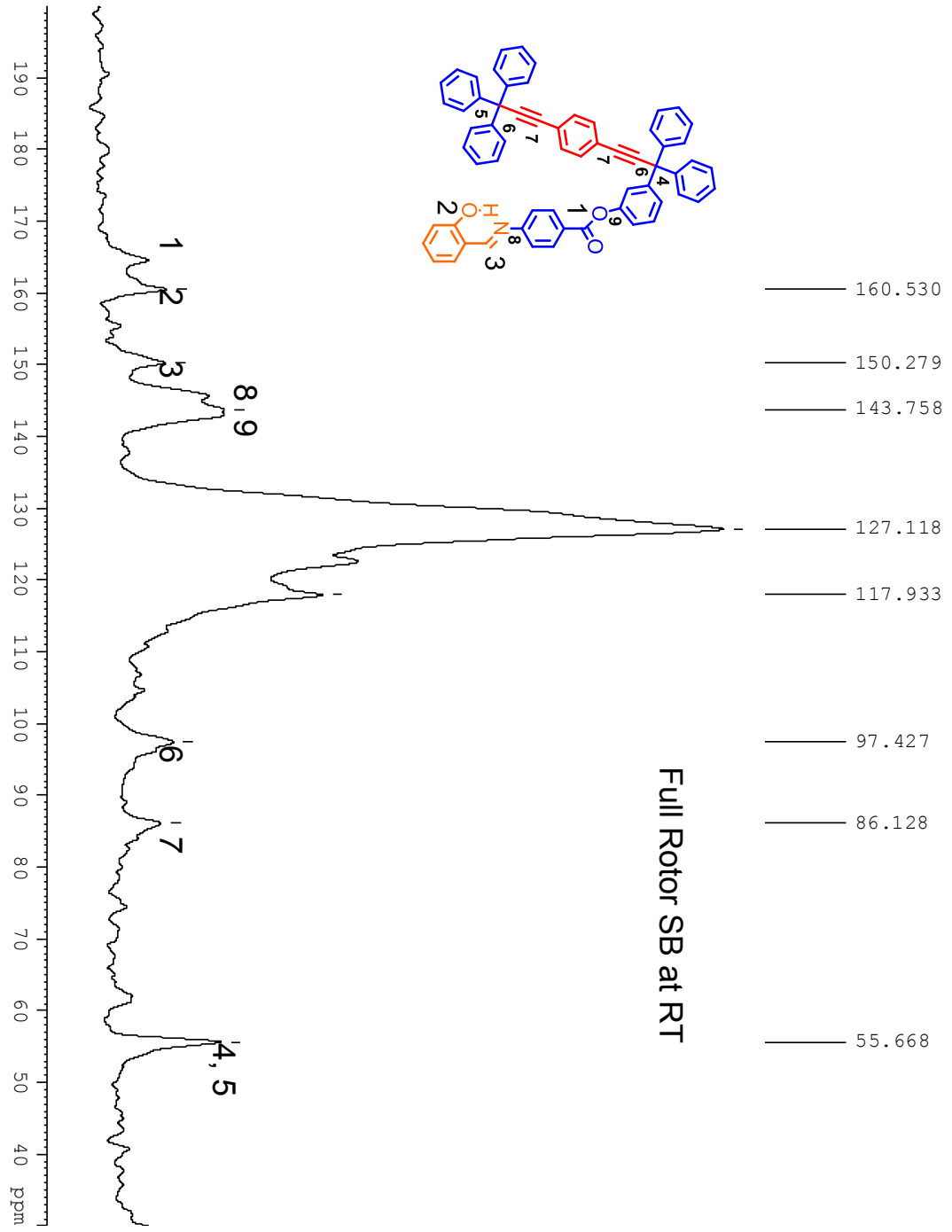

Figure S19. CPMAS of salicyladeneaniline ester linked rotor **3** at room temperature

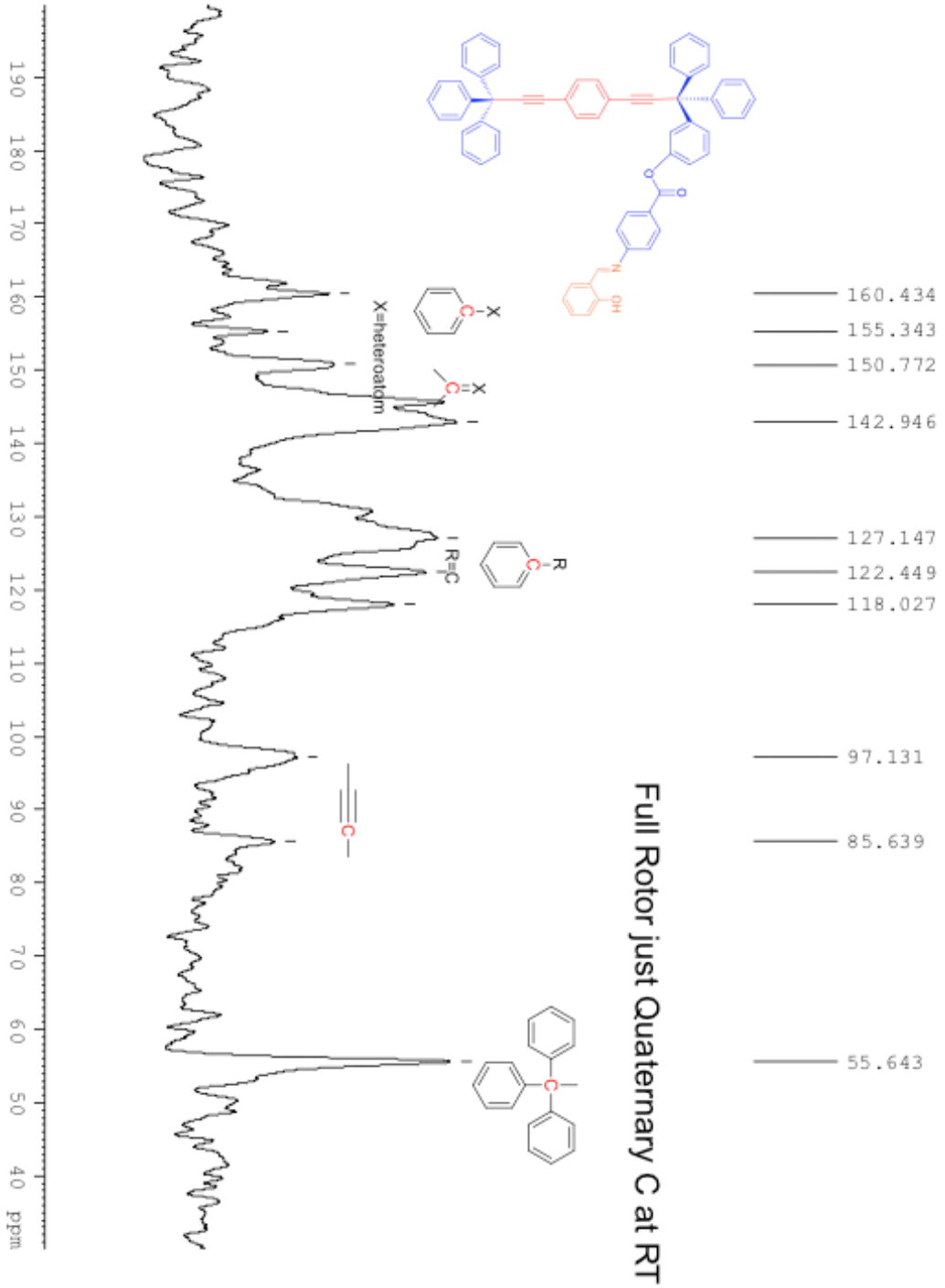

Figure S20. CPMAS of quaternary carbons of salicyladeneaniline ester linked rotor **3** at room temperature

4.7. References

[1] a) Koumura, N.; Zijlstra, R.; Delden, R.; Harada, N.; Feringa, B. *Nature* **1999**, *401*, 152. b) Balzani, V.; Credi, A.; Raymo, F.; Stoddart, F. *Angew. Chem., Int. Ed.* **2000**, *39*, 3348. c) Kelly, T. R.; De Silva, H.; Silva, R. A. *Nature* **1999**, *401*, 150. d) Karim, A. R.; Linden, A.; Baldridge, K. K.; Siegel, J. S. *Chemical Science* **2010**, *1*, 102. e) Muraoka1, T.; Kinbara1, K.; Aida, T. *Nature* **2006**, *440*, 512. f) Coskun, A.; Banaszak, M.; Astumian, D. R.; Stoddart, J. F.; Grzybowski, B. A. *Chem. Soc. Rev.* **2012**, *41*, 19. g) Browne, W. R.; Feringa, B. L. *Nat. Nanotechnol.* **2006**, *1*, 25. h) Michl, J.; Sykes, E. C. H. *ACS Nano* **2009**, *3*, 1042.

[2] a) Khuong, T.-A. V.; Nuñez, J. E.; Godinez, C. E.; Garcia-Garibay, M. A. *Acc. Chem. Res.* **2006**, *39*, 413. b) Karlen, S. D.; Garcia-Garibay, M. A. *Top. Curr. Chem.* **2006**, *262*, 179. c) Vogelsberg, C. S.; Garcia-Garibay, M. A. *Chem. Soc. Rev.* **2012**, *41*, 1892.

[3] Saebo, S.; Almolof, J.; Boggs, J. E.; Stark, J. G. *J. Mol. Struct. (Theochem)* **1989**, *200*, 361. d) Gould, S. L.; Tranchemontagne, D.; Yaghi, O. M.; Garcia-Garibay, M. A. *J. Am. Chem. Soc.*, **2008**, 130, *11*, 3246.

[4] a) Kinbara, K.; Aida, T. *Chem. Rev.,* **2005**, *105*, 1377. b) Minamino, T.; Imada, K.; Namba, K. *Curr. Opin. Struct. Biol.*, **2008**, *18*, 693.

[5] a)Samatey, F. A.; Imada, K.; Nagashima, S.; Vonderviszt, F.; Kumasaka, T.; Yamamoto, M.; Namba, K. *Nature,* **2001**, *410*, 331. b) Staehle, I. O.; Rodriguez-Molina, B.; Khan, S. I.; Garcia-Garibay, M. A. *Cryst. Growth Des,.* **2014**, *14*, 3667. c) Jones, S. E. "Dawkins on the bacterial flagellum's "tiny molecular motor" #1. http://creationevolutiondesign.blogspot.com/2005/10/dawkins-on-bacterial-flagellums-tiny.html (7/1/2014)

[6] a) Hadjoudis, E.; Mavridis, I. M. *Chem. Soc. Rev.* **2004**, *33*, 579. b) Irie, M. *Chem. Rev.* **2000**, *100*, 1683; c) Heinz Dürr, H.; Bouas-Laurent, H., Eds., Photochromism: Molecules and Systems, Elsevier, Amsterdam, 2003

[7] (a) Flynn, C. R.; Michl, J. *J. Am. Chem. Soc.* **1974**, *96*, 3280. (b) Migirdicyan, E.; Baudet, J. J. Am. Chem. Soc. **1975**, *97*, 7400.

[8] a) Koshima, H.; Matsuo, R.; Matsudomi, M.; Uemura, Y.; Shiro, M. *Cryst. Growth Des.***2013**, *13*, 4330. b) Harada, J.; Nakajima, R.; Ogawa, K. *J. Am. Chem. Soc.* **2008**, *130*, 7085. c) Amimoto, K.; Kawato, T. *J. Photochem. Photobiol. C Photochem. Rev.* **2005**, *6*, 207.

[9] Commins, P.; Nuñez, J. E.; Garcia-Garibay, M. a. *J. Org. Chem.* **2011**, *76*, 8355–8363

[10] Hadjoudis, E.; Vititorakis, M.; Moustakali-Mavridis, I. *Tetrahedron* **1987**, *43*, 1345-1360

[11] Alarchn, S. H.; Olivieri, A. C.; Nordonb, A.; Harris, R. K. *J. Chem. Soc., Perkin Trans. 2,* **1996**, 2293-2296

Chapter 5

Synthesis and Photochromic Properties of Derivatives of 1,3,5,7-tetra-*N*-Salicylideneanilineadamantane

5.1. Introduction

Some studies have been reported describing the use of adamantane-based units[1,2] to gain control of the packing in the solid state. Adamantane exhibits remarkable structural, physical, and chemical properties. Adamantane[3] molecules possess a tetrahedral shape (symmetry group T_d) that has a predisposition to form networks with a diamonoid topology (chemical formula C(4n+6)H(4n+12), where n = 0,1,2,3,...). [4,5]

The structure of adamantane has zero strain, as all C-C-C bond angles are 109.45°.[6] Adamantane also possesses a special characteristic in that it can be selectively functionalized at the four tertiary positions. This allows for controlled, three-dimensional expansion. Derivatives of adamantane attract a lot of interest as rigid molecular scaffolds with applications in the chemistry of supramolecular systems, macromolecules, dendrimers, medicinal chemistry, and polymers.[7,8] 1,3,5,7-Tetraphenyladamantane is an ideal candidate for making dendrimers, star polymers, and microporous organic frameworks.[9,10,11] However, with respect to larger tetraphenyl derivatives of adamantane, few molecules have been reported.[12,13] For example, Plietzsch et al. developed an efficient strategy for the preparation of diverse rigid 3-D tetrahedral building blocks in 2009, utilizing an adamantane core to generate a tecton library.[14] Interest for organic systems also arises from the possibility of combining other properties in the same compound to make them more viable candidates as materials. For example, Thyagarajan et al. reported a tripodal linker for metal oxide nanoparticle sensitization on TiO_2 films

made by adamantane-centered pyrene sensitizers. These compounds exhibited spectral properties typical of phenyleneethynylene-substitued pyrenes.[15]

In 2008, Zarwell et al. also reported the synthesis and evaluation of tripodal linked photoswitches on gold surfaces made by a tetrahedral adamantane core unit and an azobenzene headgroup.[16] Zarwell et al. observed the photoisomerization of this azobenzene, using a 405 nm light, and detected the isomerization by UV-Vis spectroscopy.

Although some examples of tetraphenyl derivatives of adamantane that exhibit UV-Vis absorption or fluorescence have been reported in the literature in the last ten years, photochromic functional adamantane cores have not been thoroughly explored. We report, here, organic molecules exhibiting both tetrahedral tecton building blocks and photochromic behavior.

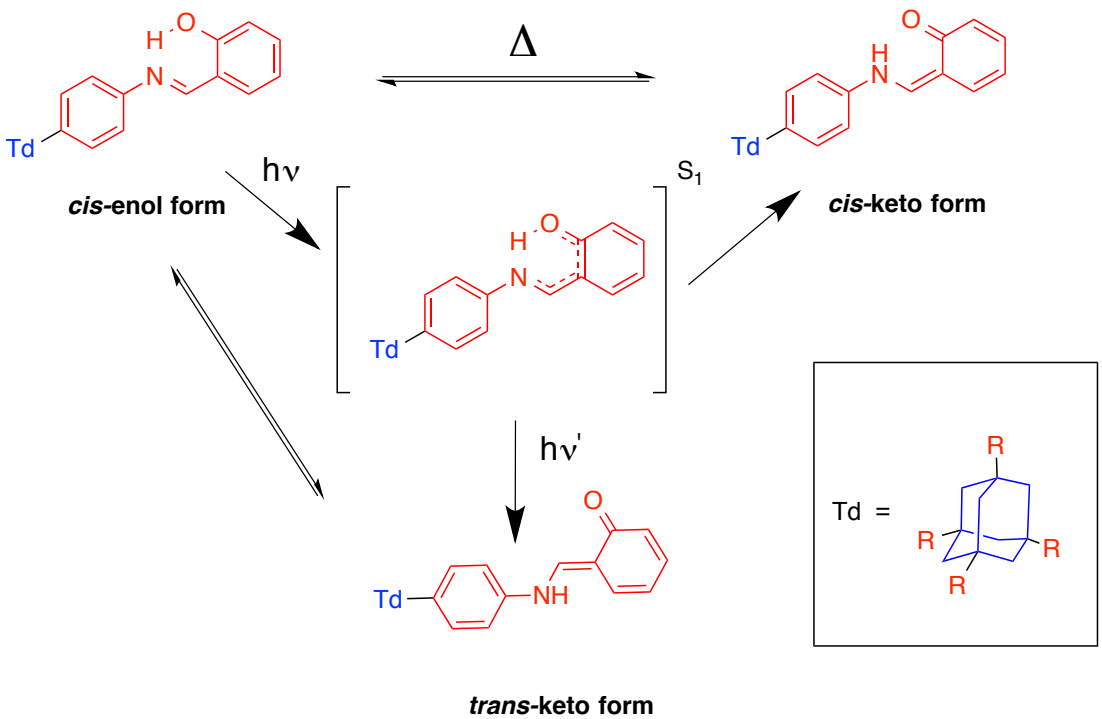

Figure 1. Representation of reversible photochromic and thermochromic processes showing just one group of the salicylideneaniline functionality in 1,3,5,7-tetra-N-salicylideneanilineadamantane 1.

5.2. Synthesis and Characterization

Photochromism is a reversible color change induced by irradiation that is exhibited by a variety of organic compounds both in the solid state and in solution. In the specific case of salicylideneanilines (SAs), they exist in thermal equilibrium between *cis*-enol and *cis*-keto tautomeric forms, as shown in Figure 1, with the aromatic hydroxyl-bearing tautomer being the most stable. The irradiation of the enol tautomer gives the electronic excited state of enol-imine form, which results in the formation of the *trans*-keto form in the ground state through the H-transfer and molecular rearrangement[17] (Figure 1).

Systems that have photoresponsiveness are the target of considerable interest in applications such as optical data processing, information storage,

electronic display systems, and ophthalmic glasses.[18] More specifically, N-salicylideneanilines have been the focus of nonlinear optical (NLO) behavior for potential applications as optical switching devices.[19] We envisioned the synthesis and study of the photochromic properties of 1,3,5,7-tetra-N-salicylideneanilineadamantane **1** and 1,3,5,7-tetra-N-3,5-di-tert-butylsalicylideneanilineadamantane **2**. We selected the "Bulky-group substitution method" in compound **2**.

This approach was considered, because Kawato et al. established the effectiveness of the introduction of the bulky tert-butyl substituents into some salicylideneanilines for improving the photoresponsiveness of the crystals. For example, 3-fluor-N-salicylideneanilines crystals did not exhibit photochromism in the solid state, but 3-fluor-N-(3,5-di-tert-butylsalicylidene)anilines showed photochromism in the solid state.[20] In addition, Amimoto et al. suggested that the bulky group could act as a space-opener in the crystal lattice, in order to increase a part of the molecular thickness to allow partial framework movement.[21] Furthermore, **1** and **2** contained four imines, which could lend themselves to applications in supramolecular chemistry and host-guest complex chemistry.[22,23] For example, Taneda et al. reported photochromic crystals of 4, 4'-methylenebis(N-salicylideneaniline), in which they exist in the syn-form and anti-form.[24] Yelamaggad et al. also reported a new class of disc-like organic molecules derived from tris(N-salicylideneanilines)(TSANs).[25] These molecules were based on the work of MacLachalan[26] and exhibited promising photophysical properties. However, few examples of photochromic tetra-imines have been described. In this paper, we

describe the synthesis as illustrated in Scheme 1 of 1,3,5,7-tetra-N-salicylideneaniline adamantane **1** and 1,3,5,7-tetra-N-3,5-di-tert-butyl salicylideneanilineadamantane **2**.

Scheme 1.

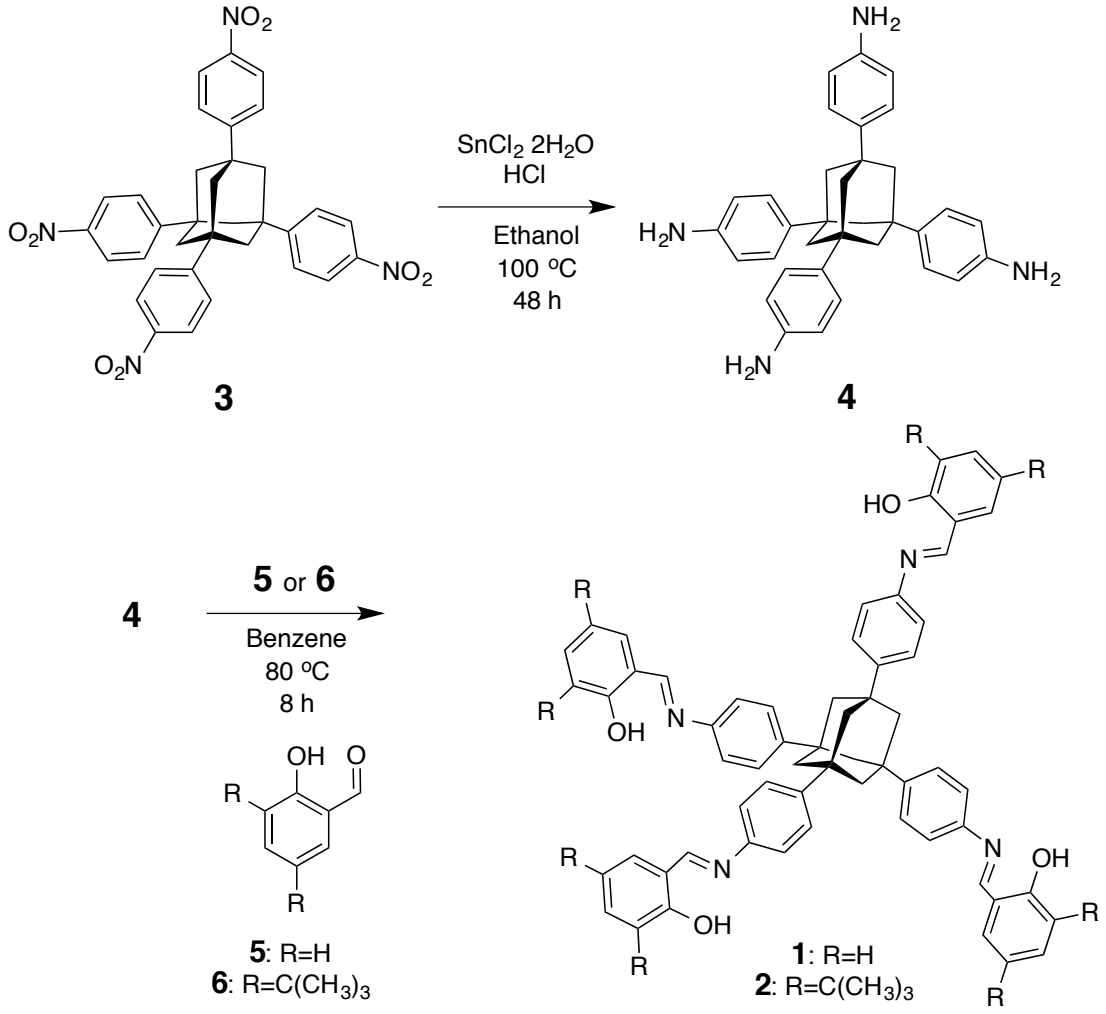

Scheme 1 shows the reduction of 1,3,5,7 tetra(4-nitrophenyl) adamanatane **3**[27] using tin chloride in ethanol, which gave 1,3,5,7-tetraaniline adamantane **4** in 90% yield. Anils **1** and **2** were synthesized by condensation with an excess of the appropriate salicylaldehyde in ca. 98% and 90% yield, respectively, after column chromatography (CH_2Cl_2: hexanes = 1:1). The structures of compounds **1** and **2**

were determined by ^{1}H NMR and ^{13}C NMR, FTIR, ESI-TOF mass spectroscopy data. The most important signals in the ^{1}H NMR of **1** were: the enol protons at δ 13.30 ppm, the aldimine protons at δ 8.65 ppm, and the adamantane protons at δ 2.18 ppm. Compound **2** showed the same important signals in ^{1}H NMR: enol protons at δ 13.80 ppm, aldimine protons at δ 8.70 ppm, and the adamantane protons at δ 2.24 ppm. There was a Δδ = 0.5 ppm shift downfield in the enol protons between compound **1** and **2,** perhaps because of the introduction of the bulky tert-butyl substituents. This significant shift was indicative of the intramolecular hydrogen bond and the resulting effect of the bulky group substitution.[20] The FT-IR spectrum of **1** showed characteristic stretching for the C=N at 1619 and 1279 cm^{-1} ,and an aromatic conjugated C=N stretching mode at 1571 cm^{-1}. The FT-IR spectrum of **2** showed the bands characteristic for C=N stretching at 1617 cm^{-1}.[17,28]

5.3. Crystallization Studies and Single Crystal X-Ray Diffraction Analyses

Crystals of **1** were grown from numerous solvent conditions, but X-ray quality single crystals could not be attained. Crystals of **2** were obtained from CH_2Cl_2 in the form of fine needles with a tendency to form twinned aggregates. X-Ray diffraction data was collected at low temperature and the connectivity was determined. The crystal structure showed a large degree of disorder in one arm, along with several highly disordered solvent molecules, as shown in Figure 2.

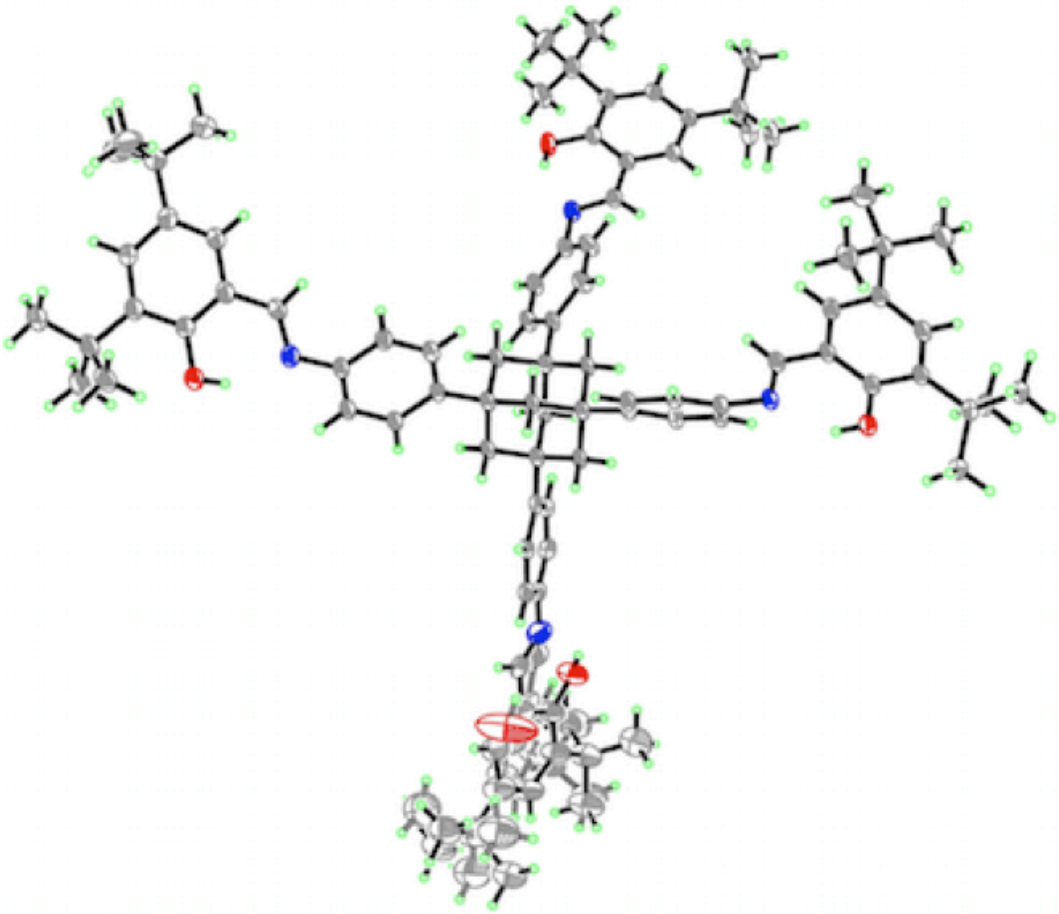

Figure 2. Crystal structure of compound **2** with a high degree of disorder in the bottom arm of the molecule. The solvent molecules were removed from the image, however, a highly disordered dichloromethane molecule was in close contact with that portion of the molecule.

This disorder may be attributed to rapid desolvation. The thermal analysis of compounds **1** and **2** showed no transitions below 500°C by DSC.

5.4. Solid State Photochromism

The photochromic and thermochromic properties of compounds **1** and **2** were evaluated. The diffuse reflectance UV-Vis spectra of **1** and **2** were recorded at

room temperature using barium sulfate to dilute the samples. Then, each sample was irradiated with ultraviolet light (high-pressure Hg 365 nm lamp, 30 W) for 12 hours for **1**, and for 20 minutes for **2**.[20,29,30] (It should be noted that the extended irradiation period for **1** was based on minimal photoisomerization after just 15 mins). Immediately after irradiation, the absorption spectrum was recorded at room temperature. The powder of **1** was pale yellow at room temperature prior to irradiation, while the photochromic powder of **2** was a slightly brighter yellow/orange. The pale yellow color of sample **1** did not change notably after irradiation. In contrast, a change of color after irradiation was easily perceived for compound **2,** as shown in the literature for photochromic solids.[31] The absorption spectrum for **1** after irradiation (green line in Figure S19 in SI) showed a rise of a broad band between 530 to 420 nm, whereas the absorption spectrum for **2** (red line in Figure 19 in SI) also showed a broad band between 550 to 450 nm, corresponding to the *cis*-keto form. For photochromic solids, as shown with compound **2**, the increase in the absorption in the range 540-580 nm was ascribed to the *trans*-keto form.[32]

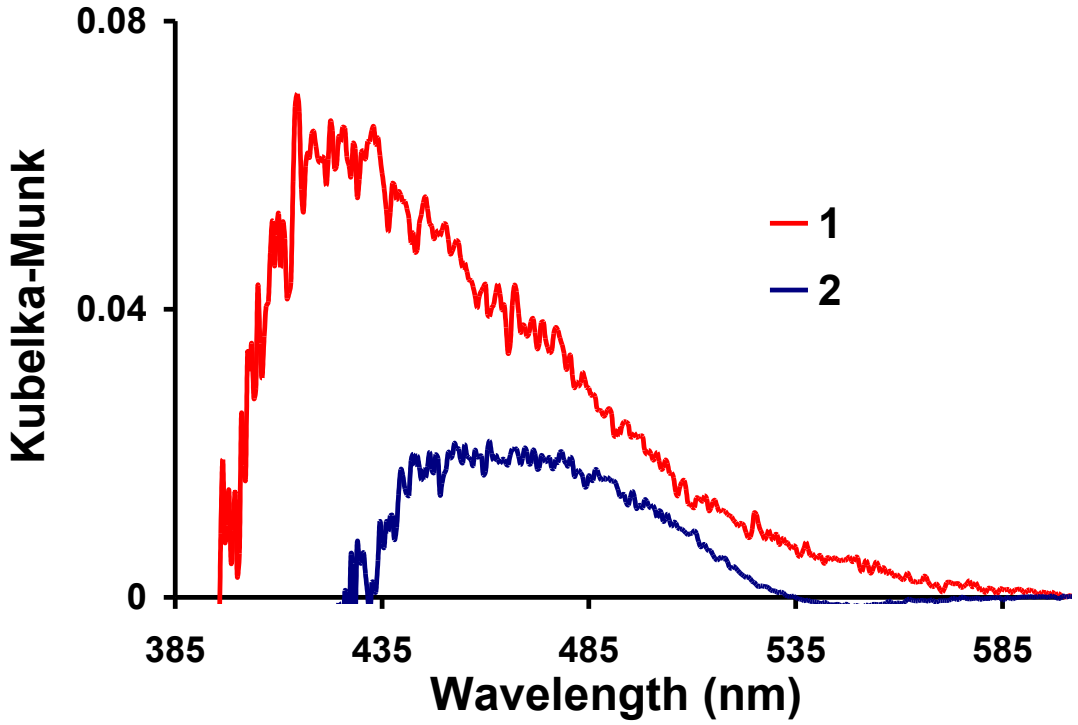

Figure 3. Difference spectra of samples after irradiation minus before irradiation transformed into Kubelka-Munk units for **1** and **2** .

The absorption spectra for **1** and **2** were converted into reflectance before and after irradiation (Figure S20 in SI). Then, Kubelka-Munk transformations were plotted, as shown in Figure 3. The Kubelka-Munk spectrum (red line in Figure 3) of **1** at 298 K exhibited a strong absorption band with a λ_{max} of 424 nm, whereas the Kubelka-Munk spectrum (blue line in Figure 3) of **2** at 298 K exhibited a strong absorption band with λ_{max} of 479 nm. The absorption band for photochromic systems that have been excited by one-photon excitation at 365 nm has a λ_{max} of 480 nm in literature. [33] In accordance with the color change, the reflectance spectrum of **2** (Figure S20 in SI) resembles that of the *trans*-keto form. Fujiwara et. al. concluded that the trans-keto form is produced not only from the excitation of the enol form with UV light, but also from that of the *cis*-keto form, which exists in equilibrium,

with visible light.[27] To test the ability of compound **2** as a photoswitch, compound **2** was irradiated for 4 cycles of 20 minutes with a 365 nm lamp, and the absorption at 500 nm was monitored up to 5-10 half-lifes.[25] Compound **2** showed reversibility, at least for 4 cycles, as shown in Figure S36 in the SI. Compound **2** showed a tri-exponential decay (Equation 1) with three lifetimes: $\tau1 = 47.615 \pm 0.1202$, $\tau2 = 311.010 \pm 70.3430$, $\tau3 = 1756.645 \pm 1.9163$ seconds (Figure 3)

1. $Y = Y0 + A1e^{-t/\tau1} + A2e^{-t/\tau2} + A3e^{-t/\tau3}$
2. where: Y = Absorbance (Arbitrary units)
3. t = acquisition time
4. τ = half-life time

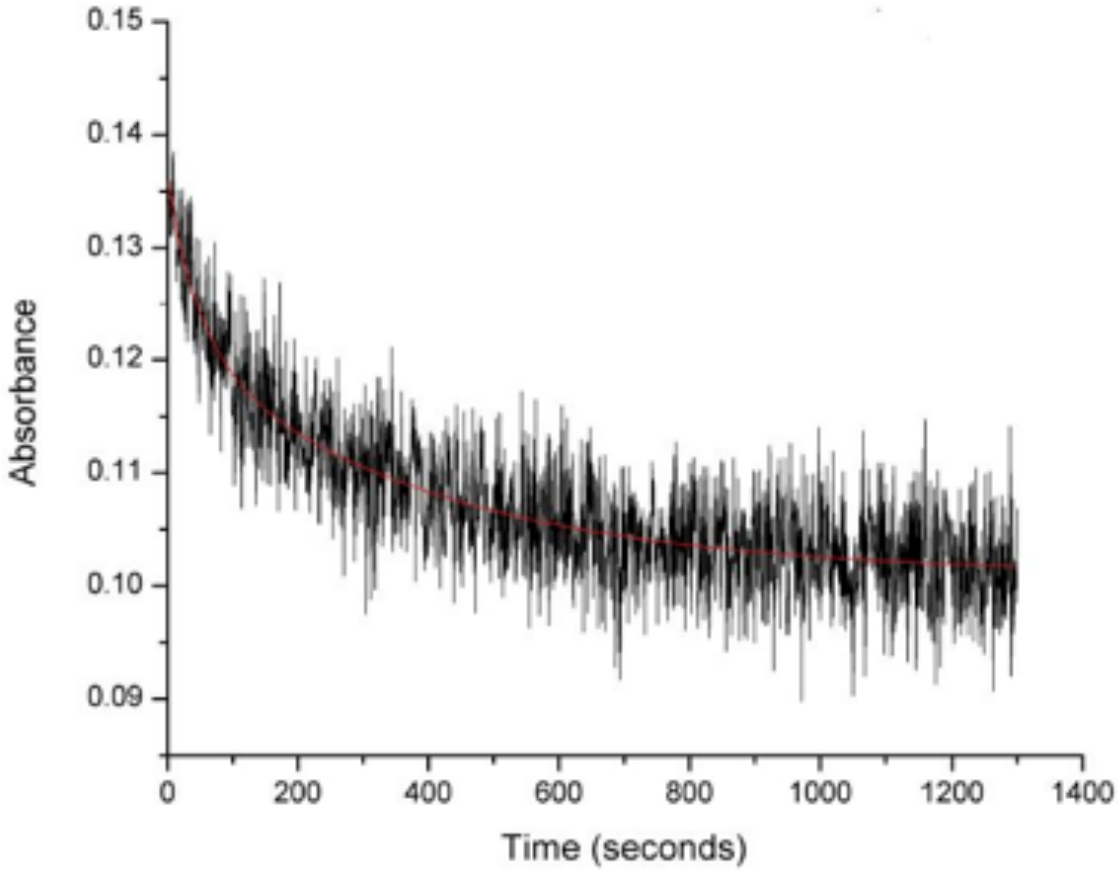

Figure 3. Tri-exponential decay of 2 (after 20 minutes of irradiation with λ = 365 nm lamp, reading at 500 nm).

In order to explain these results, we looked for the proposed mechanism for the photochromism of anils. We found that Kawato et al. proposed a possible mechanism for the photoisomerization of N-salicylideneaniline. Kawato et al. demonstrated two rate constants for this system: from trans-keto form to *cis*-keto form (k_1), and from *cis*-keto form to zwitterion-enol form (k_2). He also described a very rapid process from the zwitterion-enol form to the enol-form.[20] Due to the experimental limitations, a conclusive fitting for the decay curve was not obtained. We were unable to fit it to a biexponential with an acceptable degree of certainty. This could be explained by the fact that, theoretically, **1** and **2** can have up to 81 isomers, as shown in Figure 4. These different isomers could therefore result in different environments in the solid, which could lead to different decay curves. For this reason, the decays were arbitrarily fitted to a tri-exponetial decay as a conservative estimate of the different environments. Given these possible different environments in the solid-state, the decay curve was fitted with a tri-exponential.

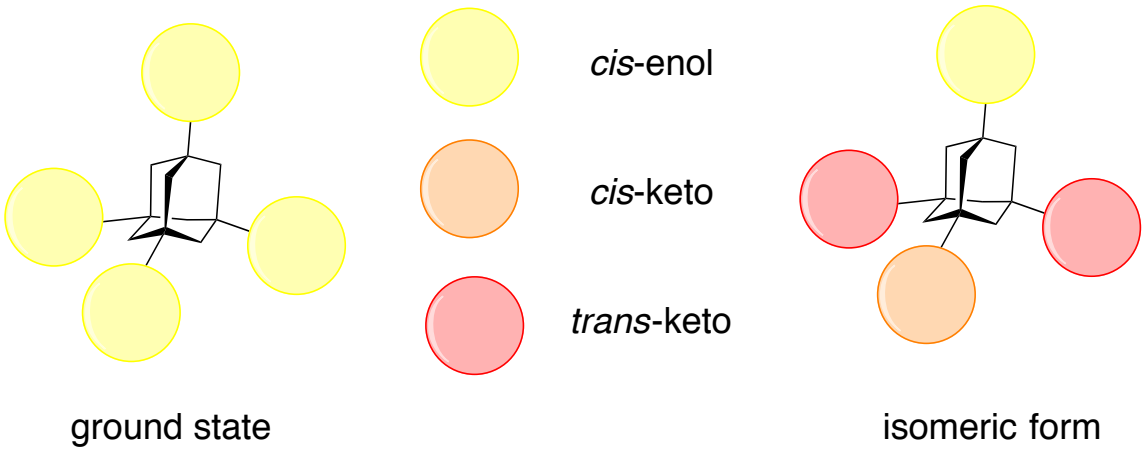

Figure 4. Each arm of the adamantane core can have three distinct forms with four arms giving rise to up to 81 isomeric forms not taking into account degeneracy.

We calculated the population of each of these three different components using equation 10:

5. $P_{total} = P1 + P2 + P3$

6. $$P = \int_0^{\infty} Ae^{-t/\tau} dt$$

7. where : P= population of specie
8. t=acquisition time
9. τ= half-life of specie
10. $P_{total} \approx A1\tau1 + A2\tau2 + A3\tau3$

In this equation, the total population was the addition of the product of the initial absorption A_n and the decay lifetime t_n. The percentage of population of each lifetime was: P1 = 2.36%, P2 = 9.88%, P3 = 87.76% (Figure S33 in SI). These results suggested that the main component during the acquisition time was the species with the longest half-life (P3 = A3τ3). Finally, the thermochromic properties of **1** and **2** were tested with varying temperature. As the temperature was lowered (77 K), the color of **2** decreased from an intense yellow to a pale yellow. Chatziefthimiou

et al. explained that some nonplanar Schiff bases could display thermochromism and photochromism simultaneously, because of the crucial factor of facile H-transfer in the imine N-atom.[34] Hadjoudis et al. proposed that in non-planar molecules the basicity of the N-imine is lower. This is because the lone pair of the nitrogen does not overlap with the π-orbitals of the aniline ring, as the aniline is rotated 55°.[35]

5.5. Conclusions

In summary, the photochromism of salicylideneanilines was based on the photo-induced proton transfer of the thermally stable enol-form and the following isomerizaton to the metastable *trans*-keto form (Figure 1). We have demonstrated that compound **2** shows reversible photochromic and thermochromic behavior. In addition, compound **2** can function as a photoswitch.

5.6. APPENDIX

General Methods

Unless stated otherwise, reactions were conducted in dried glassware under an atmosphere of argon using anhydrous solvents (freshly distilled). All commercially available reagents were used as received unless otherwise specified. Thin-layer chromatography (TLC) was conducted with EMD gel 60 F254 pre-coated plates (0.25 mm) and visualized using UV lamp. EMD silica gel 60 (particle size 0.040–0.063 mm) was used for flash column chromatography. ^{1}H NMR spectra were recorded on Bruker spectrometers at 400 MHz and are reported relative to deuterated solvent signals. Data for ^{1}H NMR spectra are reported as follows: chemical shift (ppm), multiplicity, coupling constant (Hz) and integration. ^{13}C NMR spectra are reported in terms of chemical shift. The values for $J_{AA'BB'}$ were obtained with gNMR software. IR spectra were recorded on a Perkin-Elmer 100 spectrometer and are reported in terms of frequency absorption (cm-1). Mass spectra were obtained from the UCLA Molecular Instrumentation Center (MIC) in ESI-TOF-MS and MALDI-TOF-MS.

Experimental procedures

1,3,5,7,-tetra(4-nitrophenyl)adamantane (3). A 1-L round bottom flask was charged with 1,3,5,7-tetraphenyladamantane (12.5 g, 28.4 mmol) and cooled to -42^{0}C using a CO_2/acetonitrile bath. Dropwise 90% fuming nitric acid (500 mL) was added slowly to the flask and stirred for 50 minutes. Then, the solution was transferred to a beaker containing ice water. The solid was filtered and washed with sodium bicarbonate solution, distilled water and dried with magnesium sulfate

anhydrous. The solid was crystallized in nitrobenzene (100 mL). ^{1}H NMR (400 MHz, CD_2Cl_2): δ 8.24 (m, J_{AB} = 8.10, $J_{AA'}$ = 2.75, $J_{AB'}$ = 0.20, 8H), 7.68 (m, J_{AB} = 8.10, $J_{AA'}$ = 2.75, $J_{AB'}$ = 0.20, 8H), 2.263 (s, 12H). ^{13}C NMR (360 MHz, DMSO-d_6): 156.6, 145.8, 126.9, 123.3, 44.6. MALDI-TOF-MS (*m/z*): [M+N_2O-H^+] calcd for $C_{34}H_{28}N_5O_8$ 665.83, found 665.17; IR (solid): 3126.5, 3063.4, 2935.7, 2857.1, 1593.9, 1511.9, 1451.9, 1341.5, 856.5.

1,3,5,7,-tetraanilineadamantane (4). A 100-mL three-neck round-bottomed flask equipped with a reflux condenser was charged with 1,3,5,7,-tetra(4-nitrophenyl) adamantane **3** (0.62 g, 1 mmol) and ethyl alcohol (75 mL) followed by concentrated hydrochloric acid (15 mL). Stannous chloride ($SnCl_2$-$2H_2O$, 4.1 g, 15 mmol) was added to the mixture with stirring.[28] After refluxing for 48 hours, the solvent was evaporated and water (15 mL) was added. The aqueous solution was made alkaline by adding 3 M NaOH solution and was extracted with THF (4 x 50 mL). The solvent was evaporated and the product was collected (0.5 g, 90%). ^{1}H NMR (400 MHz, DMSO-d6): δ 7.10 (d, *J*=8.6, 8H), 6.49 (d, *J*=8.6, 8H), 4.76 (s, 8H), 1.79 (s, 12H); ^{13}C NMR (360 MHz, DMSO-d_6): 146.1, 137.6, 125.1, 113.6, 47.64, 47.6, 37.7. MALDI-TOF-MS(*m/z*): [M+H^+] calcd for 501.29, found 501.38. IR (solid): 3427.2, 3334.8, 3218.8 , 3026.8 , 2922.1, 2895.9, 2848.1, 1879.1, 1622.5, 1515.8 , 1443.8, 1430.3, 1354.9, 1274.1, 1210.6 , 1187.6 , 1127.2, 1012.7, 839.5, 821.5, 772.8 , 747.4, 701.9, 644.8, 561.4 , 535.2.

1,3,5,7-tetra-*N*-salicylideneanilineadamantane (1). A 50-mL three-neck round-bottomed flask equipped with reflux condenser was charged with 1,3,5,7-tetraanilineadamantane **4** (0.160g, 0.32 mmol) and dissolved in dry benzene (15

mL) under argon atmosphere. 2-hydroxy benzaldehyde **5** (2.72 mL, 1.28 mmol) was added slowly with stirring at room temperature. The reaction mixture was heated at 80^0 C for 8 hours. The reaction was allowed to cool and evaporated to dryness. The crude product was purified by column chromatography (DCM:Hexane = 1:1) to afford 0.287 g of **3** (98% yield).^{1}H NMR (400 MHz, $CDCl_3$): δ 13.30 (s, 4H), 8.67 (s, 4H), 7.59 (d, *J* = 8.6, 8H), 7.41-7.35 (m, 8H), 7.32 (d, *J* = 8.6, 8H), 7.05 (d, *J* = 8.2, 4H), 6.94 (td, *J* = 7.5, 1, 4H), 2.18 (s, 12H); ^{13}C NMR (400 MHz, $CDCl_3$): 162.4, 161.3, 148.1, 146.8, 133.2, 132.3, 126.2, 121.3, 119.4, 119.2, 117.4, 47.4, 39.4; IR (solid): 1619, 1571, 1488, 1278, 1175, 1151, 911, 838, 755 cm^{-1}; ESI-TOF-MS (*m/z*): [M+H^+] calcd for $C_{62}H_{52}N_4O_4$ 917.40; found 917.38.

1,3,5,7-tetra-*N*-3,5-di-*tert*-butylsalicylideneanilineadamantane (2). A 50-mL three-neck round-bottomed flask equipped with reflux condenser was charged with 1,3,5,7-tetraaniline adamantane **4** (0.102 g, 0.203 mmol) and dissolved in dry benzene (15 mL) with *p*-TSA (0.5%(m/m)) and molecular sieves (4 A) under argon atmosphere. 3, 5-di-*tert*-butyl-2-hydroxybenzaldehyde **6** (0.380 g, 1.62 mmol) was added slowly with stirring at room temperature. The reaction mixture was heated until 80^0 C for 12 hours. The reaction was allowed to cool and evaporated to dryness. The same conditions for purification as compound **3** were followed. The yield of the yellow compound **5** was 90% (0.240 g).^{1}H NMR (400 MHz, $CDCl_3$): δ 13.80 (s, 4H), 8.67 (s, 4H), 7.57 (d, *J* = 8.6, 8H), 7.45 (d, *J* = 2.3, 4H), 7.32. (d, *J* = 8.6, 8H), 7.20 (d, *J* = 2.3, 4H), 2.25 (s, 12H), 1.55 (s, 36 H), 1.33 (s, 36H); ^{13}C NMR (400 MHz, $CDCl_3$): 163.5, 158.4, 147.8, 146.9, 140.7, 137.1, 128.1, 126.9, 126.2, 121.3, 118.5, 47.5, 39.4, 35.2, 34.3, 31.6, 29.6; IR (solid): 2956, 2868, 1647, 1617, 1439,

1361, 1249, 1168, 770, 735, 711 cm^{-1}; ESI-TOF-MS (*m/z*): [M+H^+] calcd for $C_{94}H_{116}N_4O_4$ 1366.95, found 1366.8.

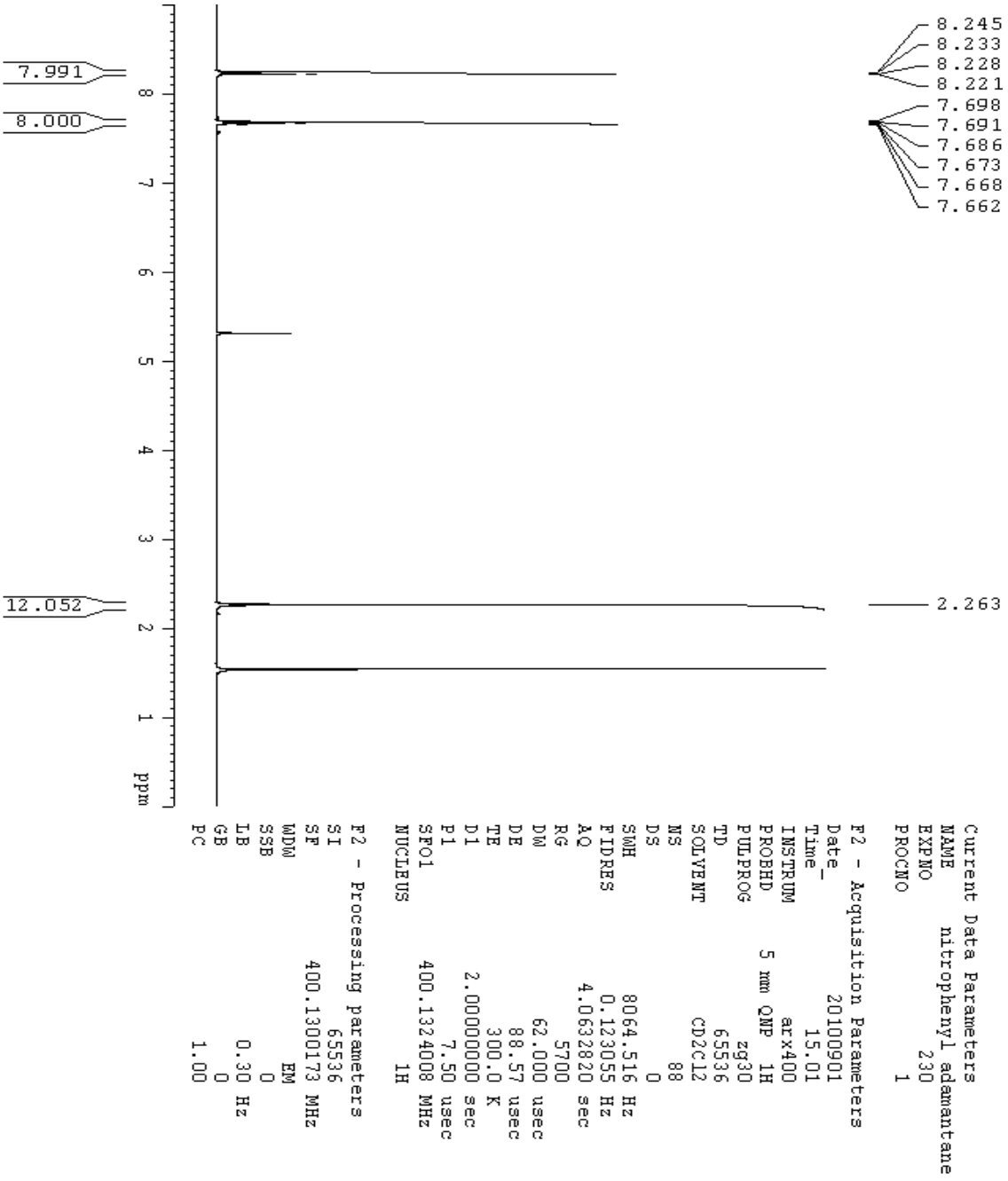

Figure S1. ^{1}H NMR for 1,3,5,7,-tetra(4-nitrophenyl)adamantane (**3**)
400 MHz ^{1}H NMR spectrum of compound **3** in $CDCl_3$

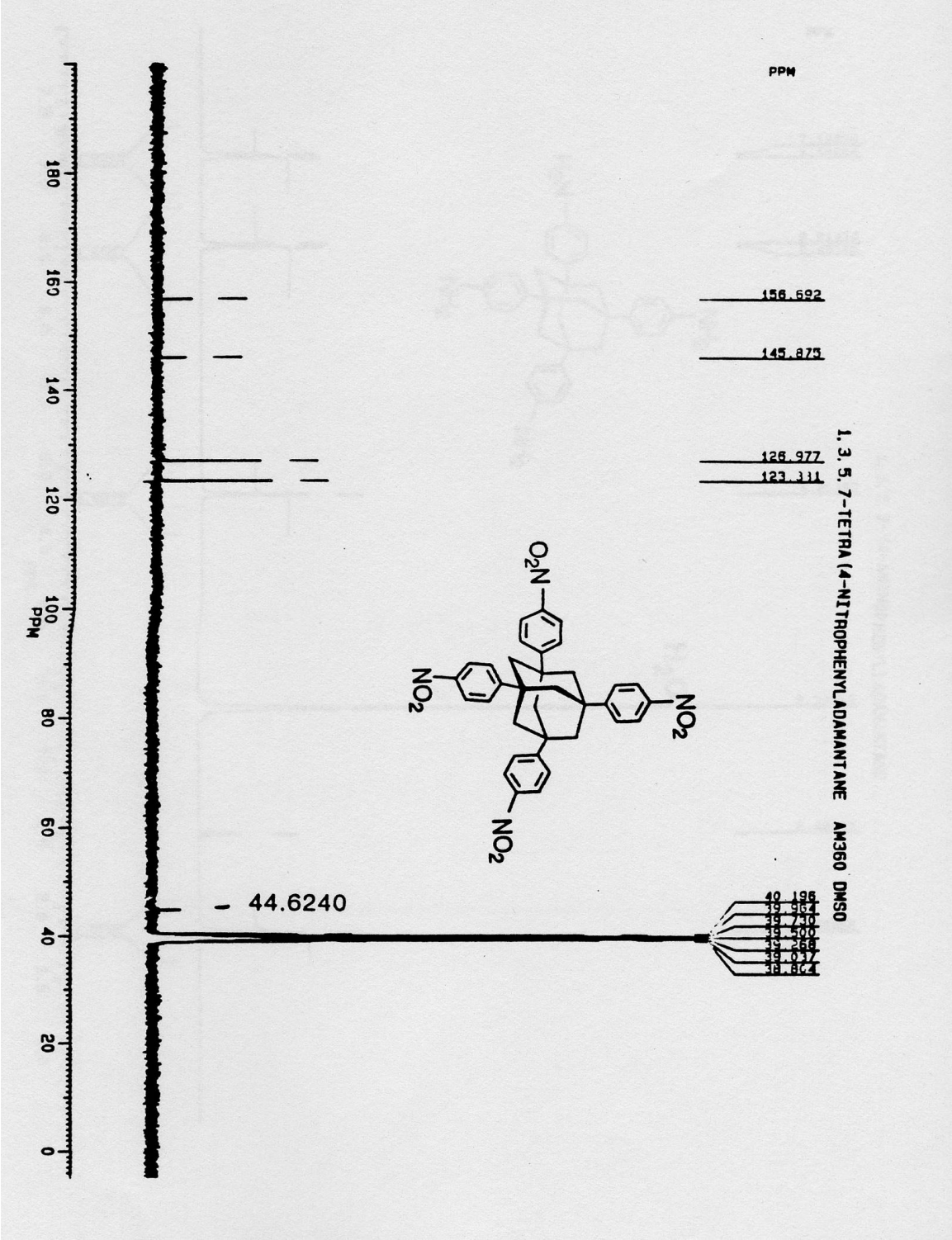

Figure S2. ^{13}C NMR for 1,3,5,7,-tetra(4-nitrophenyl)adamantane (**3**)
100 MHz ^{13}C NMR spectrum of compound **3** in $CDCl_3$

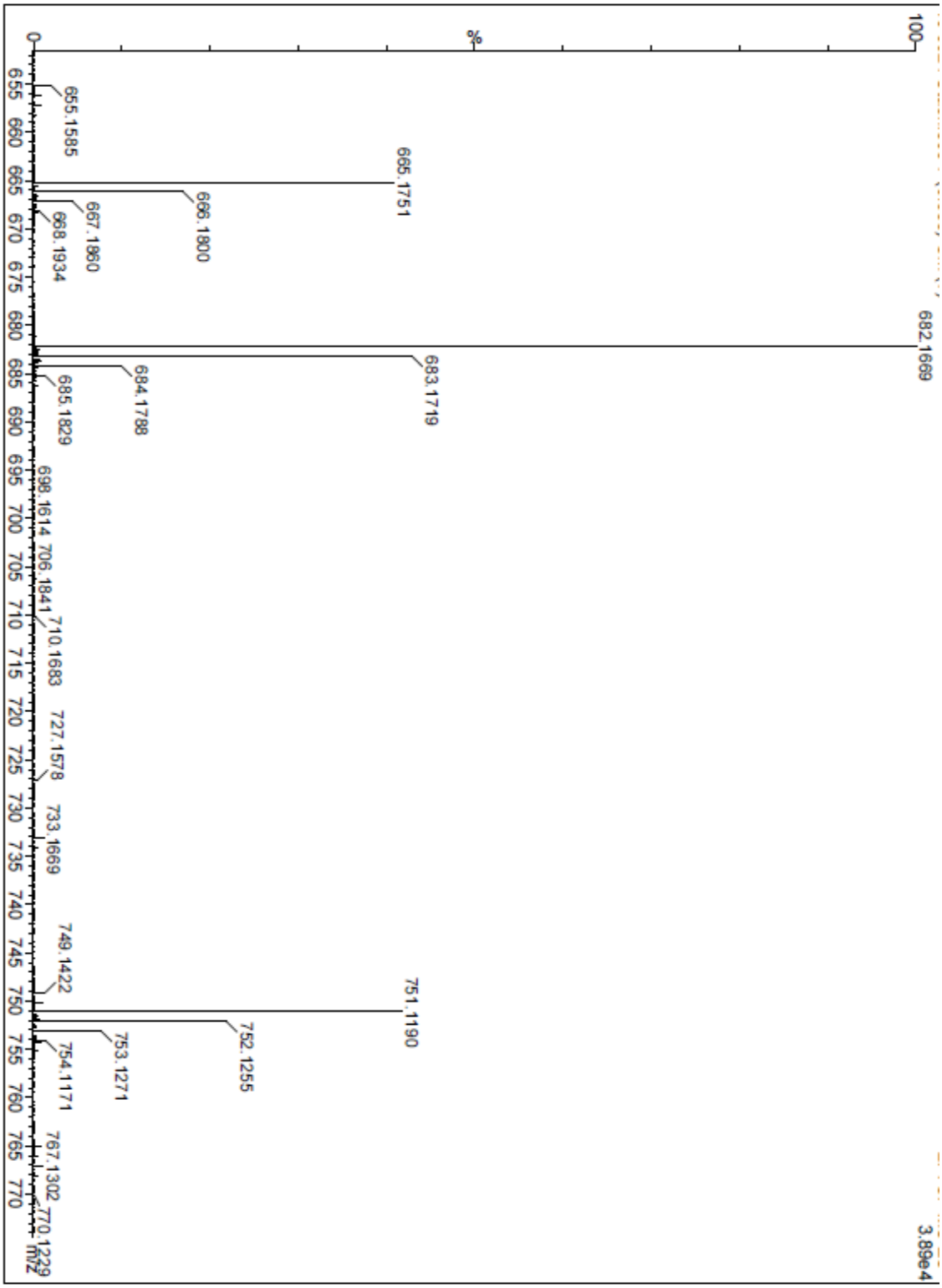

Figure S3. MALDI-TOF-MS for 1,3,5,7,-tetra(4-nitrophenyl)adamantane (**3**)

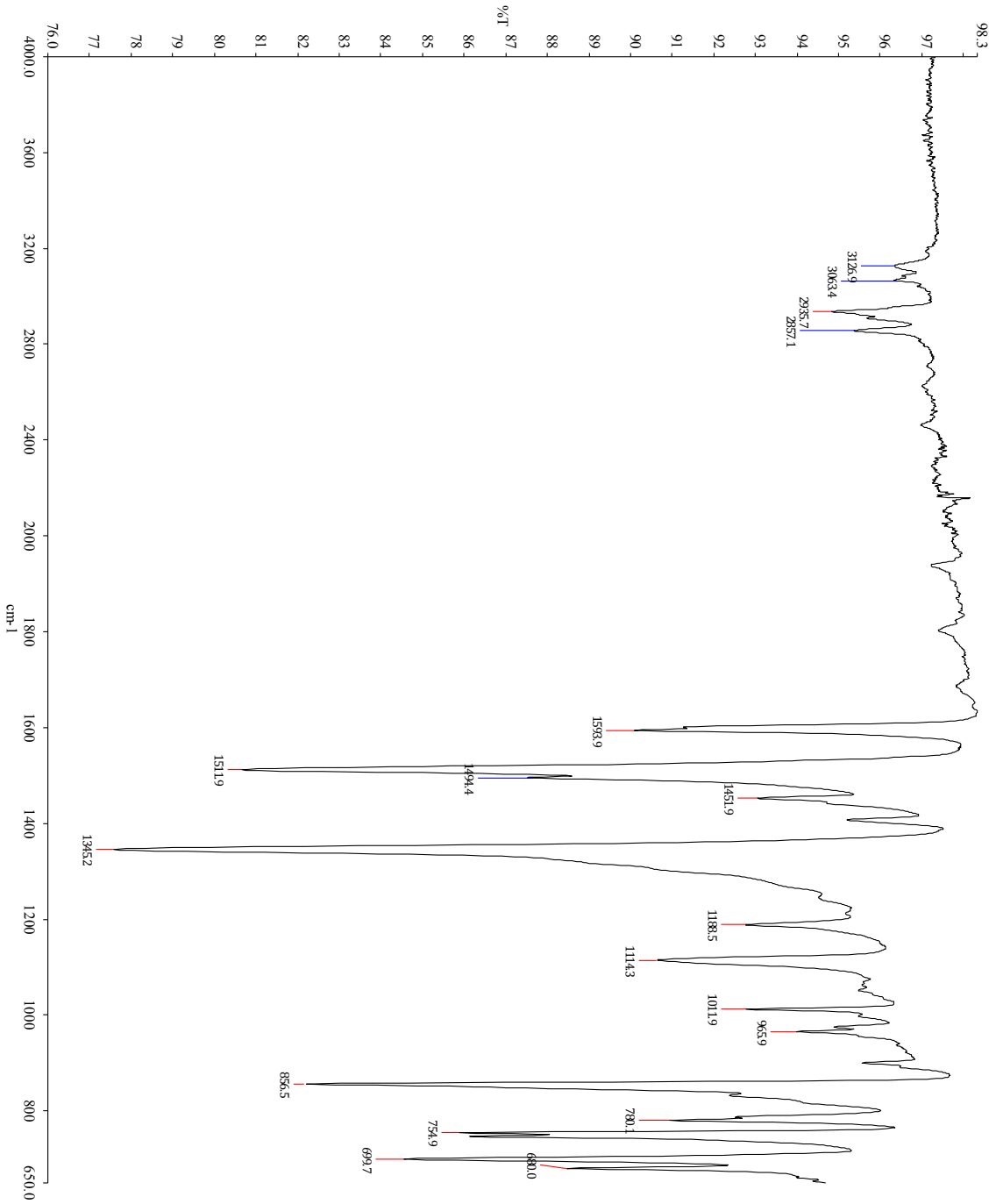

Figure S4. FTIR for 1,3,5,7,-tetra(4-nitrophenyl)adamantane (**3**)

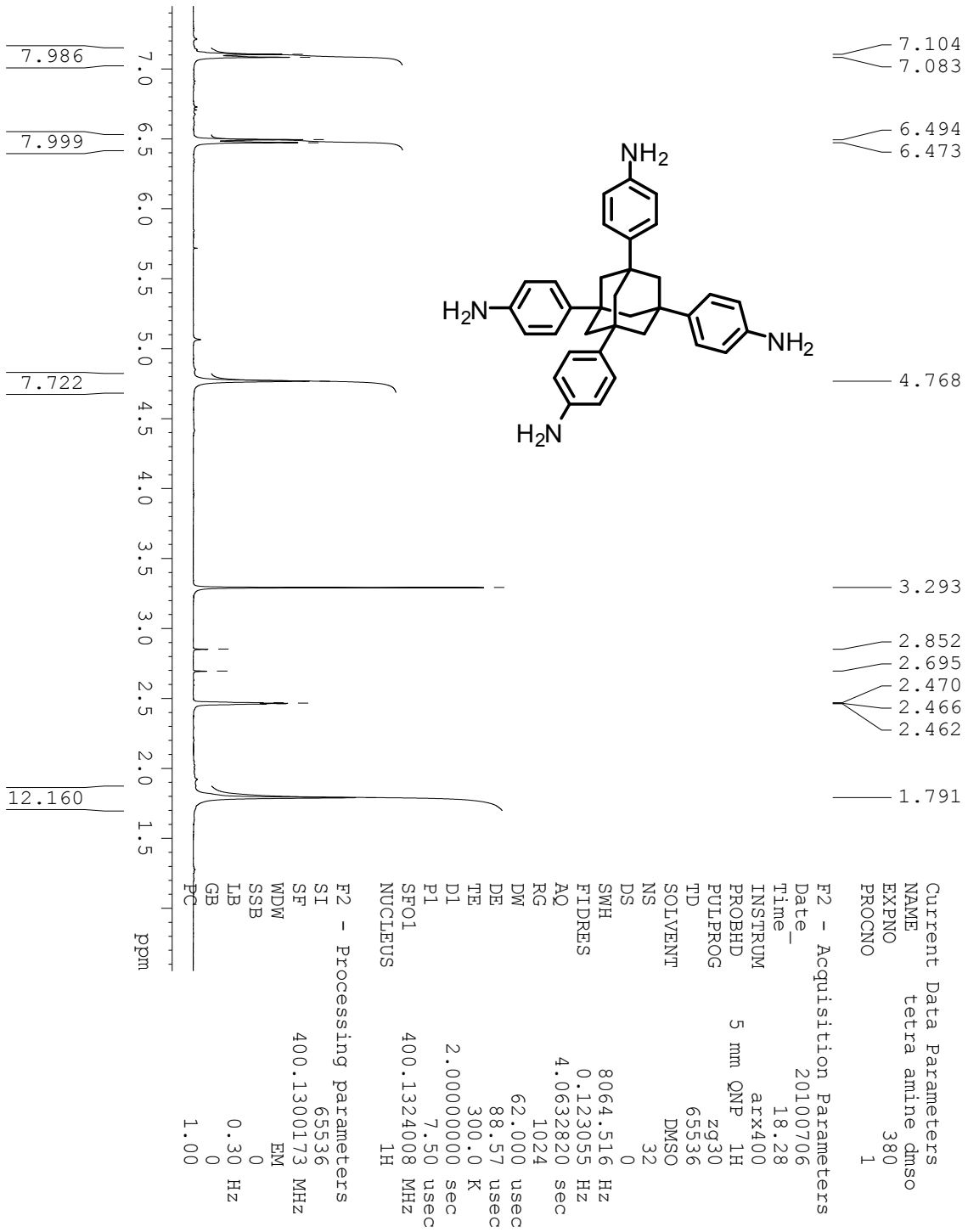

Figure S5. ^{1}H NMR for 1,3,5,7-tetraanilineadamantane **(4)**
400 MHz ^{1}H NMR spectrum of compound **4** in $CDCl_3$

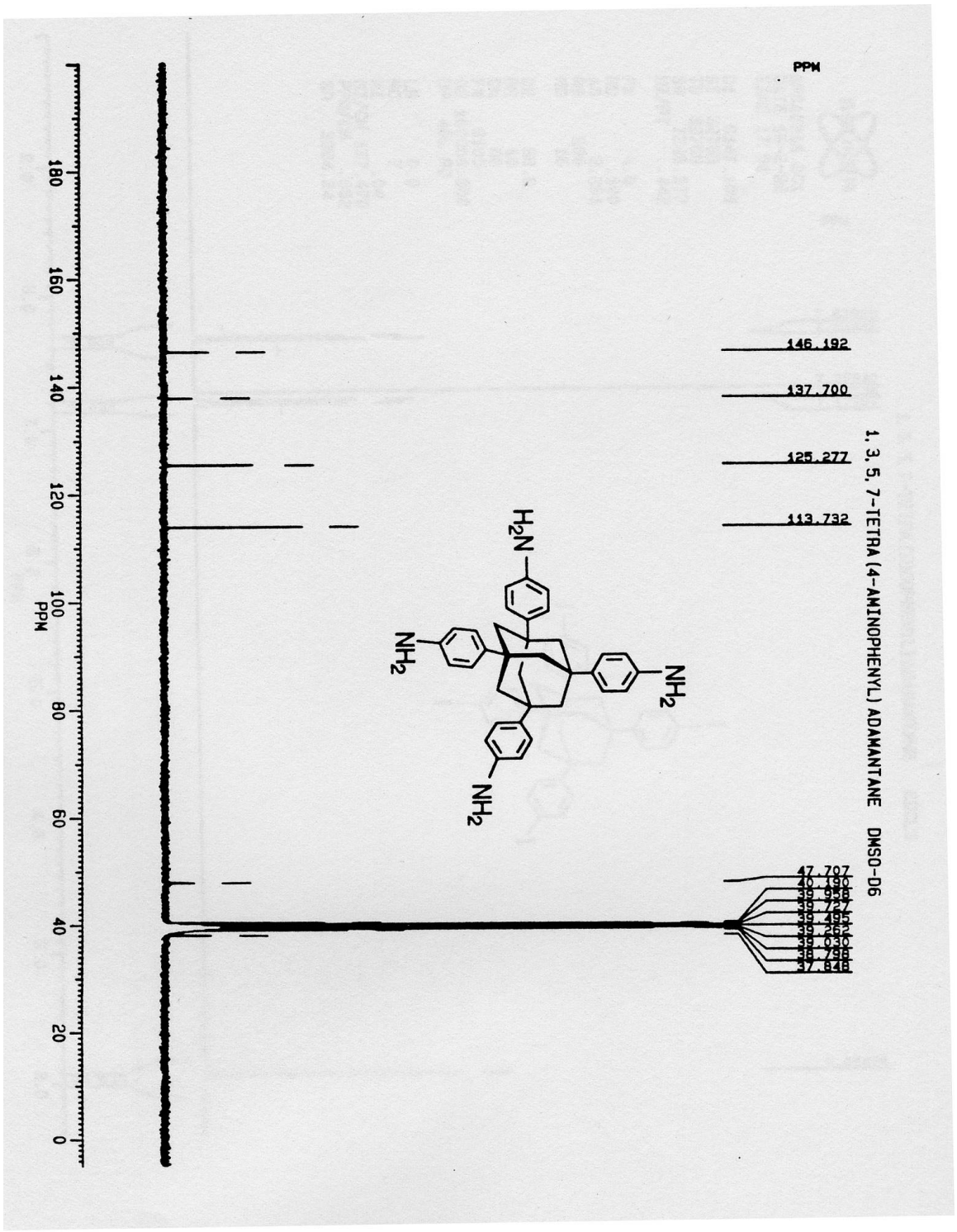

Figure S6. ^{13}C NMR for 1,3,5,7,-tetraanilineadamantane **(4)**
100 MHz ^{13}C NMR spectrum of compound **4** in $CDCl_3$

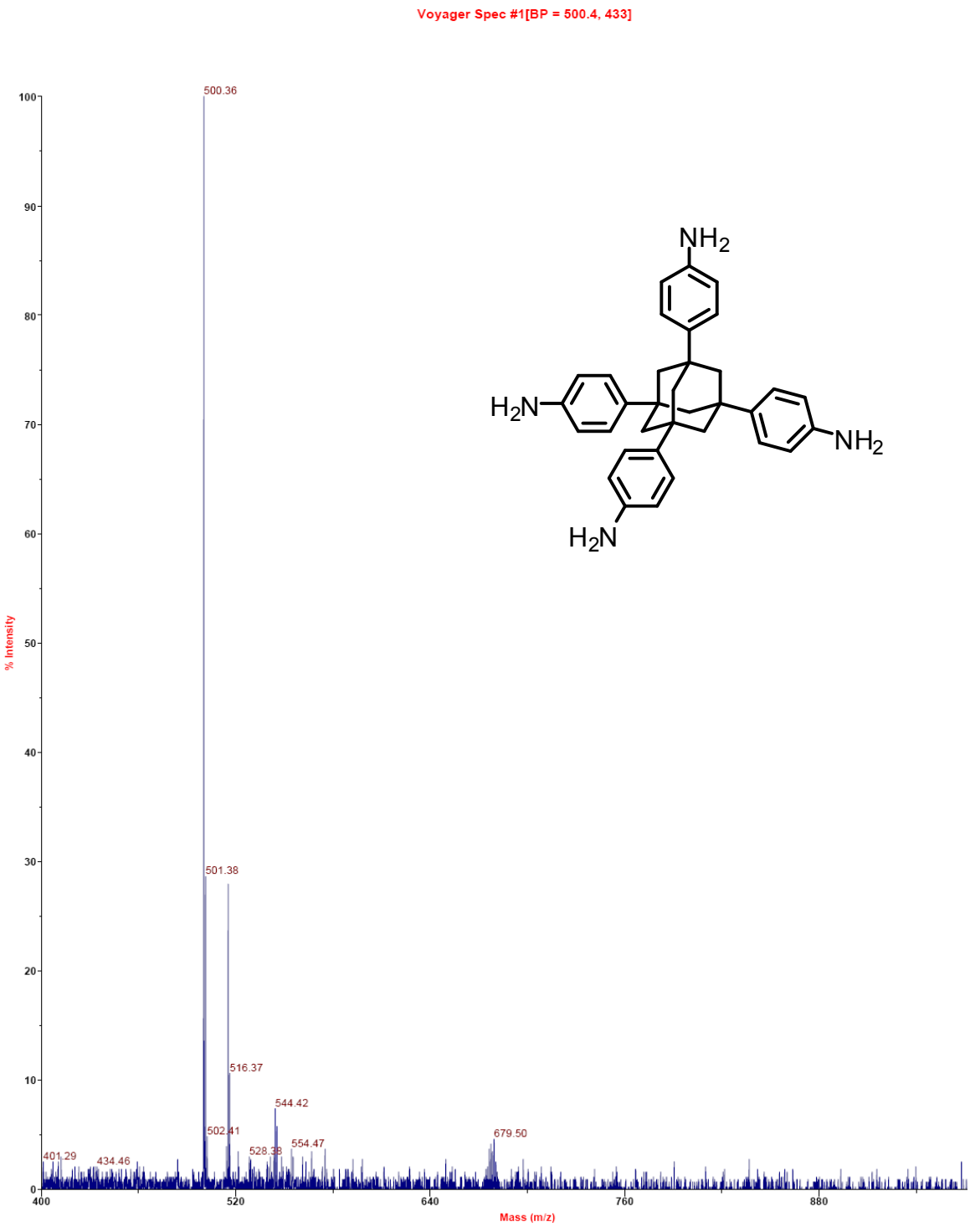

Figure S7. MALDI-TOF-MS for 1,3,5,7,-tetraanilineadamantane **(4)**

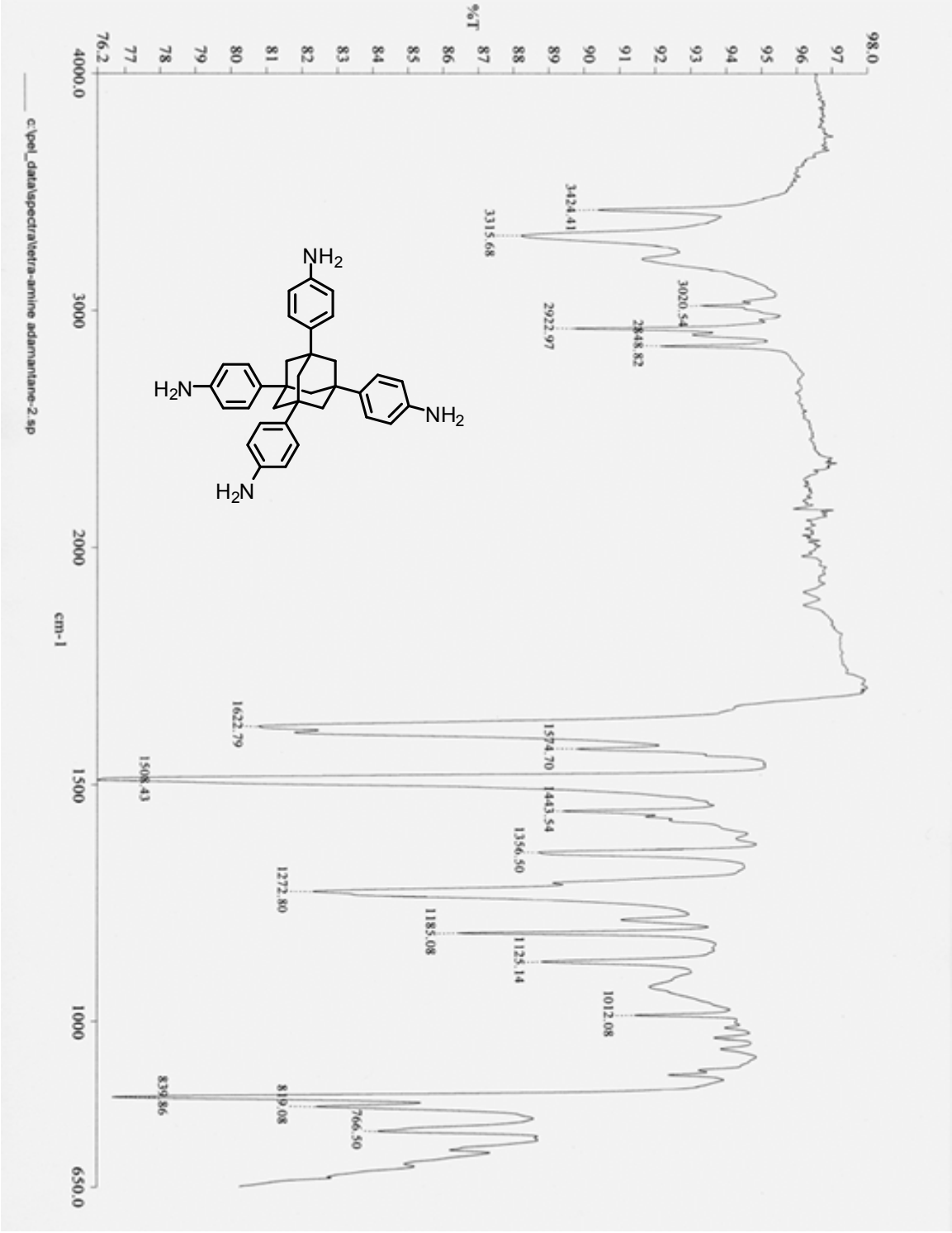

Figure S10. FTIR for 1,3,5,7,-tetraanilineadamantane **(4)**

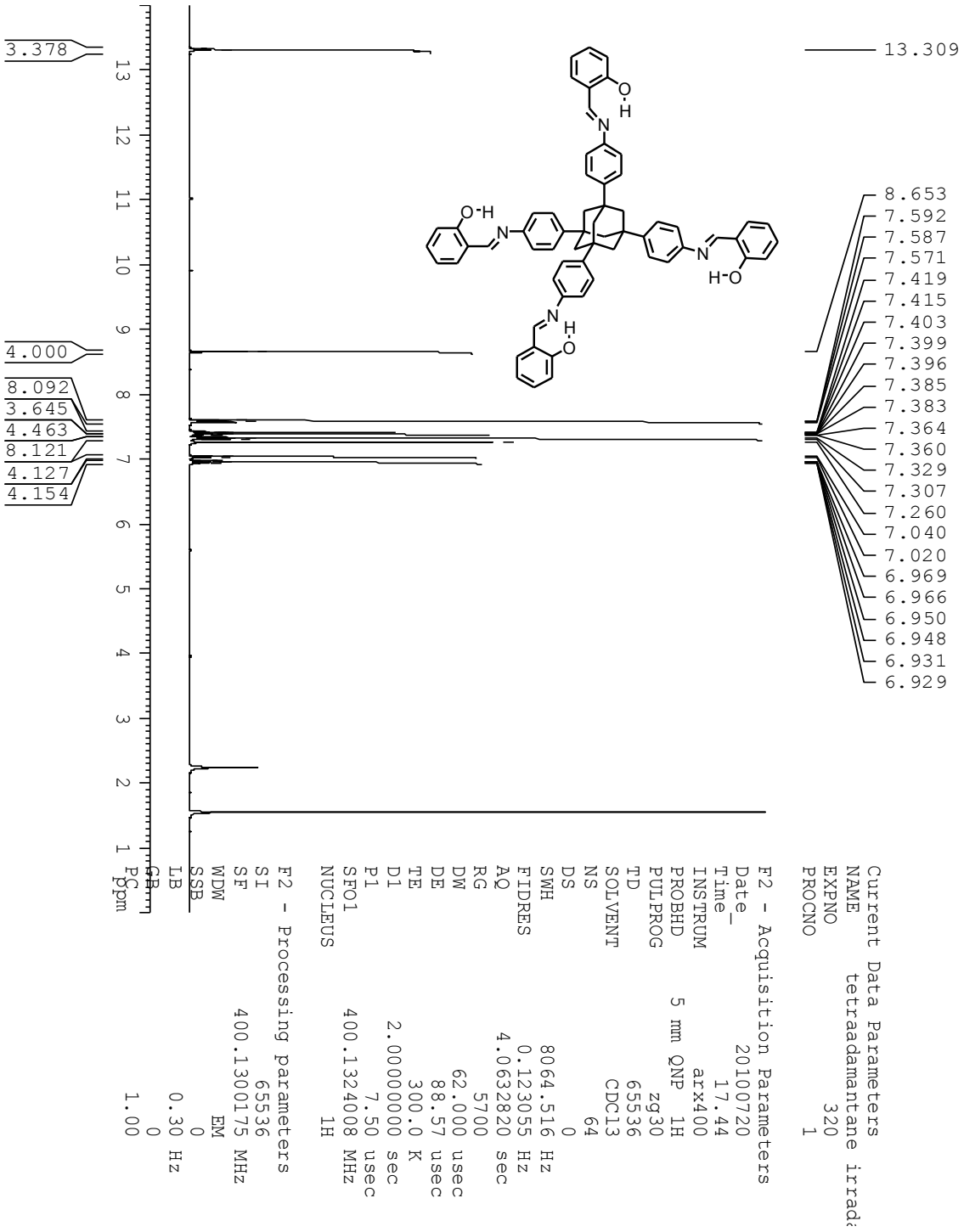

Figure S11. ^{1}H NMR for 1,3,5,7-tetra-*N*-salicylideneanilineadamantane (**1**)
400 MHz ^{1}H NMR spectrum of compound **1** in $CDCl_3$

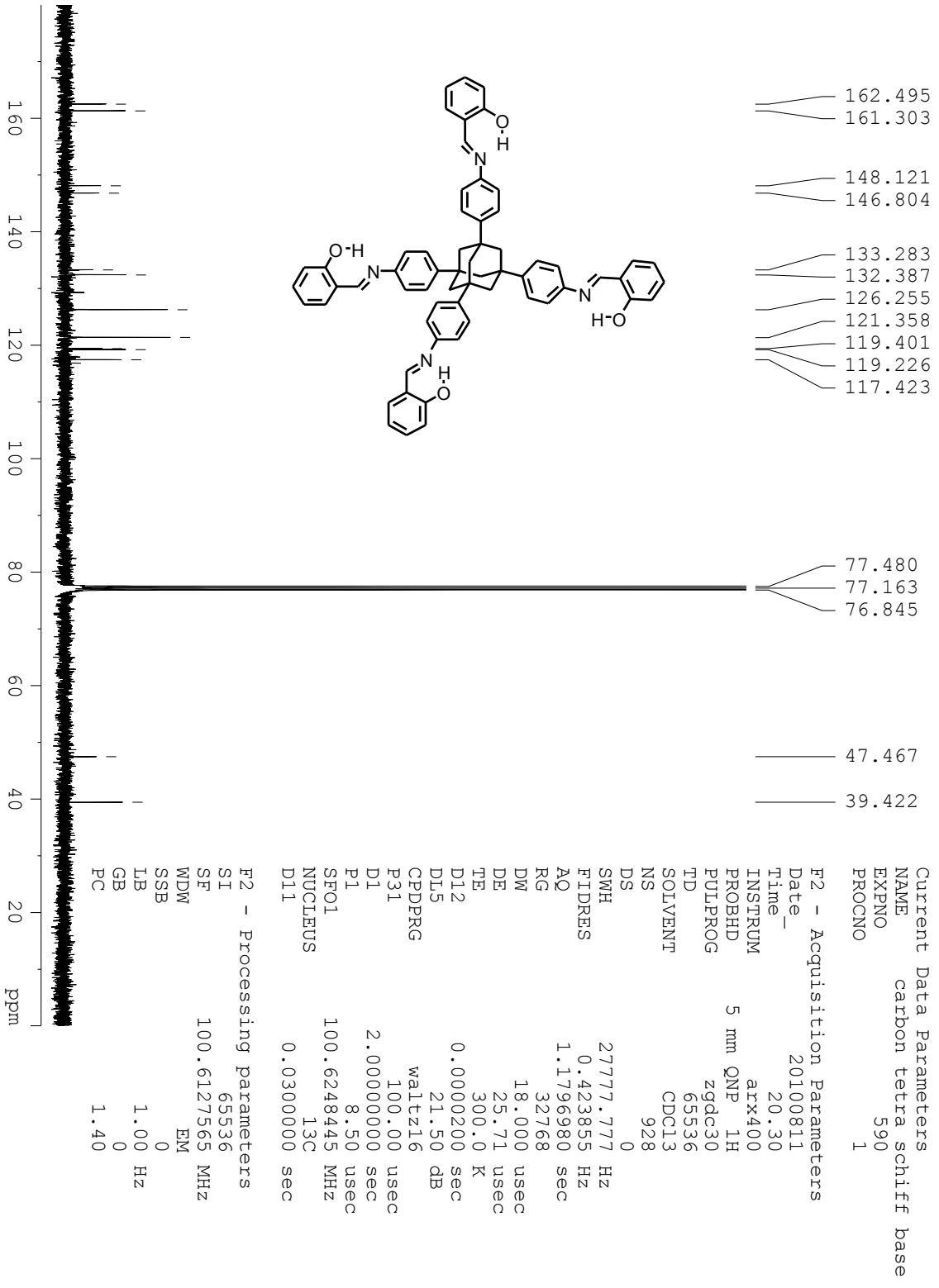

Figure S12. ^{13}C NMR for 1,3,5,7-tetra-*N*-salicylideneanilineadamantane (**1**)
100 MHz ^{13}C NMR spectrum of compound **1** in $CDCl_3$

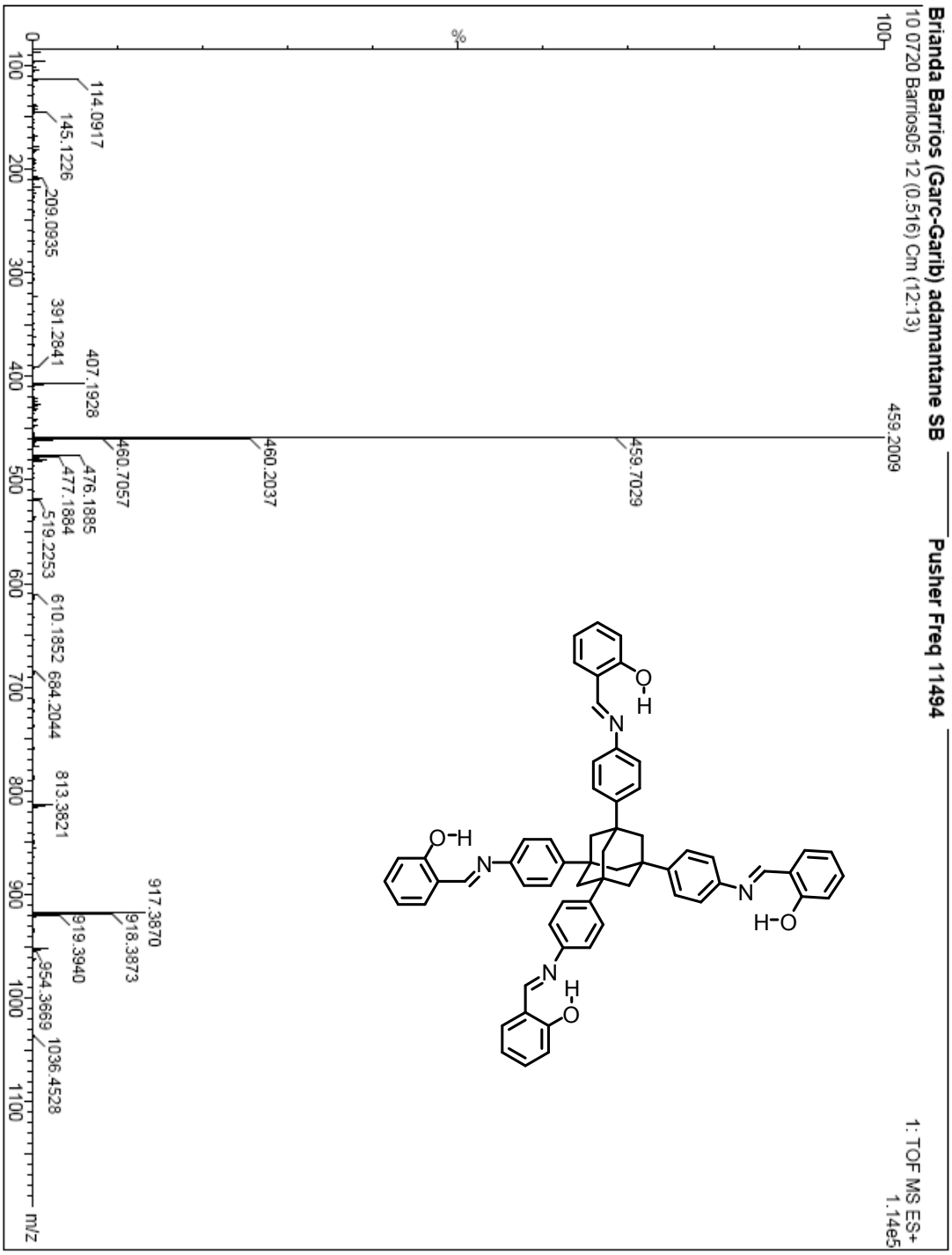

Figure S13. ESI-TOF-MS for 1,3,5,7-tetra-*N*-salicylideneanilineadamantane (**1**)

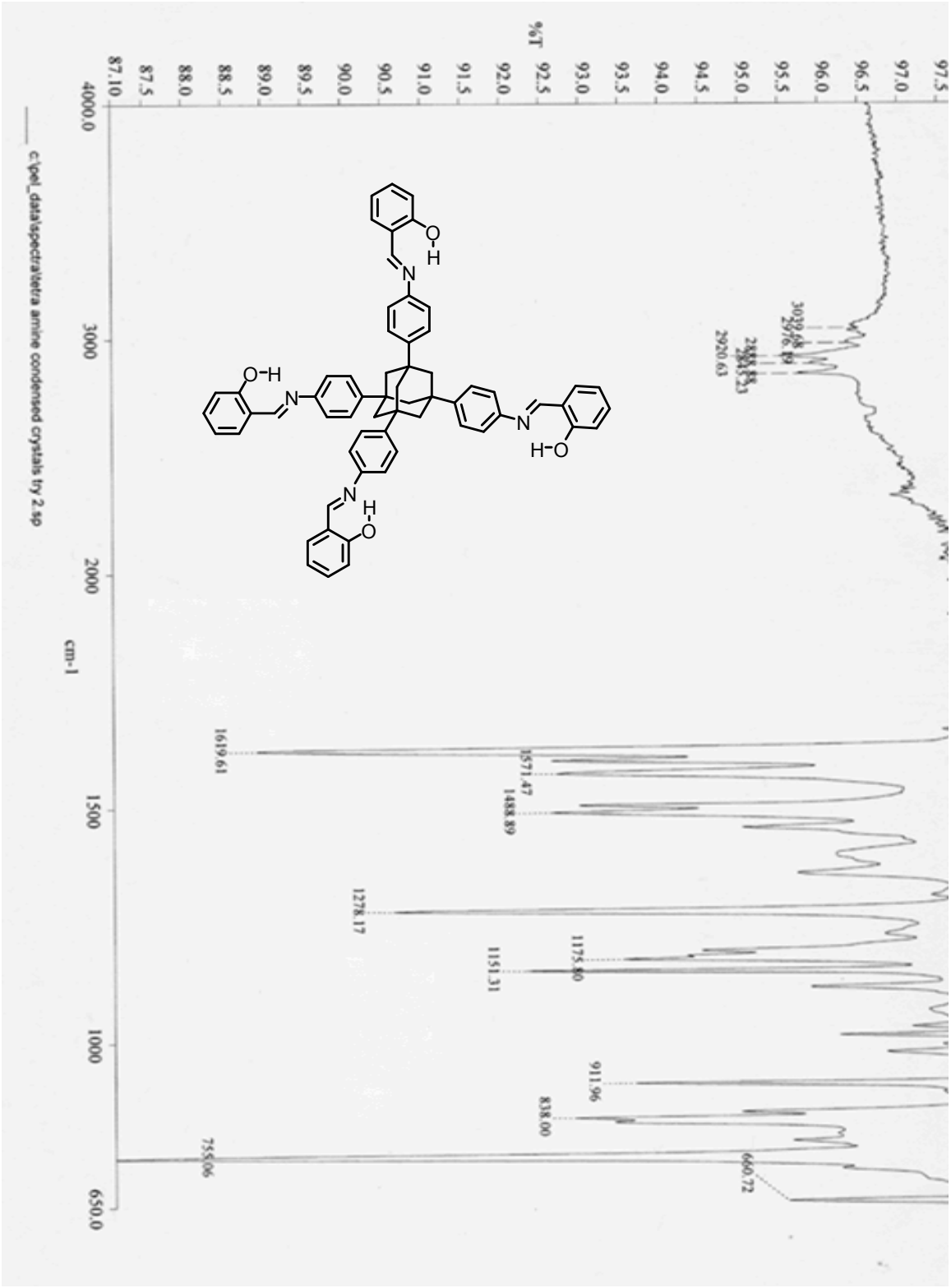

Figure S14. FTIR for 1,3,5,7-tetra-*N*-salicylideneanilineadamantane (**1**)

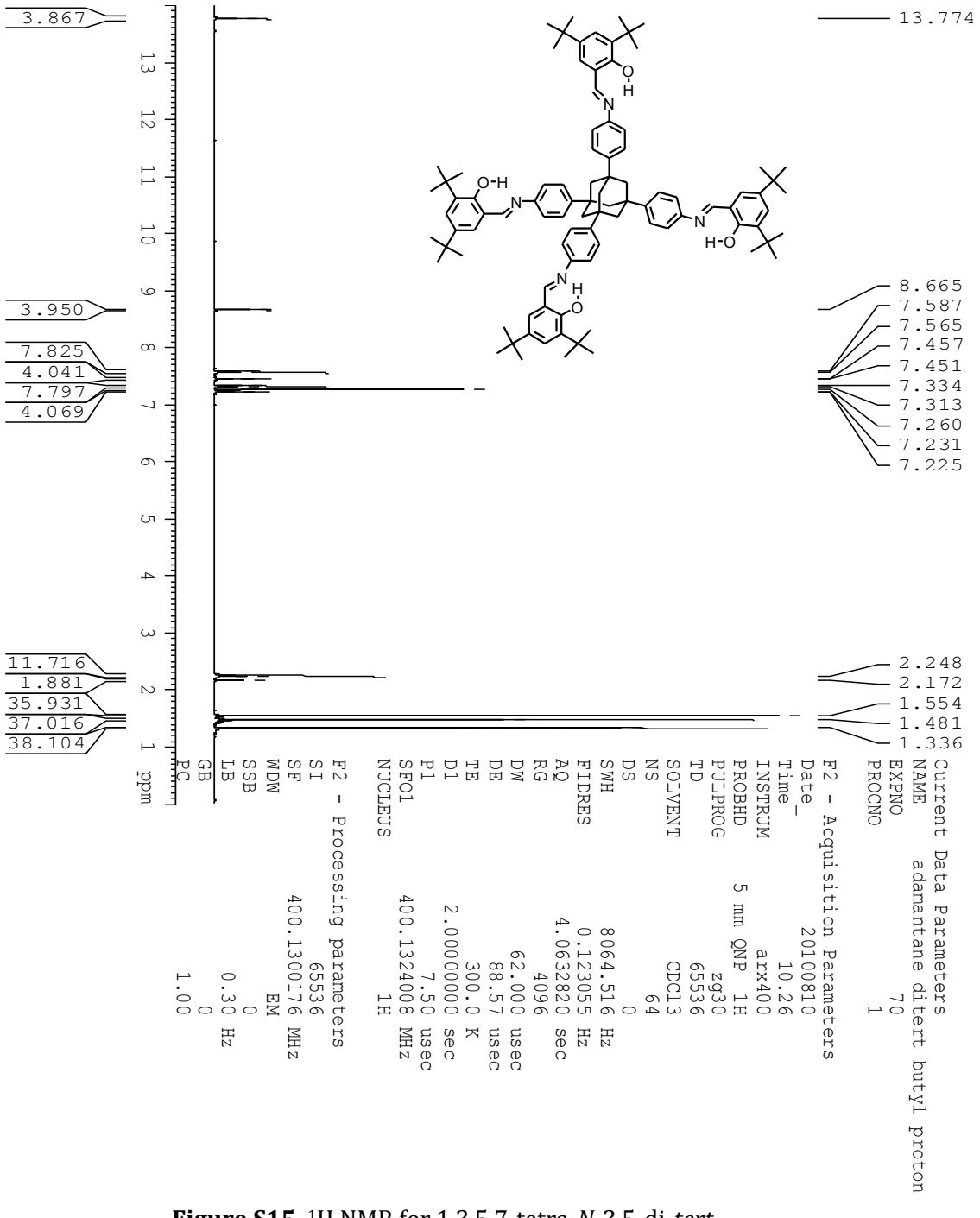

Figure S15. ^{1}H NMR for 1,3,5,7-tetra-*N*-3,5-di-*tert*-butylsalicylideneanilineadamantane**(2)** 400 MHz ^{1}H NMR spectrum of compound **2** in $CDCl_3$

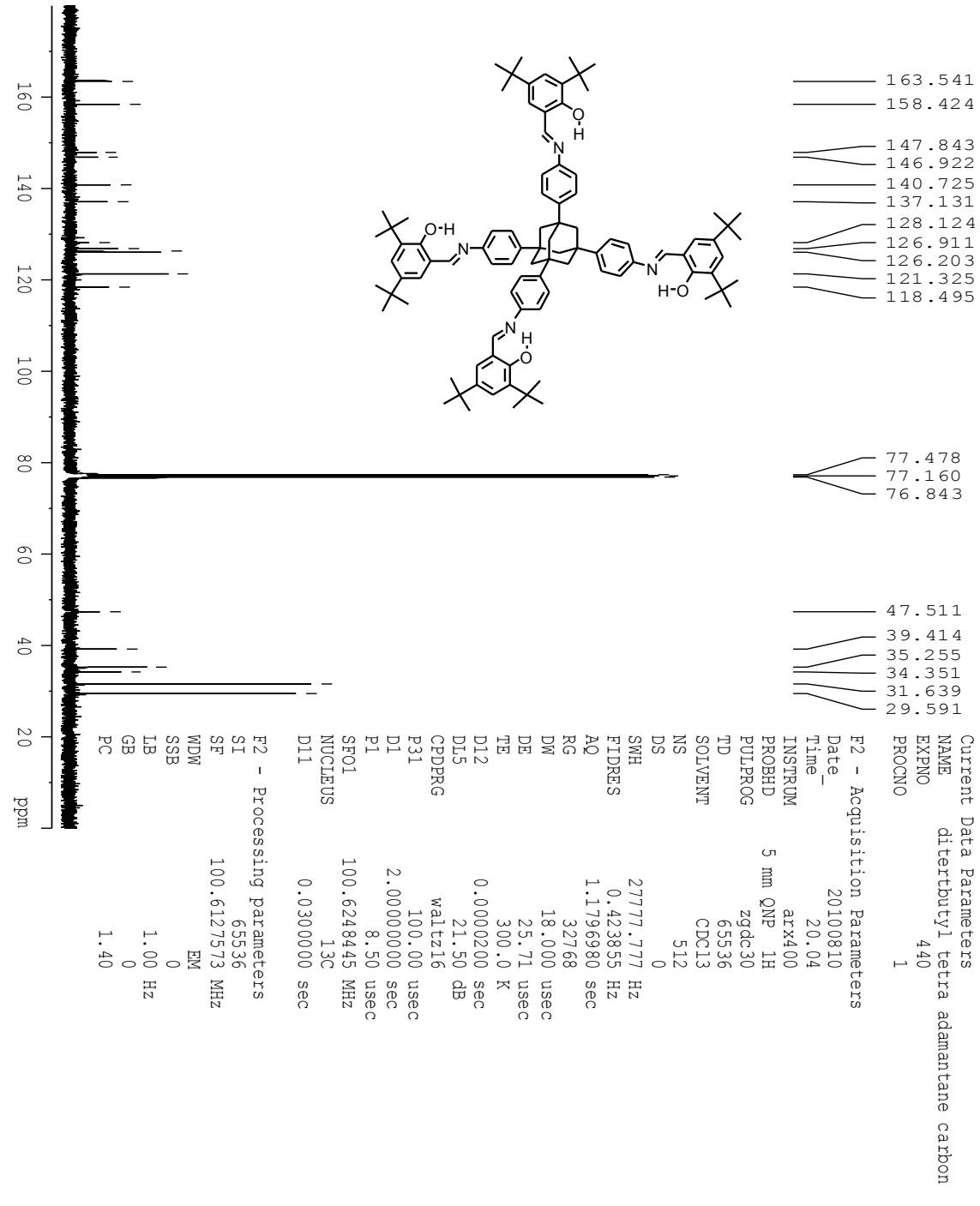

Figure S16. ^{13}C NMR for 1,3,5,7-tetra-*N*-3,5-di-*tert*-butylsalicylideneanilineadamantane **(2)** 100 MHz ^{13}C NMR spectrum of compound **2** in $CDCl_3$

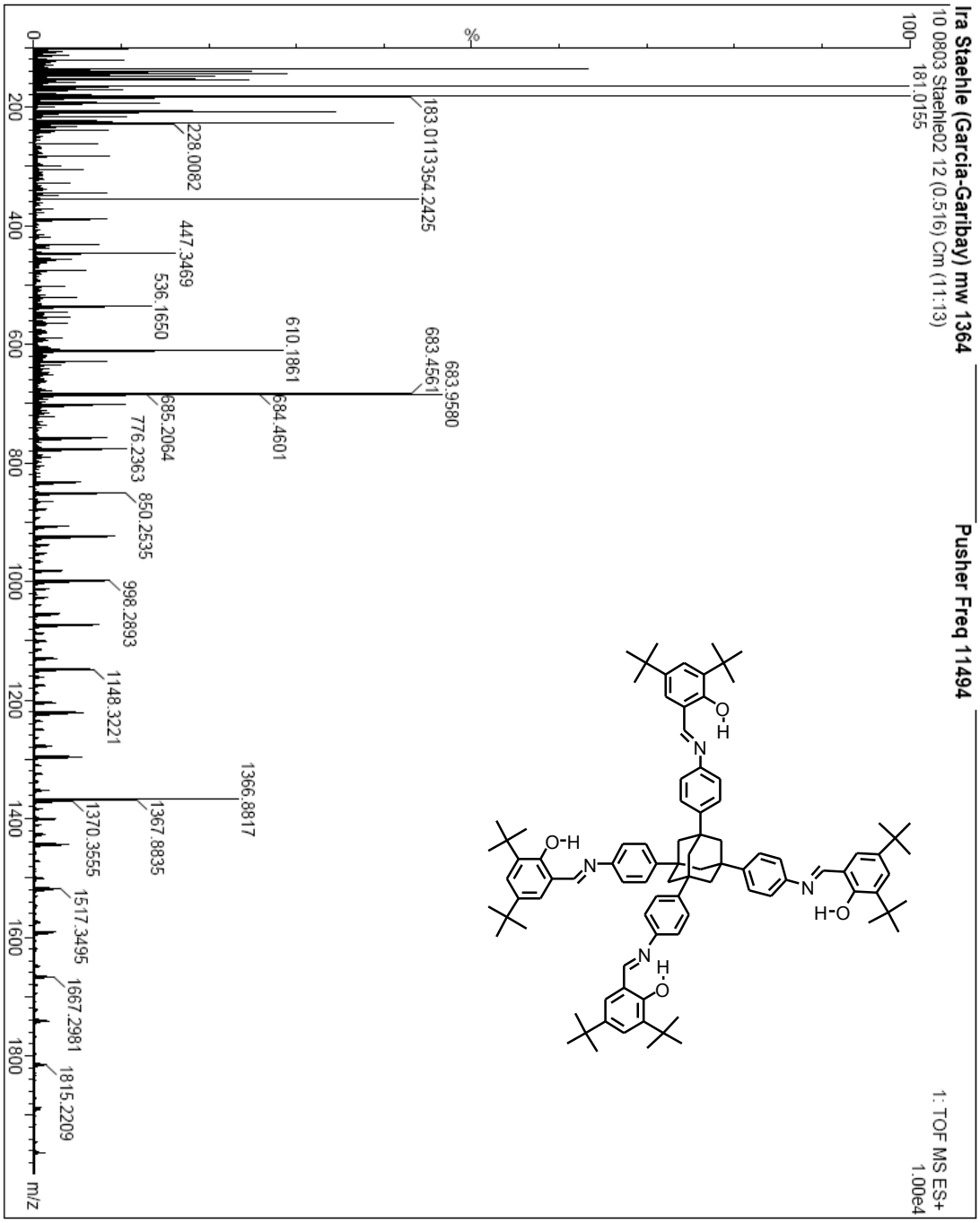

Figure S17. ESI-TOF-MS for

1,3,5,7-tetra-*N*-3,5-di-*tert*-butylsalicylideneanilineadamantane **(2)**

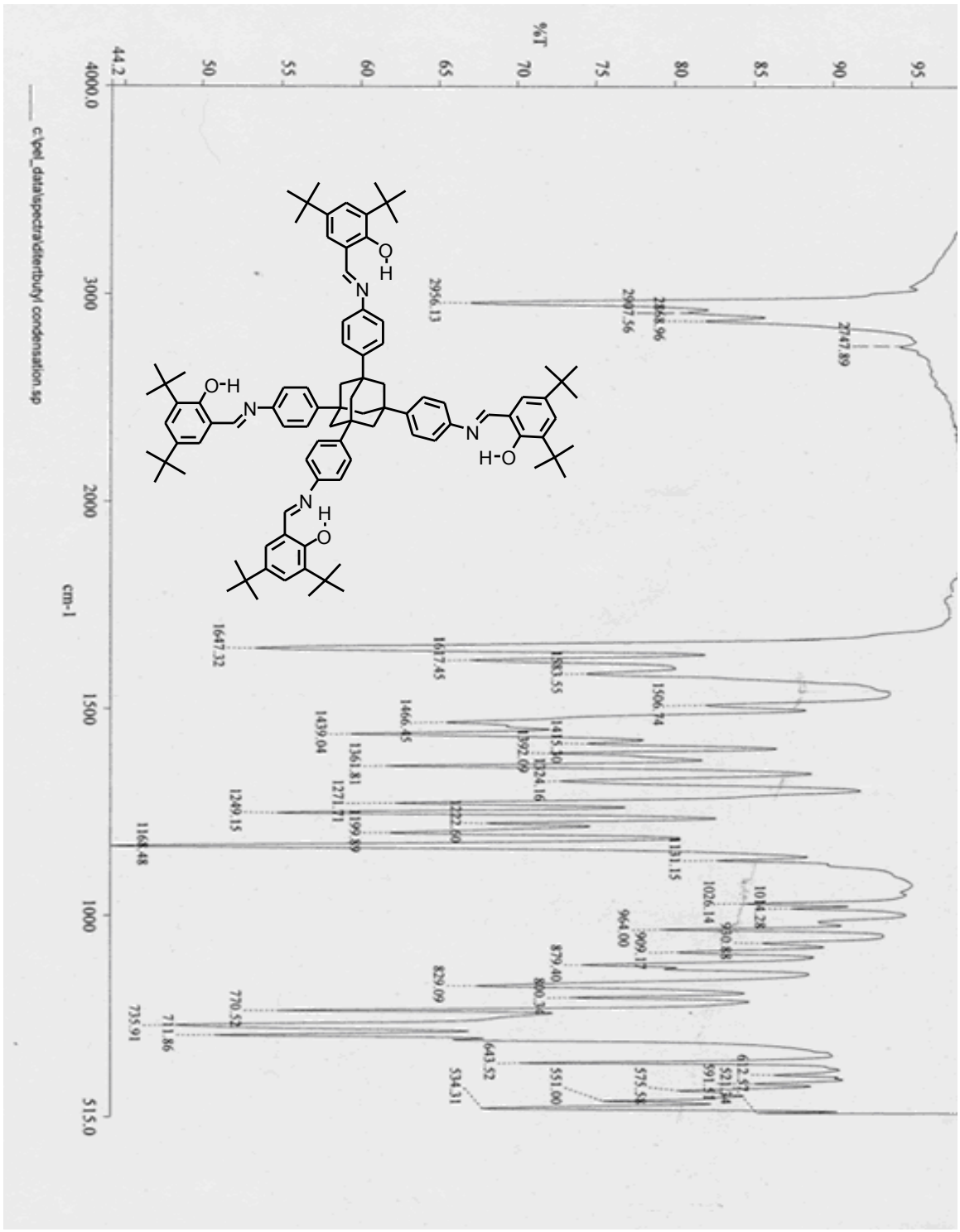

Figure S18. IR for 1,3,5,7-tetra-*N*-3,5-di-*tert*-butylsalicylideneanilineadamantane

(2)

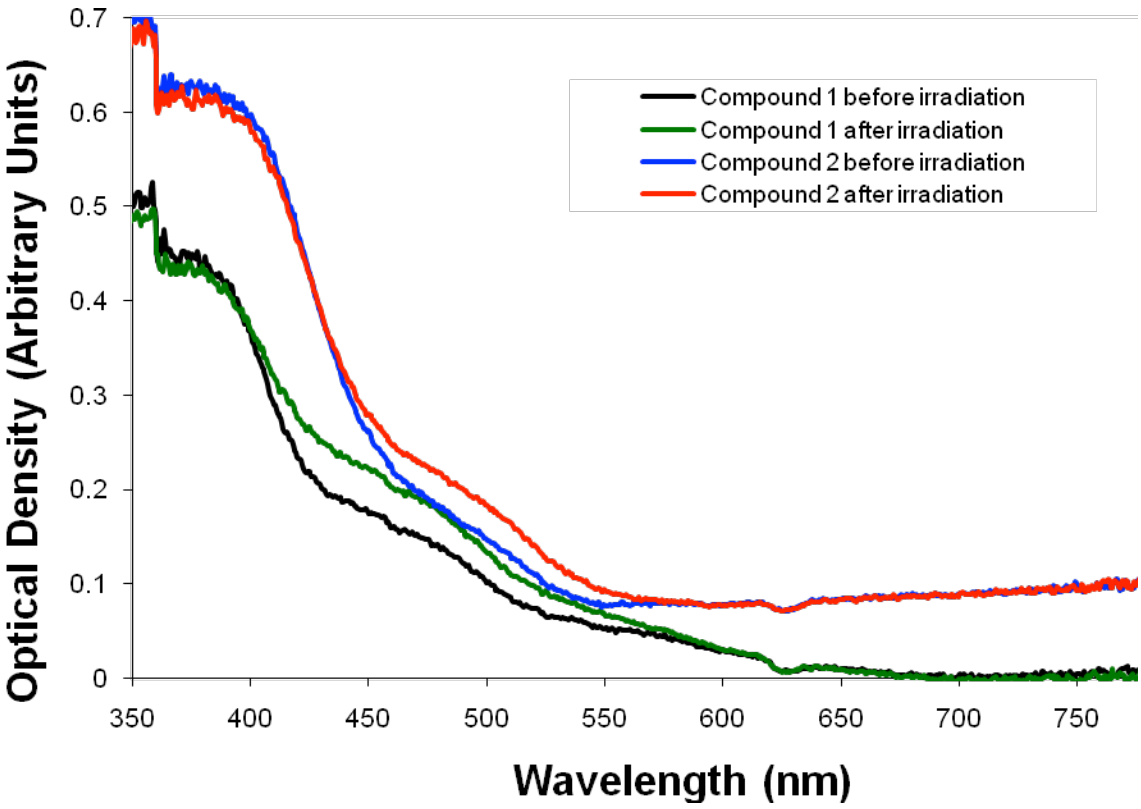

Figure S19. Diffuse Reflectance plot of **1** and **2** before and after irradiation (12 hours for **1,** 20 minutes for **2**) with λ = 365 nm light at RT

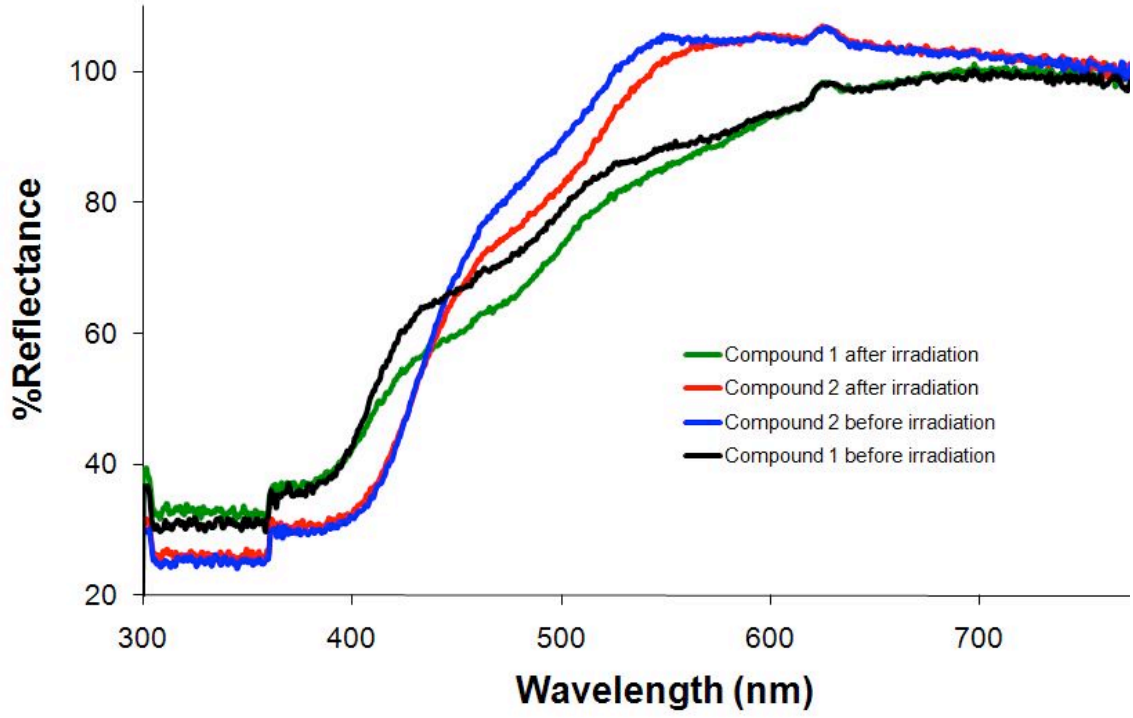

Figure S20. Reflectance plot of **1** and **2** before and after irradiation (12 hours for **1,** 20 minutes for **2**) with λ = 365 nm light at RT

Photochemical procedures

Three different sets of experiments where made with Compound **2** after irradiation for 20 minutes with λ = 365 nm light at RT**.** The conditions are described in the Table S1.

Table S1. Conditions for photochemical procedures for compound **2.**

Name of Set	**Number of Cycles in each Set**	**Total time (seconds) of reading at 500 nm**	**Time between each reading (seconds)**
Set A	**2**	**1200**	**0.2**
Set B	**4**	**3000**	**2**
Set C	**4**	**10000**	**6**

The graphs were fitted with bi-exponental formula (using Origin) as :

$$Y = Y_0 + A_1 e^{-t/\tau_1} + A_2 e^{-t/\tau_2}$$

Results of fitting for Set A (Figures S20 and S21):

cycle	set	τ 1 (seconds)	τ 2 (seconds)
1	A	51.14	422.99
2	A	48.61	395.17
	Average	49.875	
	St Deviation	1.788980156	

Results of fitting for Set B(Figures S22 to S25):

cycle	set	τ 1	τ 2
1	B	44.51	915.03
2	B	236.5099	11917.7
3	B	236.37	2523.72
4	B	107.25	1067.36
	Average	156.16	4105.953
	St Deviation	96.17287	5258.07

Results of fitting for Set C (Figures S26 to S29):

cycle	set	τ 1	τ 2
1	C	89	1589.05
2	C	136.14	1529.47
3	C	46.04	1440.88
4	C	221	1959.15
	Average	123.045	1629.638
	St Deviation	74.956639	227.9538

So, we selected two randoms cycles from Set A and Set C. Then, we fixed τ_1 (Red number) for Set C and τ_3 (Red number) for Set A and compare the fitting values. The parameters after the fitting are really close between the two samples (Figure S30 and S31)

$$\mathbf{Y = Y_0 + A_1 e^{-t/\tau_1} + A_2 e^{-t/\tau_2} + A_3 e^{-t/\tau_3}}$$

Table S2. Tri-exponential parameters for compound **2.**

	A1	τ 1	A2	τ 2	A3	τ 3	y0
cycle 2 set C	0.017	47.700	0.018	261.270	0.012	1755.290	0.258
cycle 1 set A	0.014	47.530	0.002	360.750	0.020	1758.000	0.100
Average	0.016	47.615	0.010	311.010	0.016	1756.645	0.179
standard deviation	0.002	0.120	0.011	70.343	0.006	1.916	0.112

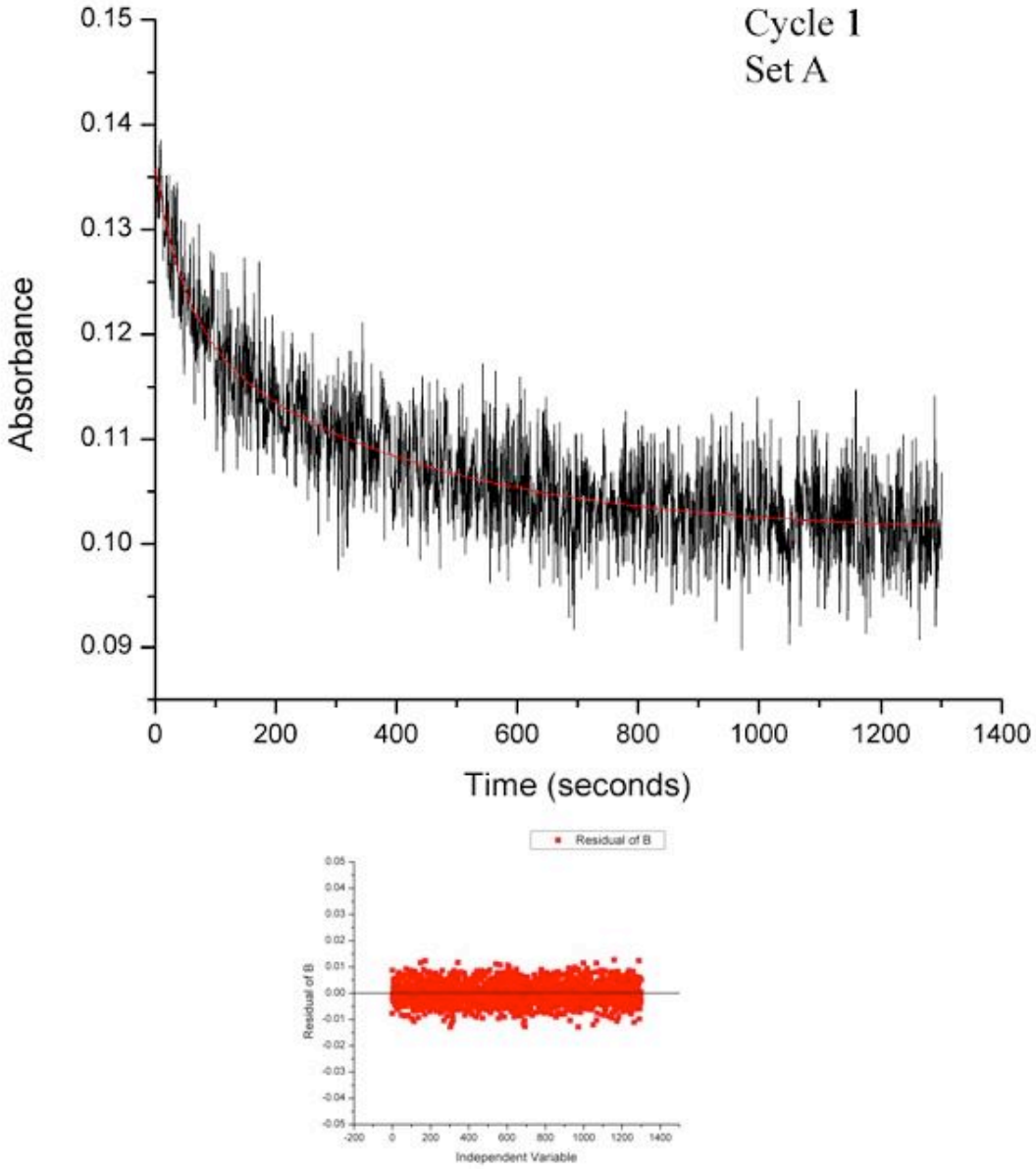

Figure S21. Plot of Cycle 1 and Residual of decay of compound **2** reading at 500 nm after 20 minutes of irradiation with 365 nm light (Acquisition time: 1200 seconds)

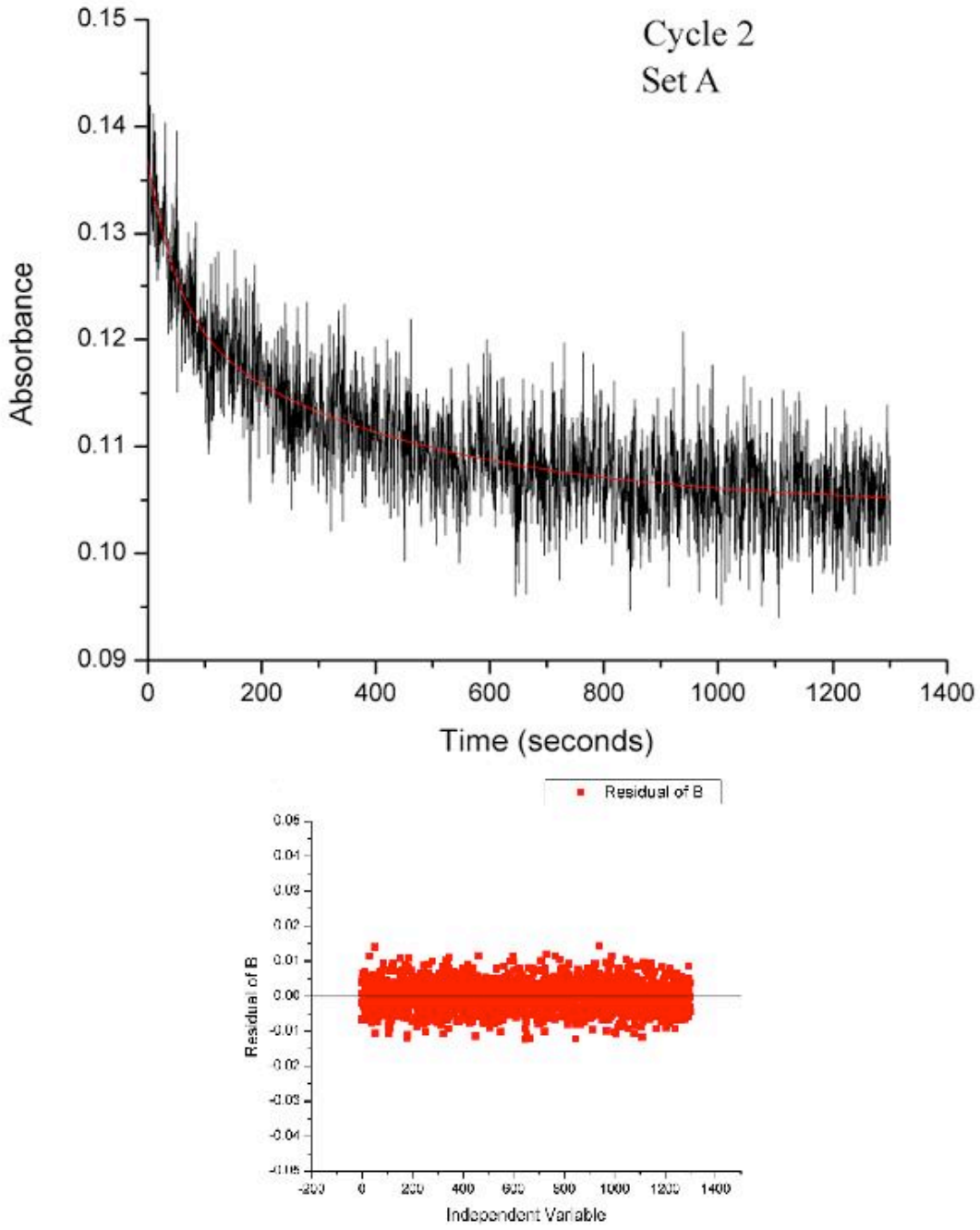

Figure S22. Plot of Cycle 2 and Residual of decay of compound **2** reading at 500 nm after 20 minutes of irradiation with 365 nm light (Acquisition time: 1200 seconds)

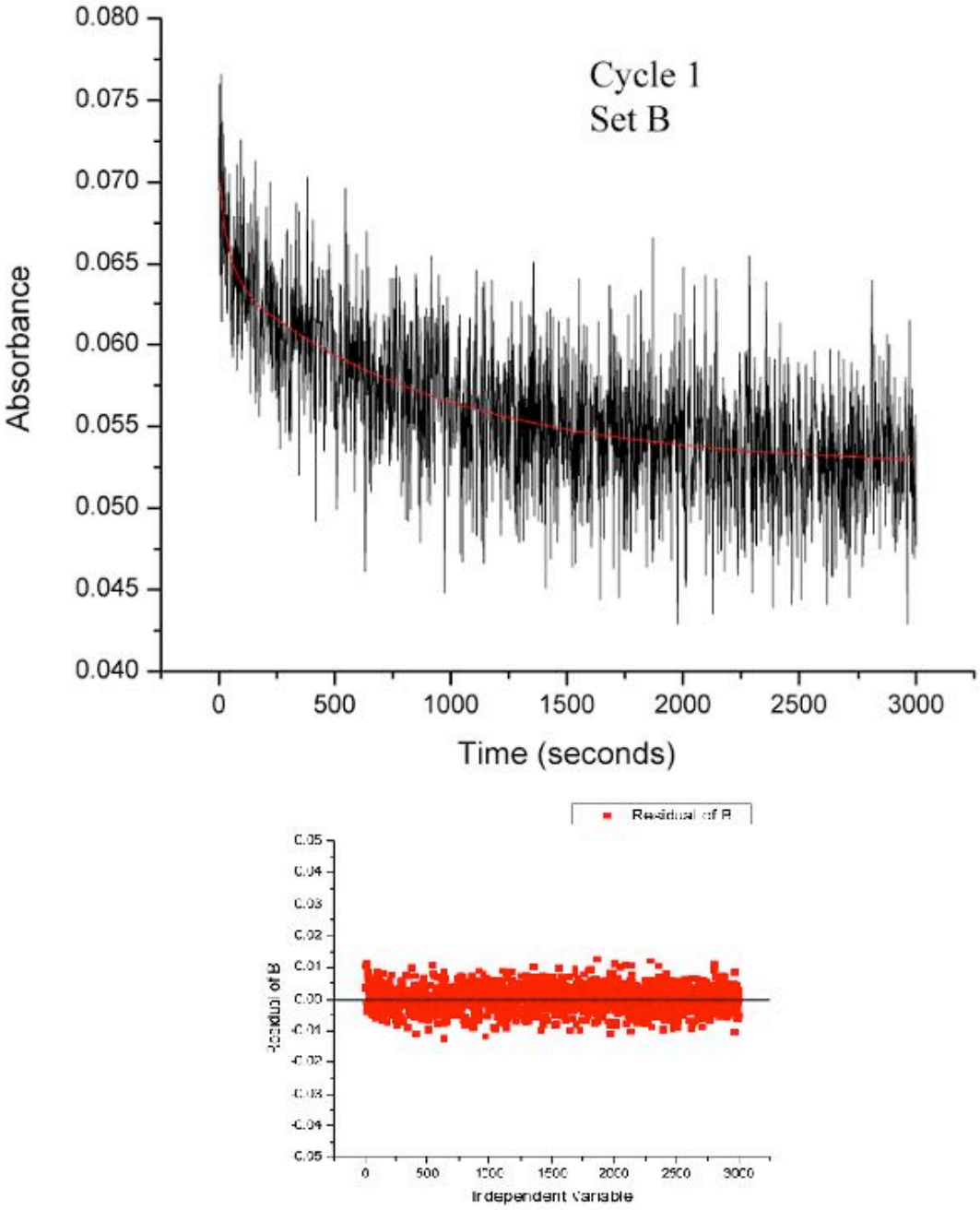

Figure S23. Plot of Cycle 1 and Residual of decay of compound **2** reading at 500 nm after 20 minutes of irradiation with 365 nm light (Acquisition time: 3000 seconds)

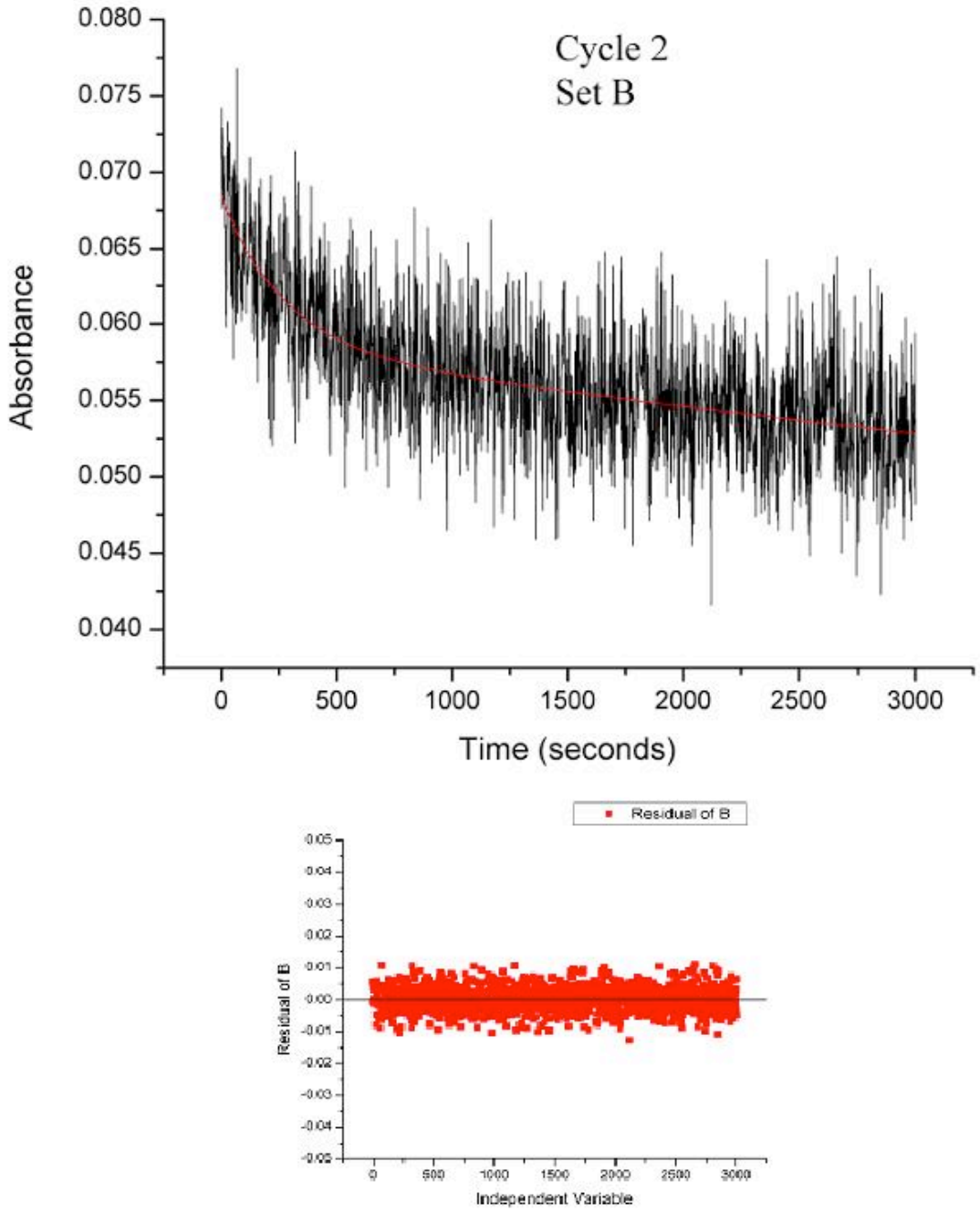

Figure S24. Plot of Cycle 2 and Residual of decay of compound **2** reading at 500 nm after 20 minutes of irradiation with 365 nm light (Acquisition time: 3000 seconds)

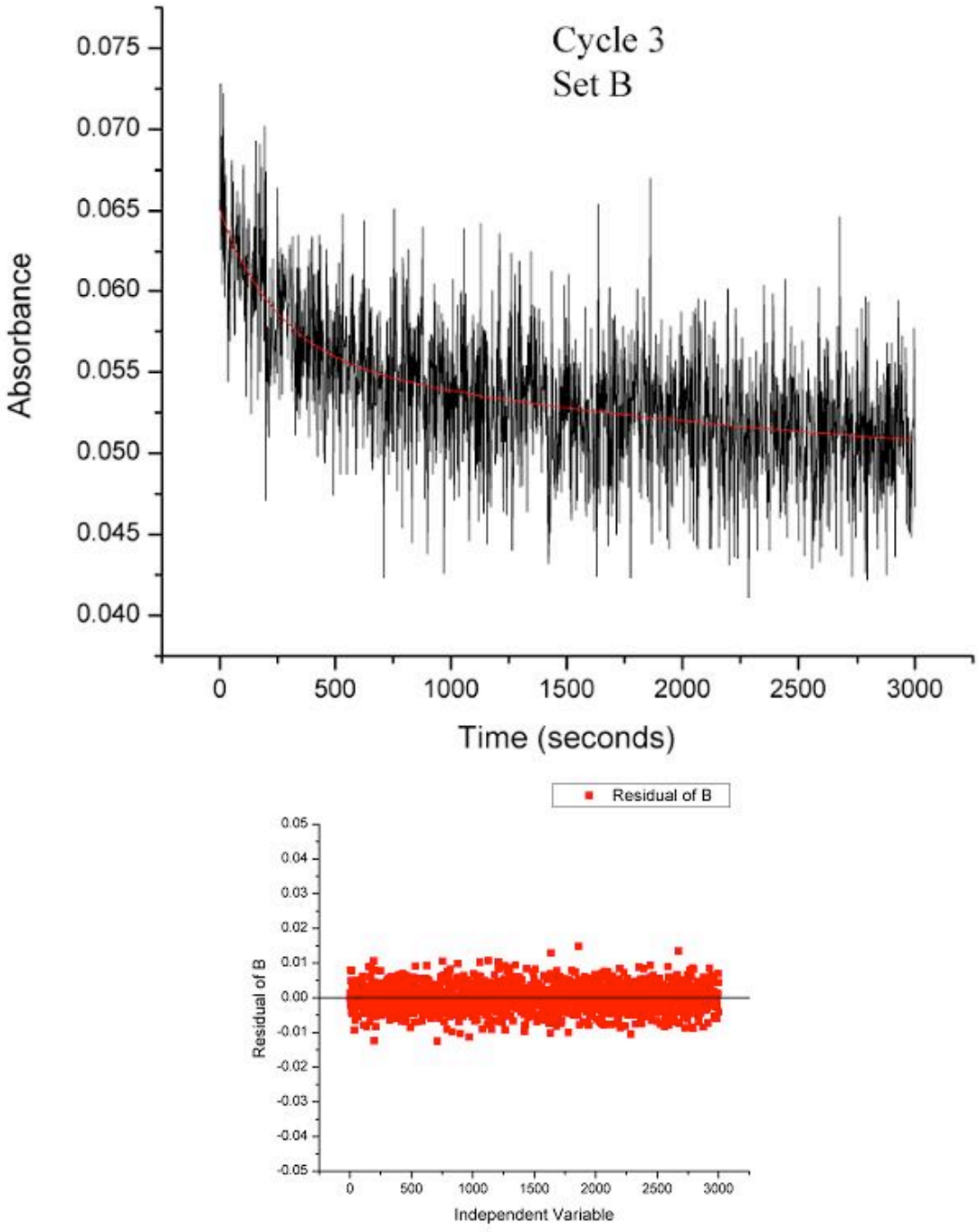

Figure S25. Plot of Cycle 3 and Residual of decay of compound **2** reading at 500 nm after 20 minutes of irradiation with 365 nm light (Acquisition time: 3000 seconds)

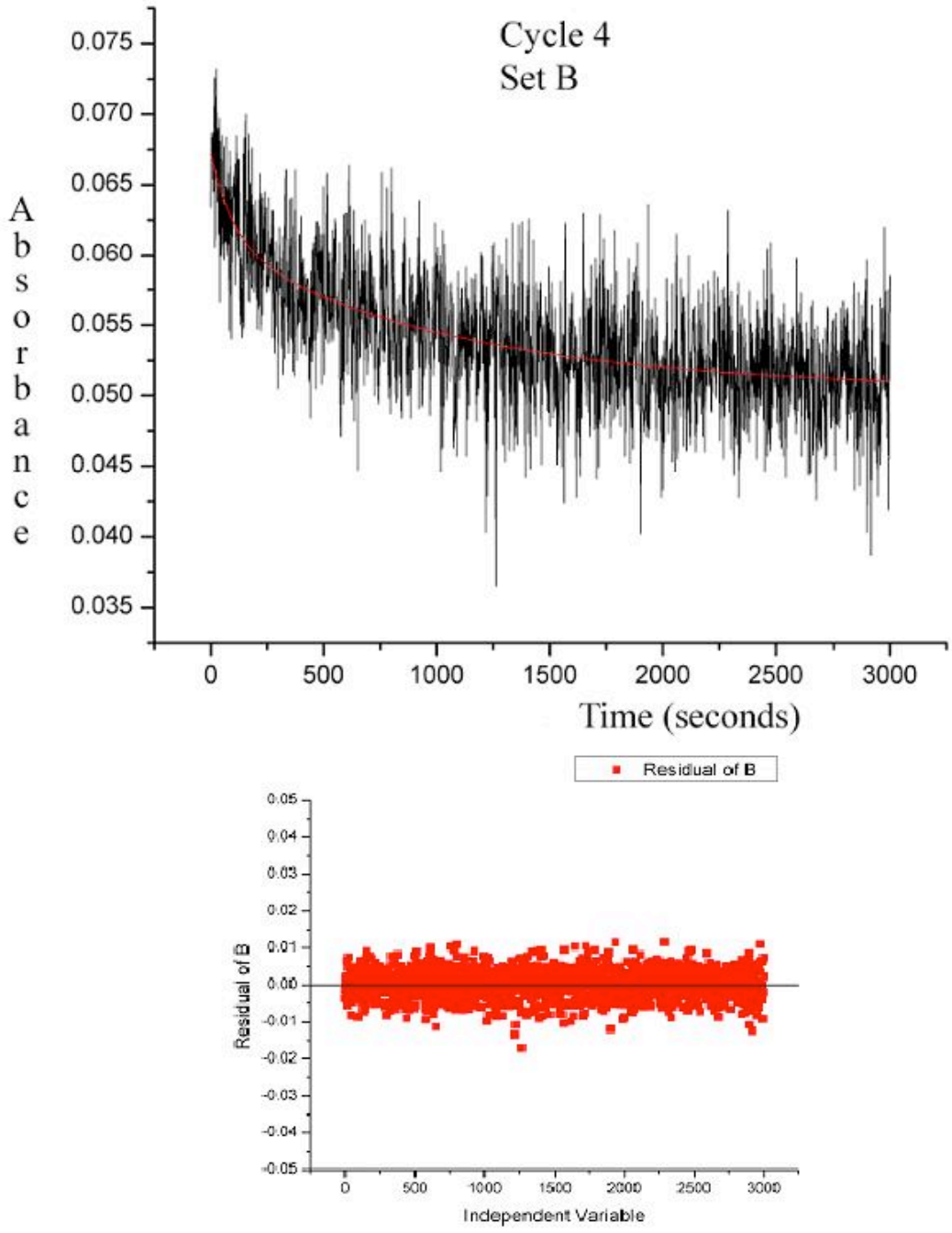

Figure S26. Plot of Cycle 4 and Residual of decay of compound **2** reading at 500 nm after 20 minutes of irradiation with 365 nm light (Acquisition time: 3000 seconds)

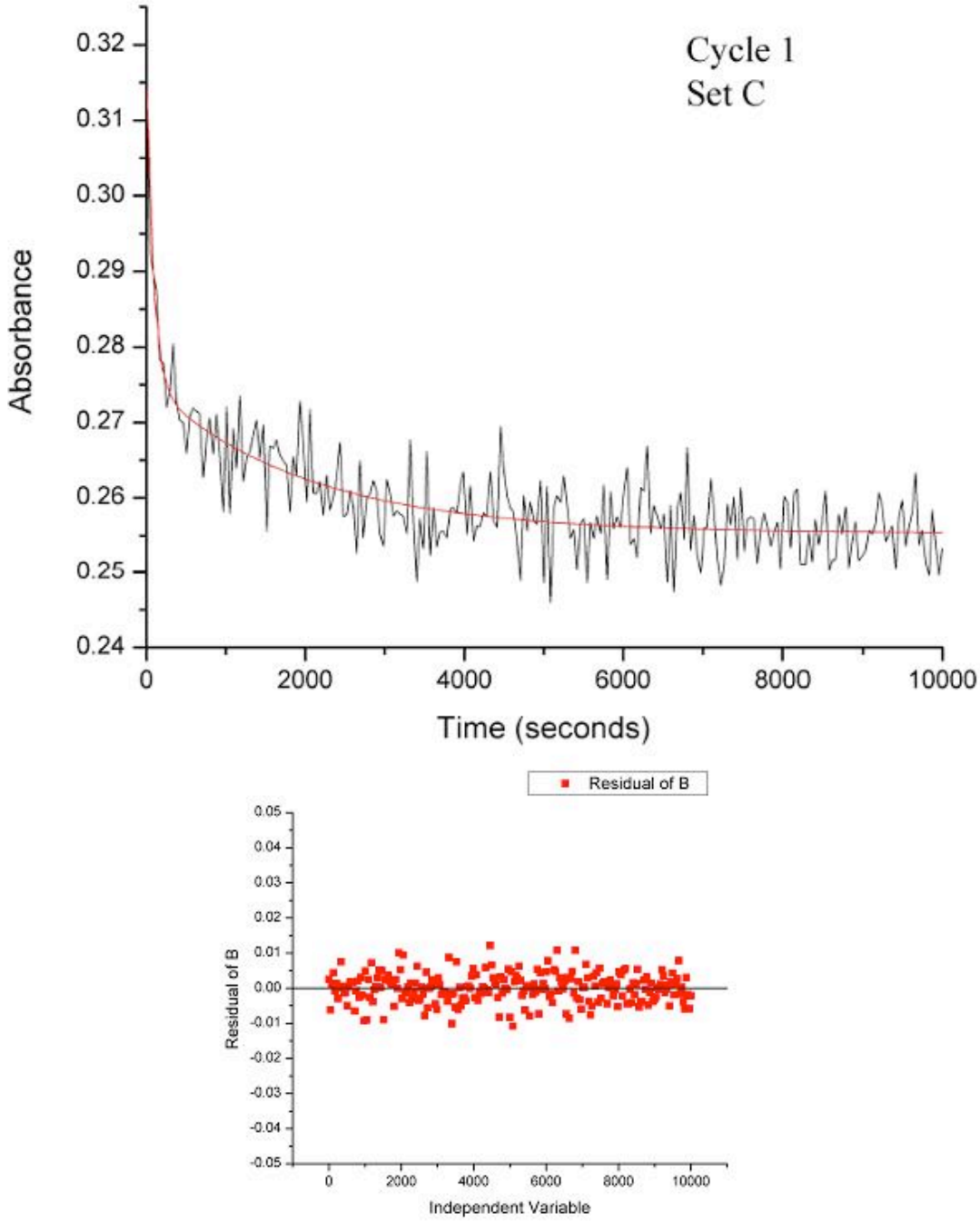

Figure S27. Plot of Cycle 1 and Residual of decay of compound **2** reading at 500 nm after 20 minutes of irradiation with 365 nm light (Acquisition time: 10000 seconds)

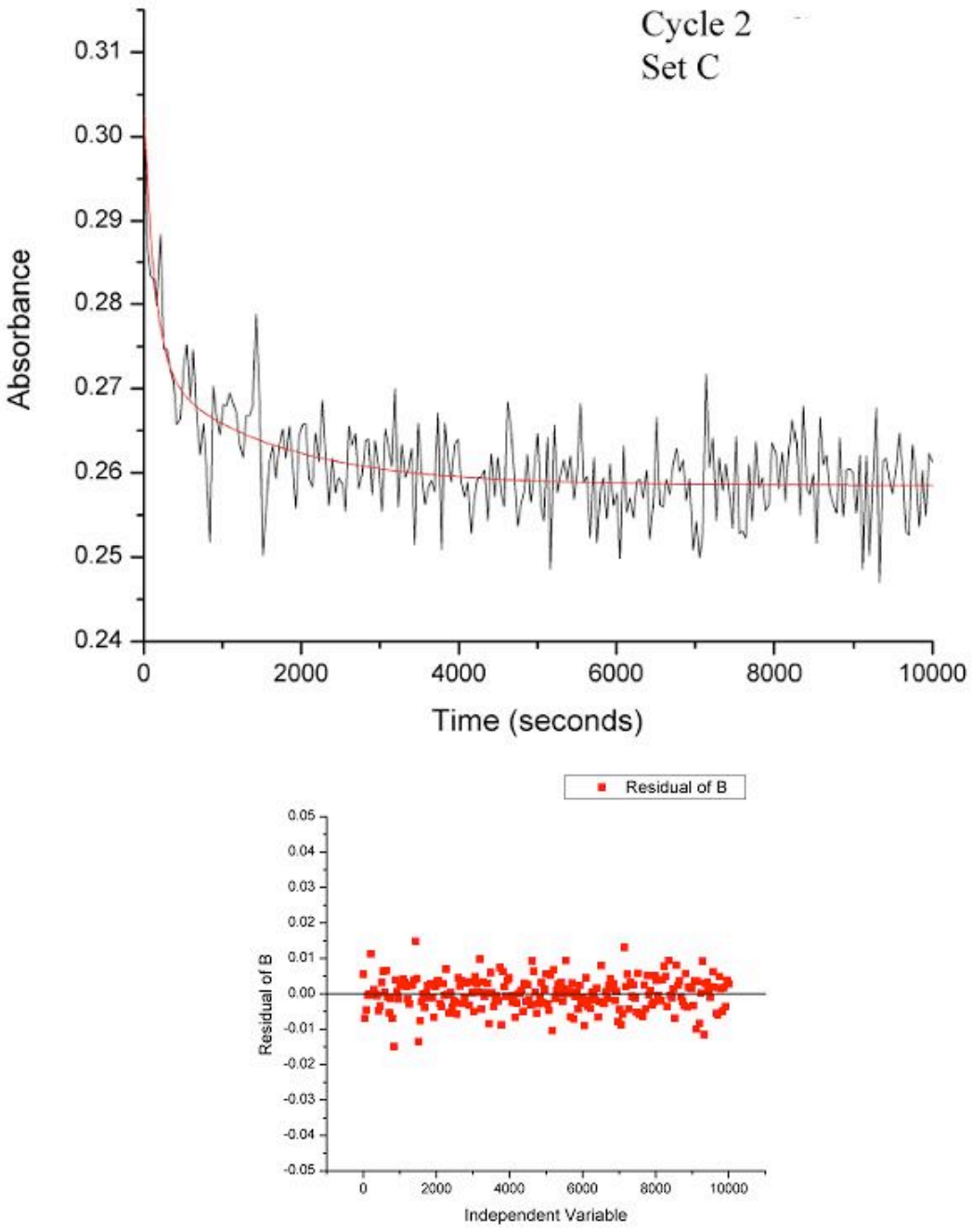

Figure S28. Plot of Cycle 2 and Residual of decay of compound **2** reading at 500 nm after 20 minutes of irradiation with 365 nm light (Acquisition time: 10000 seconds)

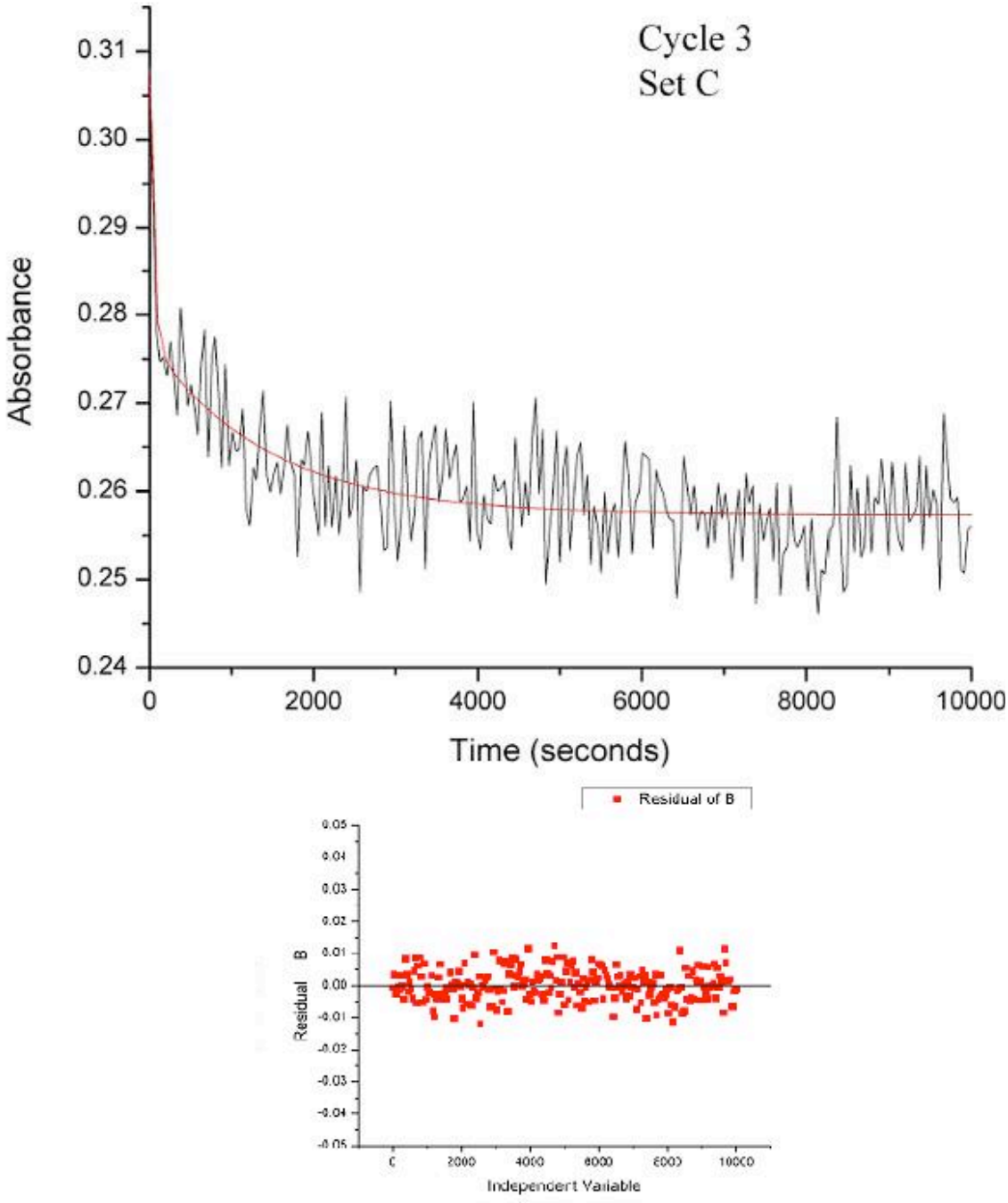

Figure S29. Plot of Cycle 3 and Residual of decay of compound **2** reading at 500 nm after 20 minutes of irradiation with 365 nm light (Acquisition time: 10000 seconds)

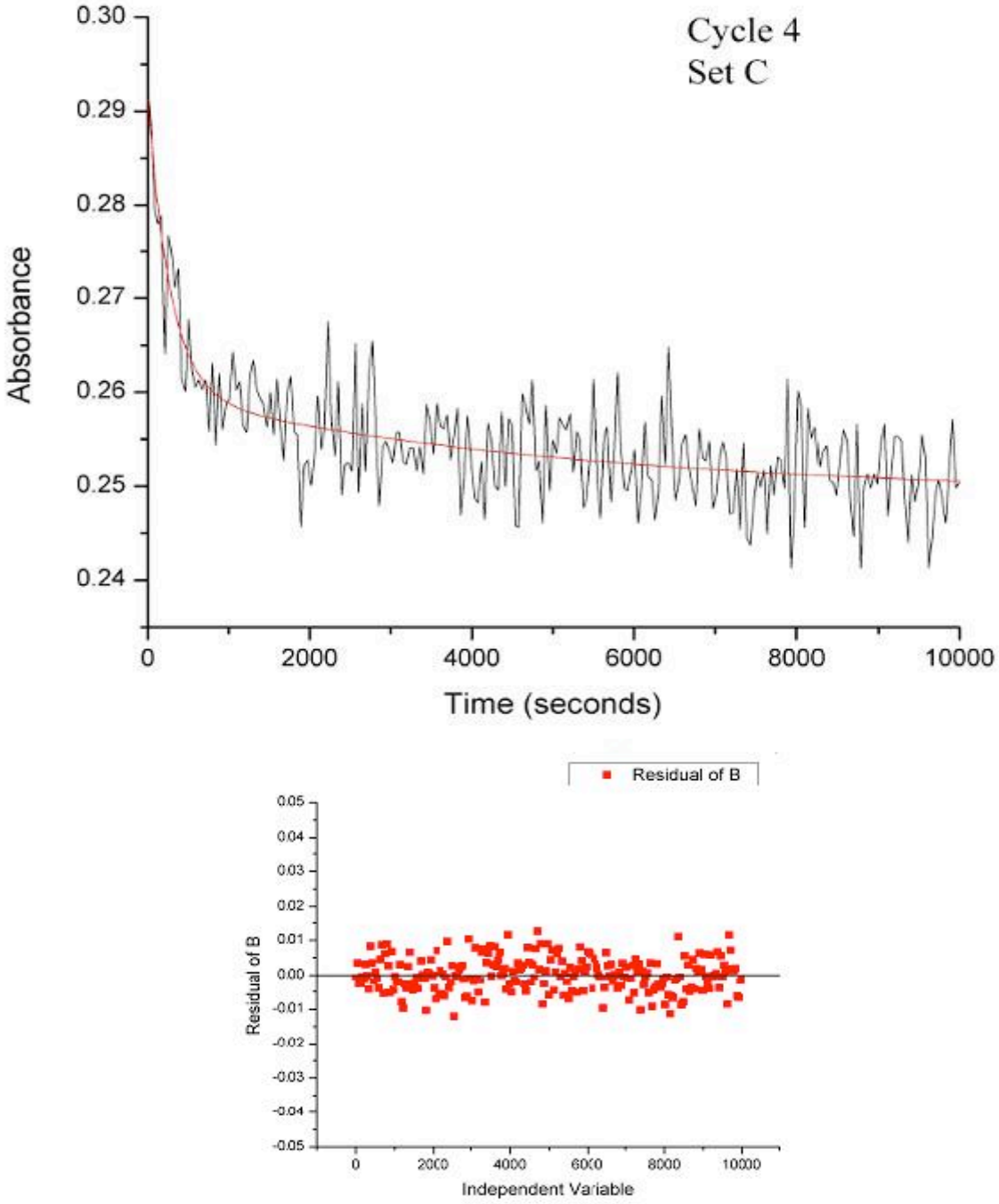

Figure S30. Plot of Cycle 4 and Residual of decay of compound **2** reading at 500 nm after 20 minutes of irradiation with 365 nm light (Acquisition time: 10000 seconds)

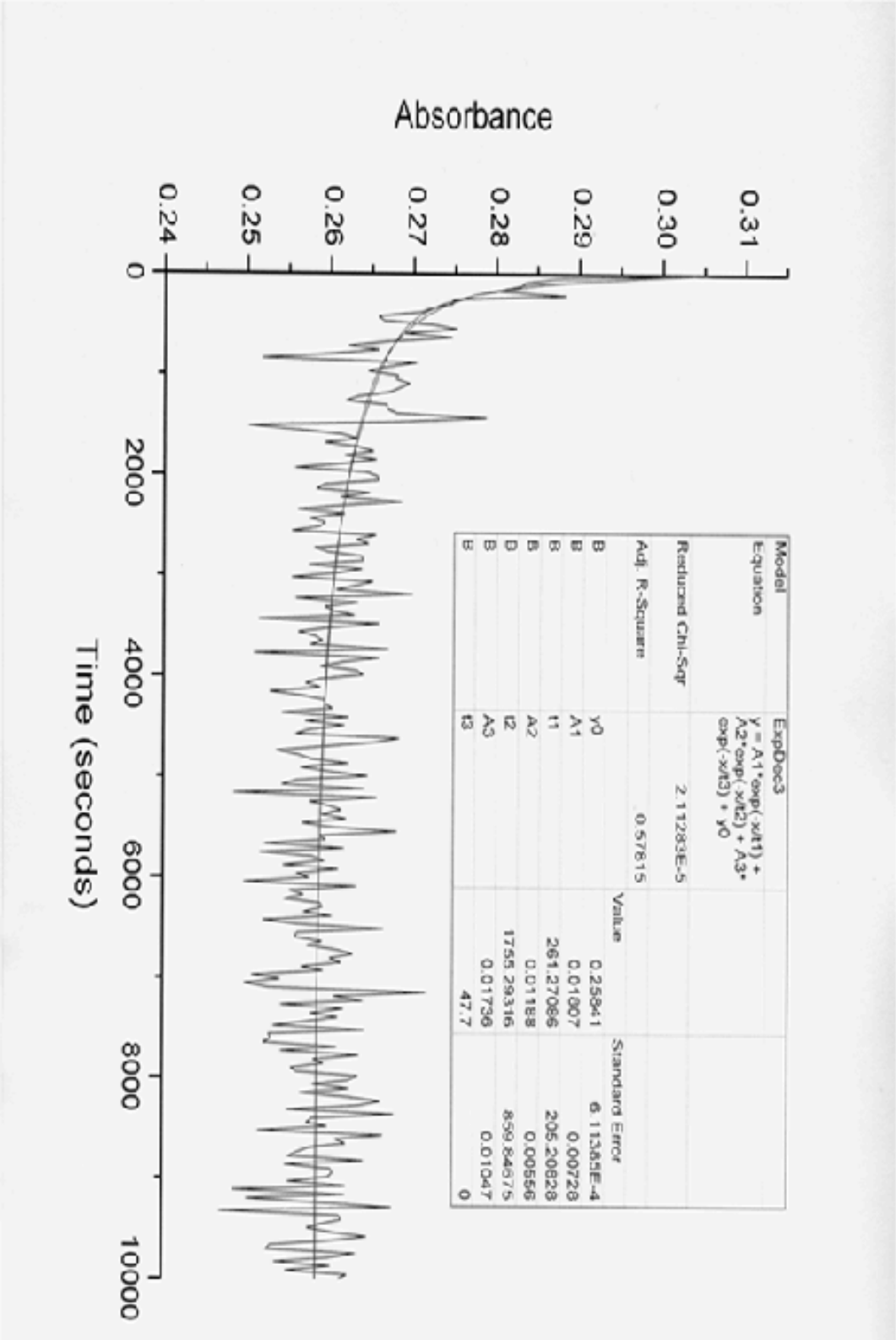

Figure S31. Plot of Tri-exponential fitting of Cycle 2 of Set C.

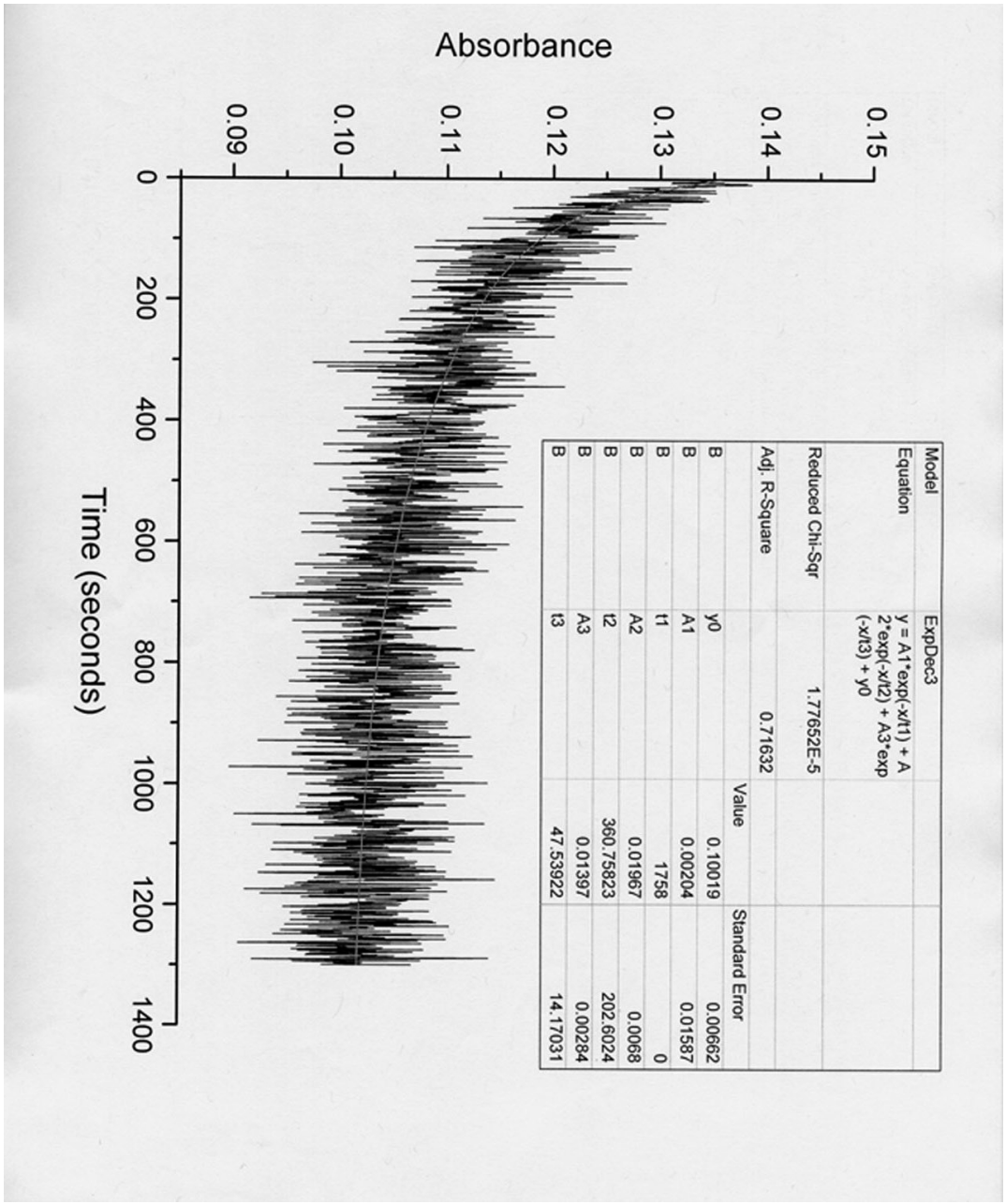

Figure S32. Plot of Tri-exponential fitting of Cycle 1 of Set A .

From Table S2, we took the values of each A and τ and plotted them using this equation: $Y=A_n e^{-t/\tau_n}$ (Figure S32).

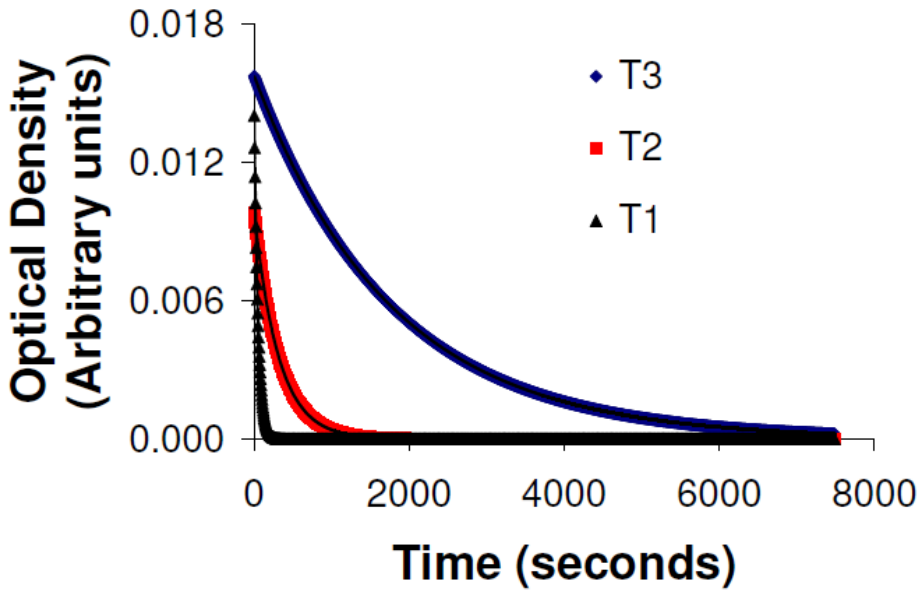

Figure S33. Plot of compound **2** using mono-exponential fitting for τ_n (Total time: 7000 seconds).

Table S3. Population of each "species" during the adquisition time.

	population 1 (p1)	population2 (p2)	population 3 (p3)	pTotal (p1+p2+p3)
An* τ n	3.12098535	27.71107488	0.74422245	31.57628268
(An* τ n) /p(total	0.098839543	0.877591424	0.023569033	
percentage	9.88	87.76	2.36	100.00

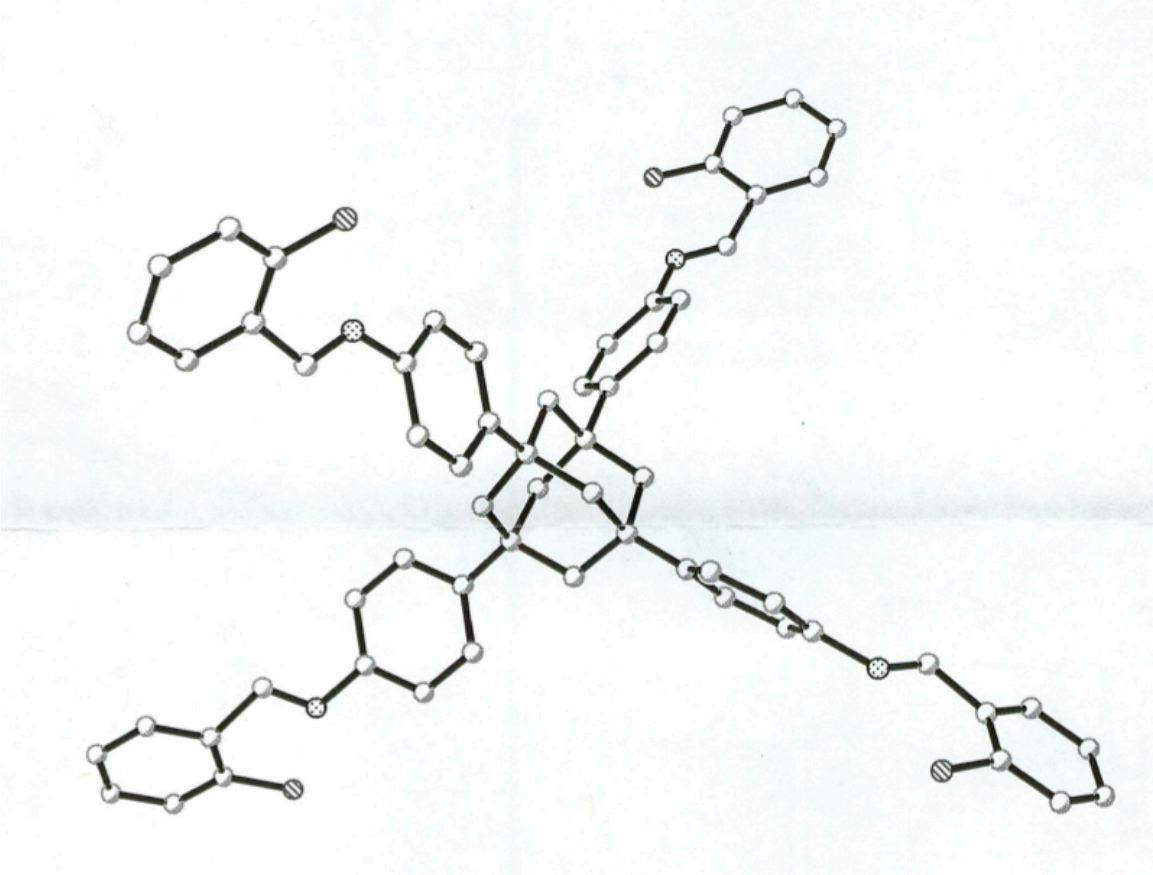

Figure S34. Crystal structure of **1**, connectivity only from heptane and THF.

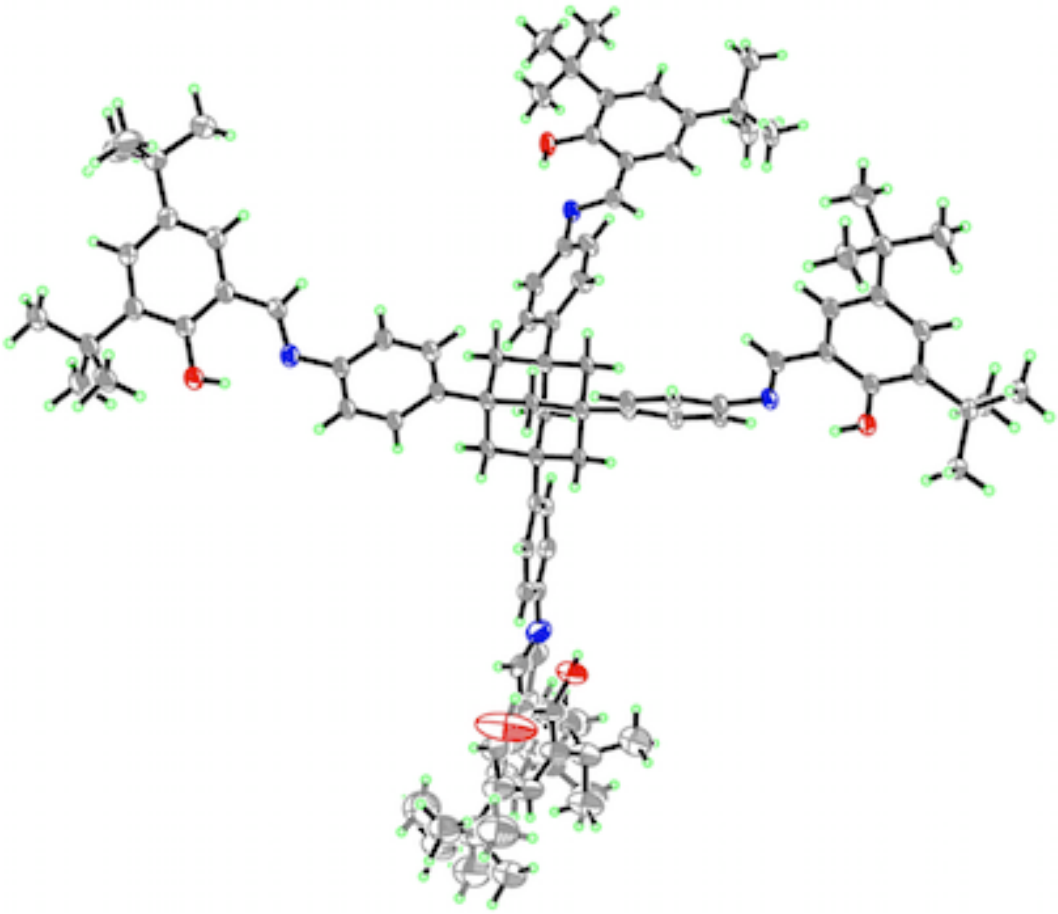

Figure S35. Crystal structure of **2** with disorder in one arm, possibly due to rapid loss of solvent.

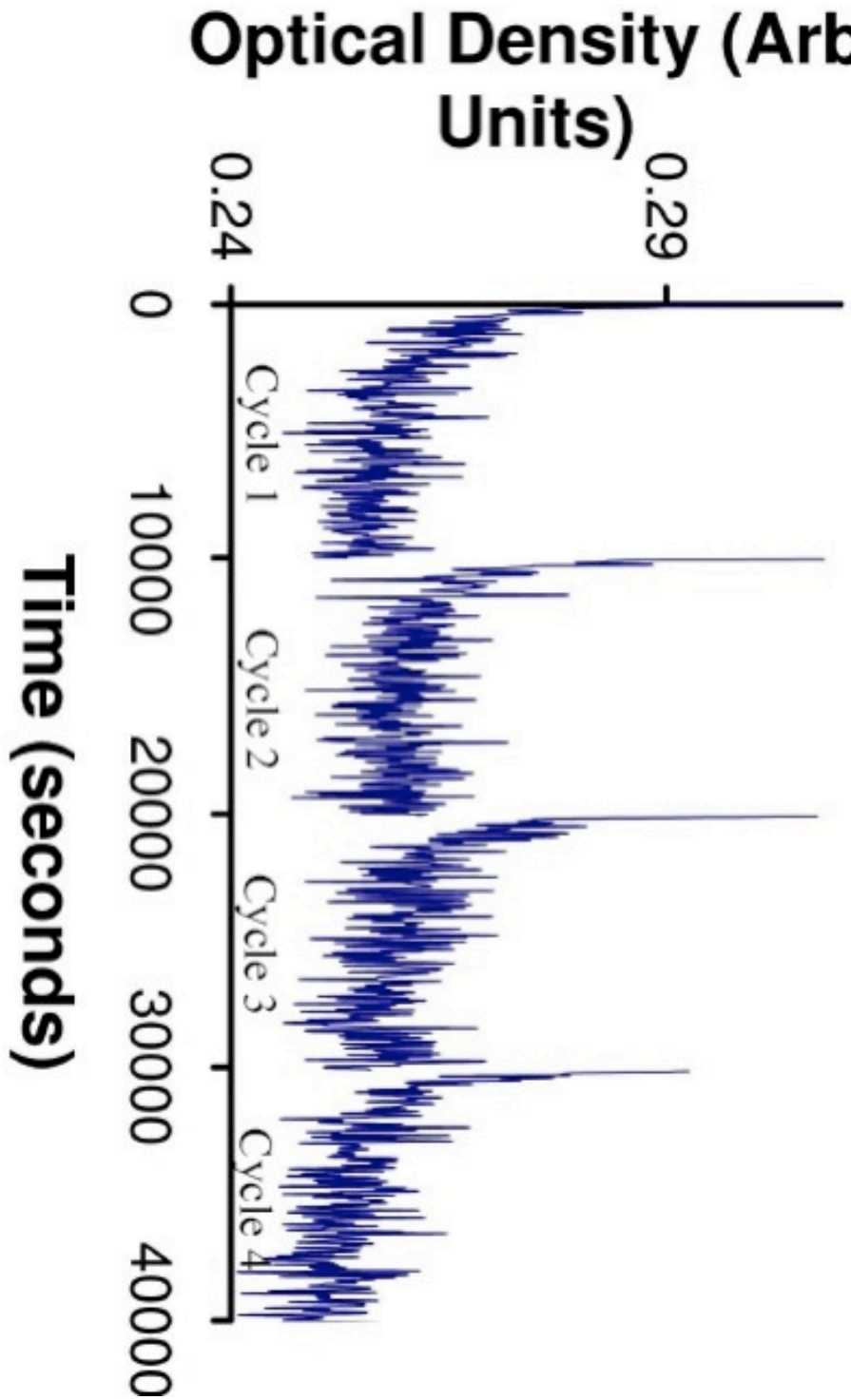

Figure S36. Diffuse reflectance showing the cyclability of **2.**

5.7. References

[1] Hoffart, D. J.; Cote, A. P.; Shimizu, G. K. H. *Inorg. Chem.* **2003**, *42*, 8603-8605.
[2] Wang, S.; Oldham, W.J.; Hudack, R.A.; Bazan, G.C. *J. Am. Chem. Soc.* **2000**, *122*, 5695-5709.
[3] Vittal, J. J. *Polyhedron* **1996**, *15*, 1585-1642.
[4] El-Kaderi, H. M.; Hunt, J. R.; Mendoza-Cortes, J. L.; Cote, A. P.; Taylor, R. E.; O'Keeffe, M.; Yaghi, O. M. *Science* **2007**, *316*, 268-272.
[5] Guo, W., Galoppini, E., Gilardi, R., Rydja, G., Chen, Y. *Crystal Growth and Design*, **2001**, *1*, 3, 231-237.
[6] Tiwari, R. N.; Chang, L. *J. Appl. Phys.* **2010**, 107, 103305-1-103305-7.
[7] Boldog, I.; Lysenko, A. B.; Rusanov, E. B.; Chernega, A. N.; Domasevitch, K. V. *Acta Crystallogr., Sect. C: Cryst. Struct. Commun*. **2009**, *65*, 248-252.
[8] Lamoureux, G.; Artavia, G. *Curr. Med. Chem*. **2010**, *17*, 2967-2978.
[9] Reichert, V. R.; Mathias, L. J. *Macromolecules* **1994**, *27*, 7024-7029
[10] Lim, H.; Chang, J. Y. *Marcomolecules* **2010**, *43*, 6943-6945.
[11] Reichert, V. R.; Mathias, L. J. *Marcomolecules* **1994**, 27, 7015-7023.
[12] Jones, K.; Mahmoudkhani, A. H.; Chandler, B. D.; Shimizu, G. K. H. *Cryst. Eng. Comm*. **2006**, *8*, 303-305.
[13] Kim, J.; Chen, B.; Reineke, T. M.; Li, H.; Eddaoudi, M.; Moler, D. B.; O'Keeffe, M.; Yaghi, O. M. *J. Am. Chem. Soc.* **2001**, *123*, 8239-8247.
[14] Plietzsch, O.; Schilling, C. I.; Tolev, M.; Nieger, M.; Richert, C.; Muller, T.; Brase, S. *Org. Biomol. Chem.* **2009**, *7*, 4734-4743.
[15] Thyagarajan, S.; Liu, A.; Famoyin, O. A.; Lamberto, M.; Galoppini, E. *Tetrahedron* **2007**, *63*, 7550-7559.
[16] Zarwell, S; Ruck-Braun, K. Tetrahedron Lett. **2008**, 49, 4020-4025.
[17] Hadjoudis, E.; Chatziefthimiou, S.D.; Mavridis, I.M. *Curr. Org. Chem.* **2009**, *13*, 269-286.
[18] Asahi, T.; Masuhara, H.; Nakatani, K.; Sliwa, M. *Mol. Cryst. Liq. Cryst.* **2005,** *431*, 241-248.
[19] Sliwa, M.; Letard, S.; Malfant, I.; Nierlich, M.; Lacroix, P.G.; Asahi, T.; Masuhara, H.; Yu, P.; Nakatani, K. *Chem. Mater.* **2005,** *17,* 4727-4735*.*
[20] Kawato, T.; Koyama, H.; Kanatomi, H.; Tagawa, H.; Iga, K. *J. Photochem. Photobiol. A: Chem.,* **1994**, *78,* 71-77.
[21] Amimoto, K.; Kawato, T. *J.Photochem. Photobiol.,C* **2005**, 6, 207-226
[22] Shokova, E. A.; Kovalev, V. V. *Russ. J. Gen. Chem.* **2008**, *78*, 2082-2093.
[23] Ziolek, M.; Burdzinski, G., Filipczak, K.Karolczak, J.; Maciejewski, A. *Phys. Chem. Chem. Phys.* **2008**, *10*, 1304-1318.
[24] Taneda, M.; Amimoto, K.; Koyama, H.; Kawato, T. *Org. Biomol. Chem.* **2004**, *2*, 499-504.
[25] Yelamaggad, C. V.; Achalkumar, A. S.; Shankar Rao, D. S.; Krishna Prasa, S. *J. Org. Chem.* **2007**, *72*, 8308-8318.
[26] Chong, J. H.; Sauer, M.; O. Patrick, B.; MacLachlan M. J. *Org. Lett.* **2003**, *5,* 3823-3826.

[27] Shen, D.; Chapman, O. L.; Lin, L.; Ortiz, R. (Mobil Oil Co., USA). Method for direct arylation of diamondoids. US Patent 5,347,063, September 13, 1994.
[28] Nakagaki, R.; Kobayashi, T.; Nakamura, J.; Nagakura, S. *Bull. Chem. Soc. Jpn.* **1997**, 50, *8*, 1909-1912.
[29] Kawato, T., Koyama, H., Kanatomi, H., Isshiki M. *J. Photochem.* **1985**, *28*, 103-110.
[30] Kawato, T.; Kanatomi, H.; Koyama, H. Igarashi, K. *J.Photochem. Photobiol.,A* **1986,** *33,* 199-208.
[31] Fujiwara, T.; Harada, J.; Ogawa, K. *J. Phys. Chem. B* **2004**, *108*, 4035-4038.
[32] Fukuda, H.; Amimoto, K., Koyama, H., Kawato, T*. Org. Biomol. Chem.* **2003**, *1*, 1579-1583.
[33] Hadjoudis, E. *Mol. Eng.* **1995**, *5,* 301-337.
[34] Chatziefthimiou, S.D., Lazarou Y. G., Hadjoudis, E., Dziembowska, T., Mavridis, I.M. *J. Phys. Chem. B* **2006,** *110,* 23701-23709.
[35] Hadjoudis, E.; Mavridis, I. M. Chem. Soc. Rev., **2004,** *33, 579-588.*